HYDROLOGIC AND WATER QUALITY CHARACTERISTICS OF A SMALL WETLAND - UPPER DORN CREEK WETLAND, WISCONSIN

by

Justin S. Rogers

A thesis submitted in partial fulfillment of

the requirements for the degree of

Master of Science

(Civil and Environmental Engineering)

at the

UNIVERSITY OF WISCONSIN-MADISON

2006

ABSTRACT

Wetlands are well known to provide the functions of peak flow reduction, sediment and nutrient trapping, and hydrologic storage during storm events. However, few comprehensive field studies have been conducted to demonstrate these characteristics. This paper reports on a study of a small 44.9 hectare degraded wetland in a predominately agricultural watershed in southern Wisconsin. The goal of the study was to quantify the hydrologic and water quality characteristics of this wetland through the use of both measurements and modeling. The hydrologic behavior of this wetland was investigated by measuring flood hydrographs during storm events at several locations upstream and downstream of the wetland. The results of the observed hydrology indicated that the wetland attenuated flood peaks for events of up to a 1.5 year recurrence interval. Wetland flood storage was significant for events of 1-2 recurrence interval, but was not significant for small events. Hydraulic modeling was performed using the HECRAS model with LIDAR and site surveyed data inputs. Results of hydraulic modeling indicate that the wetland was inundated 7% at baseflow, 64% at the largest observed event (1-2 year recurrence) and 76% for a hypothetical 5-year recurrence event. Suspended sediment and phosphorous (P) loadings entering and exiting the wetland were determined for each event using direct sampling; these results showed net deposition during very small events and net loss during large events. There was a net export of sediment from the wetland of 156,600 kg and 98% of this sediment was moved in the two largest observed events. Total P loads entering and leaving the wetlands were 602 kg and 585 kg, respectively, over the duration of the study period. Laboratory determination of

critical stress on sediment cores showed that flow conditions in storm events exceeded the critical shear threshold, showing that the suspended sediment samples were the result of channel and wetland erosion.

ACKNOWLEDGEMENTS

Professor Ken Potter – My advisor

Professors John Hoopes and Chin Wu – My committee members

The following people provided tremendous help with the project:

Adam Hoffman, Professor David Armstrong, Professor Mike Penn (UW–Platteville), Evan Murdoc, Josh Anderson, Mitch Asch, Corey Alfred, Chris Parrish, Mike Aslaksen, and Jason Woolard

The following people were very generous in allowing us to work on their property:

Jeff Kippley, Vernon Ripp, Al Dorn, Sophie Wagner, and Cyril Statz

Funding for this project was provided by:

Arthur D. Frazier Fellowship, US Environmental Protection Agency, Wisconsin Department of Natural Resources, NOAA/NGS

I would also like to thank my family and friends for their continued support. The following people provided additional help editing this thesis:

Minna Rogers and Hans Obma

Most importantly I would like to acknowledge my wife, Minna who has put up with many long hours and late nights so I can pursue my dreams. Thank you and I love you so much.

Finally, I would like to give credit to God who has granted me a mind to work, the opportunities to learn and the continual grace of a loving Father.

TABLE OF CONTENTS

LIST OF FIGURES

LIST OF TABLES

1. INTRODUCTION

Wetlands are unique features of landscapes that significantly influence the hydrology and water quality of surface and ground waters (Brinson et al 1995, NWPF 1988). Through the temporary storage of storm runoff, wetlands can reduce flood peaks (Bullock and Acreman 2003). Storage also enables wetlands to retain sediment and associated nutrients, such as phosphorous. Although these effects of wetlands are well accepted, quantification of them has proven difficult.

It is also becoming recognized that some of these wetland characteristics may be conflicting, particularly in watersheds that have been significantly altered by human activities (Ehrenfeld 2004, Hansson et al 2005). For example, in agricultural watersheds the habitat functions of wetlands are likely to be degraded by trapping of excess amounts of sediment and nutrients. Hence in agricultural regions, it may be desirable to suppress the hydrologic and water quality functions of wetlands that provide exceptional habitat. At the same time, it may be advantageous to restore degraded wetlands in some rural and nearby urban areas to reduce flood peaks and trap sediments and nutrients.

It is commonly proposed that the hydrology in a wetland involves temporary storage, energy dissipation, and peak flow reduction (Brinson et al 1995). However, a review of 169 wetland research projects by Bullock and Acreman (2003) revealed that there was a large variation in wetland capacity to reduce or delay floods. There does seem to be widespread agreement that wetlands can exert a significant influence on flood hydrology

and that initial wetland storage is crucial in determining how a wetland behaves hydrologically (Krause 1999, McKillop 1999, and Potter 1994).

Wetlands present a complex hydraulic region with typically very low slopes, shallow water depths, and meandering channels. The hydraulic characteristics of wetlands have not been well studied, partly because the concepts developed for floodplains, reservoirs and natural channels can be applied to wetland conditions. Nevertheless, hydraulic modeling of wetlands is complex and is significantly affected by the roughness coefficient (Hall 2005) and microtopography (French 2003). In addition to these influences, the relationship between stage and storage in the overbank areas is complex and involves hysteretic effects (Hughes 1979, Lewin and Hughes 1980).

One of the most often cited characteristics of wetlands is their ability to retain suspended sediments and substances absorbed to them (Kleiss 1996, Brinson 1995). Numerous studies support this feature and have shown that wetlands serve to trap sediments (Cooper et al 1987, Craft and Casey 2000, Hupp and Bazemore 1993, Hupp et al 1993, Johnston 1984, Kleiss 1996, Lowrance 1986, Mitsch et al 1979, Wilson 2005). However, it has also been observed that resuspension of sediments during individual storm events can transform wetlands into sediment sources (Jordan 2003, Kleiss 1996, Phillips 1989, Wilson 2005). Therefore, it appears that wetlands generally trap sediments but may be sediment sources under certain conditions.

The sediment transport within a system is controlled by two primary factors: sediment supply; and sediment transport capacity (Julien 1998). Sediment supply is the amount of

sediment available to the stream system for transport. Sediment transport capacity is the ability of the water to carry sediment and is typically related to the bed shear stress (Lee et al 2004, Julien 1998). The interaction of sediment supply and transport capacity leads to the rate of sediment transport. Sediment rating curves in natural channels have been observed to have several shapes, which are related to a combination of temporal, spatial, hydrological, hydraulic, and meteorological factors (Sichingabula 1998).

Another important characteristic of wetlands is their retention of nutrients, such as phosphorous (P), which improves the water quality in downstream aquatic systems (Johnston, 1991). The impact of P on water quality in freshwater lakes is widely recognized (Schindler 2006; Carpenter, 2005), and excessive P loadings may lead to eutrophication of the receiving water body. While regulations have resulted in decreased loading from point sources, nonpoint sources, including agricultural runoff, are an increasing problem for lakes and rivers (Carpenter et al., 1998; Newman, 1995). Wetlands are important landscape features that can modify the amount, timing, and composition of P and sediments delivered to downstream sites and waterbodies.

This paper reports on a study of a degraded wetland in a predominately agricultural watershed in southern Wisconsin. The goal of the study was to quantify the hydrologic and water quality characteristics of this wetland through the use of both measurements and modeling.

2. SITE DESCRIPTION

Appendix A in this report contains additional site description information.

The Dorn Creek Watershed (Figure 1) is located within Dane County, Wisconsin, between the Town of Waunakee and the City of Middleton. Dorn Creek is a tributary to Sixmile Creek, which flows directly into Lake Mendota. It is approximately 18.2 kilometers long and has a total watershed area of 32.82 square kilometers (USGS 1983). The land surrounding the creek is primarily agricultural, although there is a small residential area at the far western edge of the watershed.

There are three distinct wetland areas along Dorn Creek. The wetlands were outlined based on review of topographic mapping (USGS 1983), aerial photographs and land use mapping (Dane County 2006). The largest and most downstream wetland is known as the Dorn Creek Wetland and has a total area of 153.0 hectares. The second wetland upstream is known as Upper Dorn Creek Wetland, with a total area of 44.9 hectares. The most upstream wetland is a small unnamed wetland of approximately 9.7 hectares. The focus of this investigation is on the Upper Dorn Creek Wetland and associated channel. The Upper Dorn Creek Watershed is composed of 5 major sub-watersheds based on USGS mapping (USGS1983) which have been named A through E (Figure 1). Watersheds B, D, and E are internal subwatersheds contributing to channel reaches.

Most areas of the Upper Dorn Creek Wetland are classified as a shallow marsh, but some areas are sedge meadow to mesic prairie (Eggers and Reed 1997). Major portions of the wetland are covered by Reed Canary Grass, a non-native, invasive species.

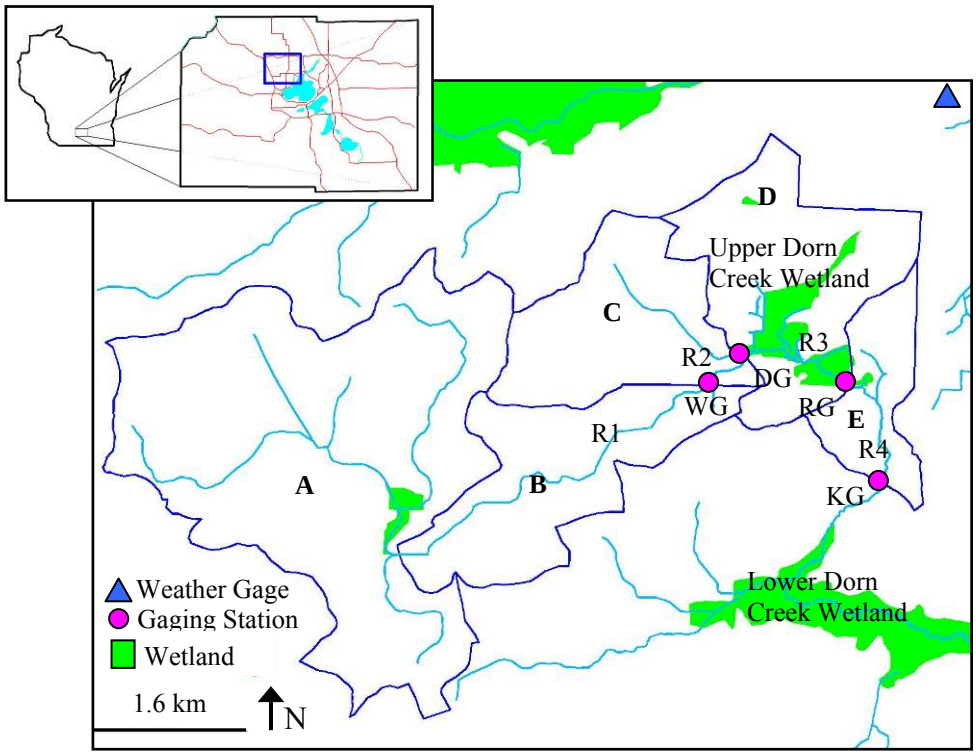

Figure 1: Project Location With Sub-Watersheds (A,B,C,D and E) and Major Reaches (R1-R4) of Upper Dorn Creek Watershed Showing Wetlands and Gaging Stations: Wagner (WG), Dorn (DG), Ripp (RG), and Kippley (KG)

Watershed	Area (km^2)	% Impervious	Flow Length (km)	Elevation Change (m)
A	8.79	7.04	4.33	57.9*
B	2.86	0.98	3.85	12.2*
C	2.56	2.62	2.21	43.5**
D	3.23	1.91	3.54	36.7**
E	1.19	2.18	2.35	23.5**

Table 1: Watershed Characteristic Summary. * Based on USGS (1983) Data. **Based on LIDAR Survey Data.

Table 2 is a summary of the channel reach characteristics within the watershed. Reaches were defined based on the location between gages (Figure 1), and slopes were determined by the total elevation drop within the reach.

Reach	Length (km)	Elevation Change (m)	Slope (m/m)	General Description
1	3.77	12.21	0.003236*	Grass-lined excavated channel, soil is primarily silt-loam.
2	0.46	0.83	0.001824**	Small incised main channel surrounded by floodplain, with silt-clay sediment bottom
3	1.42	2.37	0.001668**	Wetland reach, wide and shallow, with silt-clay sediment bottom
4	1.25	5.00	0.004006**	Deeply incised channel with hard clay and sand bottom and boulder groups

Table 2: Reach Characteristic Summary. * Based on USGS (1983) Data. **Based on LIDAR Survey Data

The current land use is primarily agricultural, although numerous residential and commercial structures are located within the watershed (Murdoc 2006). Based on review of aerial photos (Dane County 2006), soil data (Dane County 1996) and geological data (Clayton and Attig 1997), of current and probable historic wetlands within the Dorn Creek Watershed, the Dorn Creek Watershed has experienced an estimated 54% loss of wetlands.

The primary mechanisms for wetland loss are the installation of drain tiles and agricultural ditches to convey water away from former wetlands and subsequent conversion of the land to agricultural use. Most of the major wetlands in the area have experienced loss of area due to encroachment, but some of the smaller wetlands have been completely removed. Within the Upper Dorn Creek Wetland, several agricultural channels have been cut into the wetland to provide drainage. These channels have a significant effect on the hydrologic and water quality behaviors of the wetland.

3. METHODS AND INSTRUMENTATION

Appendices B and F in this report contain additional information on methods and instrumentation.

Four gaging stations were set up along Dorn Creek, as shown in Figure 1, for the 2006 season. The gaging stations were named, based on the property owners of the sites. The Wagner and Kippley gaging stations were run with Campbell Scientific Dataloggers (CR-10X and CR-10), and the Dorn and Ripp gaging stations were monitored by Isco 6712 Samplers. Data were recorded on one-minute intervals, and averaged over 15-minute intervals.

Gage	Contributing Watersheds
Wagner	A+B
Dorn	A+B+C
Ripp	A+B+C+D
Kippley	A+B+C+D+E

Table 3: Gages and Contributing Watersheds

3.1 Water Level Measurement

Water level data were obtained at all four gage sites using pressure differential transducers. At the Ripp and Dorn Sites, Isco 720 Submerged Probes were attached to the Isco Samplers, mounted to the bed of the channel. At the Kippley and Wagner sites, Global Water WL-400 pressure transducers were installed in stilling wells (mounted in the channel), and connected to the dataloggers.

3.2 Meteorological

Weather data were taken from a privately owned weather station (KWIWAUNA2), which is part of the Weather Underground network of weather stations (WU 2006). The gage was an Oregon Scientific WMR968 Wireless Weather Station using VWS (v.12.08) software. It was located 1.32 km from the watershed edge and 4.70 km from the watershed centroid as shown on Figure 1. This data include 5-minute precipitation as well as other weather data.

3.3 Rating Curves and Baseflow

Standard methods for measuring streamflow, as described by (Herschy 1995), and (Chow et al. 1988), were used. Flow measurements were made, using calibrated electro-magnetic velocity meters (Marsh McBirney 201 and 711), seven times from April through June, during flood and baseflow conditions. For flowrates above measured conditions, the calibrated HECRAS model was used to develop rating curves. Stormflow was separated from baseflow using a linear method for each event. An initial point was selected before stormflow rise, and the ending point was taken between 4 to 7 days after the initial event. This assumption was based on site investigations, which indicated that the system was well drained after 7 days even for the larger events.

3.4 Sediment and Phosphorous Analysis

Suspended sediment concentration in the flow was obtained by two principle methods. One D&A Instrument Optical Backscatter (OBS-3) device was installed at the Kippley

Site for continuous turbidity measurement, and two Isco Model 6712 Portable Samplers were installed at the Dorn and Ripp Sites for automated stormflow sampling.

The OBS-3 probe was installed in the flow at the protruding end of the stilling well. The OBS instrument was calibrated in the field by simultaneous measurement of the OBS response and a direct sample of the flow. This sample was later filtered, using methods described below, to obtain suspended sediment concentration.

The Isco Portable Samplers were programmed to collect 24 flow samples during storm events (every 2 hours for the first 12 samples and then every 8 hours for the last 12 samples). The sampler was set to begin sampling when a set threshold of water level was measured by its water level probe. The threshold level was set, based on observed storm data, in the range of 2 to 5 cm. After stormflow events, the samples were recovered, and stored in acid washed polyethylene bottles at 4°C until analysis. Total phosphorous (P) was measured, after a persulfate digestion (APHA, 1992), in all neutralized P aliquots using the method of Murphy and Riley (1962).

Analysis of the samples for total suspended solids involved filtering a known volume of sample, using a pre-weighed, Whatman Nuclepore, polycarbonate membrane filter with a pore size of 0.40 μm. The filter was then dried and weighed, and the total suspended sediment concentration determined (UW 2006). Additional analysis of the stormflow samples was performed using a Sequoia Laser In-Situ Scattering and Transmissometer (LISST), model 100X. Sampling was performed according to the manufacturer's recommendations. A linear regression was performed to correlate volume per volume,

given by the LISST, and transmission response to a mass concentration. A combination of the LISST and filter data was used to determine the final TSS values.

Total sediment budget results were based on a mass balance of the system (Figure 2). At each gaging station, the stormflow volume and sediment mass were known for each storm event. However, there was additional input from the local watershed between the gages that was unknown.

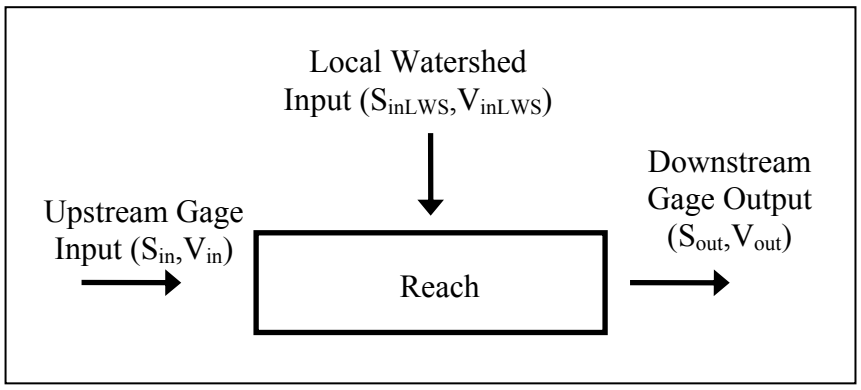

Figure 2: Mass Balance Diagram for Storm Runoff Volume (V) and Sediment (S)

The runoff volume and sediment concentration were estimated using a mass balance. Because of the potentially large and uncertain amounts of water stored in the wetland, the storm runoff volume and sediment yield for the watershed surrounding the wetland (Watershed D) were estimated using the runoff coefficient and sediment yield characteristics of the upstream Watershed C. Similar methods were applied to Reach 4 and Watershed E, except that the storm runoff volume was available from the gage data. Therefore, a simple mass balance for sediment accumulation in a reach is:

$$S_{inDorn} + S_{inWSD} - S_{outRipp} = \text{Accumulation(Reach 3)}$$

$$S_{inRipp} + S_{inWSE} - S_{outKippley} = \text{Accumulation(Reach 4)}$$

These relations assume that Watersheds C, D and E are similar in their runoff and sediment yield characteristics. Based on the site and watershed information in Table 1, this is a reasonable assumption.

3.5 Flume Core Testing and Local Bed Shear Analysis

Cores were taken from steel core pipes driven into the bed sediments at the four gaging stations. Both ends of the core were capped; and care was taken to minimize disturbance to the sample. Testing of the sediment cores was performed, using the methods of Lee et al. (2004), except that erosion detection was visual rather than automated. The testing was performed in a 23.2 cm wide flume with variable slope. The soil core was pushed through the tube until it was flush with the channel, and the channel was run until the critical shear stress was obtained. Testing of the cores was conducted for every 5 cm of soil core depth.

Typical design flow conditions and schematic diagram are similar to those of Lee et al. (2004). Due to difficulty in determining slopes to the accuracy needed, a friction drag method was adopted to determine the critical shear stress values. Based on Lee et al. (2004), the friction coefficient (C_f) was related to the Reynolds number. Using this relationship, the bed shear was calculated from:

$$\tau_b = \frac{\rho C_f U^2}{2}$$

Actual determination of the local bed shear for natural channels is complex, as flows are nonuniform and unsteady in flood conditions. For steady, uniform flow, the bed shear stress is determined by $\tau_0 = \gamma R_h S_0$ (Munson et al 2005). For nonuniform conditions, a one-dimensional momentum balance for steady flow gives (Lee et al 2004):

$$\tau_b = \gamma R_h \left(S_0 - \frac{dD}{dx}(1 - F^2) \right)$$

$dD/dx = S_0 - S_w$ = spatial rate of change of the water depth, S_w = water surface slope, R_h = hydraulic radius, and F = Froude number.

Using this relationship, the bed shear stress was calculated for the gaging sites for the 2006 season. The friction slope (S_w) and Froude number (F) were determined using the HECRAS model and then related to the depth. The hydraulic radius (R_h) was determined from site surveyed data and recorded water depth.

3.6 Surveying and DTM Generation

LIDAR (Light Detection and Ranging) data were obtained for the project area to support the hydrodynamic modeling. The data for this project were acquired on June 24, 2006, using an Optech ALTM 3100 and waveform digitizer installed on a Dynamic Aviation Beechcraft King Aircraft. The GPS/IMU data were processed and used to generate georeferenced, ASCII mass point files. The raw, last return data were interpolated to a

one-meter grid using a Kriging algorithm. The one-meter (xy) grid was then converted to an AutoCAD, digital topographic format using Surfer (V7.02) program. Three contour intervals of the digital topographic maps were generated of the system: 5-meter, 1-meter, and 0.2-meter. Cross sections were surveyed at each of the four gaging stations and at fifteen additional sites for the hydraulic modeling.

3.7 HECRAS Modeling

HECRAS (v.3.1.1) was used to estimate steady-state water surface profiles in the stream and wetland at peak flowrates interpolated between gages, as well as at other flow rates. The use of observed flowrates accounts for some attenuation from storage and unsteady flow effects. Within the digital AUTOCAD drawing, a principal channel centerline was established for the project area. Channel stationing was established in feet beginning at Dorn Creek and County Highway K (STA 0) and continuing upstream to Dorn Creek near Pheasant Branch Road (STA 14430). Figure 10 shows the cross section locations along the channel. The cross section geometry was based on a combination of the digital LIDAR data and surveyed cross sections. LIDAR topographic data has been used successfully for hydraulic modeling under similar applications (French 2003). Accurate hydraulic modeling of wetland areas is difficult. Within the North Wetland, the main channel bottom is elevated up to 1.2 feet above the lowest point in the wetland. In order to account for this elevated main channel effect, ineffective flow areas were added to the outer banks of the observed main channel to the elevation of the main channel banks.

Based on the field measurements of flowrate and stage for several stormflows, the Manning's n roughness coefficients for the main channels were directly determined for the four gaging stations, using the HECRAS model and a maximum difference of ±0.01 feet between measurements and model results. These values agreed with published values by Chow (1959) and Haan (1994) for observed channel type.

Several model scenarios were run using the observed flowrates for the 2006 season. For low flow events, flowrates were applied to sections slightly upstream of the gaging stations at areas of known inflow. For higher flowrates, these flow values obtained from the gaging stations were linearly interpolated for cross sections between the gaging stations. The total wetland inundation was calculated using the water top width and weighted cross section length from the HECRAS model

4. RESULTS AND DISCUSSION

Appendices C, D and E in this report contain additional results and data analysis.

4.1 Precipitation

The 2006 season had many precipitation events, with widely varying duration and intensity. The major storm events of the 2006 season are summarized in Table 4.

Event Name	Event Approx. Date	Precip. Total (cm)	Duration (hr)	Avg. Intensity (cm/hr)	Max. Intensity (cm/hr)	Days since Last Rain	Conditions	Approx. 8-hr Rec. Int. (yr)
1	4/3	2.90	18.8	0.15	0.89	15	dry	0.3
2	4/7	2.92	10.1	0.29	0.71	4	wet	0.4
3a	4/16	2.01	13.3	0.15	0.79	9	wet	0.1
3b	4/30	3.40	26.7	0.13	0.61	14	dry	0.2
4	5/11	3.00	31.1	0.10	0.51	11	dry	0.1
5	5/24	3.00	3.5	0.87	2.49	7	wet	0.2
6	6/25	6.30	4.6	1.37	2.39	16	dry	1.5
7	7/11	5.41	7.5	0.72	2.01	16	dry	1.8
8	7/27	2.59	1.8	1.47	2.59	7	wet	0.6
9	8/23	9.09	39.8	0.23	1.60	17	dry	0.5
10	9/12	6.25	46.1	0.14	1.19	6	wet	0.2

Table 4: Major Event Precipitation Summary for 2006

Analysis of the frequency of these precipitation events was based on Huff and Angel (1992) for an 8-hour duration. Review of the storm hydrographs showed that the watershed had a typical time of concentration approximately 8 hours. Additional analysis comparing peak flowrate and an 8-hour rainfall duration showed good agreement as compared to other durations. It should be noted that this recurrence interval analysis was

based on precipitation data, which may not correspond well to the recurrence interval for peak flowrates due to initial conditions and other factors. The local regression equations, developed by Walker and Krug (2003) for peak flowrate, gave a 1.5 year recurrence interval for Event 6 at the Dorn Gage.

Historical monthly precipitation from 1948 to 2005 (NCDC 2006) was compared to the 2006 observed precipitation (Figure 3). Based on these results, all months except September were statistically wetter than average. The period of April to September 2006 was the 10th wettest on record for monthly precipitation.

Month	Observed Precip. (cm)	Rank of 1948-2005	Quantile (Weibull)	Avg. Precip. 1948-2005 (cm)	Sdev. 1948-2005 (cm)
Apr-06	14.12	3	0.05	7.88	3.27
May-06	11.51	12	0.20	8.84	4.78
Jun-06	11.51	22	0.37	10.49	5.98
Jul-06	11.33	19	0.32	10.29	4.55
Aug-06	12.32	19	0.32	9.66	5.03
Sep-06	6.53	29	0.48	7.66	5.48

Table 5: Comparison of Historical and 2006 Observed Monthly Precipitation Data

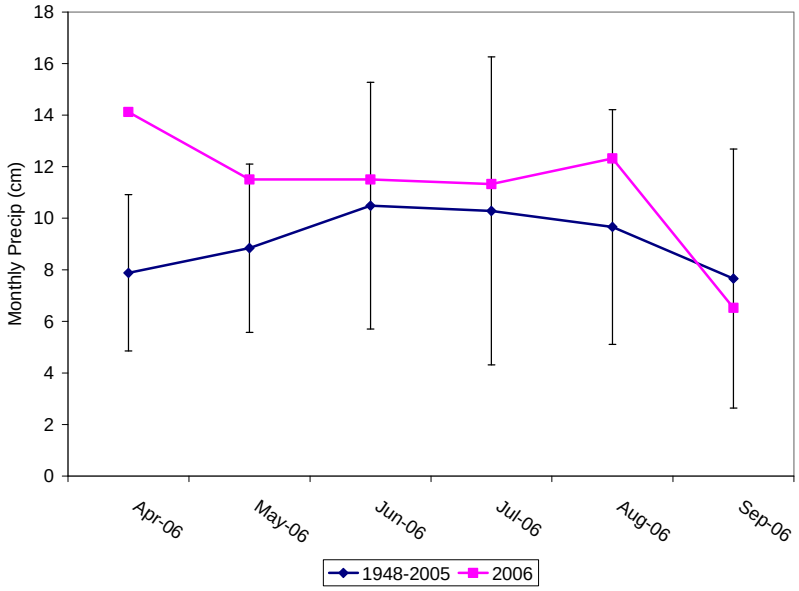

Figure 3: Historical and 2006 Observed Precipitation

4.2 Hydrograph Analysis

The following figures show the observed peak flowrates and stormflow volumes for the 11 recorded events. Figure 4 clearly shows that peak flowrates are better correlated with runoff depth than total precipitation. This is due to antecedent conditions as well as other factors, such as rainfall intensity. Events 5 and 6 were the highest recorded events in terms of both peak flowrate and storm flow volume.

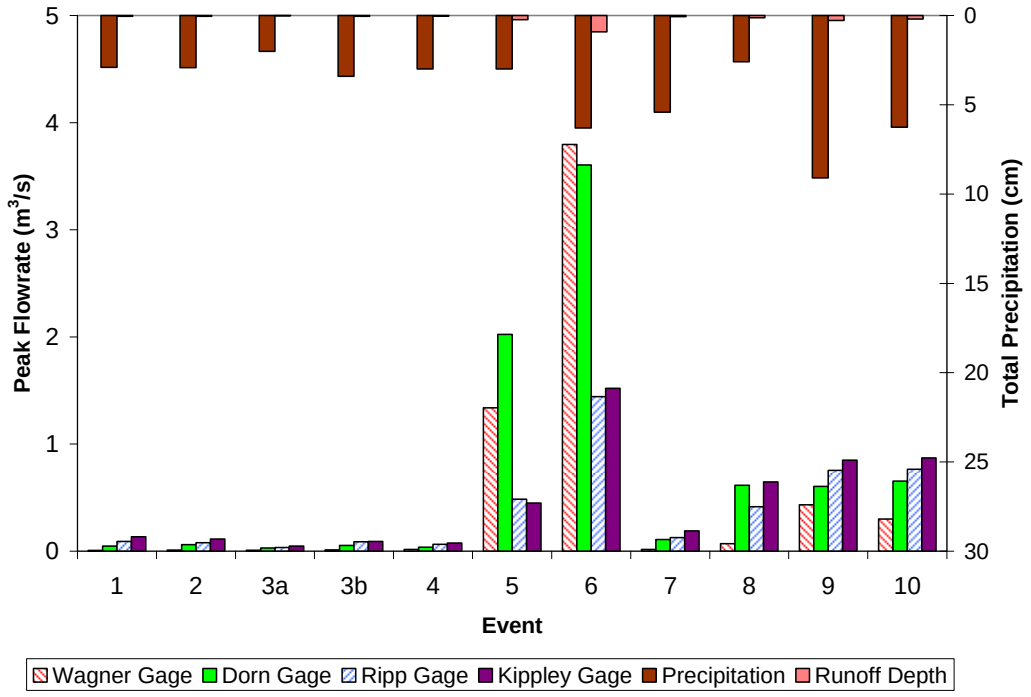

Figure 4: Peak Flowrates for 2006 Season

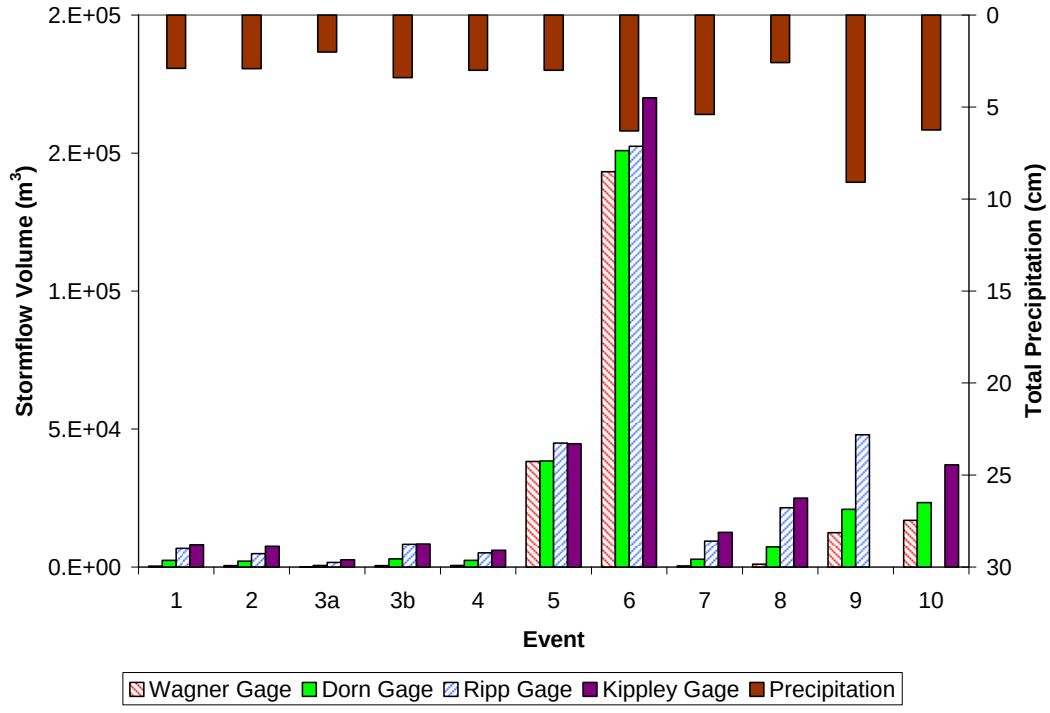

Figure 5: Stormflow Volumes for 2006 Season (Note: data was not available for the Kippley Gage Event 9 or Ripp Gage Event 10).

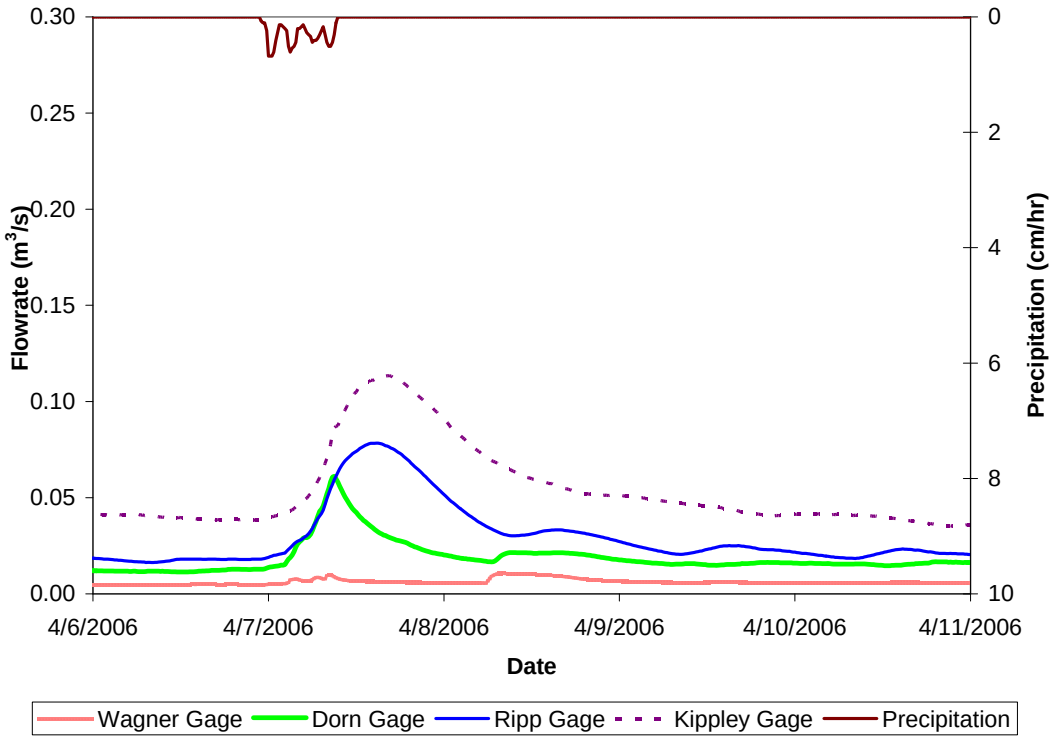

Figure 6: Typical Small Hydrograph (Event 2)

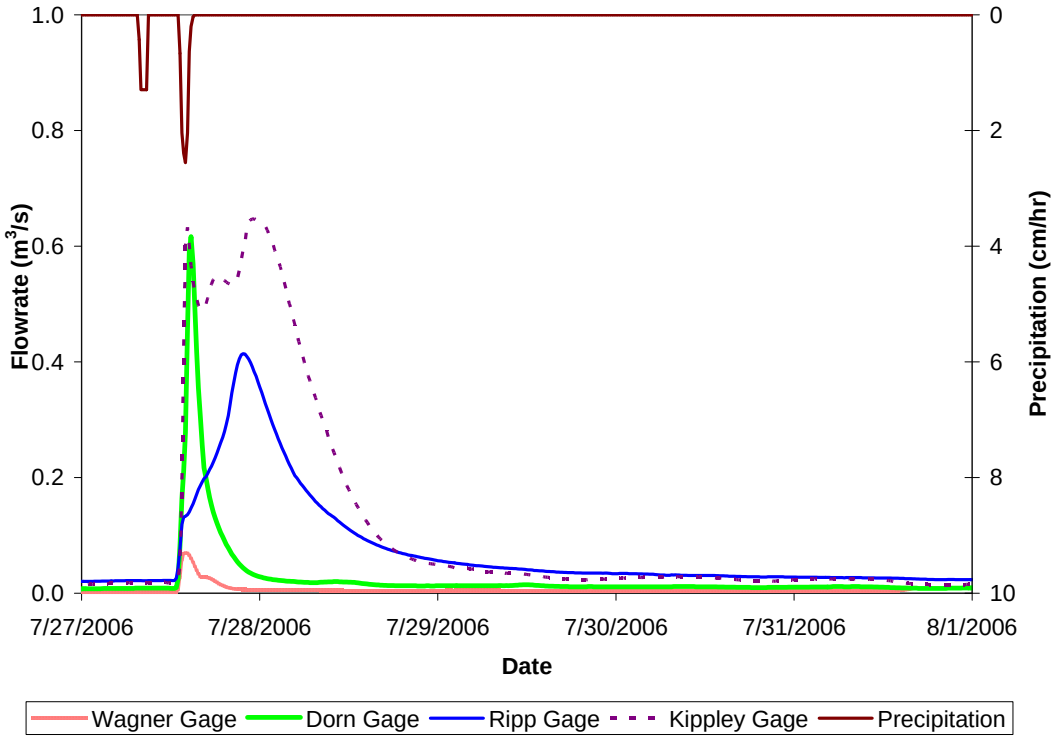

Figure 7: Typical Mid-Sized Hydrograph (Event 8)

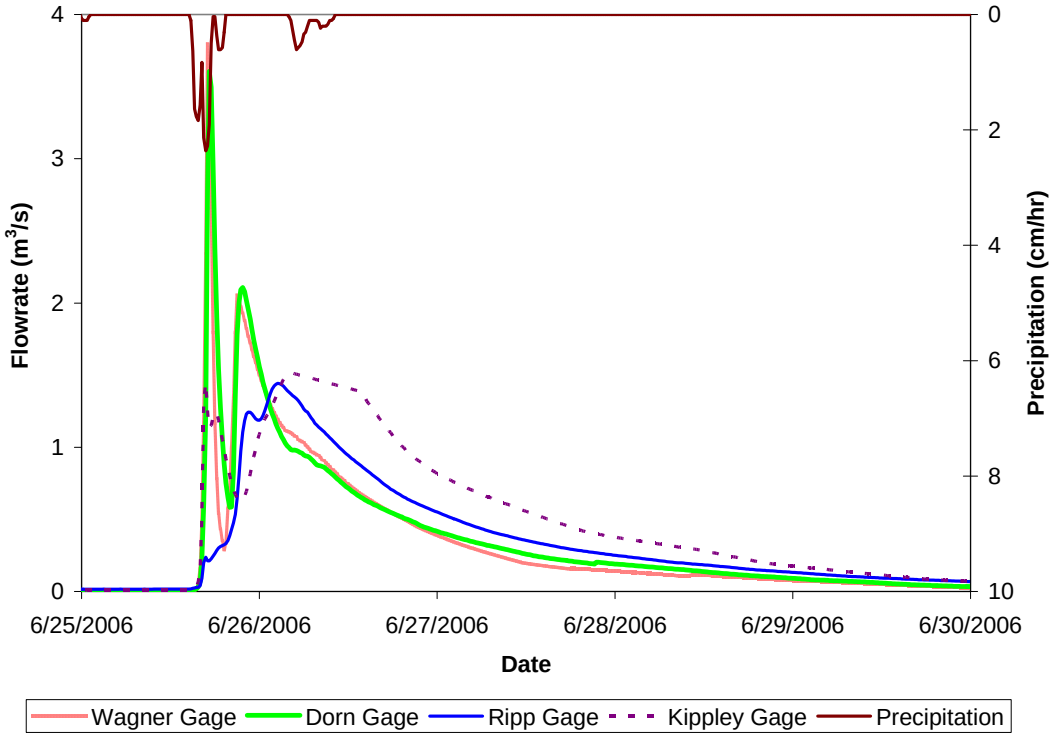

Figure 8: Largest Measured Hydrograph (Event 6)

Figures 6, 7 and 8 present hydrographs for small, mid-sized and large storm events respectively.

As shown in Figure 6, the hydrologic response to a small storm event is uniform, and peaks show typical smooth hydrograph flow response. This event resulted from a low intensity storm of 2.92 cm of rainfall in 10.1 hours. Flood wave progression down the watershed was fairly uniform, and total peak flowrates increased at successive downstream gaging stations. Of note is the most upstream gage (Wagner), which shows very little flow response, even though it accounts for 63% of the watershed area above the most downstream gage (Kippley Gage). This pattern is apparent in other storms and

may be due to high watershed infiltration rates. Peak flows through the wetland (Dorn to Ripp Gages) are lagged, but not attenuated. In fact, flowrates increase through the wetland. As stated previously, this is not a closed system, as Watershed D adds flow to the Creek between the gages, which accounts for the increase in peak flow. Overall, the wetland does not seem to affect peak flows in a typical small event.

As shown in Figure 7, the hydrologic response to a mid-sized event shows a dramatically different response. This event was a high intensity storm of 2.59 cm of rainfall in 1.8 hours. Again, the response at the Wagner Gage is disproportionately low. The Dorn Gage shows a clear sharp peak, which is a combination of flow from Watersheds B and C. This represents the major flow input to the wetland. As mentioned before, there are several small tributaries, which add additional flow to the wetland from Watershed D. The peak flow at the Ripp Gage is significantly smaller than at the Dorn Gage, although the total volume is much larger. This peak flow attenuation is due to the overflow into the wetland. The Kippley Gage shows three distinct peaks. From comparison to the Ripp Gage, it is clear that peaks 1 and 2 result from Watershed E. The third peak corresponds to the main flood wave and is significantly higher than at the Ripp Gage.

Figure 8 shows the largest observed event for the 2006 season. This event was the result of 6.30 cm of precipitation in 4.6 hours and has an estimated recurrence interval of 1.5 years. Two peaks are seen at the Wagner Gage representing Watersheds A and B respectively. Based on analysis of the volume, Watersheds A and B (which represent 63% of the watershed area) are contributing 69% of the storm volume. Clearly,

Watersheds A and B are fully contributing in this event. Flood hydrographs between the Wagner and Dorn Gages have very similar flowrates and flood hydrograph shape. The hydrograph at the Dorn Gage is delayed slightly, but not significantly changed from upstream. Flow between the Dorn and Ripp Gages shows significant peak attenuation. The hydrograph is much lower and shows three distinct peaks. The first peak appears to come from areas near the gage in Watershed D. The two remaining peaks come from a combination of the input hydrograph at the Dorn Gage, and the bulk of Watershed D. In other events, this double peak was observed, even when there was only a single peak observed at the Dorn Gage. This indicates that peaks 2 and 3 observed here are the results of the incoming hydrographs in combination with flows from Watershed D, and not from rainfall variability. The exact hydrologic reasons for the appearance of this double main peak remain unclear. Flow between the Ripp and Kippley Gages shows two distinct peaks. The first peak is a result of flow from areas in Watershed E. The second peak is clearly a result of the delayed hydrograph, observed at the Ripp Gage.

4.3 Wetland Peak Reduction

For the observed record, flood peak reduction occurs for large events but not for small events (Figure 4). Large flows show a clear attenuation, while lower flowrate peaks are higher at the outlet. The transition occurs at approximately 0.65 m^3/s of the incoming flowrate. Thus, near 0.65 m^3/s, flows enter into significant portions of the wetland, and wetland storage becomes significant. Figure 9 shows a plot of peak flowrates at the wetland inlet and outlet normalized by the total storm volume. These results indicate

peak reduction for all events. Inflow from the local Watershed D and the agricultural ditching in the outer areas of the wetland affect this relation. Local inflow will increase the water in the channels, causing faster conveyance through the wetland, and more inundation of the wetland by water from the inlet. Ditching allows faster conveyance of flows and forces more flow into channels. For small events (below bankfull), ditching would allow faster conveyance of flows, as water is no longer entering the wetland.

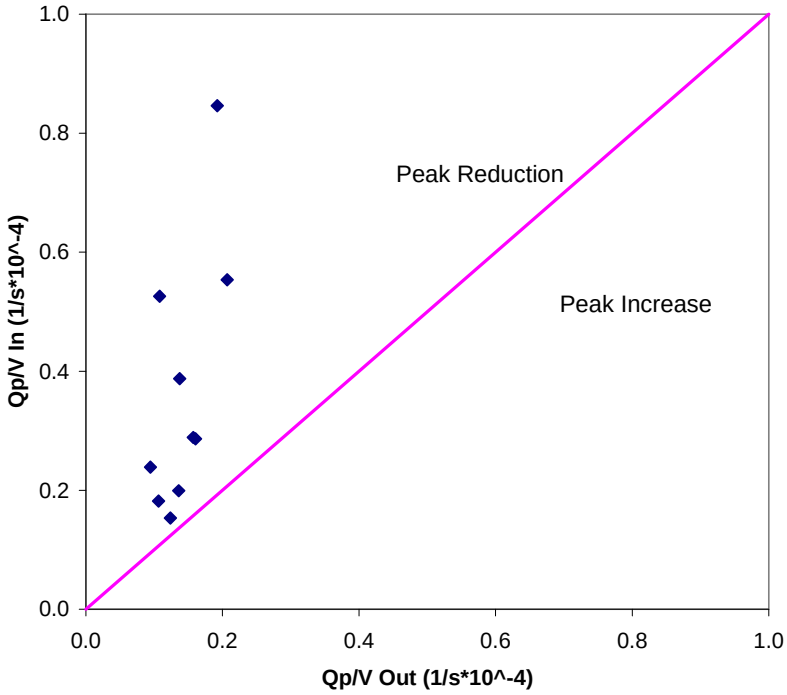

Figure 9: Incoming and Outgoing Peak Wetland Flowrates (Q_p) Normalized by Storm Volume (V) for the 2006 Season

For all of the recorded events, the peak time lag was recorded. Using this information and the known distance between gages, the average and standard deviation of the flood wave speed were 0.25±0.20, 0.058±0.012, and 0.24±0.10 m/s for Reaches 2, 3 (wetland) and 4 respectively. The Kinematic Wave speed was calculated for each reach based on

the HECRAS model with good agreement for Reaches 2 and 4. However, this method highly over predicted the wave speed for the wetland reach (3). Theoretically, the flood wave speed will vary as a function of depth; however, channel roughness and storage influence the flood wave speed, which explains the discrepancy. These results show that flood wave propagation through the wetland is much slower compared to the other steeper reaches.

4.4 Wetland Inundation

HECRAS was run for the 12 flow conditions measured to estimate the probable extent of flooding. The maximum extent of flooding obtained from the HECRAS results under the peak flows for Events 2 and 6, are shown on the AUTOCAD drawing in Figure 10. The shaded coloring represents all predicted depths of storm inundation; thus, areas of the outer floodplain will have low water depths.

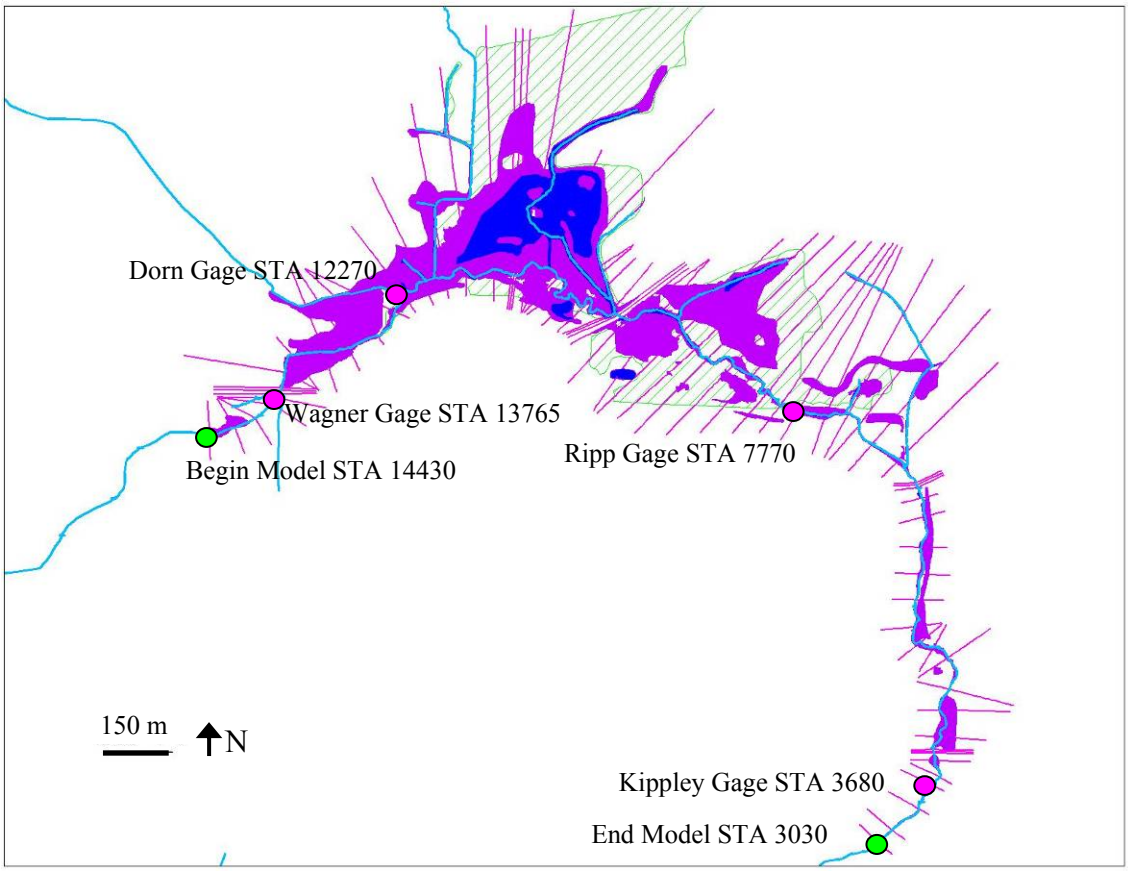

Figure 10: Overall Modeled Flood Extents for Small Event 1 (Dark Shading), and Larger Event 6 (Light Shading)

Figure 10 shows a wide range of flood inundation for the 2006 measurements. For a representative small event (dark shading), Event 2, most stormflow is contained within the main channel. In the northern part of the wetland, there is a distinct area of inundation; this region is constantly inundated and is probably fed from groundwater sources. The portion of the southern wetland experiences almost no inundation for these low flow events. The total wetland inundation is 12% for this event. The typical inundation under baseflow conditions is approximately 7%.

During the largest observed event (light shading), Event 6, significant portions of the wetland are inundated in both the northern and southern sections of the wetland. Downstream of the wetland, the channel is typically at bankfull conditions, and in some cases there is significant overtopping. The inundation of the wetland is 64% for this event. A 5-year event ($Q_{p\ in}$ = 6.5 m^3/s, $Q_{p\ out}$ = 2.7 m^3/s) was run in the HECRAS model, and gave a 76% inundation.

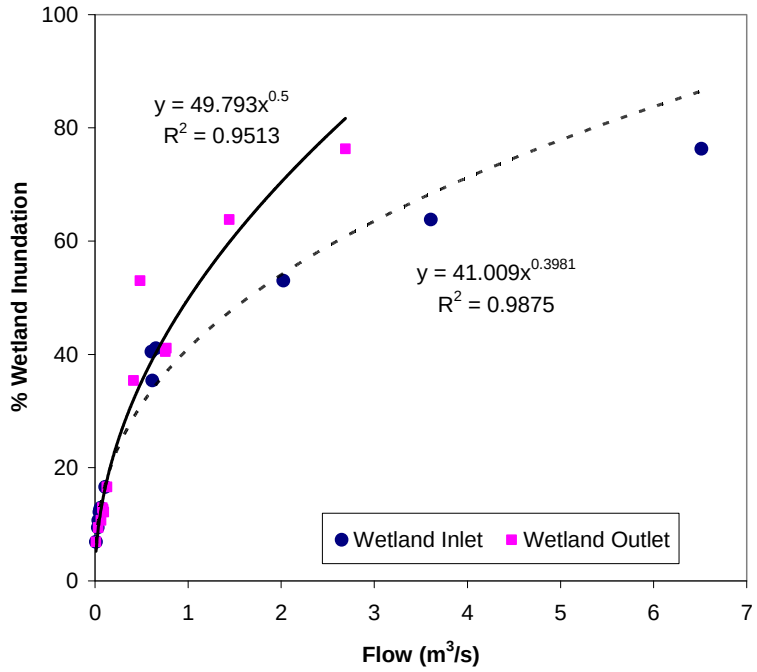

Figure 11: Percent Wetland Inundation as a Function of Incoming Flowrate and Outlet Flowrate

Figure 11 shows the variation of inundation with peak inflow to and outflow from the wetland for all 11 measured events (return periods up to 1.5 years), and the simulated, 5-year return interval event. Differences in storage and initial conditions are the primary causes of scatter in the data. Large peak inflows are attenuated in the wetland, indicated by the increasing difference between peak flowrate in an out of the wetland for increasing

inundation. Extrapolation of these curves beyond the measured data is not recommended, as storage and other nonlinear effects become more influential in large events.

4.5 Sediment and Phosphorous Transport

Table 6 presents results of sediment calculations at the Dorn, Ripp and Kippley Gages, watershed sediment inputs to the channel, and deposition (erosion) in reaches. The calculation methods are explained in Section 3.4 of this report.

	Measured Sediment Load (kg)			Watershed Sediment Input (kg)			Reach Deposition (Erosion) (kg)	
Event	Dorn Gauge	Ripp Gauge	Kippley Gauge	A+B+C	D*	E *	Dorn-Ripp (Wetland)	Ripp-Kippley
1	437	321	2,217	437	392	231	508	(1,665)
2	62	102	876	62	49	76	9	(698)
3a	112	75	313	112	102	182	139	(56)
3b	NA	NA	606	NA	NA	NA	NA	NA
4	330	173	933	330	261	123	418	(637)
5	40,288	69,283	173,370	40,288	271	121	(28,724)	(103,966)
6	35,641	165,097	68,832	35,641	1,880	4,146	(127,576)	100,411
7	139	180	307	139	122	159	80	32
8	398	532	1,644	398	354	190	219	(922)
9	1,785	4,218	NA	1,785	753	NA	(1,680)	NA
10	NA	NA	1,934	NA	NA	NA	NA	NA
Total**	79,191	239,981	251,032	79,191	4,183	5,227	(156,607)	(7,502)

Table 6: Sediment Transport Data for 2006 Season. NA = Not Available. *Computed based on assumed values described in methods section. **Totals cannot be directly compared as data is not available for all events at each site.

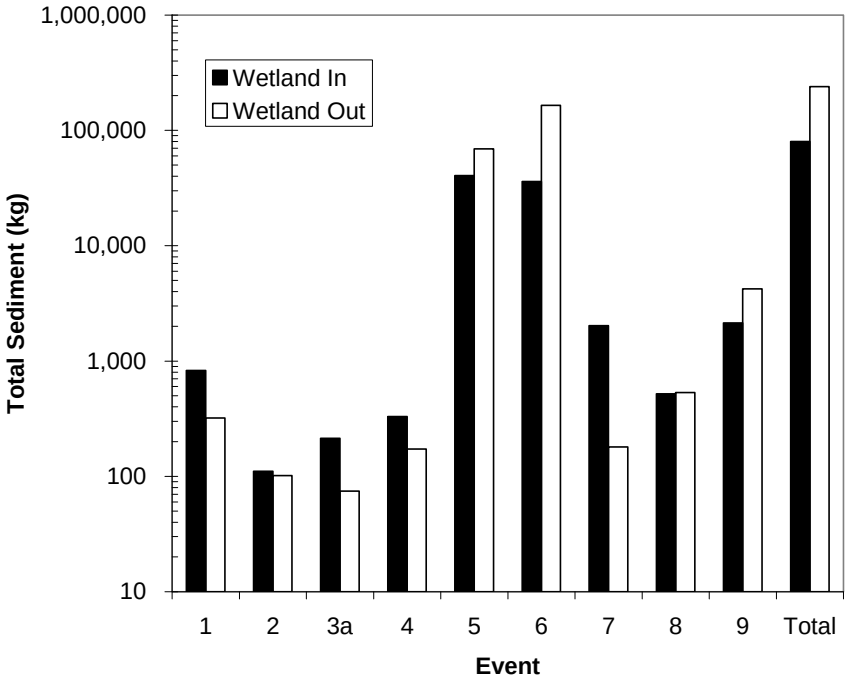

Figure 12: Total Sediment Flux In and Out of Wetland for Each Event in the 2006 Season

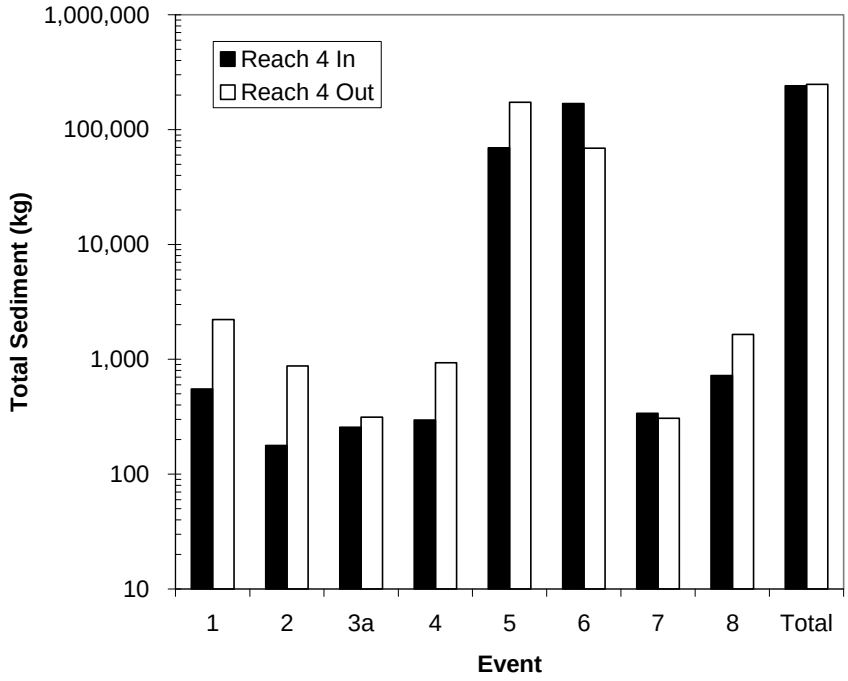

Figure 13: Total Sediment Flux In and Out of Reach 4 for Each Event in the 2006 Season

These results indicate that sediments were deposited in the wetland area for most of the small rainstorm events. However, larger events show a net export of sediments. For the total observed record, the calculations show that the wetland exported 156,607 kg of sediment, which is 65% of the total sediment load at the wetland outlet. Reach 4 shows erosion for most events; however, deposition from Events 6 and 7 balances the sediment load at the Kippley Gage. Total erosion from Reach 4 was 7,502 kg which is 3% of the total sediment transported. Site investigations after Events 5 and 6 indicated significant erosion and a lack of channel sediments in some of the wetland areas, and a large deposition of channel sediment just downstream of the Ripp Gage. These observations concur with the calculated results.

Of note is the magnitude of sediment transport for each of the events. The largest observed event (6) transported nearly 69% of the total load past the Ripp Gage. Both Events 5 and 6 combined transported 98% of the total load past the Ripp Gage for the 2006 season. This result indicates the importance of larger events in the sediment transport process and the relative unimportance of very small events, in terms of total sediment transport.

The impact of the assumed volumes and concentrations for Watersheds D and E are small in comparison to the overall sediment budget. For Watershed D, the inflow sediment concentration would need to be 112,000 mg/l and 14,600 mg/l for Events 5 and 6 for the wetland to have a net sediment balance of zero. These concentrations are orders of magnitude greater than anything observed in the system during the 2006 season.

Additionally, a review of watershed characteristics shows that Watersheds C, D and E are very similar and would therefore have similar sediment runoff and sediment yields.

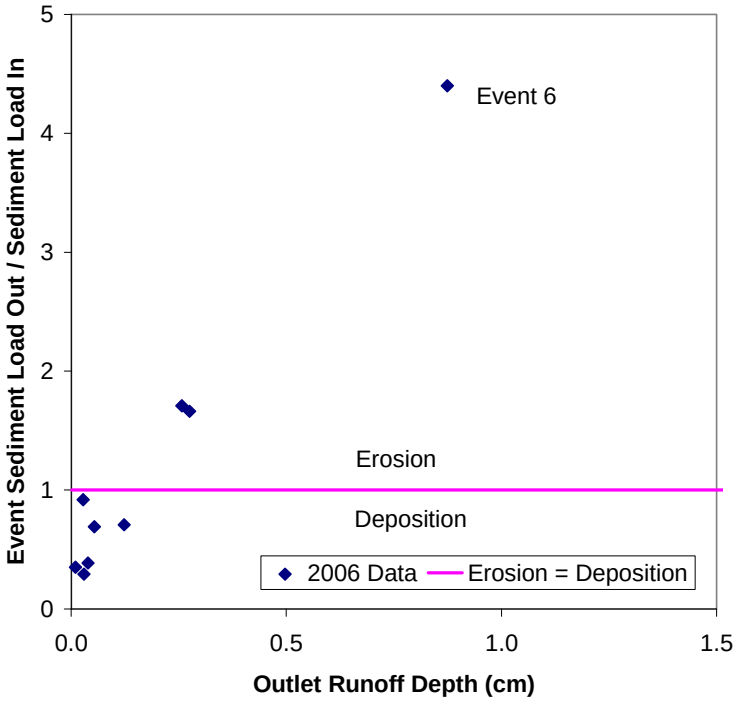

Figure 14: Wetland (Reach 3) Erosion and Deposition for 2006 Season

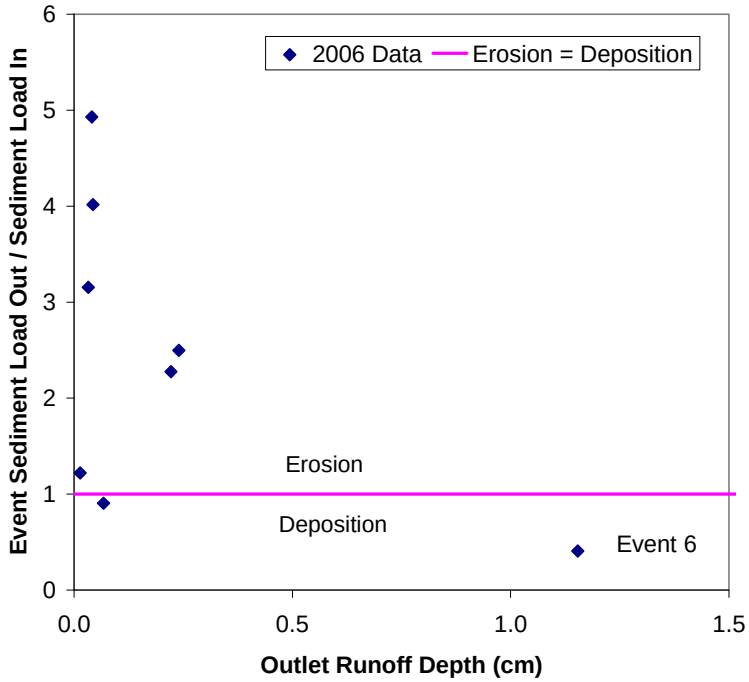

Figure 15: Reach 4 Erosion and Deposition for 2006 Season

Figures 14 and 15 show the relationship between total storm volume at the outlet divided by the watershed area upstream of the outlet (runoff depth) and the ratio of sediment load out to sediment load in, in Reaches 3 (wetland) and 4. Within the wetland (Reach 3), there appears to be a relationship between storm volume and net sediment deposition or erosion, which indicates that the wetland is capacity limited for sediment transport. This result concurs with the presence of large sediment deposits within the wetland. Reach 4 does not show a clear relationship between storm volume and net sediment deposition or erosion, which indicates that Reach 4 is supply limited for sediment transport.

Based on the flow and sediment measurements for each of the events, sediment rating curves were determined for the Dorn, Ripp, and Kippley Gages. These results are plotted in Figures 16, 17 and 18.

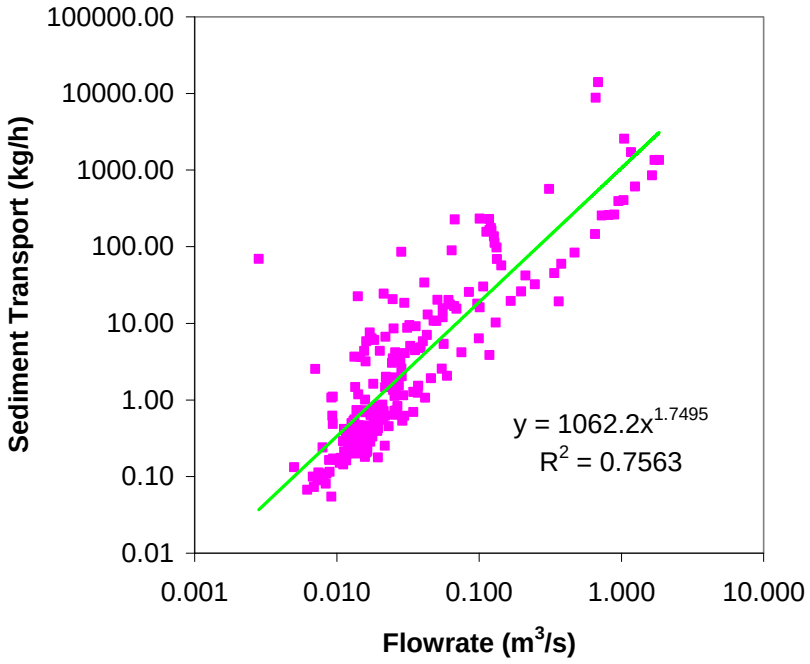

Figure 16: Dorn Gage Sediment Rating Curve

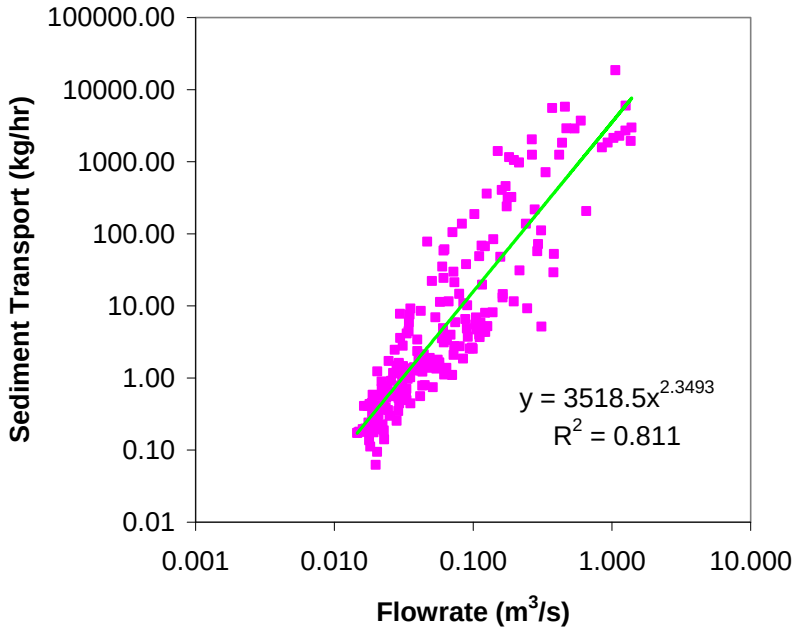

Figure 17: Ripp Gage Sediment Rating Curve

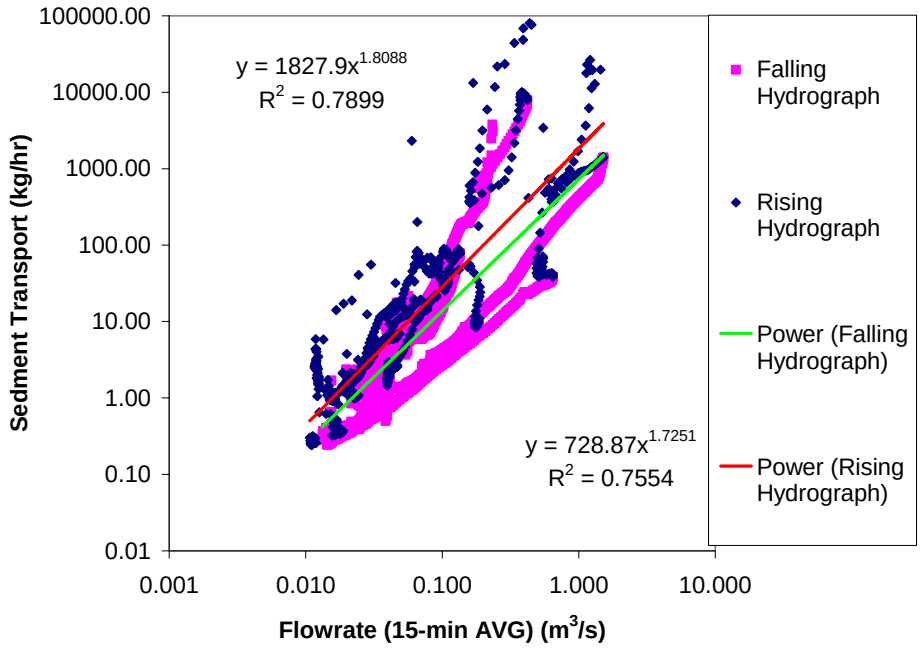

Figure 18: Kippley Gage Sediment Rating Curve

Analysis of the sediment rating curves indicates several key conclusions concerning sediment transport in the system. The Dorn and Ripp Gages (Figures 16 and 17) show some variation in the data; overall, there is a clear relationship between flowrate and sediment transport. There was no statistical difference in the rising and falling limbs of the hydrograph in terms of sediment transport. These results support the conclusion that the wetland is strongly controlled by sediment transport capacity, and agree with the previous analysis of total sediment transport.

The sediment rating curve for the Kippley Gage (Figure 18) shows a clear difference between the rising and falling limbs of the hydrograph. Analysis of the individual storm events shows a hysteresis for all events with higher transport in the rising limb of the hydrograph. The large spread in the data for the sediment transport at the same flow or flow at the same transport, which supports the conclusion that the sediment transport in

the reach is strongly controlled by sediment availability and that sediment entering the reach is quickly flushed through the reach.

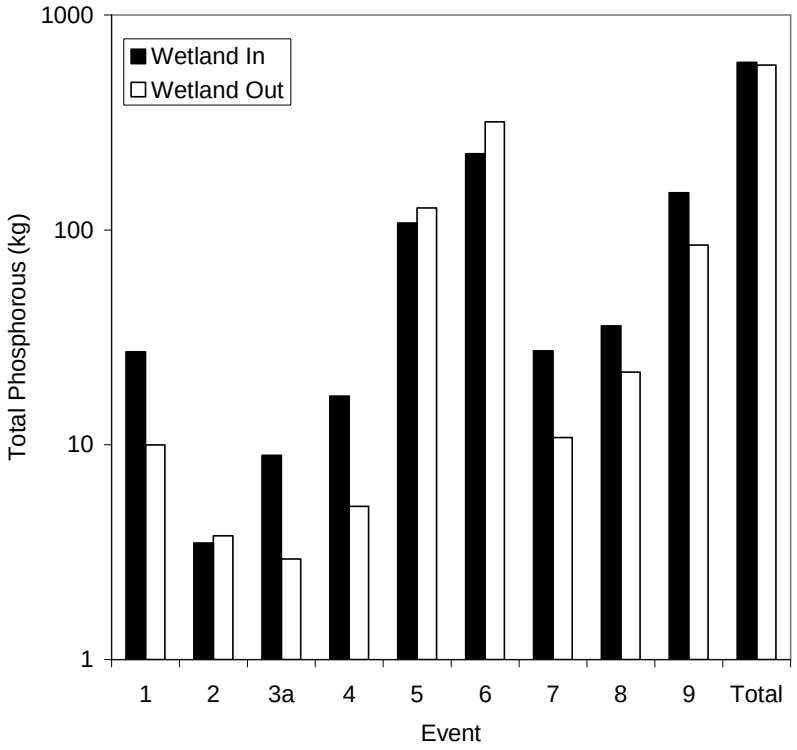

Figure 19: Total P Load Transported by Nine Storm Events During Study Period (Note Log Scale) (Hoffman et al., to be submitted)

The P entering and leaving the wetland for nine runoff events are shown in Figure 19. Events 5 and 6 account for 22 and 55% of the total loads moved into and out of the wetland during the study period. The wetland was primarily a P sink for small storm events, and a P source for large events. The total P load entering the wetland were 602 kg and the total P load leaving the wetland was 585 kg for the duration of the study period. The P load was not solely explained by rainfall amount, as intensity of rainfall and duration since last rainfall, affected the P transport. The proportions of dissolved

reactive P and bioavialable P varied depending on the event but made up a large component of the TP load (Hoffman et al., to be submitted).

4.6 Bed Shear Analysis

Figures 20 and 21 present results of laboratory flume testing of sediment cores. Figures 22 and 23 present calculations of the bed shear stress and sediment flux (= [suspended sediment concentration]*[average flowrate of water]) entering and leaving the wetland. The bed shear stress was calculated assuming nonuniform flow at each tine through an event (See 3.5 Methods).

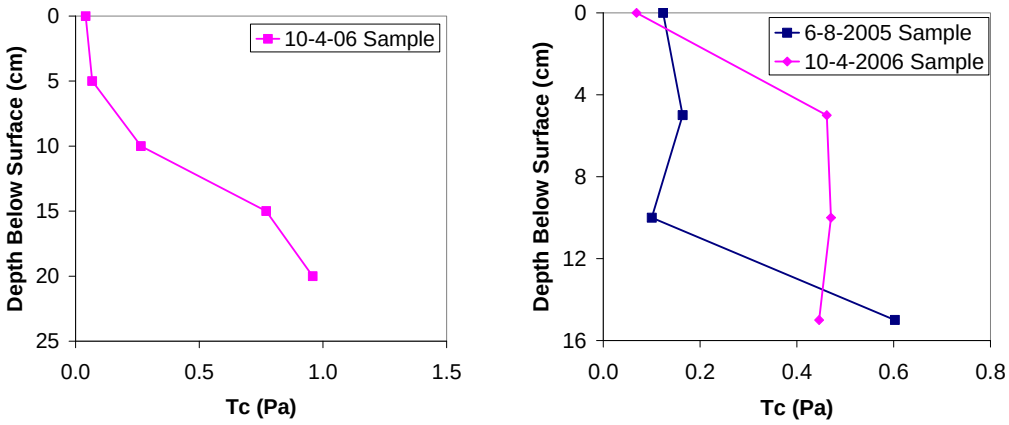

Figures 20 and 21: Critical Shear Profile for Dorn and Ripp Gage Sites

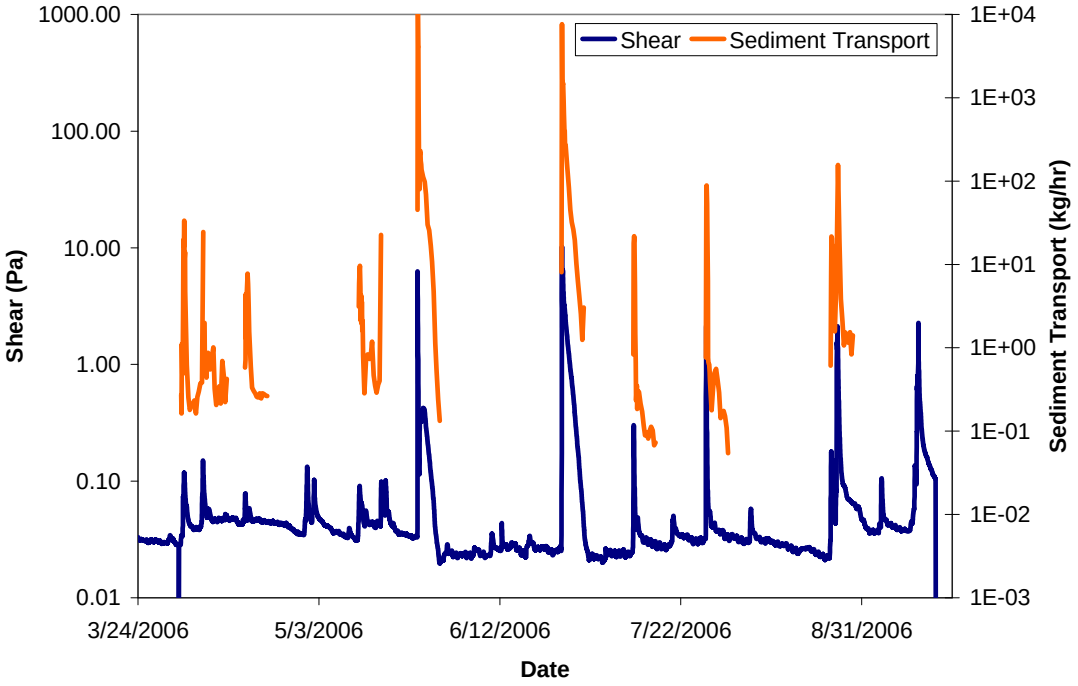

Figure 22: Bed Shear Stress and Observed Sediment at Dorn Site. Note: not all events were sampled for sediment concentration.

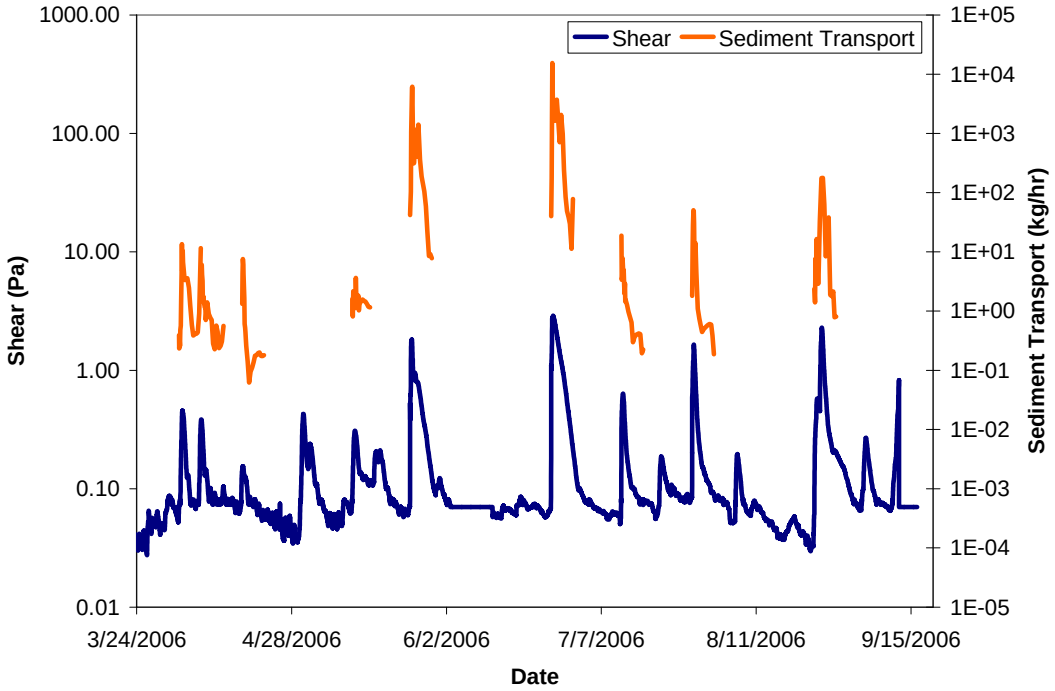

Figure 23: Bed Shear Stress and Observed Sediment at Ripp Site. Note: not all events were sampled for sediment concentration.

The results of the shear testing (Figures 20 and 21) indicate a top region of sediment with a low critical shear value. These values are consistent with the literature values presented for non-cohesive, unconsolidated silt (Julien 1998). Deeper in the samples, the critical shear values increased, indicating cohesion and consolidation of the sediments. High levels of roots and other vegetative matter were observed deeper in the sediment cores, indicating higher shear strength.

The bed shear stress levels show base level shear stress below or near the critical shear stress at the bed surface. Much higher shear stress levels are observed during storm events, and agree with corresponding observed increase in suspended sediment concentration. This data clearly supports the agreement of field shear stress and observed sediment transport with the laboratory critical shear results. Field observation at the Dorn Gage after Events 5 and 6 indicated a hard clay bed bottom and a lack of soft sediment top layer. Observation at the Ripp Gage indicated a deposit of loose bed material. These observations concur with the mass transport results, bed shear, and sediment critical shear values.

5. CONCLUSIONS

Several key features of the Upper Dorn Creek Wetland were revealed through the hydrologic and sediment monitoring and the hydraulic modeling. The 2006 season was a statistically wet year, with 11 storm events. The measured events ranged from very small to a 1.5 year recurrence interval event. The creek and wetland have remarkably different hydrologic response between small and larger events. For small flow events, the large upstream area does not contribute to the system, the hydrologic response is uniform, and the wetland shows moderate attenuation for flowrate peaks. This result is influenced by the agricultural ditching around the wetland area.

Large events have a complex flood hydrograph, which is a function of many factors. The large upstream watershed (A and B) begin to contribute to the system, and other peaks are observed that are not evident in small events. Peak attenuation through the wetland is very good for larger events and increases with incoming flowrate. The wetland was found to have an average flood wave speed of 0.058±0.012 m/s.

HECRAS modeling of the wetland showed the degree of inundation for various flow conditions. The wetland is 7% inundated for baseflow conditions (primarily due to long-term ponded water and groundwater discharge). For a low flow storm event, it was approximately 16% is inundated. For the largest observed event (1.5 year recurrence), it was approximately 64% inundated. For a hypothetical 5-year event, it was approximately 76% inundated. This analysis indicates that only larger events overflow into the main

portions of the wetland area, while most small flood events do not enter into main wetland areas.

Sediment transport analysis of the wetland area indicated that deposition occurred within the wetland for small events and net erosion for large events. For the season measured, the wetland exported 156,607 kg of sediment, (= outflow – inflow = ~64% of total sediment load outflow). Ninety-eight percent of the sediment was transported in the two largest observed events. For the season, Reach 4 had a small erosion of 7,502 kg of sediment (= ~3% of reach sediment load outflow). Sediment rating curves indicated that sediment transport in the wetland was capacity controlled, while Reach 4 was supply controlled. The wetland seemed to act as a P sink during small storm events and as a P source for large events. Total P loads entering the wetland were 602 kg and total P loads leaving the wetland was 585 kg for the duration of the study period. Critical shear tests on sediment cores in the wetland agree with published values for silt grain size, and a rise in bed shear stress over the critical shear stress value due to storm events caused erosion and a rise in sediment concentration.

The export of sediment during specific flood events has been observed at other wetlands (Jordan 2003, Kleiss 1996, Phillips 1989, Wilson 2005). A longer record is necessary to determine the long-term erosion or deposition rates in this wetland. Sediment transport in the wetland (Reach 3) and lower Reach 4 for the observed record were controlled by the two largest events. A succession of small depositional events within the wetland may balance the sediment budget. However, the net erosion observed in 2006 may have been

caused by of large deposition of sediment from previous years that has since changed to lower sediment loadings, and thus overall net erosion within the wetland as the system adjusts geomorphologically (Phillips 1989).

Future hydraulic work for the Dorn Creek system would primarily include the development of a more robust hydraulic model. A two-dimensional, unsteady model would be a much better representation of the wetland and allow for a greater understanding of the system. Additionally, a full hydrologic model, calibrated to the observed data and coupled with some additional gaging within the wetland, would allow a more complete understanding of the complex dynamics and hydrology of the wetland. Additional sediment work could include dating of sediment cores and sediment monitoring to determine long term sedimentation rates within the wetland.

6. REFERENCES

American Public Health Association (APHA). 1992. *Standard Methods for Examination of Water and Wastewater, 18th ed.* Washington, DC: American Public Health Association.

Brinson, M.M, F.R. Hauer, L.C. Lee, W.L. Nutter, R.D. Rheinhardt, R.D. Smith, and D.F. Wigham. 1995. *Guidebook for Hydrogeomorphic Assessments to Riverine Wetlands*. U.S. Army Engineer Waterways Experiment Station, Vicksburg, MS. Wetlands Research Program Technical Report WRP-DE-11.

Bullock, A. and M. Acreman. 2003. The Role of Wetlands in the Hydrological Cycle. Hydrology and Earth System Sciences 7(3): 358-389.

Carpenter, S.R., N.F. Caraco, D.L. Correll, R.W. Howarth, A.N. Sharpley, and V.H. Smith. 1998. Nonpoint Pollution of Surface Waters with Phosphorus and Nitrogen. Ecol. Appl. 8:559–568.

Carpenter, S.R. 2005. Eutrophication of Aquatic Ecosystems: Bistability and Soil Phosphorus. Proc. Natl. Acad. Sci. 102:10002-10005.

Chow, V.T. 1959. *Open Channel Hydraulics*. New York: McGraw Hill, Inc.

Chow, V., D. Maidment, and L. Mays. 1988. *Applied Hydrology*. New York: McGraw Hill, Inc.

Clayton, L. and J. Attig. 1997. *Pleistocene Geology of Dane County, Wisconsin, Bulletin 95.* Madison, Wisconsin: Wisconsin Geological and Natural History Survey.

Cooper, J., et al. 1987. Riparian Areas as Filters for Agricultural Sediment. Soil Science Society of America Journal 51: 416-420.

Craft, C., and W. Casey. 2000. Sediment and Nutrient Accumulation in Floodplain and Depressional Freshwater Wetlands of Georgia, USA. Wetlands 20(2): 323-332.

Dane County. 1996. *Dane County Soils*. Madison, Wisconsin: Natural Resource Conservation Service (NRCS).

Dane County. 2006. "Dane County DCiMap". Dane County (WI) Land Information Office. http://dcimap.co.dane.wi.us/dcimap/index.htm.

Eggers, S. and D. Reed. 1997. *Wetland Plants and Plant Communities of Minnesota and Wisconsin, 2nd Ed.* St. Paul, Minnesota: US Army Corps of Engineers.

Ehrenfel, J.G. 2004. The Expression of Multiple Functions in Urban Forested Wetlands. Wetlands 24.4: 719-733.

French, J. 2003. Airborne Lidar in Support of Geomorphological and Hydraulic Modeling. Earth Surface Processes and Landforms 28: 321-335.

Haan, C.T., B.J. Barfield, and J.C. Hayes. 1994. *Design Hydrology and Sedimentology for Small Catchments*. New York: Academic Press.

Hall, J, et al. 2005. Distributed Sensitivity Analysis of Flood Inundation Model Calibration. Journal of Hydraulic Engineering 131 (2): 117-126.

Hansson, L.A., et al. 2005. Conflicting Demands on Wetland Ecosystem Services: Nutrient Retention, Biodiversity, or Both? Freshwater Biology 50: 705-714.

Herschy, R. 1995. *Streamflow Measurement, 2nd Edition*. Cambridge, UK: E&FN SPON.

Hoffman, A., et al. Phosphorous and Sediment Transport in the Upper Dorn Creek Wetland. University of Wisconsin-Madison. To be Submitted.

Huff, F.A., and J.R. Angel. 1992. *Rainfall Frequency Atlas of the Midwest, Bulletin 71*. Midwestern Climate Center Research Report: 92.03.

Hupp, C., and D. Bazemore. 1993. Temporal and Spatial Patterns of Wetland Sedimentation, West Tennessee. Journal of Hydrology 141: 179-196.

Hupp, C., et al. 1993. Sediment and Trace Element Trapping in a Forested Wetland, Chikahomony River, Virginia. Wetlands 13(2): 95-104.

Hughes, D.A. 1979. Floodplain Inundation: Processes and Relationships with Channel Discharge. Earth Surface Processes 5: 297–304.

Johnston, C.A., et al. 1984. Nutrient Trapping by Sediment Deposition in a Seasonally Flooded Lakeside Wetland. Journal of Environmental Quality 13(2): 283-290.

Johnston, C.A. 1991. Sediment and Nutrient Retention by Freshwater Wetlands: Effects on Surface Water Quality. Crit. Rev. Environ. Control 21:491-565.

Jordan, T., et al. 2003. Nutrient and Sediment Removal by a Restored Wetland Receiving Agricultural Runoff. Journal of Environmental Quality 32: 1534-1547.

Julien, P. 1998. *Erosion and Sedimentation*. New York: Cambridge University Press.

Kleiss, B.A. 1996. Sediment Retention in a Bottomland Hardwood Wetland in Eastern Arkansas. Society of Wetland Scientists. Wetlands 16(3): 321-333.

Krause, A.F. 1999. Modeling the Flood Hydrology of Wetlands using HEC-HMS. MS Thesis. University of California Davis.

Lee, C., et al. 2004. Automated Sediment Erosion Testing System Using Digital Imaging. Journal of Hydraulic Engineering 130(8): 771-782.

Lewin, J., and D. Hughes. 1980. Welsh Floodplain Studies II: Application of a Quantitative Inundation Model. Journal of Hydrology 46: 35-49.

Lowrance, R., et al. 1986. Long-Term Sediment Deposition in the Riparian Zone of a Coastal Plain Watershed. Journal of Soil and Water Conservation 41:266-271.

McKillop, R., et al. 1999. Modeling the Rainfall-Runoff Response of a Headwater Wetland. Water Resources Research. 35(4): 1165-1177.

Mitsch, W. et al. 1979. Ecosystem Dynamics and Phosphorous Budget of an Alluvial Cypress Swamp in Southern Illinois. Ecology 60(6): 1116-1124.

Muson, B., et al. 2005. *Fundamentals of Fluid Mechanics 5th Ed.* New York: John Wiley and Sons.

Murdoc, E. 2006. Transport and Storage of Sediments and Solutes in a Small Agricultural Stream, Dane County, Wisconsin. MS Thesis. University of Wisconsin – Madison.

Murphy J., and J.P. Riley. 1962. A Modified Single Solution Method for the Determination of Phosphate in Natural Waters. Anal. Chim. Acta. 27:31-36.

National Climate Data Center (NCDC). 2006. Madison, Wisconsin Historical Data. National Oceanic and Atmospheric Administration (NOAA). http://www4.ncdc.noaa.gov/cgi-in/wwcgi.dll?wwDI~StnSrch~StnID~20020992.

National Wetlands Policy Forum (NWPF). 1988. Protecting America's Wetlands: An Action Agenda. Conservation Foundation, Washington, D.C.

Newman, A. 1995. Water Pollution Point Sources Still Significant in Urban Areas. Environ. Sci. Technol. 29:114.

Phillips, J. 1989. Fluvial Sediment Storage in Wetlands. Water Resources Bulletin 25(4): 867-873.

Potter, K. 1994. Estimating Potential Reduction Flood Benefits of Restored Wetlands. Water Resources Update 97: 34-37.

Schindler, D.E. 2006. Recent Advances in the Understanding and Management of Eutrophication. Limnol. Oceanogr. 51:356-363.

Sichingabula, H. 1998. Factors Controlling Variations in Suspended Sediment Concentration for Single-Valued Sediment Rating Curves, Frazier River, BC. Hydrological Processes 12: 1869-1894.

University of Wisconsin (UW). 2006. "SOP for Suspended Particulate Matter (SPM) Filter Weighing" The University of Wisconsin – Madison, Environmental Chemistry & Technology Program, Mercury Research Group. http://www.engr.wisc.edu/groups/mercury/SOP%20for%20Suspended%20Particulate%20Matter.htm.

US Geological Survey (USGS). 1983. *7.5 Minute Quadrangle Maps: Springfield Corners, WI, and Waunakee, WI.* Madison, Wisconsin: Wisconsin Geological and Natural History Survey.

Walker, J.F., and Krug, W.R. 2003. *Flood-Frequency Characteristics of Wisconsin Streams*. USGS WRI Report: 03-4250.

Weather Underground (WU). 2006. "Weather Station History, KWIWAUNA2 Northwest of Waunakee Airport, Waunakee, Wisconsin" The Weather Underground, Inc. http://www.wunderground.com/weatherstation/WXDailyHistory.asp?ID=KWIWAUNA2

Wilson, C., et al. 2005. Transport of Fine Sediment Through a Wetland Using Radionuclide Tracers: Old Woman Creek, OH. Journal of Great Lakes Research 31: 56-67.

APPENDIX A – ADDITIONAL SITE OVERVIEW INFORMATION

A.1 Introduction

This appendix contains additional site overview information not presented in Section 2 of this report.

The Dorn Creek Watershed is located within Dane County, Wisconsin between the Town of Waunakee and the City of Middleton. The creek is a tributary to Sixmile Creek, which flows directly into Lake Mendota. Dorn Creek is approximately 11.28 miles long and has a total watershed area of 12.67 square miles (USGS 1983). The land surrounding the creek is primarily agricultural, although there is a small residential area at the far western edge of the watershed. The total impervious area for the watershed is calculated as 3.66 percent.

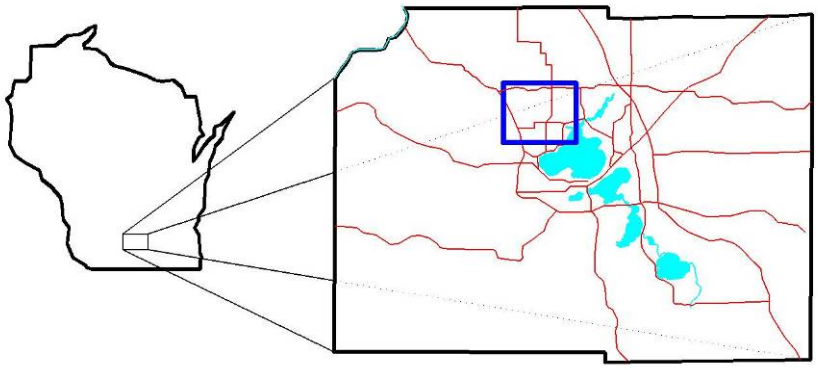

Figure 24: Dane County, Wisconsin Showing Project Location

There are three distinct wetland areas along Dorn Creek. Based on review of topographic mapping (USGS 1983), aerial photographs (Dane County 2005) and land use mapping (Dane County 2006) the wetlands were outlined. The largest and most downstream is known as the Dorn Creek Wetland and has a total area of 378 acres. The second wetland

upstream is known as Upper Dorn Creek Wetland, with a total area of 111 acres. The most upstream wetland is a small unnamed wetland of approximately 24 acres.

The focus of this investigation is on the upper 7.5 miles of the Dorn Creek Watershed and the Upper Dorn Creek Wetland. Meffert Road crosses the wetland at approximately the midpoint, and divides the wetland into two distinct parts, a northern and southern section. The two sections are similar in their characteristics, although the northern section is generally more inundated with deeper water levels.

Stream gages were installed at four locations in the project area, and are shown in Figure 26. Two gages are upstream of the wetland, and two are downstream. The instrumentation of these gages is described in detail in Section 3 of this report.

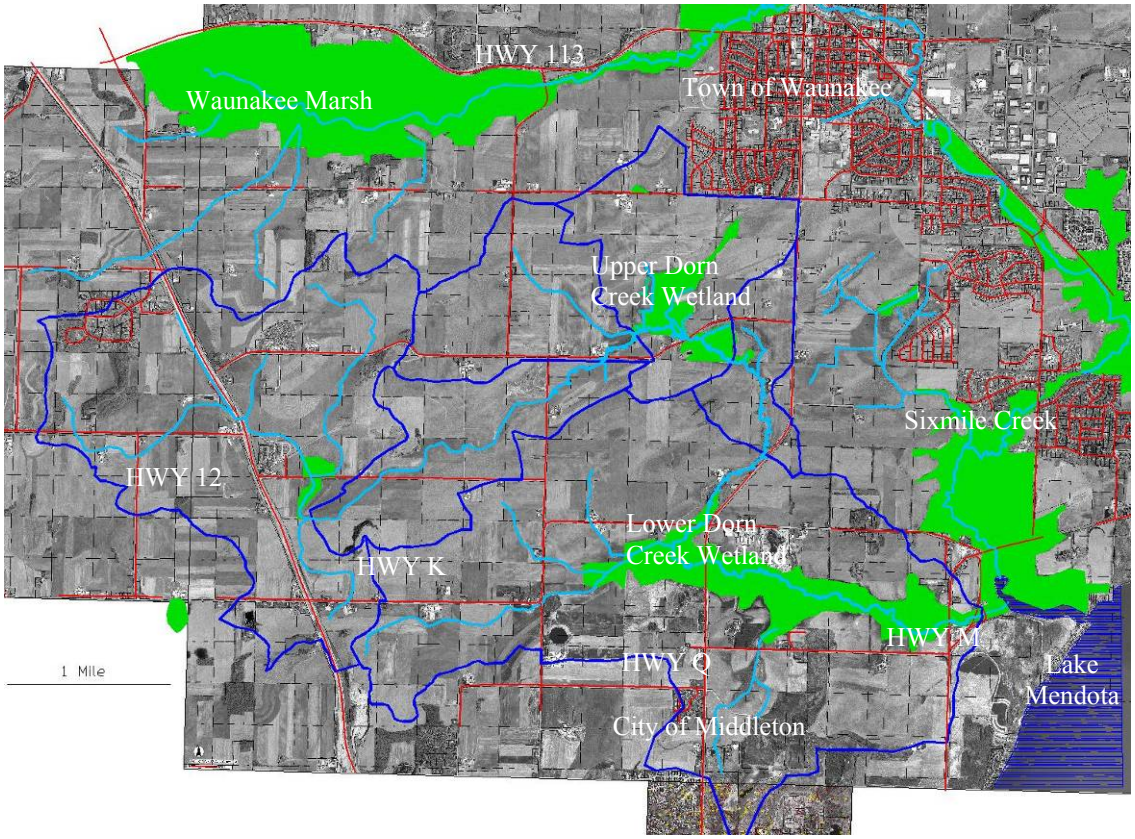

Figure 25: Dorn Creek Watershed Overview (Watershed in Blue, Watercourses in Light Blue, Wetlands in Green, Roads in Red) Compiled from USGS (1983) and Dane County (2006) sources. Orthophoto courtesy of Dane County (2005), used by permission.

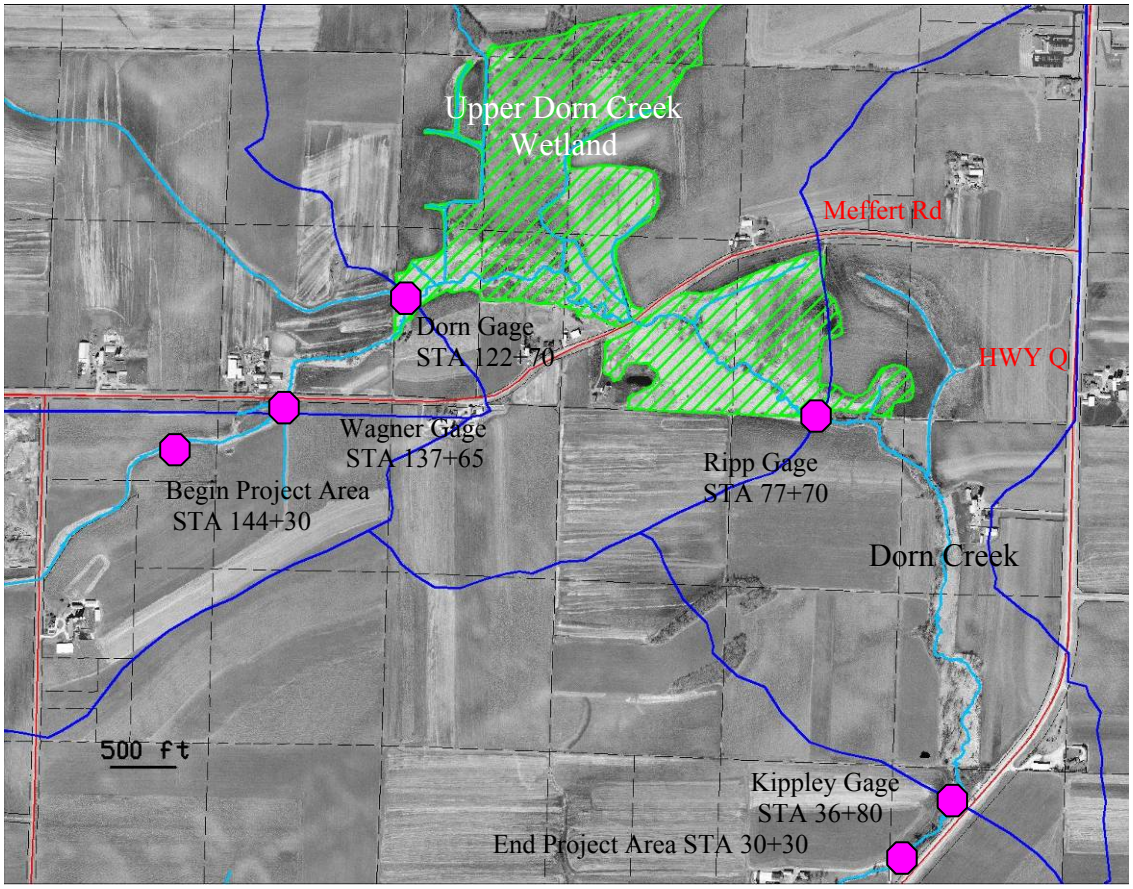

Figure 26: Project Area and Gaging Stations. Stationing measured from County Highway K and Dorn Creek in feet. Orthophoto courtesy of Dane County (2005), used by permission.

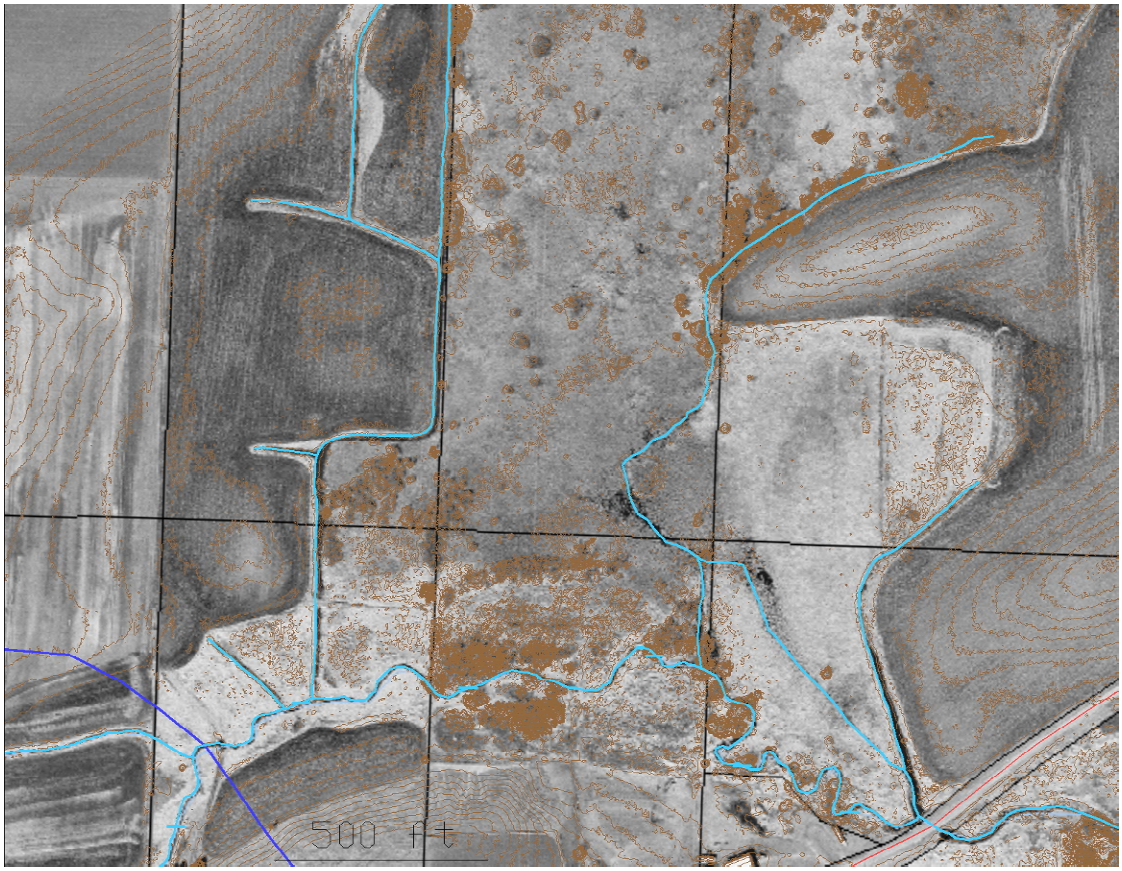

Figure 27: North Upper Dorn Creek Wetland with 1m Topography. Orthophoto courtesy of Dane County (2005), used by permission.

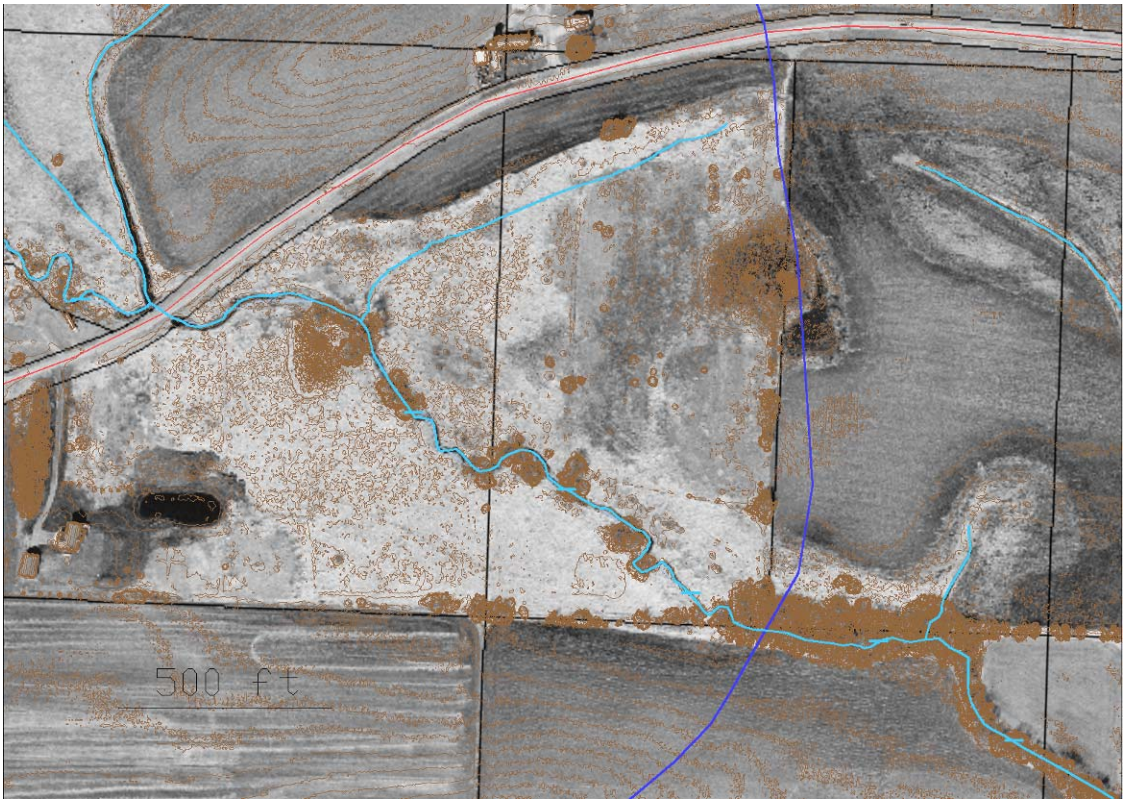

Figure 28: South Upper Dorn Creek Wetland with 1m Topography. Orthophoto courtesy of Dane County (2005), used by permission.

Most areas of the Upper Dorn Creek Wetland are classified as a shallow marsh, but some areas are Sedge Meadow to Mesic Prairie (Eggers and Reed 1997). Major portions of the wetland are covered by Reed Canary Grass, a non-native invasive species. The biological diversity within the wetland is immense, supporting numerous species of birds, grasses, trees, amphibians, mammals, and other plant and animal life.

A.2 Historical Perspective

Changes to the Dorn Creek Watershed due to human impacts have been significant. The primary current land use is agricultural, although numerous residential and commercial structures are also within the watershed. Based on review of aerial photos (Dane County 2005), soil data (Dane County 1996), and geological data (Clayton and Attig 1997), Figure 29 was complied indicating current and probable historic wetlands within the Dorn Creek and Sixmile Creek Watersheds. According to this analysis, the Dorn Creek Watershed has experienced a 54% loss of wetlands and the Sixmile Creek Watershed has experienced a 37% loss of wetlands, largely due to human impacts.

The primary mechanism for wetland loss is the installation of drain tiles and agricultural ditches to convey water away from former wetlands and subsequent conversion of the land to agricultural use. As shown in Figure 29, most of the major wetlands in the area have experienced loss of area due to encroachment. However, some of the smaller wetlands have been completely removed.

Within the Upper Dorn Creek Wetland, several agricultural channels have been cut into the wetland to provide draining for agricultural land. As will be described later, these channels play a significant effect on the hydrology and sediment transport through the wetland.

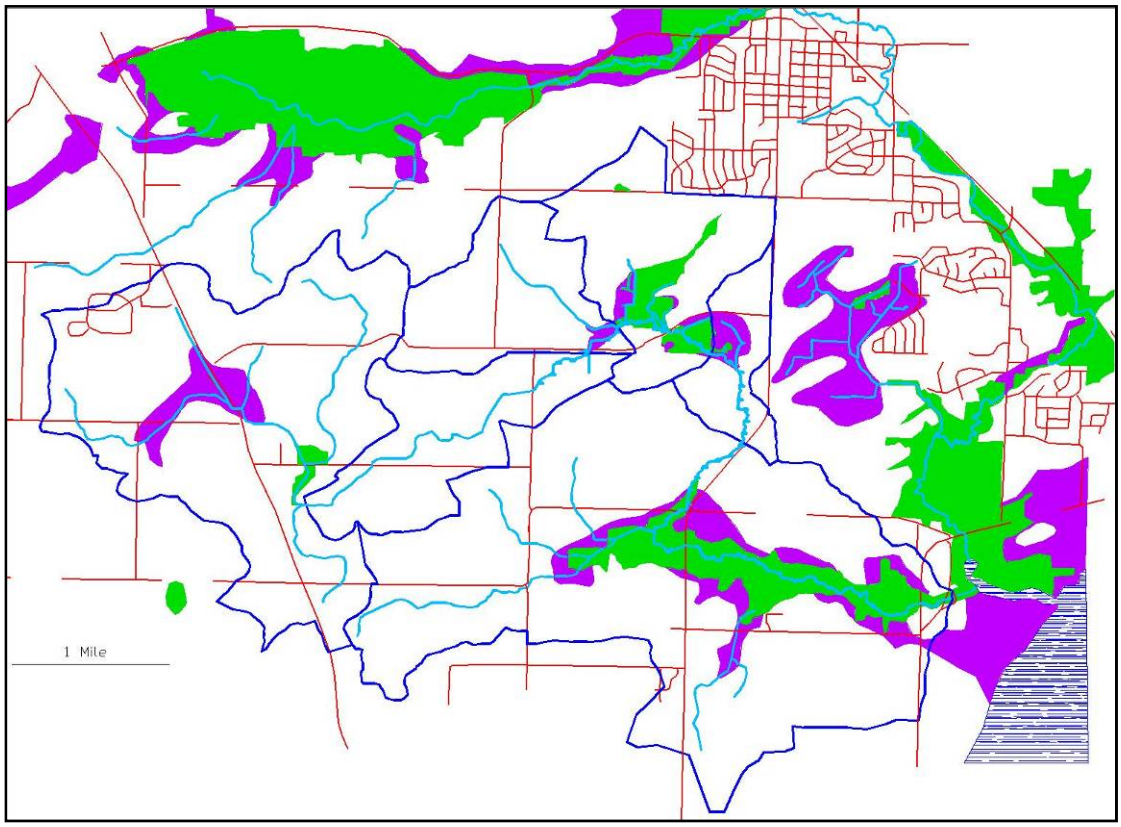

Figure 29: Probable Historic (Purple) and Current (Green) Wetlands in the Dorn Creek and Sixmile Creek Watersheds

A.3 Geology and Geomorphology

The geology of the project area is primarily glacial till underlain by Franconia Sandstone with bedrock depths ranging from 20 to 90 feet (Cline 1979). However, there are several areas of glacial offshore lake sediment, most notably the Upper Dorn Creek Wetland.

In Pleistocene times, the wetland was most likely a glacial lake, which has since drained and become a wetland. The northern section of the wetland is predominantly offshore lake sediment overlain by a few meters of post glacial peat, which results in flat topography (Clayton and Attig 1997). The southern section of the wetland is also predominantly offshore lake sediment but is mostly uncollapsed with slightly hummocky topography (Clayton and Attig 1997).

The soils in the areas surrounding the wetland are primarily comprised of silt loam to silty clay loam (Dane County 1996). However, pockets of coarser materials do exist in portions of the watershed.

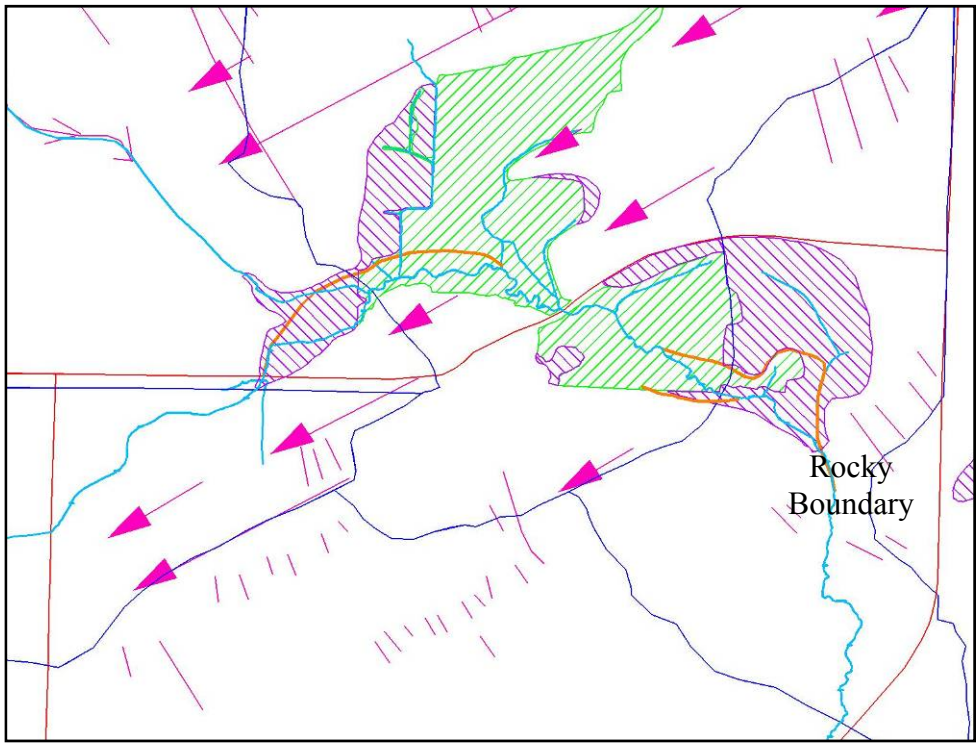

Figure 30: Glacial Geology of Project Area with Historic and Current Wetlands. Drumlins are pink arrows, moraines are small pink perpendicular lines, and historic channels are orange. Adapted from Clayton and Attig (1997)

The predominant Pleistocene geologic formations surrounding the wetland are glacial drumlins and small moraines. As shown in Figure 30, the southern end of the wetland is bordered by several moraines. Site inspection of this material indicates very rocky, gravely material. The presence of this material as well as low depth to bedrock forms a geomorphically hard surface, and thus creating the downstream boundary for the wetland.

The geomorphology of the project area is complex, and although not the focus of this project, some interesting aspects were discovered. Based on site observations and review of topography, several former main channels through the wetland were observed and are shown in orange in Figure 30. Historic data seems to confirm these findings (Cline 1979). It is unclear if these channel changes are a result of natural geomorphology or from human impacts.

A.4 Geometry

Large scale topographic data of the project area is quite comprehensive and easily obtainable. Mapping of the area from the USGS (1983) gives 10 foot contour intervals, and Dane County (2006) mapping provides 4 foot resolution mapping. However, for the purposes of this study much higher resolution was required to effectively model the wetland system. As described in Section 3 of this report, high resolution LIDAR data were taken of the project area and subsequently converted to 0.2 meter (0.66 foot) digital contours in AutoCAD.

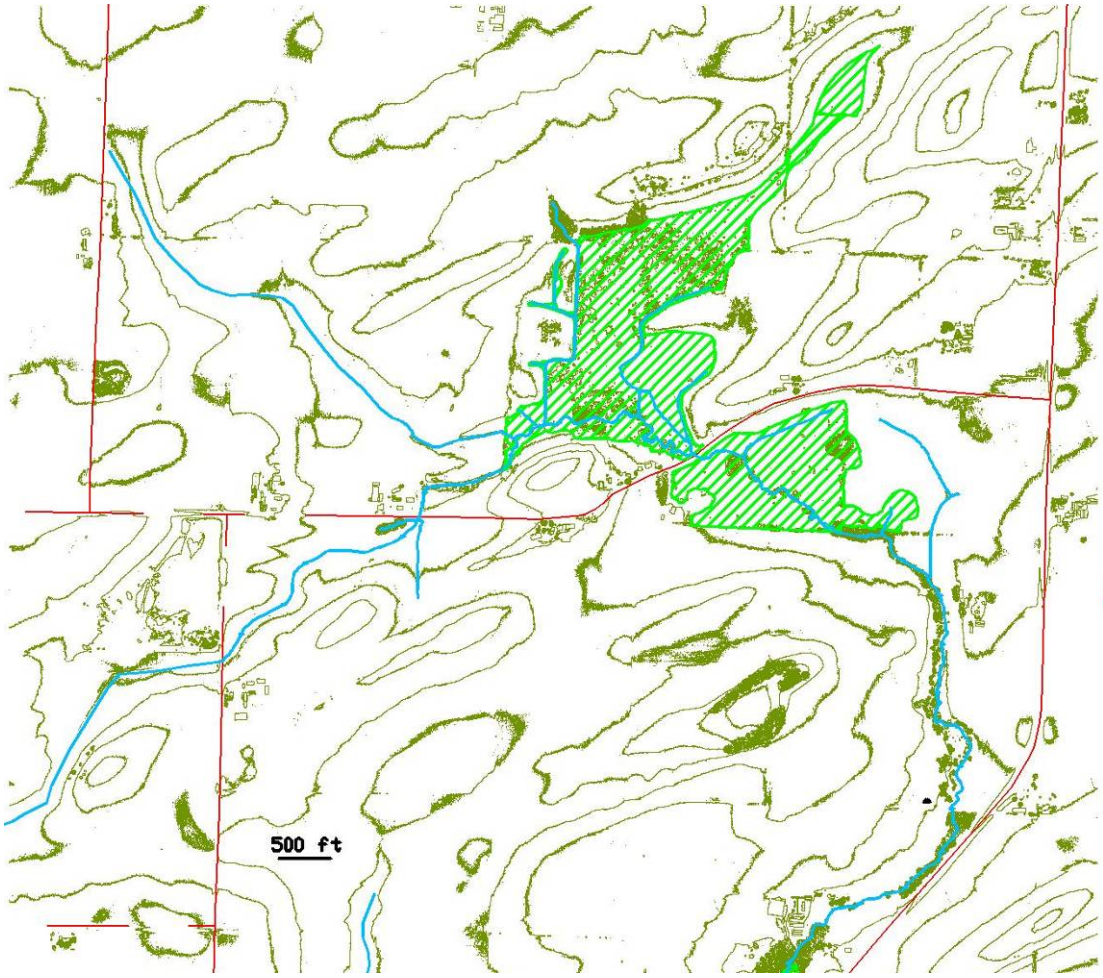

Figure 31: 5m Contour LIDAR Topographic Mapping of Project Area

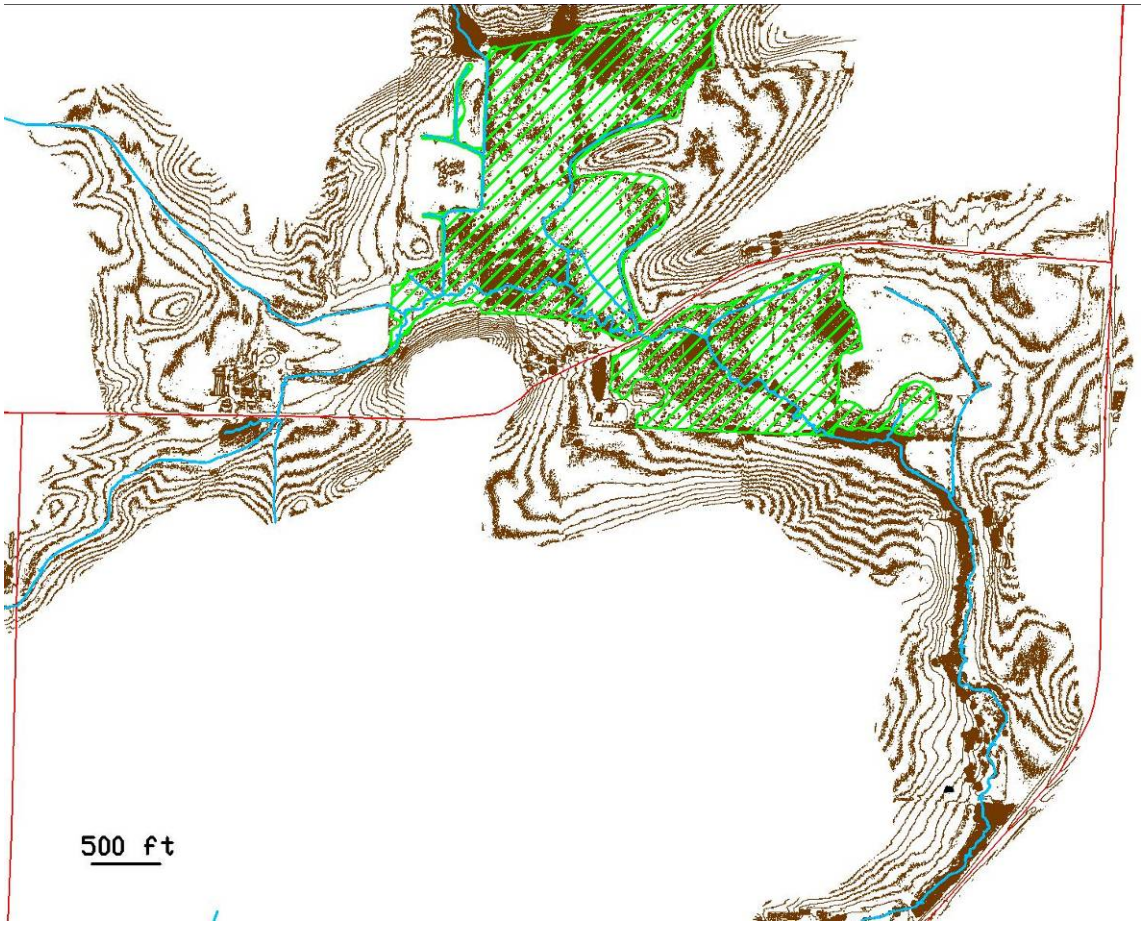

Figure 32: 1m Contour LIDAR Topographic Mapping of Project Area (only topography near Dorn Creek was computed)

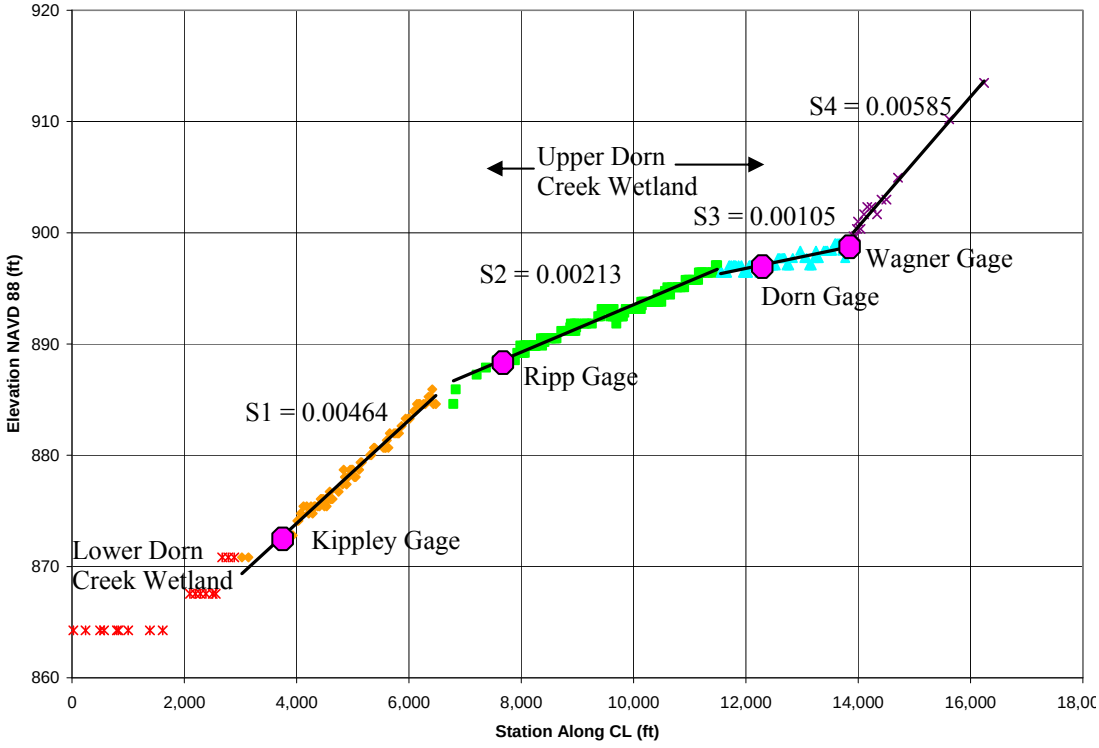

Figure 33: Dorn Creek Profile Based on LIDAR Mapping. Stationing from Confluence with Highway K

The bottom channel elevations were plotted along the centerline of Dorn Creek starting at Highway K. From Figure 33, it is clear that there are four distinct slope reaches within the project area. Each reach has distinct characteristics and will be discussed separately.

Figure 34: Typical S1 Cross Section (at Kippley Gage, March 2006)

The most downstream reach (S1) is a relatively high slope, and is characterized by a deeply incised channel. The channel is generally composed of a hard clay bottom, with boulder groups at various locations.

Figure 35: Typical S2 Cross Section (at Meffert Rd, March 2006)

The second slope (S2) is located mostly within the wetland. The hingepoint between S1 and S2 is located at a narrowing of the valley, and change in bed material type, as described above. The channel is generally wide and shallow, with silt-clay sediment bottom.

Figure 36: Typical S3 Cross Section (at Dorn Gage, March 2006)

The third slope (S3) is located just downstream of the Dorn Gage. The hingepoint between S2 and S3 occurs within the wetland. A series of trees occur at this location, but it is unclear geomorphically why the slope changes at this point. The upper portion of this reach was most likely part of the wetland in previous times, but has been dredged significantly, which may contribute to the slope change. Channel type is generally a small incised main channel surrounded by floodplain and soil types are silty-clay sediment.

Figure 37: Typical S4 Cross Section. Main Channel Center, Groundwater Spring Tributary Lower Left (at Wagner Gage, March 2006)

The fourth slope (S4) is located upstream of the final gage. The slope is steep and the channel is generally incised. From interviews of property owners, it was determined that this channel was dug, and did not exist prior to excavation. Historically, flows through this area did not have a defined channel. The channel is generally silty loam soil, covered by thickets of grass.

Using the methods described in Section 3 of this report, compilation of LIDAR topographic and site surveying allowed delineation of 70 cross sections of the channel. These cross sections were the primary input for the HECRAS modeling described in Section 3 of this report.

A.5 References

Cline, D. 1979. Geology and Ground-Water Resources of Dane County, Wisconsin. US Geological Survey Water-Supply Paper 1779-U.

Clayton, L. and J. Attig. 1997. *Pleistocene Geology of Dane County, Wisconsin, Bulletin 95.* Madison, Wisconsin: Wisconsin Geological and Natural History Survey.

Dane County. 1996. *Dane County Soils*. Madison, Wisconsin: Natural Resource Conservation Service (NRCS).

Dane County. 2005. *Dane County Land Information Office and Fly Dane Partnership, 20060317, One-Foot Resolution Digital Orthophotography.* Madison, Wisconsin: Dane County Land Information Office. Available at: http://dcimap.co.dane.wi.us/dcimap/index.htm

Dane County. 2006. "Dane County DCiMap". Dane County (WI) Land Information Office. http://dcimap.co.dane.wi.us/dcimap/index.htm

Eggers, S. and D. Reed. 1997. *Wetland Plants and Plant Communities of Minnesota and Wisconsin, 2nd Ed.* St. Paul, Minnesota: US Army Corps of Engineers.

US Geological Survey (USGS). 1983. *7.5 Minute Quadrangle Maps: Springfield Corners, WI, and Waunakee, WI.* Madison, Wisconsin: Wisconsin Geological and Natural History Survey.

APPENDIX B – ADDITIONAL INSTRUMENTATION AND METHODS INFORMATION

B.1 Overview

This appendix contains additional instrumentation and methods information not presented in Section 3 of this report.

The primary goals of this project involved field investigations of the hydrology, hydrodynamics and sediment transport characteristics of the Upper Dorn Creek Wetland. To accomplish these goals, accurate instrumentation and measurement were essential. For investigation of the hydrology, measurement of water levels, meteorological data, and rating curves was needed. For investigation of the hydrodynamics, accurate knowledge of the geometry, roughness, stream velocity and flowrates was needed. Finally, for investigation of the sediment transport, measurement of total sediment concentrations, particle distributions, bed shear and stream velocity measurements were required.

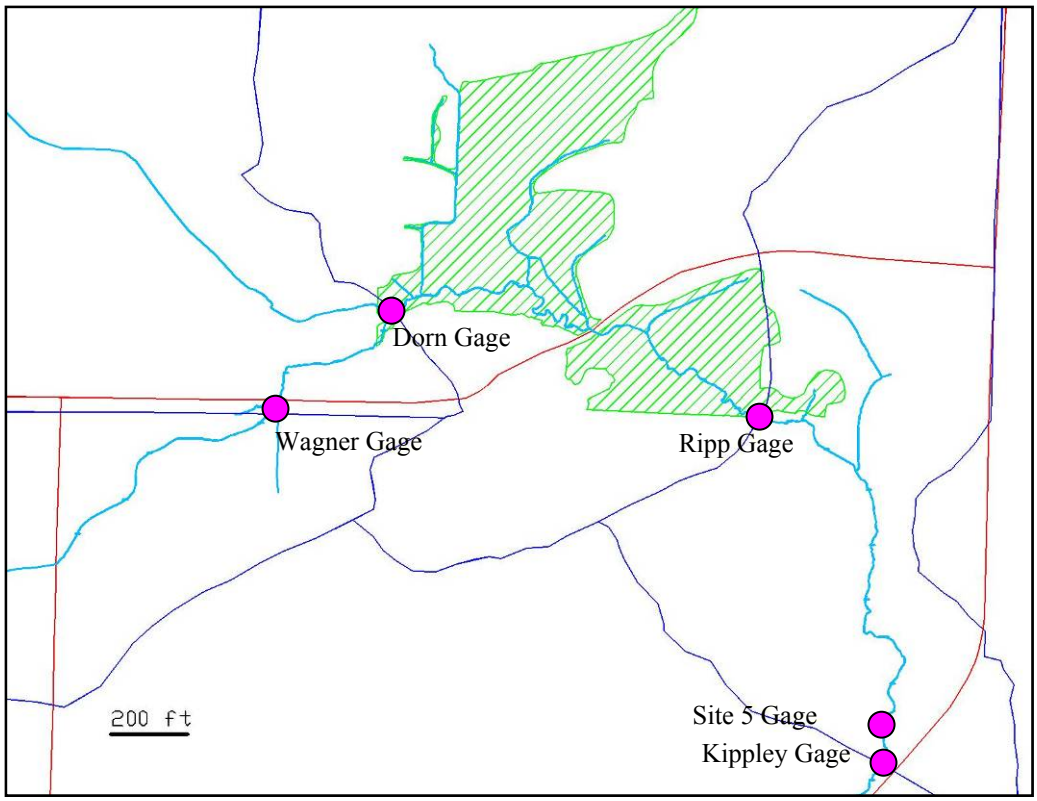

Figure 38: Gaging Station Locations

Monitoring of the Dorn Creek system has been ongoing since 2003. Evan Murdoc worked on the project from 2003 to 2005 and the results of his findings are summarized in his master's thesis (Murdoc 2006). To ensure a comprehensive report, his monitoring scheme is summarized in this section, however, all details contained in this section relating to calibration and methods apply to the 2006 season only. Specifics related to Evan Murdoc's work can be found in his thesis (Murdoc 2006).

Parameter	**Kippley Gage**
Data Storage	CS Datalogger
Water level	WL-400 Press Tans
Sediment	OBS-3
Temperature	None

Velocity	None

Table 7: 2003 Season Monitoring Scheme (Murdoc 2006) (CS=Campbell Scientific, OBS=Optical Backscatter, WL=Water Level)

Parameter	**Site 5 Gage**	**Kippley Gage**
Data Storage	CS Datalogger	CS Datalogger
Water level	WL-400 Press Tans	WL-400 Press Tans
Sediment	OBS-3	OBS-3
Temperature	None	None
Velocity	None	None

Table 8: 2004 Season Monitoring Scheme (Murdoc 2006)

Parameter	**Wager Gage**	**Kippley Gage**
Data Storage	CS Datalogger	CS Datalogger
Water level	WL-400 Press Trans	WL-400 Press Tans
Sediment	OBS-3	OBS-3
Temperature	None	None
Velocity	None	None

Table 9: 2005 Season Monitoring Scheme (Murdoc 2006)

For the 2006 season, the monitoring scheme was expanded substantially from previous years. Four gaging stations were set up along the creek, as shown in Figure 38 for the 2006 season. Two of the gaging stations were run by Campbell Scientific dataloggers, and two by Isco Samplers. Due to several instances in previous seasons of loss of instruments due to flooding, stilling wells of 4" PCV pipe were installed at the Wagner and Kippley Gages. The Isco Samplers were installed at locations away from flood potential and anchored in place.

Parameter	**Wager Gage**	**Dorn Gage**	**Ripp Gage**	**Kippley Gage**
Data Storage	CS CR-10 Datalogger	Isco 6712 Sampler	Isco 6712 Sampler	CS CR-10X Datalogger
Water level	WL-400 Press Trans	Isco 720 Probe	Isco 720 Probe	WL-400 Press Tans

Sediment	OBS-3	Direct Sampling	Direct Sampling	OBS-3
Temperature	CS T-107	None	None	CS T-107
Velocity	None	None	None	MMB ECM-201

Table 10: Gaging Station Setup for 2006 Season (CS=Campbell Scientific, MMB=Marsh McBirney, OBS=Optical Backscatter, WL=Water Level)

Figure 39: Wagner Gage Site, Showing Stilling Well (March 2006)

Figure 40: Dorn Gage Site, Showing Sampler Housing (March 2006)

Figure 41: Ripp Gage Site, Showing Sampler (March 2006)

Figure 42: Kippley Gage Site, Showing Stilling Well (March 2006)

B.2 Water Level Gages

Water level data were obtained at all four gage sites using pressure differential transducers. At the Ripp and Dorn sites, Isco 720 Submerged Probes were attached to the Isco samplers. At the Kippley and Wagner sites, Global Water WL-400 pressure transducers were used in connection with the Campbell Scientific Dataloggers.

Figure 43: Global Water WL-400 Water Level Gage

Figure 44: Isco Model 720 Submerged Probe

The Isco 720 Probes were internally calibrated, and listed by the manufacturer as having an accuracy of ± 0.01 ft (for 0.1<D<5.0 ft), a temperature coefficient of ± 0.005 ft/°F, and a maximum depth of 20 feet (Isco 1996). The probes were mounted to the bed of the channel using wooden stakes and plastic ties. The line was secured to the bottom of the channel using metal stakes and covered by sediment to avoid contact with debris during flood events. The water level data were stored every minute and downloaded from the Isco sampler using an Isco 581 Rapid Transfer Device. This data were then downloaded to a computer using Isco Flowlink (v.4.16) software.

The WL-400 water level gages were connected to the Campbell Scientific Dataloggers as described in Appendix F. The gages were calibrated by placing them in a tube of known depth and sequentially filling the tube and reading the output voltage from the datalogger. This calibration was performed in the Fluid Mechanics Lab at the University of Wisconsin-Madison and the results are shown below. The WL-400 gages were installed in the stilling wells so that the probe was just above the bottom, hanging vertically. Plastic ties were used to secure the line to the wall of the stilling well, and assure that no creep occurred during monitoring.

One major disadvantage of these instruments was their maximum listed depth of 3 feet (Global Water 2003). On several occasions, water level depth exceeded this maximum, and thus critical data were lost at some flood stage peaks.

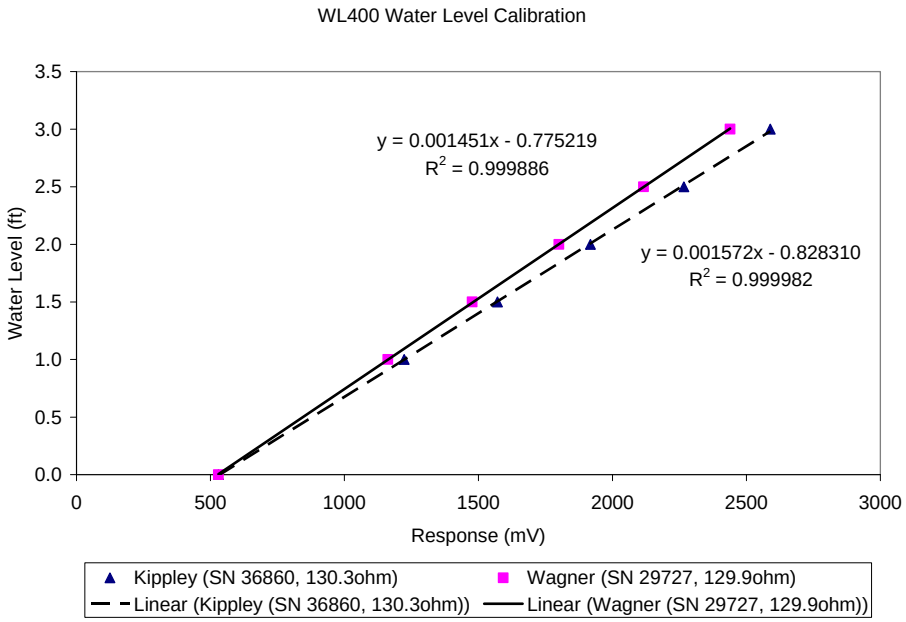

Figure 45: Calibration of WL-400 Water Level Sensors

For all of the gages, the measurement of the water depth at the measured cross section was very important. The height of the probe above the bed at the surveyed cross section was added to the gage depth to obtain the true water depth. For the Isco samplers, this was accounted for in the program setup. With the WL-400 gages, it was included in the calibration curve for conversion from response to true water level.

B.3 Sediment Sampling

The accurate measurement of suspended sediment concentration (SSC) during stormflow events was essential for this project. Suspended sediment concentration in the flow was obtained by two principle methods. Two D&A Instrument Optical Backscatter (OBS-3) devices were installed at the Kippley and Wagner sites for continuous turbidity

measurement. Two Isco Model 6712 Portable Samplers were installed at the Dorn and Ripp sites for automated stormflow sampling.

The optical backscatter devices function based on the reflectivity of suspended sediment particles. According to the manufacturer, the OBS-3 samples in the following way (D&A 2006):

A water sample… is illuminated by an [infrared] light source… and one or more photodetectors convert the light radiated from the sample to photocurrent. The amount of photocurrent depends mainly on the area of the illuminated particles but also on particle size, shape and reflectivity. Since the area of the illuminated particles is directly proportional to the suspended-sediment concentration, SSC, measurements of light scattering provide a way to estimate SSC.

Figure 46: OBS-3 Probe with Protective Stilling Well Pipe

The OBS-3 probes were connected to the Campbell Scientific Dataloggers as described in Appendix F. They were installed in the stilling wells, at the mouth of the protruding pipe, in the flow. The probes were oriented to point downstream and perpendicular to the flow. Calibration of the OBS units was essential, due to the variability of sediment types, and non-linearity in response. The OBS instruments were calibrated in the field by stirring up sediments in the channel upstream of the gage. The OBS response was measured and a direct sample of the flow was taken simultaneously for different concentration levels. The samples were then filtered using methods described below to

obtain suspended sediment concentration. The results of the calibration are presented below.

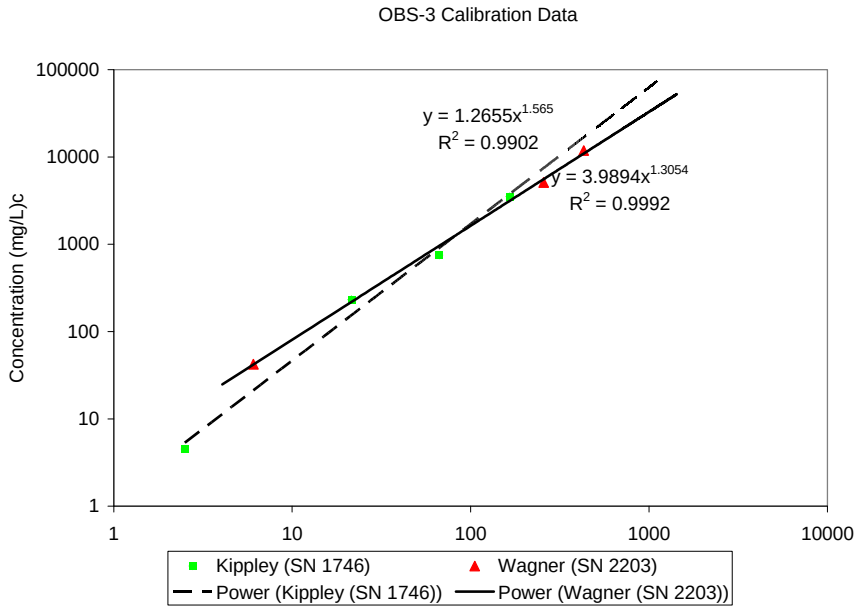

Figure 47: OBS-3 Calibration Results

Although field calibration of the OBS instruments showed excellent agreement, there were several concerns involving possible inaccuracies. E. Murdoc (2006) expressed concern over the accuracy of this method to determine SSC. Fouling of the OBS lens by biological growth was observed to affect response levels tremendously. The lenses were cleaned once or twice per week to minimize these effects. However, at certain dates, errors may be present in the data due to these effects.

Another hindrance in using these instruments is deposition of fine sediments on the OBS lens. At the Wagner site, very low flow rates allowed deposition to occur on the lens and significantly affected results. Due to this error, the sediment data obtained by OBS

methods for the Wager site was determined to be unusable, and is not included in this report. Flowrates at the Kippley site were sufficiently high so deposition on the lens was not an issue.

At the Dorn and Ripp sites, Isco Portable Samplers were installed. These samplers are programmed to collect 24 flow samples following a user-specified scheme. For these sites, the samplers were programmed to collect samples every 2 hours for the first 12 samples (1 day), and then every 8 hours for the last 12 samples (4 days). The sampler was set to begin sampling when a rise in water level was measured by the water level probe. The sampler collection head was installed in the channel using wooden stakes, and secured to the channel bottom.

After stormflow events, the samples were recovered from the samplers, and placed in plastic bottles. The samples were then stored in a cool condition in the Water Chemistry Lab at the University of Wisconsin-Madison and later analyzed by Adam Hoffman. Analysis of the samples for total suspended solids involved use of a procedure developed by the University of Madison Mercury Research Group (UW 2006). A known volume of sample was filtered using a pre-weighed Whatman Nuclepore Polycarbonate membrane filter, (47mm diameter) with a pore size of 0.40 μm. The filter was then dried and weighed, and the total suspended sediment concentration determined.

The accuracy of this method is excellent, and preferable to optical methods. This is primarily because it is a direct mass measurement and not affected by particle shape, color, or other variables. Due to extensive time to run samples using this method, only

some of the stormflow samples were analyzed. Data obtained from the LISST particle analyzer was combined with this filtered data to yield the final SSC values.

B.4 Velocity and Flowrate

There were two primary velocity meters used during this project. Early in the 2006 season the Marsh McBirney ECM-201 was used as a portable gage to measure velocities at different locations in the system. After April 2006, this velocity meter was installed at the Kippley site. The Marsh McBirney ECM-711 meter was then used as a portable meter for velocity measurements within the creek system.

The two velocity meters function on essentially the same principle. According to the manufacturer (MMB), the velocity meter:

…measures flow using the Faraday principle which states that as a conductor moves through and cuts the lines of magnetic flux, a voltage is produced. The magnitude of the generated voltage is directly proportional to the velocity which the conductor moves through the magnetic field…a pair of electrodes that measure the voltage produced by the velocity of the conductor, which, in this case, is the flowing liquid.

Based on the age of the instruments, it was determined that the readout velocity of both meters should be calibrated. Additionally, the output voltage of the 201 meter was calibrated. The calibration was conducted at the Fluid Mechanics Lab at University of Wisconsin-Madison in a large uniform flume under steady flow conditions. A Sontek SP-AV10M01 Acoustic Doppler Velocity meter (ADV) was used to measure the velocity at a set point, and subsequently the ECM-201 readout velocity, ECM-201 voltage output, and ECM-711 readout velocity were recorded at the same location. The ADV velocity meter is considered extremely accurate, and is adequate for this calibration.

For the installation at the Kippley site, the ECM-201 was placed in a plastic box and wired to the datalogger. A power scheme was developed to allow for longer lasting external lead-acid batteries to run the instrument. The wiring schematics, as well as pin outputs are located in Appendix F. The ECM-201 probe was fixed to a bar that was driven into the streambed at the Kippley cross section. The probe was vertically located approximately 1 inch from the bottom of the bed, and laterally at the location of approximate average velocity within the creek.

Several problems were experienced with this instrument, which were not fully resolved. The instrument would experience random losses in signal to the datalogger, usually for several hours, after which it would start functioning again. Additionally, during storm events, the front probe of the ECM would tend to get clogged by debris, and thus yield inaccurate results. Attempts were made to produce reliable data, although there are many areas where continuous data is not available. The results of this measurement are shown in Appendix C.

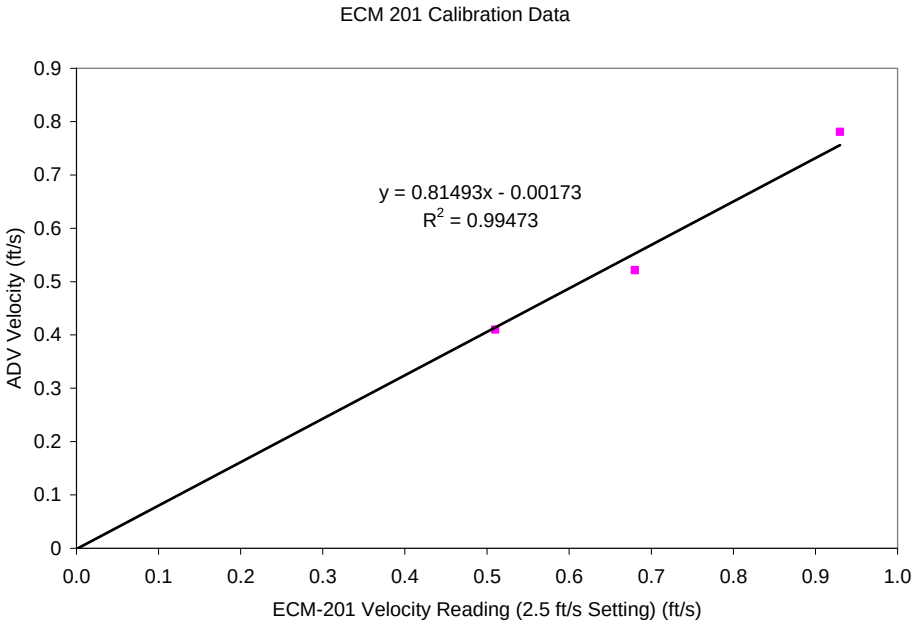

Figure 48: ECM-201 Calibration - Readout Velocity to ADV Velocity

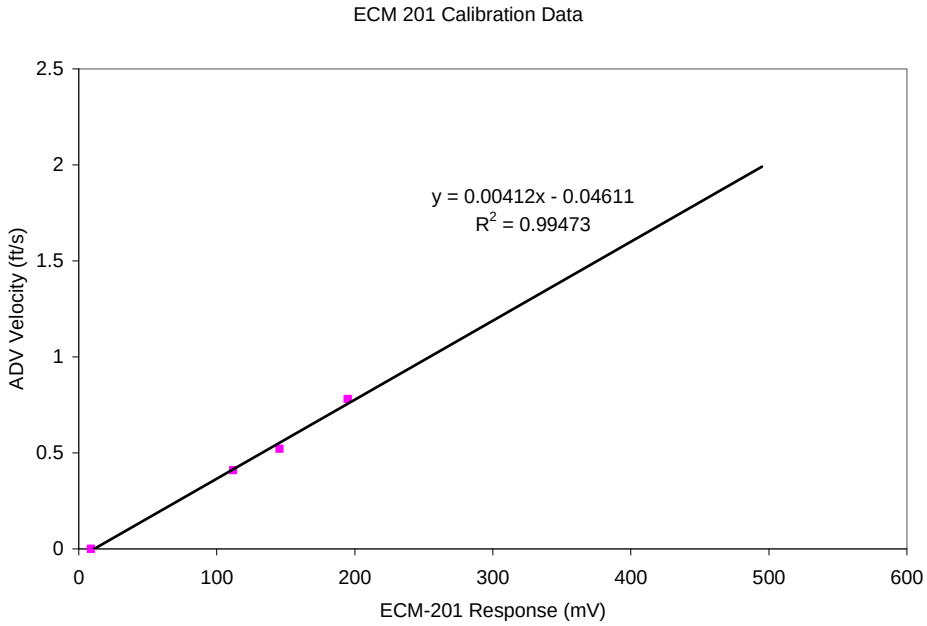

Figure 49: ECM-201 Calibration - mV Response to ADV Velocity

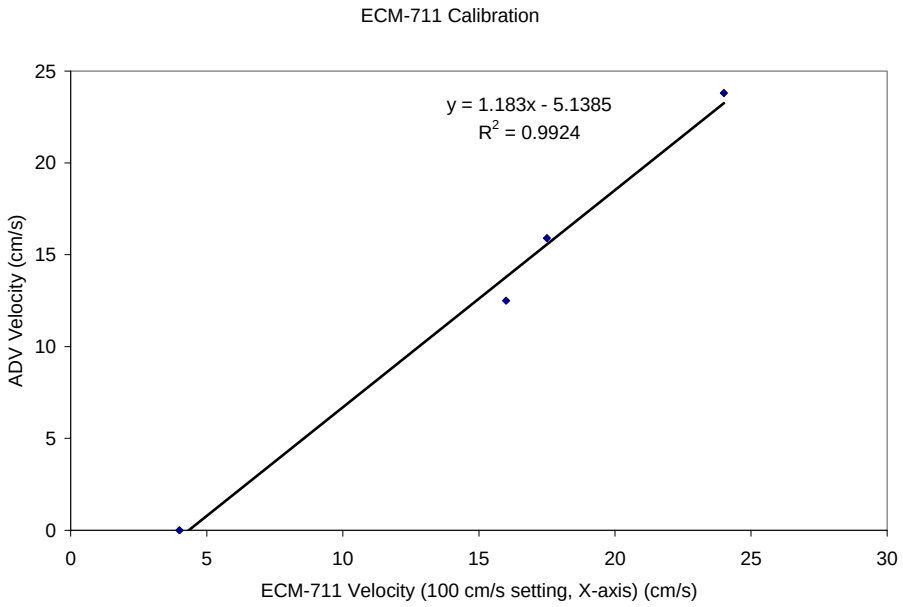

Figure 50: ECM-711 Calibration - Readout Velocity to ADV Velocity

The primary use of the portable velocity meters was to determine the flowrate in the creek at the gage sites. The compilation of this stage and flowrate data allowed formation of rating curves for each of the sites. The final rating curves are a result of a combination of field data and HEC-RAS modeling as described in Appendix C.

Figure 51: Typical Flowrate Measurement (J. Anderson at Ripp Gage)

The methods used for measuring flowrate are typical for small streamflow measurement and are described by (Herschy 1995), and (Chow et al. 1988). Each cross section of interest was divided into 1 foot sections. Using the results of the channel survey, the velocity (V) was measured at 0.6 times the total depth at 1 foot increments (w) along the stream. The total flowrate (Q) is then defined by:

$$Q = \sum_{i=1}^{n} V_i d_i \Delta w_i$$

B.5 Temperature Sensors

Temperature in Dorn Creek was monitored at two locations, the Wagner Gage and the Kippley Gage, in connection with Campbell Scientific dataloggers. The temperature sensors used were Campbell Scientific T-107 Temperature Sensors. The manufacturer lists the measurement range of -35 to 60 °C, and a margin of error of ± 0.2 °C (CS 2004). The measurements were checked using a mercury thermometer with excellent correlation, and therefore no calibration of this device was needed. The sensors were installed at the protruding end of the stilling wells so that the probe was in the stream flow.

Figure 52: Campbell Scientific T-107 Temperature Sensor

B.6 Rainfall/Meteorological

The rainfall and meteorological data requirements included incremental precipitation and ambient temperature. In an ideal situation, finances would be available for purchase of a weather station. However, due to budget limitations, weather data were obtained through third party sources.

For the 2003 to 2005 seasons, data were obtained from a USGS gaging station along the Pheasant Branch Creek in Middleton, Wisconsin (Gage 05427948) (USGS 2005). The gage is located at N 43°06'12", W 89°30'42", which is approximately 2.16 miles from the edge of the watershed and 4.07 miles from the centroid of the watershed. This dataset included 15-minute precipitation data for the site, as well as stage and flowrate for the Pheasant Branch Creek (neighboring watershed to the southwest). The precipitation gage ceased functioning in the spring of 2006, which led to the use of another weather station.

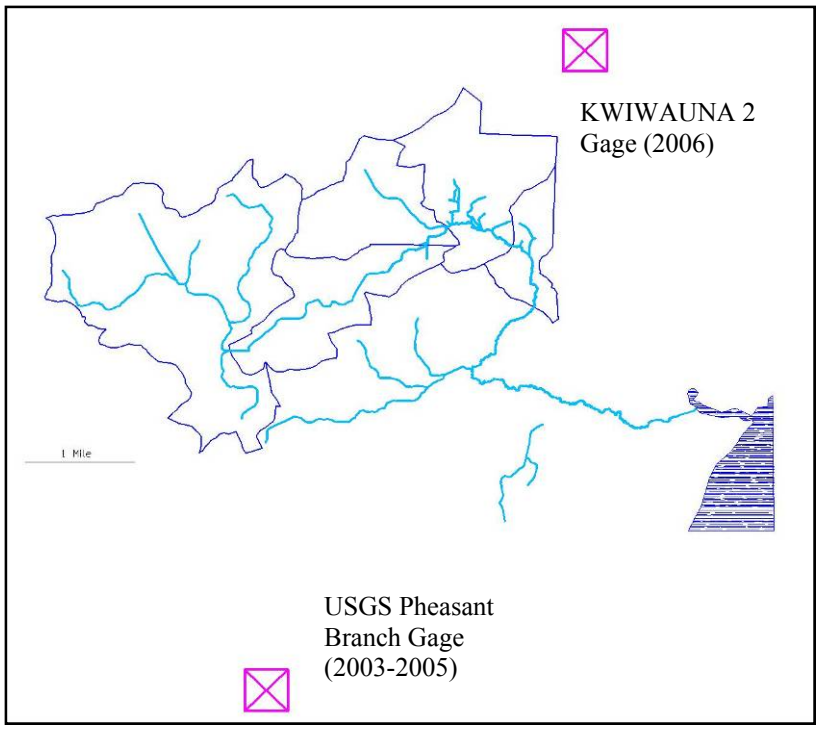

Figure 53: Location of Weather Stations in Relation to Dorn Creek Watershed

For the 2006 season, weather data were taken from a privately owned weather station, which is part of the Weather Underground network of weather stations (Gage KWIWAUNA2) (WU 2006). The gage is an Oregon Scientific WMR968 Wireless Weather Station using VWS (v.12.08) software. The gage is located northwest of the Waunakee Airport at N 43°11'18", W 89°27'25", which is located 0.82 miles from the watershed edge and 2.92 miles from the watershed centroid. This dataset included 5-minute weather data including ambient temperature, incremental and cumulative rainfall, wind speed, wind direction, barometric pressure and other meteorological parameters. In several instances where this gage was down for maintenance, the data were supplemented by nearby weather stations. None of these downtimes occurred during major rainfall events.

Due to weather patterns and rainfall variability, errors in estimation of the precipitation may be significant. This is especially true during summer months when storms are shorter, more intense, and more localized.

B.7 Particle Size (LISST)

To analyze stormflow samples obtained from the Isco samplers, a Sequoia Laser In-Situ Scattering and Transmissometry (LISST) model 100X was used. The LISST determines particle size and concentration by using laser diffraction. According to the manufacturer, the LISST (Sequoia):

…consists of optics for producing a collimated laser beam, a specially constructed detector array, electronics for signal preamplification and processing… After recovery of the instrument, small-angle scattering data are off-loaded from the instrument and subsequently inverted mathematically on a PC to produce the particle size distribution…The principal measurement—angular scattering distribution— is obtained over 32 ring-detectors whose radii increase logarithmically from 102 to 20,000 microns.

The testing of the storm samples was carried out in the Water Chemistry Lab at University of Wisconsin-Madison. The procedure for testing began with cleaning and background scatter detection of the device using distilled water. The stormflow samples were shaken to suspend particles and subsequently poured into the LISST. The sample was stirred in the LISST and data were recorded to a computer every second using the LISST SOP (v.4.65) software. For many of the samples, the concentrations were too high for the LISST (measured by monitoring the transmission parameter). These samples were diluted using volumetric glassware and poured into the LISST.

The LISSTS gives results in a volume per volume measurement for each particle size. For correlation to sediment results obtained by other methods, it was necessary to convert this volume/volume concentration to a mass/volume measurement. This conversion was achieved by correlation of the LISST data with samples using the filtration techniques described in Section 3. A linear regression equation was determined using the filtered results, LISST response and the LISST transmission parameter (T). The results of the calibration are shown below.

$$mg/l = 1.202 + 0.0113*(LISST\ \mu l/l) - 21.34*Ln(T)$$

In addition to total concentration and particle distribution, the LISST software computes the mean particle diameter (D50), as well as the standard deviation of the particles. A comparison of the calculated concentration and filtered results are shown below.

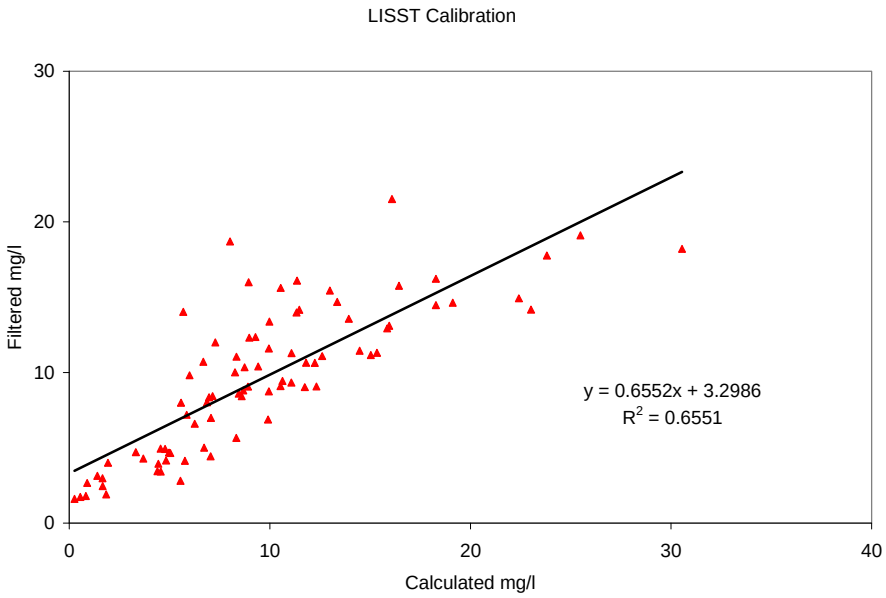

Figure 54: LISST Calibration Results

B.8 Dataloggers

At the Kippley and Wagner gaging stations, Campbell Scientific Dataloggers were used (CR-10X and CR-10 respectively) as the primary recording devices. As described in Section 3, the two gages had essentially the same instrumentation: WL-400 water level meter, OBS-3 backscatter device, and T-107 water temperature probe. Additionally, at the Kippley Gage, channel velocity was recorded using an ECM-201 velocity meter.

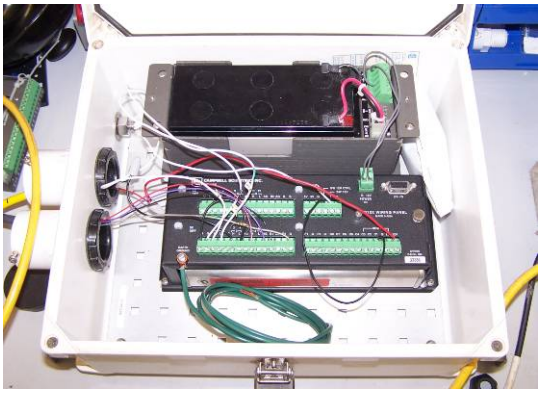

Figure 55: Typical Campbell Scientific Datalogger Setup

The programs used for running the dataloggers, wiring diagrams and setup configurations are located in Appendix F. The dataloggers were programmed to take readings of the instruments every 10 seconds, and record the average of those readings every minute. Therefore, the resulting data files contained 1 minute data points.

The dataloggers were placed inside plastic sealed boxes with a desiccant to prevent water damage. The baseplate and ground connection were grounded to a stake in the soil outside the box. Power was obtained from external 12 volt lead-acid batteries which were charged regularly.

Connection to the datalogger was done using Campbell Scientific PC200W (v.3.1) program with direct connection to a portable computer. The dataloggers were connected to Campbell Scientific SM16M storage modules, which allowed for data storage. Data were removed from the storage modules using Campbell Scientific Storage Module System (SMS v.4) program with direct connection to a portable computer.

B.9 Data Compilation

The compilation of data required merging of datasets from the four gaging stations, as well as meteorological data into a single format. Data from the Campbell Scientific Dataloggers was received in one minute resolution, comma delimited files. The data from the Isco Samplers was received through the Flowlink 4 program, and subsequently exported to one-minute comma delimited files. Meteorological data were downloaded from online sources and converted to 5-minute Microsoft Excel format. The data from these three sources was then combined into one single Microsoft Excel file for each month. The appropriate calibration curves were applied to the water level gages, OBS instruments, and any abnormal results were corrected.

Due to space limitations, the one minute data were converted to 15-minute data using the following methods. For the water level, water temperature, and OBS sediment concentration data, the fifteen minute average was taken. For the ambient air temperature, the 12-hour average temperature was taken. This was done to reduce the variability of the ambient temperature and allow for better comparison to water temperatures, which are much more subdued in their fluctuations.

The sediment concentration data samples obtained from the Isco Samplers were analyzed using filtration and LISST methods. Due to time constraints, not all of the samples were run using the filtration techniques. Where only one data point was available (i.e. either filtration or LISST), the available point was used. Where both LISST and filtration data points were available, the filtration data were used. Where no concentration was available (due to lost samples), the average of the neighboring points was taken. Most the major events of the 2006 season were computed using these methods, and the results are presented in Section 4 and Appendix E.

The final 15-minute dataset and the final sediment concentration data were then merged into a single Microsoft Excel file for the entire 2006 season. Various parameters were then calculated using this data such as flowrate, bed shear, hydraulic radius, mass transport, volume transport. Additionally, graphs were generated using this data, as presented in Section 4 and Appendix E.

B.10 Flume Core Testing

The primary objective in the flume core testing was to accurately determine the critical bed shear for erosion to occur at several of the gaging sites. Shelby tube cores were taken by driving steel core pipes into the bed sediments. The bottom and top end were capped, care was taken to not disturb the sample.

Testing of the sediment cores was performed using methods used by Lee et al. (2004). However, the soil core was advanced by hand cranking and no automated camera system

was used. The testing was performed in a 0.76 foot wide flume with variable slope at the University of Wisconsin Fluid Mechanics Lab. The soil core was pushed through the tube until it was flush with the channel, and then covered. The pump was then begun with the desired slope, flowrate and water elevation. The downstream water surface was adjusted to obtain nearly uniform flow in the channel, and the channel was allowed to reach steady state. The cover over the soil core was then removed and exposed to the flow. The core was observed visually for any signs of erosion. If no erosion occurred, the sample was covered and the procedure repeated with a higher shear stress.

Parameters recorded were flowrate (Q), depth at three locations (PG1, PG2, PG3), and bed slope (DG1, DG2). Typical design flow conditions and schematic diagram are listed in Lee et al. (2004). Testing of the cores was conducted for every 5 cm of soil core depth.

B.11 Surveying

There were several sites where very detailed cross section information was required beyond the LIDAR (Light Detection and Ranging) mapping accuracy. At each of the four gaging stations, a cross section survey was conducted. Additionally, fifteen cross sections located mainly near the Kippley and Ripp Gages were surveyed for the HEC-RAS model due to excessive vegetation and lack of LIDAR data in those areas. Finally, bathymetry measurements were conducted for six cross sections to track long term changes in the cross section due to erosion or deposition.

The methods for determining the cross sections at the gaging stations involved tying a taut, level string across the channel. The distance between the string and the channel was measured and recorded at one foot increments along the channel.

The methods for determining the fifteen HEC-RAS cross sections involved placing a level 22-foot bar across the channel. The distance between the channel and the bar was measured and recorded at one foot increments. These cross sections were related to total elevation from the LIDAR mapping by locating these cross sections in areas where there were visible gaps in the vegetation (where the LIDAR obtained a ground reading). The lowest channel measurement was then given the observed LIDAR elevation.

The methods for determining the bathymetric measurements are similar to those stated above, and are described by Murdoc (2006). A 22-foot bar was placed across the channel, and fit into rebar posts of known elevation. These posts were assumed to remain stable, and thus allowing repeatable measurements. The distance between the bar and the channel was then measured at one foot increments.

B.12 Mapping/LIDAR

Due the need for detailed topographic data for hydrodynamic modeling, LIDAR (Light Detection and Ranging) data were obtained of the project area. LIDAR is an active remote sensing technique that involves the use of pulses of laser light directed toward the ground and measuring the time of pulse return to determine elevation (Lillesand, et al 2004). One of the distinct advantages of LIDAR technology is the ability to sense several

return pulses, and distinguish tree canopy vs. bare ground, and penetrate water to give stream or lake bottom elevations.

The data for this project was acquired on June 24, 2006 using an Optech ALTM 3100 and waveform digitizer (operated by Kutalmis Saylam of Optech) installed on a Dynamic Aviation Beechcraft King Air (piloted by Paolo Ramella and Sue Ossler). The flight mission parameters are listed in Table 11.

Parameter	**Value**
Flying height	800 m (AGL)
Flying speed over ground	135 kts
Scan frequency	49.8 Hz
Scan angle	± 17.3 deg
Pulse repetition frequency (PRF)	70 kHz
Laser beam divergence	Narrow (0.3 mrad)
Laser footprint diameter	0.2 m
Swath width	500 m
Strip overlap	125 m
Nominal point spacing in X and Y	0.7 m

Table 11: LIDAR data acquisition parameters for June 24, 2006 flight mission

A temporary station located 13 km from the center of the project area was used for the GPS base station. This station was processed with respect to the National Geodetic Survey (NGS) Continuously Operating Reference Station (CORS) network using the NGS Online Positioning User Service (OPUS). The OPUS output is summarized below:

REF FRAME: NAD_83 (CORS96) (EPOCH:2002.0000)
LAT: 43 07 56.17199 0.009 (m)
E LON: 270 42 33.82045 0.005 (m)
W LON: 89 17 26.17955 0.005 (m)
EL HGT: 258.000 (m) 0.022 (m)

The sensor-to-antenna offset vector ("lever arm") components were determined by Optech using a total station and refined in Applanix POSPROC: revised lever arms (m) GPS to sensor, x= 0.045, y= -0.070, z= -1.591.

Jason Woolard of NOAA/NGS processed the GPS/IMU data and generated the georeferenced ASCII mass point files. All data for this project were referenced to NAD83 and projected in UTM (Zone 16N) and all elevation values were calculated as GRS80 ellipsoid elevations. The raw last return data were interpolated to a one meter grid by Chris Parrish of NOAA using a Kringing algorithm supplied by Michael Sartori of the University of Florida. Funding for the LIDAR data was supplied by Mke Asleksen, Chief of NGS Remote Sensing Division.

The one-meter (xy) grid was then converted to an AutoCAD digital topographic format using Surfer (V7.02) program. Due to the very large data size, only the project area was converted to the digital AutoCAD format. Three contour intervals of the digital topographic maps were generated: a 5-meter, 1-meter, and 0.2 meter.

In addition to the LIDAR topographic data, other elements were included in the AutoCAD mapping. Elements from the Dane County digital mapping website such as stream channels, buildings, land use, soil mapping, and aerial photographs were included (Dane County 2006). Additionally, the USGS 7.5 Minute Quadrangle maps were scanned into the drawing, and used primarily for watershed delineation (USGS 1983). Other information from various sources such as geologic features and bedrock elevations

were included. Every effort was made to assure correct scaling and orientation of the various components. Results of the mapping for the area are presented in Section 2.

B.13 References

Campbell Scientific (CS). 2004. *Model T-107 Temperature Probe Instruction Manual*. Logan, Utah: Campbell Scientific, Inc.

Chow, V., D. Maidment, and L. Mays. 1988. *Applied Hydrology*. New York: McGraw Hill, Inc.

Dane County. 2006. "Dane County DCiMap". Dane County (WI) Land Information Office. http://dcimap.co.dane.wi.us/dcimap/index.htm

D & A Instruments. 2005. "OBS- Turbidity Sensor Basics" D & A Instrument Company. http://www.d-a-instruments.com/measure_turbidity.html

Global Water. 2003. *Water Level Sensor: WL400 Instruction Manual*. Gold River, California: Global Water, Inc.

Herschy, R. 1995. *Streamflow Measurement, 2nd Edition*. Cambridge, UK: E&FN SPON

Isco. 1996. *720 Submerged Probe Manual*. Lincoln, Nebraska: Isco, Inc.

Lee, Cheegwan, Chin Wu, and John Hoopes. 2004. Automated Sediment Erosion Testing System Using Digital Imaging. Journal of Hydraulic Engineering, ASCE 130: (8) 771.

Lillesand, Thomas, Ralph Kiefer, and Jonathan Chipman. 2004. *Remote Sensing and Image Interpretation*. Hoboken, New Jersey: John Wiley and Sons, Inc.

Marsh McBirney. *Model 201 Portable Water Flow Meter Instruction Manual*. Frederick, Maryland: Marsh McBirney, Inc.

Murdoc, Evan. 2006. Transport and Storage of Sediments and Solutes in a Small Agricultural Stream, Dane County, Wisconsin. MS Thesis. University of Wisconsin – Madison.

Sequoia Scientific. *LISST 100-X Particle Size Analyzer User's Manual, Version 4.6*. Bellevue, Washington: Sequoia Scientific, Inc.

University of Wisconsin (UW). 2006. "SOP for Suspended Particulate Matter (SPM) Filter Weighing" The University of Wisconsin – Madison, Environmental Chemistry & Technology Program, Mercury Research Group.

.http://www.engr.wisc.edu/groups/mercury/SOP%20for%20Suspended%20Particulate%20Matter.htm

US Geological Survey (USGS). 1983. *7.5 Minute Quadrangle Maps: Springfield Corners, WI, and Waunakee, WI.* Madison, Wisconsin: Wisconsin Geological and Natural History Survey.

USGS. 2005. "USGS 05427948 Pheasant Branch at Middleton, Wisconsin Gaging Station." USGS Wisconsin Water Science Center. http://nwis.waterdata.usgs.gov/wi/nwis/nwisman/?site_no=05427948&agency_cd=USGS

Weather Underground (WU). 2006. "Weather Station History, KWIWAUNA2 Northwest of Waunakee Airport, Waunakee, Wisconsin" The Weather Underground, Inc. http://www.wunderground.com/weatherstation/WXDailyHistory.asp?ID=KWIWAUNA2

APPENDIX C – ADDITIONAL HYDRAULIC DATA

0.1 Overview

This appendix contains additional hydraulic information not presented in Section 4 of this report.

0.2 HECRAS Model

The HECRAS (Hydraulic Engineering Center River Analysis System) model was selected for this project due to its ease of use, general acceptance in the engineering community, and ability to meet the goals stated above. The HECRAS model is a public use program developed by the US Army Corps of Engineers (USACE). For this project, HECRAS (v.3.1.1) was used for all modeling.

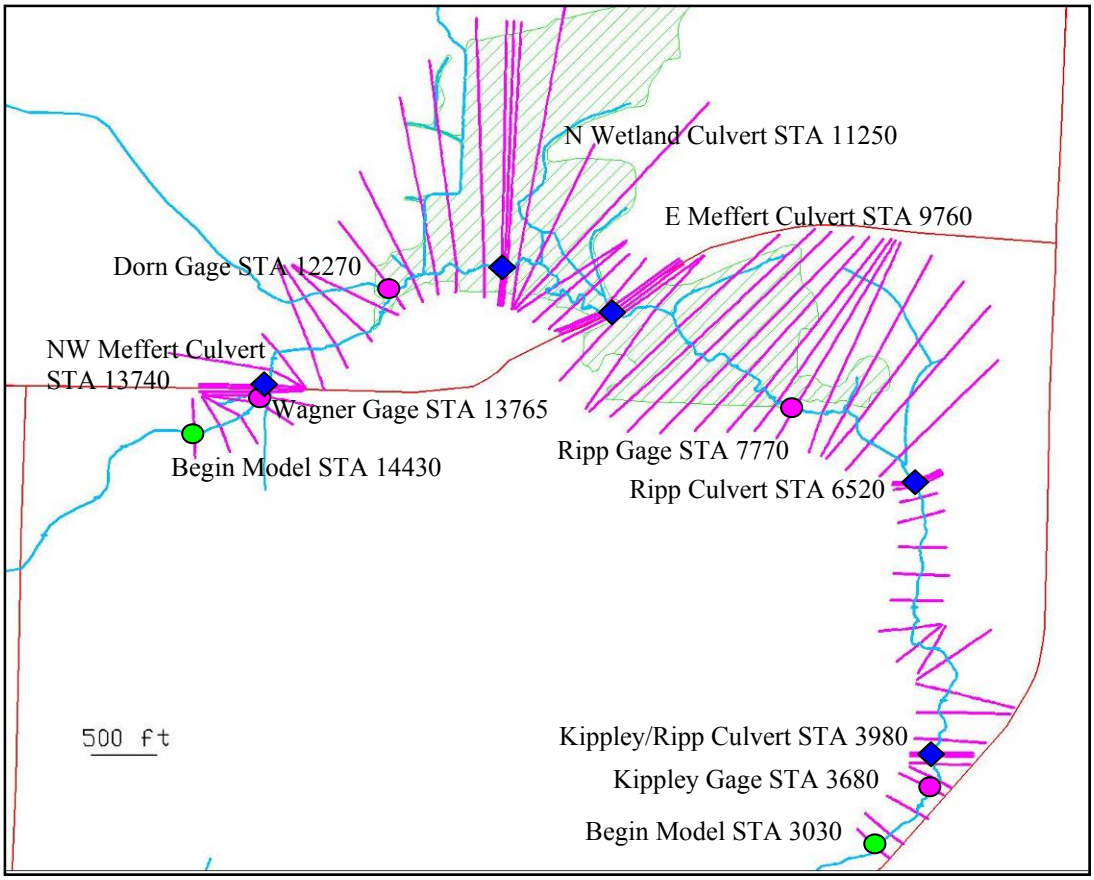

Figure 56: HECRAS Cross Section Locations and Key Hydraulic Elements

0.2.1 Theory and Limitations

The HECRAS model is based on the solution of the one-dimensional energy equation (USACE 2006). According to the USACE, energy losses (USACE 2006):

…are evaluated by friction (Manning's equation) and contraction/expansion (coefficient multiplied by the change in velocity head). The momentum equation may be used in situations where the water surface profile is rapidly varied. These situations include mixed flow regime calculations (i.e. hydraulic jumps), hydraulics of bridges, and evaluating profiles at river confluences (stream junctions)…The effects of various obstructions such as bridges, culverts, weirs, and structures in the flood plain may be considered in the computations.

As stated above, the energy equation is used to evaluate water surface profiles using Manning's equation and contraction/expansion coefficients. Mathematically, this becomes an iterative process:

$$z_1 + h_1 + \frac{\alpha_1 V_1^2}{2g} = z_2 + h_2 + \frac{\alpha_2 V_2^2}{2g} + h_L$$

Losses due to friction and contraction/expansion are calculated as follows:

$$h_L = LS_f + C\left|\frac{\alpha_2 V_2^2}{2g} - \frac{\alpha_1 V_1^2}{2g}\right|$$

$$S_f = \left[\frac{Q}{K}\right]^2$$

$$K = \frac{1.486}{n} AR^{2/3}$$

HECRAS uses the momentum equation in select cases such as hydraulic jumps, stream junctions and bridge constrictions and drop structures for determining the water surface profile. A momentum balance of a body of water enclosed by two cross sections yields:

$$P_2 - P_1 + W_x - F_f = Q\rho V_x$$

Expansion of these terms leads to:

$$\frac{Q_2\beta_2}{gA_2} + A_2 h_2 + \left(\frac{A_1 + A_2}{2}\right)LS_0 - \left(\frac{A_1 + A_2}{2}\right)LS_f = \frac{Q_1\beta_1}{gA_1} + A_1 h_1$$

Additional information on additional parameters and the notation used within this report can be found in the HECRAS Hydraulic Reference Manual (USACE 2002).

Modeling of Dorn Creek was performed using steady flow analysis option within HECRAS. This approach assumes that the flow is steady, gradually varied, one dimensional, and that slopes are small (USACE 2002). Additionally, the model assumes a rigid impervious boundary and a linear stage-discharge response. These assumptions are valid for most areas of Dorn Creek, although there are some notable exceptions.

The flows in the non-wetland areas of the creek can be approximated reasonably well as one-dimensional flows, as there is typically a well-defined main channel. However, flows within the wetland itself follow shallow, winding and often diverging/converging channels, which may not be well approximated by a one-dimensional flow analysis. This is especially true in the North Wetland, where several tributaries, ponding, and very low slopes produce flow directions that may not be parallel to the main channel.

The assumption of steady-state flow through the system has several limitations, most notably inaccurate modeling of storm hydrographs. Attempts were made to model the flow using the unsteady flow option, but the model was unstable, and a solution could not be obtained. In an effort to model the observed hydrographs through the system, the actual observed peak flowrates from the four gaging stations were used, and flowrates linearly interpolated between cross sections. In effect, this method accounts for the unsteady flows and storage by using a steady flow analysis method and observed

flowrates. Results are therefore representative of maximum stage, velocity and flowrates at each cross section for that event.

The assumption of a rigid, impervious boundary is generally true for the Dorn Creek system. Erosion and deposition rates have been observed to be slow (on the order of years for observable change). The impervious boundary assumption is also generally true for the system, especially in areas with a deeper more defined main channel. One notable exception to this assumption is within the wetland itself. Throughflow between the vegetative surface, and harder soil bottom may be significant in wetland areas, as the grass/peat material typical of the wetland is extremely porous. Groundwater discharge also has been observed to be significant within the wetland.

The assumption of a linear stage-discharge response is probably valid for most of the Dorn Creek system especially where the main channel is deep and well defined, and flows are not rapidly varied. However, D.A. Hughes (1979) noted that hysteretic effects of inundation and recession of stormflows to and from the floodplain may be significant. He concludes that the movement of inundating water is shown to depend upon the shape of the flood hydrograph and the prevailing form of the floodplain; and that the degree of hysteresis depends on the conductivity of the floodplain/flood event combination. Therefore, these effects may be significant within the wetland area, and are not accounted for in the modeling.

The final assumptions of small slopes and gradually varied flow are generally valid through the system. Low slopes are typical of the Dorn Creek system, and site

observations have shown no significant structures that would violate the gradually varied flow assumption under flood conditions.

0.2.2 Cross Section Geometry

Within the digital AUTOCAD drawing, a principal channel centerline was established for the project area. Channel stationing was established in feet beginning at Dorn Creek and County Highway K (STA 0) and continuing upstream to Dorn Creek near Pheasant Branch Road (STA 14430). This stationing was used to identify cross sections and other geometric elements within the HECRAS model.

The geometric inputs to the HECRAS model primarily consist of cross section data at intervals along the channel centerline. For this model, cross section spacing along the channel range from 311 to 26 feet but are typically near 200 feet and drawn perpendicular to channel flow. Figure 56 shows the cross section locations along the channel. Cross sections were located at closer intervals where required, such as channel bends, culverts, and bridges as described in the HECRAS User's Manual (USACE 2002).

The geometric coordinates of the cross sections were primarily determined using the LIDAR 0.5 meter digital topographic mapping described in Section 3. In the AUTOCAD digital drawing, cross sections were located were overlain over the topography in 3D space. The properties of these 3D cross section lines were then exported to xyz coordinates. Within Microsoft Excel, the xyz coordinates were converted to distance

from the end point and elevation (d,z) points in feet which were subsequently copied to the HECRAS model.

There were several cross sections where the LIDAR data were incomplete due to vegetation. The surveyed cross section data were combined with the LIDAR digital data to produce a complete cross section. For model stability, cross sections were interpolated at 40-foot intervals using the automated cross section interpolator in HECRAS. The calculated results for these interpolated sections were not included in the results, but were used to help "smooth out" transitions within the model.

0.2.3 Inneffective Flow Areas

As described previously, accurate hydraulic modeling of wetland areas is difficult. Within the North Wetland, it has been observed that the main channel bottom is elevated up to 1.2 feet above the lowest point in the wetland as shown in Figure 57. This is probably a result of vegetative growth on the channel banks serving to "harden" the banks from erosion, and possible settlement of low-ponded areas. Additionally, there is a small northern tributary that enters near this location that may affect the geomorphology. The low area shown in the figure is typically ponded with water under baseflow conditions. The location of the main channel has been field verified, and agrees with Dane County (2006) mapping.

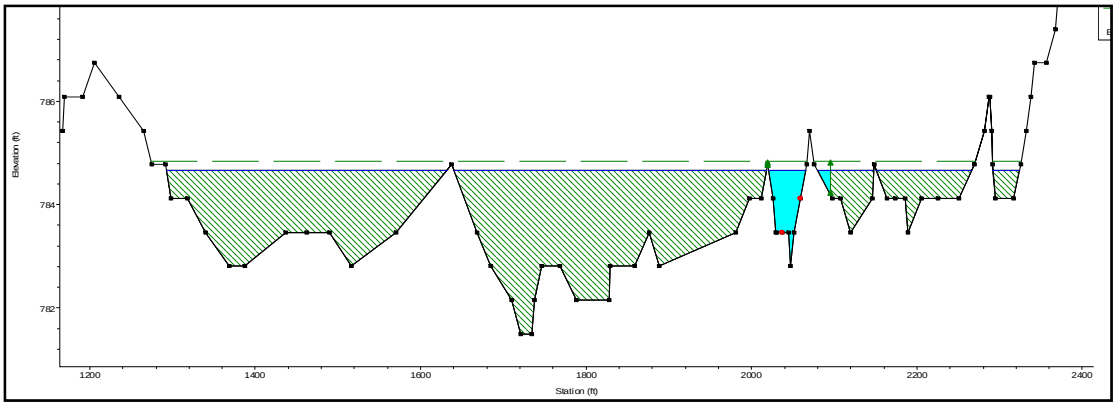

Figure 57: Typical North Wetland Cross Section (STA 1110). Main Channel is to the Center Right. 6-25-06 Event Simulation

In order to account for this elevated main channel effect, ineffective flow areas were added to the outer banks of the observed main channel to the elevation of the main channel banks as shown in the figure. Although this is not a perfect method, it does force the water to move through the main channel for low flows (while the main wetland is inundated but does not contribute to the conveyance). Higher flows above the main channel banks are allowed to go into the main wetland which contributes to the conveyance. This produces the net result of what is believed to actually occur in the wetland based on field observations of stormflows.

In addition to ineffective flow areas used for the wetland areas, these were also used for bridges and culverts to block areas that do not contribute the conveyance as described in the User's Manual (USACE 2002). Additionally, this method was used to block areas such as ponds and canals that did not contribute to the conveyance.

3.2.4 Bridges and Culverts

There are several bridges and culverts within the Dorn Creek system. Table 12 is a list of the bridges and culverts within the system with pertinent details. All information was field measured.

Name	Northwest Meffert	North Wetland	East Meffert	Ripp	Kippley/ Ripp
Channel Station	13740	11250	9760	6520	3980
Shape	Pipe Arch	Semicircle	Conspan Arch	Conspan Arch	Box Bridge
Headwall	45 Degree Concrete	Flush to Soil	45 Degree Concrete	Mitered to Slope	90 Degree Concrete
Bridge/ Culvert Material	Corrugated Steel	Corrugated Steel	Concrete	Concrete	Concrete Sides, Steel Top
Bottom Material	Sediment	Sediment/ Grass	Sediment	Rocks	Rocks
Length (ft)	38	24	40	14	23
Width (ft)	9	5	14	8	14
Height (ft)	7	3	7	4	5

Table 12: General Bridge and Culvert Properties

The culvert and bridge properties were inputted into the HECRAS model as described in the User's Manual (USACE 2002).

0.2.5 Manning's Roughness

The Manning's n roughness coefficient is a representation of the total roughness of the entire section. Within the HECRAS model, separate roughness coefficients can be used for the main channel, right overbank and left overbank. The estimation of the roughness coefficient is very significant to the value of the computed water surface and depends on

many variables (USACE 2002). It is also usually one of the least known parameters in hydraulic modeling.

Published results of Manning's n coefficients from field studies in various channels are primarily based on V.T. Chow (1959). More recent field studies of Manning's n coefficients for wetland and floodplain areas are widely varied from 0.039 to 2.4 (Krause 1999). The primary difficulty in estimation of the Manning's n value is that it is a bulk roughness coefficient, and does not account for changes in roughness due to depth or other hydraulic parameters. The best method for determination of the Manning's n value is direct measurement during flood conditions.

Based on the field measurements of flowrate and stage for several stormflows, the Manning's n coefficients for the main channels were directly determined for the four gaging stations using the HECRAS model. More details of this procedure are contained in the calibration section of this report. Essentially, the Manning's roughness coefficient was varied so that for a given observed flowrate, the observed and predicted water levels were the same. It should be noted that the largest available flowrates were use to calibrate these values so roughness is representative of higher stage levels. These values agree with published values by Chow (1959) and Haan et al. (1994) for observed channel type.

Gage	Station (ft)	Calibrated main channel Manning's n
Wagner	13765	0.020
Dorn	12270	0.076
Ripp	7770	0.053

Kippley	3680	0.061

Table 13: Calibrated Main Channel Manning's n values at Gaging Stations

The overbank Manning's n coefficients were selected based on site observations of roughness and correlations to published values. Values selected for overbank Manning's n values range from 0.05 to 0.11. Table 14 summarizes the Manning's n values used for the HECRAS model, and is a compilation of calibrated, interpolated and inferred values.

Start Station (ft)	End Station (ft)	Applied Mannings's n			Main Channel Description	Overbank Description
		Right OB	Main Channel	Left OB		
13080	14430	0.050	0.020-0.060	0.050	Transition from thick grass to loose sediment to weedy wetland	Cornfields and grass
8090	13080	0.080-0.110	0.070-0.110	0.080-0.110	Very weedy to deep weedy pools and brush	Wetland with open grass to trees and heavy brush
6520	8090	0.100	0.053	0.100	Weedy with fallen trees	Trees and brush (former wetland)
3980	6520	0.080	0.070	0.080	Weedy to loose sediment	Heavy grass
3030	3980	0.100	0.061	0.100	Clay bottom with boulder clusters	Trees and brush

Table 14: Typical Manning's n values used for HECRAS modeling by reach type. (OB = overbank)

0.2.6 Flowrate and Boundary Conditions

A steady state model was run using HECRAS. As described in the assumptions section, several model scenarios were run using the observed flowrates for the 2006 season. The following is a summary of the peak flowrates observed at each gaging station, based on

the rating curves. It should be noted that these values are not a snapshot in time, but peak values for each event, which occur at staggered timing as the flood wave travels down the system (see Appendix D for more hydrologic information).

For low flow events, flowrates were applied to sections slightly upstream of the gaging stations at areas of known inflow. For higher flowrates, these flow values obtained from the gaging stations were linearly interpolated for cross sections between the gaging stations. Not all events of the 2006 season were run in the HECRAS model; rather a representative group was used as shown below.

Storm Event Date	**Peak Observed Flowrate (cfs)**			
	Wagner Gage	Dorn Gage	Ripp Gage	Kippley Gage
4/3/2006	0.28	1.72	3.27	4.77
4/7/2006	0.37	2.16	2.77	4.01
4/16/2006	0.34	1.11	1.24	1.72
4/28/2006 Baseflow	0.169	0.370	0.391	0.560
4/30/2006	0.47	1.92	3.08	3.21
5/11/2006	0.59	1.31	2.27	2.74
5/24/2006	47.27*	71.46	17.13	15.89
6/25/2006	134.02*	127.34	50.94	53.66*
7/11/2006	0.54	3.88	4.53	6.71
7/27/2006	2.46	21.77	14.62	22.86
8/23/2006	15.30	21.35	26.66	30.00*
9/12/2006	10.58	23.07	27.00*	30.77*
Theoretical High Flowrate**	250.00	230.00	95.00	95.00

Table 15: Observed Event Flowrates Used for HECRAS Modeling. (*extrapolated value) (Hypothetical event, relative flowrates based on observed conditions for lower flowrates)**

The boundary conditions used in the model were critical depth at both the inlet and outlet of the system. Although these values are not truly representative of conditions at the boundary, the boundaries are located far away from the areas of interest so that this error does not have an observable effect on the model results.

3.2.7 Calibration

Calibration of the model is important to assure that model results are representative of the real conditions in the field. In a theoretical sense, many parameters could be varied to assure agreement such as water depth, flowrate, roughness, channel geometry and slope. For the modeling of the Dorn Creek system, geometry, slope, water depth and flowrate were fixed parameters, and known to a certain degree of accuracy. Therefore, the Manning's n roughness value is the clear calibration parameter for this project.

The calibration of the HECRAS model was primarily accomplished by the changing of the main channel Manning's n resistance factors to match observed water depths. This is an iterative process and required many simulations to obtain a converged solution within 0.01 feet. Final values were compared to those listed by Chow (1959), and Haan et al (1994) with excellent agreement.

Calibration was not possible for overbank Manning's n resistance factors due to stage-flow data not being available for highly flooded conditions. Therefore, Manning's n values were selected from the literature for observed overbank type.

3.2.8 Results

The HECRAS model was developed for the Dorn Creek system to accomplish three goals. The first goal was to determine the probable extent of flooding for observed flow conditions within the wetland itself, and to map the limits of flooding. The second goal was to use the model to supplement the rating curves for the sites for flowrates above the field measured values. Finally, the hydraulic model would aid in sediment transport modeling by showing probable velocity and bed shear distributions within the wetland system.

The results of the HECRAS modeling agree with observed conditions in the field. The water surface profile from three model runs for a representative small event, large event and baseflow conditions is shown in Figure 58 below. The profile shows increasing water levels with increasing flowrate.

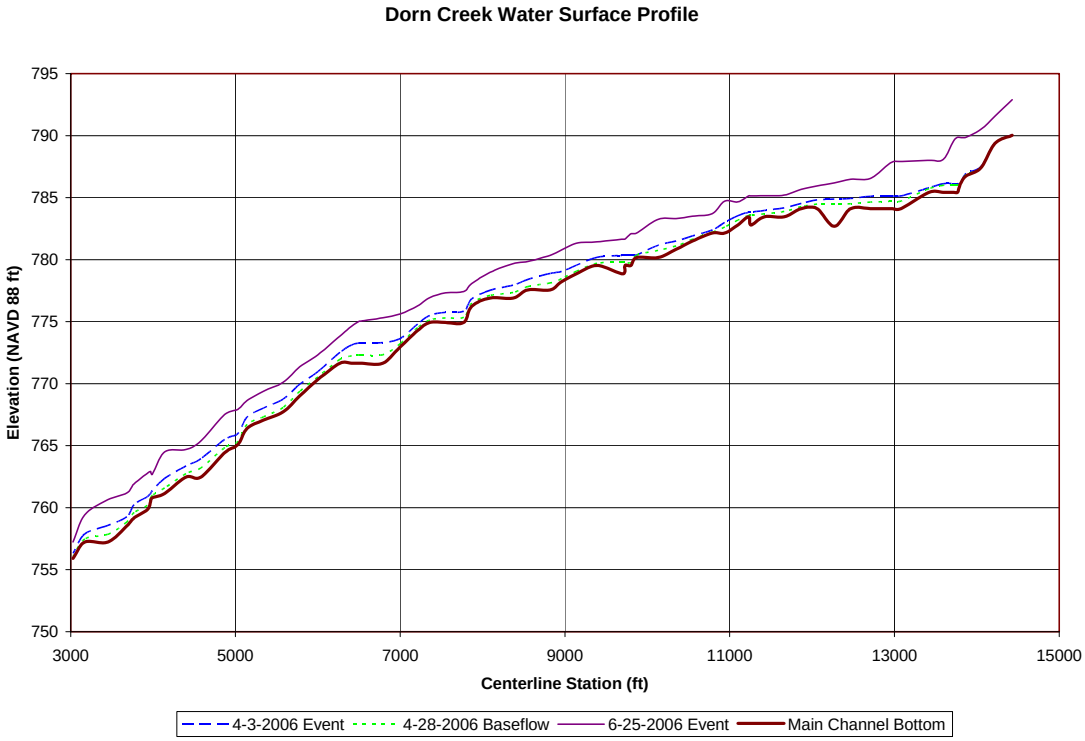

Figure 58: HECRAS Water Surface Profile for Small Flowrate, Larger Flowrate and Baseflow Conditions

The probable extent of flooding was determined for a small event (4/23/2006), and the largest observed event (6/25/2006). The extent of flooding for each cross section from the HECRAS results was mapped in the AUTOCAD drawing. The results of that mapping are shown in Figure 59, Figure 60 and Figure 61. The shaded coloring represents any predicted depth of storm inundation, and therefore many areas of floodplain may have very low water depths.

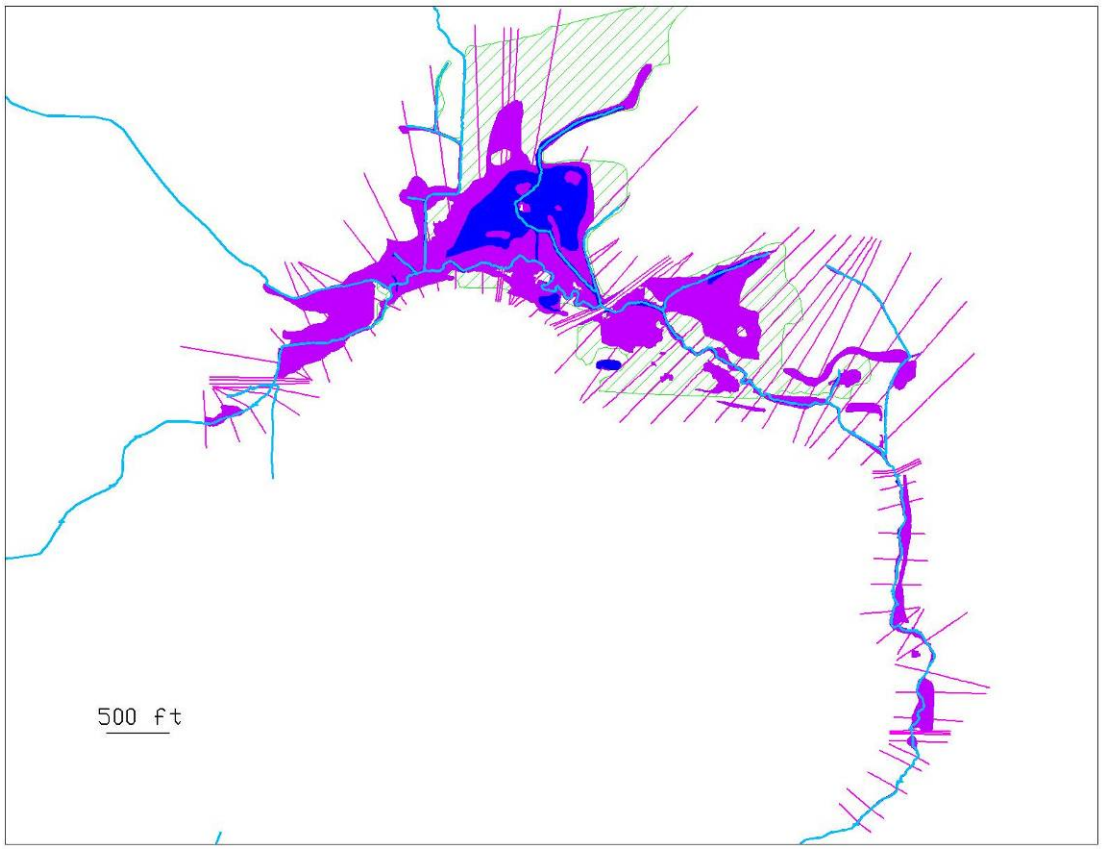

Figure 59: Overall Modeled Flood Extents for Small 4/3/2006 (Blue), and Large 6/25/2006 (Purple), events

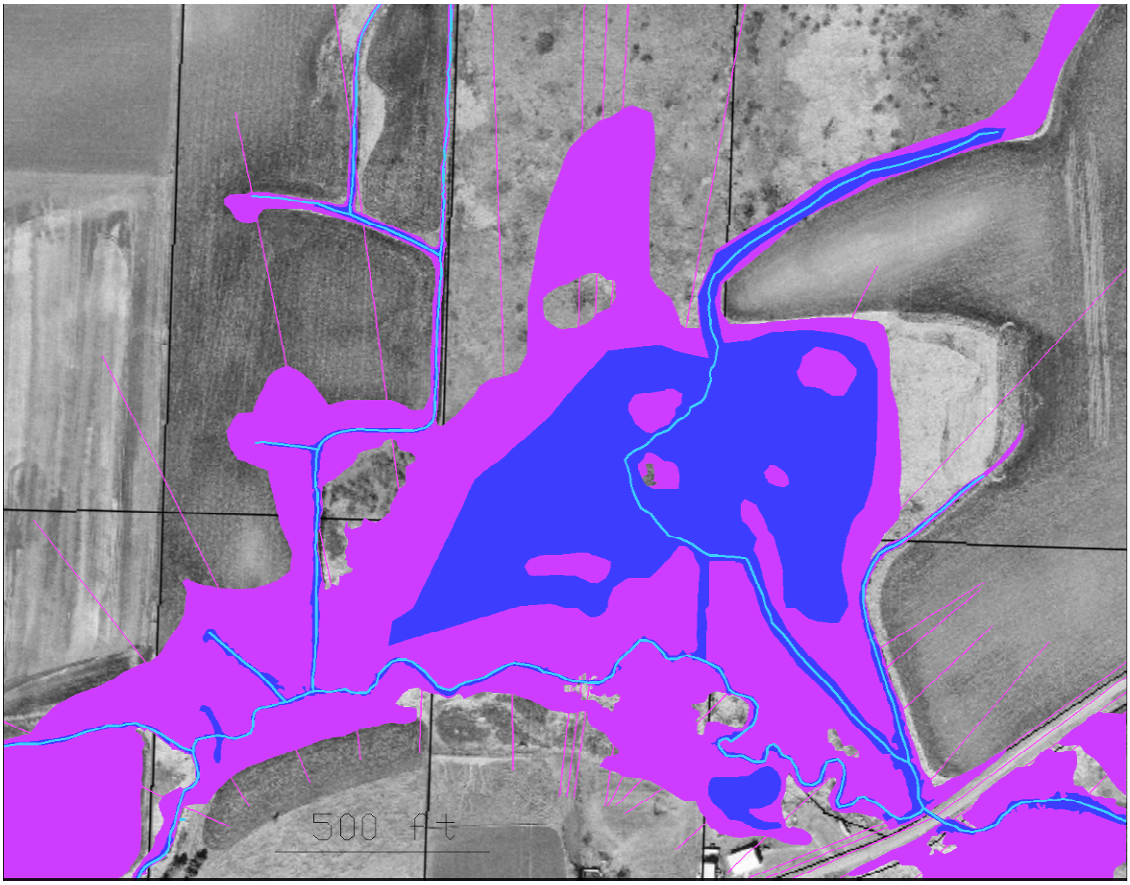

Figure 60: Modeled Flood Extents for North Wetland for Small 4/3/2006 (Blue) and Large 6/26/2006 (Purple) Events. Othophoto Courtesy of Dane County (2006). Used by Permission

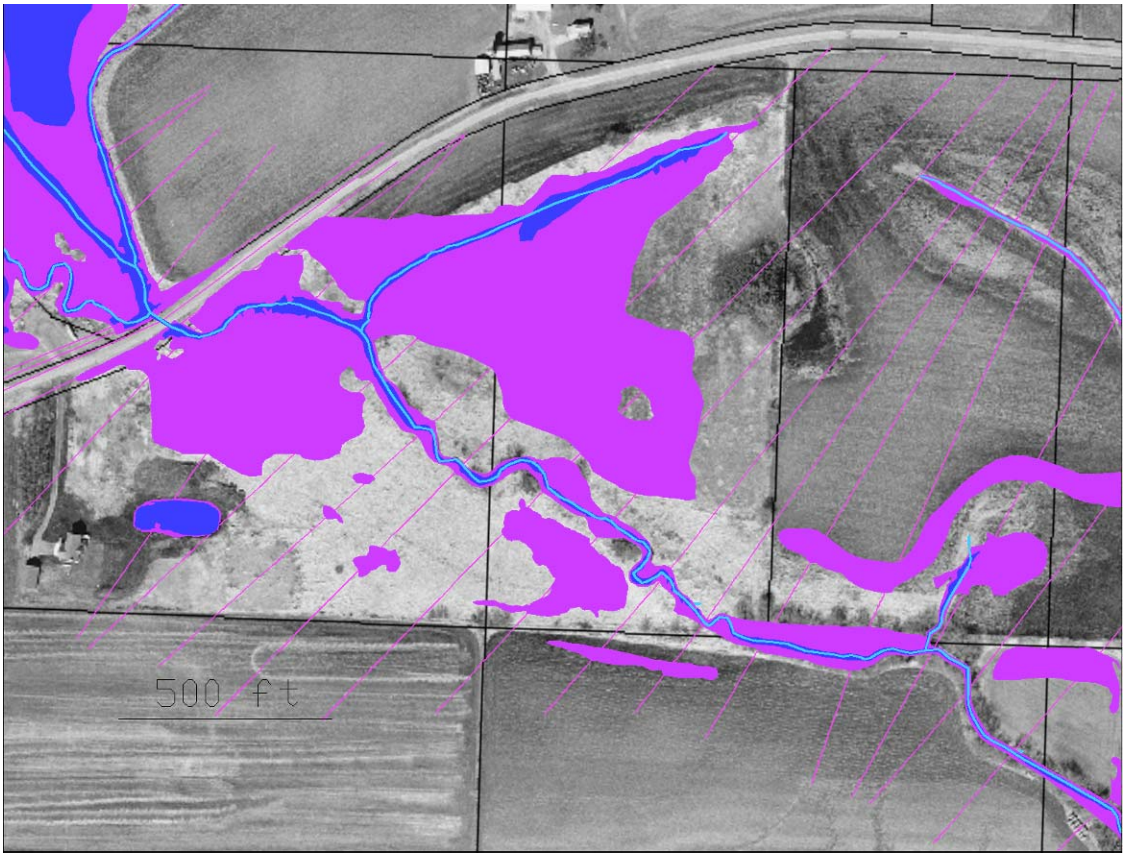

Figure 61: Modeled Flood Extents for South Wetland for Small 4/3/2006 (Blue) and Large 6/26/2006 (Purple) Events. Othophoto Courtesy of Dane County (2006). Used by Permission

As shown in the previous figures, there was a wide-range of flood extent during the 2006 season. The blue color represents the extent from a typical, small flood event. From the figures, it is clear that for small events, most stormflow is contained entirely within the main channel. In the north wetland, there is a distinct area of inundation. However, this region is subjected to almost constant water inundation and is probably fed from groundwater sources. This area is also the area in which the main channel is elevated above the wetland as discussed in the section on ineffective flows. It should be noted that the southern wetland experiences almost no inundation for these low flow events. The total wetland inundation for the low flow event is calculated at 12%. As a comparison, typical inundation under baseflow conditions was calculated as approximately 7% of the wetland area.

The purple shading represents probable inundation from the largest observed storm event. Significant portions are inundated, in both the northern and southern sections of the wetland. In the southern reaches of the system below the wetland, the channel is typically at bankfull conditions and in some cases there is significant overtopping. For the largest observed event, the percentage of inundation of the wetland is estimated at 64%. Additionally, the large hypothetical event (of approximately 5-year recurrence interval), showed an inundation of 76%.

The model was run for the 12 scenarios shown in the flowrate section of this report. The total wetland inundation was calculated using the water top width and weighted cross section length from the model. These two quantities were multiplied to give top surface

area for that cross section. The total cross sections over the wetland area were then summed and divided by the total area to give the percent inundation.

The results of the analysis used to determine the bed shear and velocities are shown below for both a representative small (4/3/2006) and large (6/25/2006) event, as well as baseflow conditions.

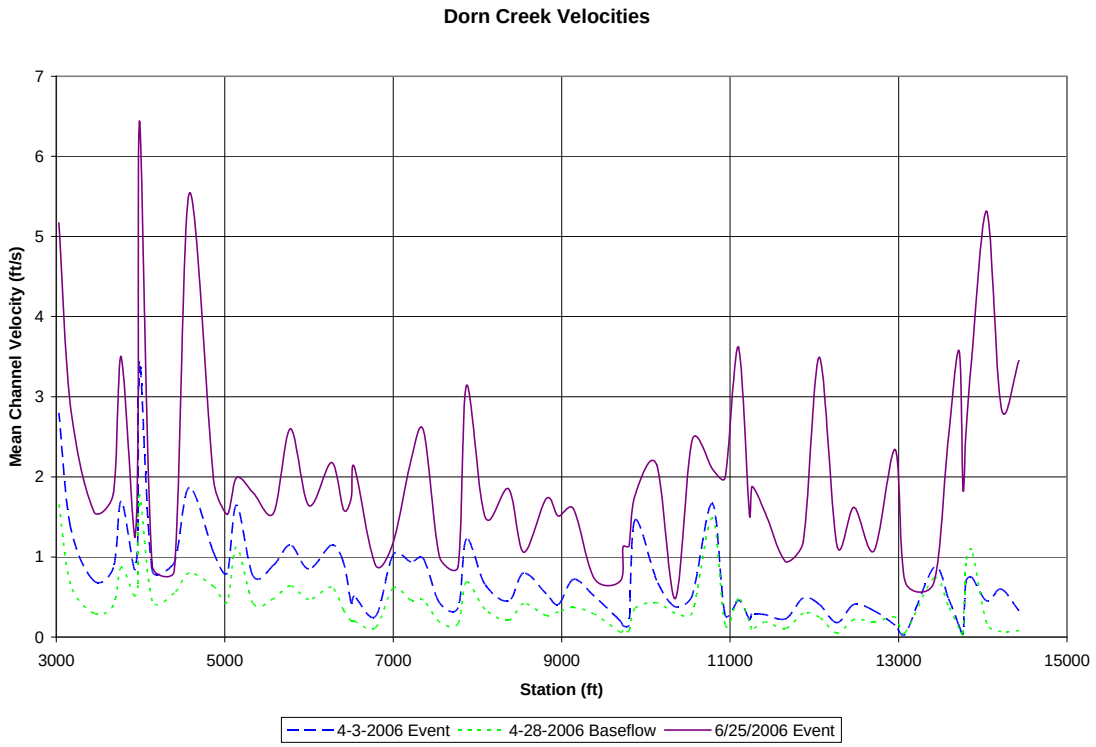

Figure 62: HECRAS Velocity Profile for Representative Large, Small and Baseflow Conditions

The results of the HECRAS modeling show velocity distributions through the system ranging from 0.04 to 1.78 ft/s for baseflow conditions, 0.04 to 3.44 ft/s for the small event and 0.48 to 6.43 for the large event. The velocity has a high variability changes significantly between cross sections.

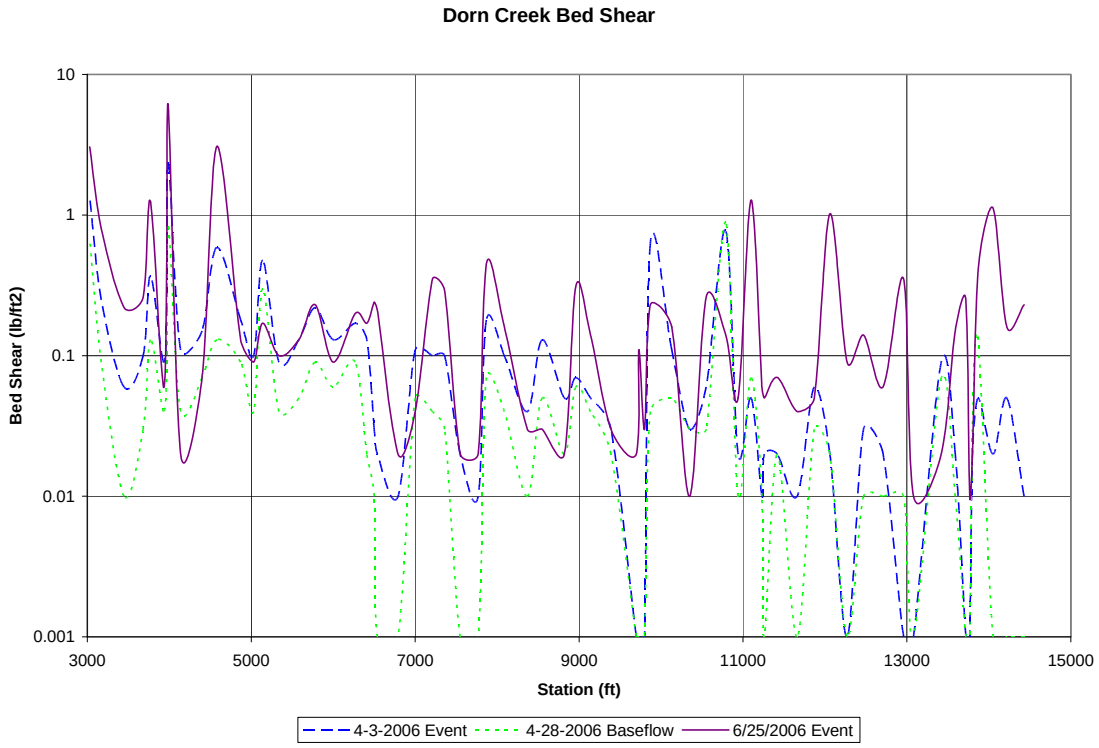

Figure 63: HECRAS Bed Shear Profile for Representative Large, Small and Baseflow Conditions

The results of the HECRAS modeling show bed shear distributions through the system ranging from 0.00 to 0.89 lb/ft^2 for baseflow conditions, 0.00 to 2.35 lb/ft^2 for the small event and 0.01 to 5.66 lb/ft^2 for the large event. The bed shear has a high variability and changes significantly between cross sections.

Clearly there are limitations to these modeling results. The HECRAS model results are reasonable and calibrated, however may be inaccurate for the reasons listed in the assumptions section. Therefore it can be considered as a good first approximation to the hydraulic properties of the system.

For future work, a more detailed hydraulic model would give a more comprehensive understanding of the system. Ideally, a 2-dimensional, unsteady model would give much more refined results. The LIDAR dataset could provide the necessary geometric information, if coupled with a site channel survey. This improved model could allow modeling of the hydrograph recession and attenuation, give a better understanding of the wetland storage properties, and better approximate the complex flow patters within the wetland.

0.3 Rating Curves

Conversion of water depth measurements to flowrate involves the use of rating curves. Rating curves have been used extensively in natural channels for flowrate measurement (Herschy 1995). The methods used for measuring flowrate are typical for small streamflow measurement and are described by (Herschy 1995), and (Chow et al. 1988). Each cross section of interest was divided into 1 foot sections. Using the results of the channel survey, the velocity (V) was measured at 0.6 times the total depth at 1 foot increments (w) along the stream. The total flowrate (Q) is then defined by:

$$Q = \sum_{i=1}^{n} V_i d_i \Delta w_i$$

These measurements are ideally made for a wide range of flowrate conditions. The flowrate and stage data points are then plotted, and a regression relationship is determined.

In the Dorn Creek system, measurements of flow and stage levels were conducted at seven times during the season from April through June for flood and baseflow conditions at the four gages. These results are presented in Figure 64 for low flowrates. It was found through regression analysis that the quadratic form best approximated the stage discharge relationship for this data. Based on results of Carter and Anderson (1963), the estimated standard deviation for the methods used is 4-6%.

For flowrates above measured conditions, the HECRAS model was used to develop rating curves. For each site, a desired flowrate was run through the model, assuming observed scaling of peak flowrates through the system to account for any backwater effects. The observed stage levels were then recorded and plotted on Figure 65. It was found through regression analysis that the power law form best approximated the Dorn and Wagner sites, and the cubic form best approximated the stage discharge relationship at the Ripp and Kippley sites for the high flowrates. The basis for two rating curves separating high and low flowrates is commonly used and is described by Gupta (1995). The error for this data is essentially the same as the error for the HECRAS model, which is discussed in the assumptions section.

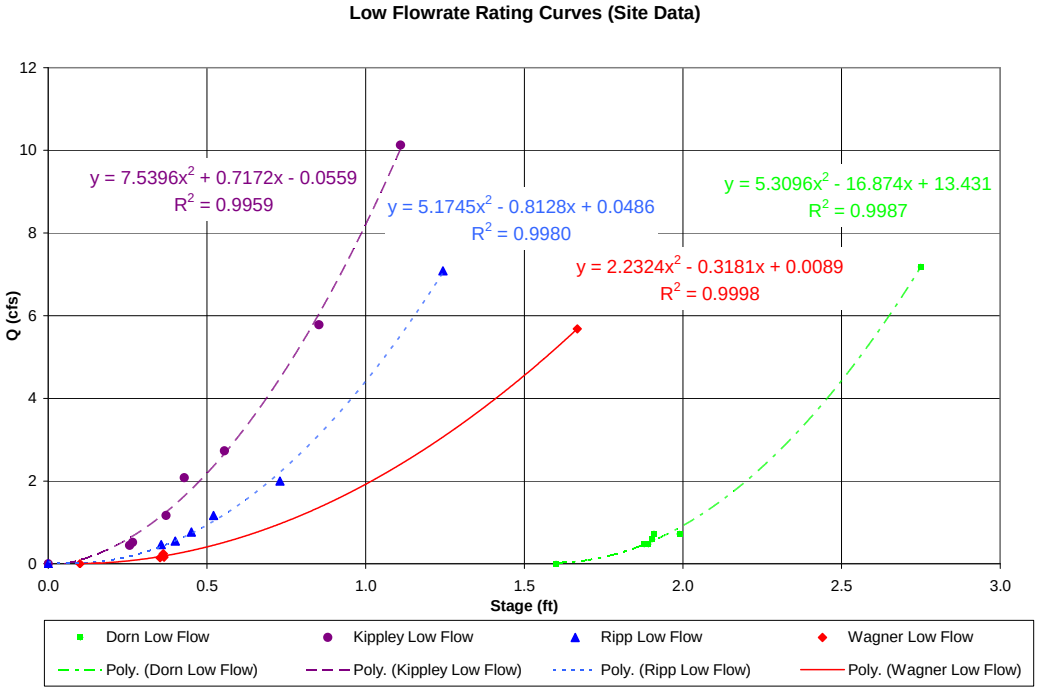

Figure 64: Site Observed Low Flowrate Rating Curves for Sites

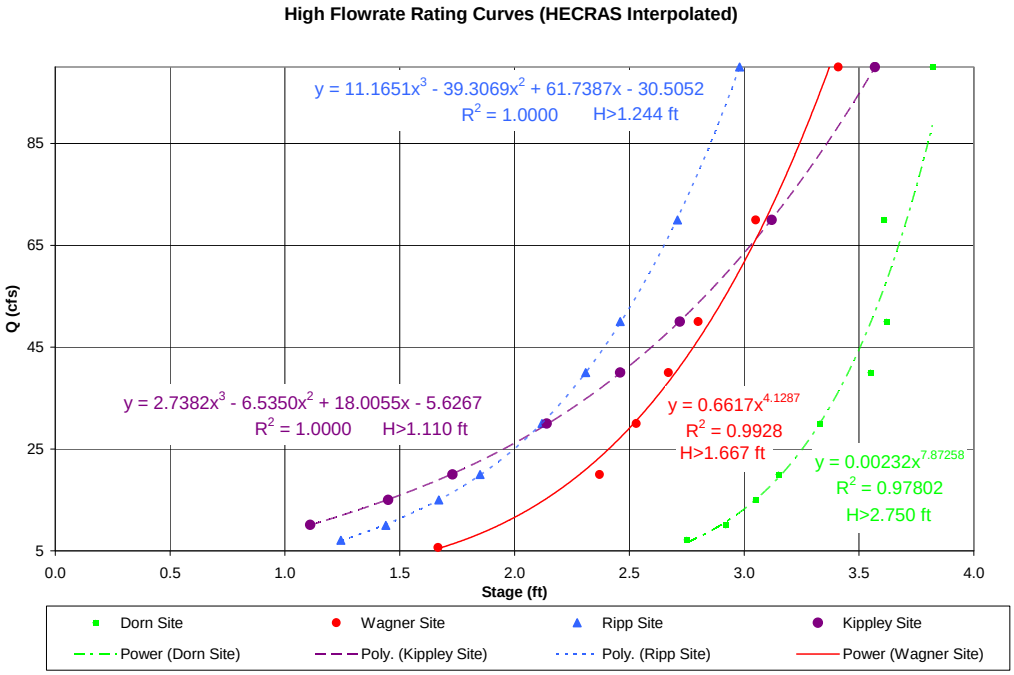

Figure 65: HECRAS Developed Rating Curves for High Flowrates

There are some limitations to using the rating curve method to determine flow. Most notably, it assumes a unique relationship between stage and discharge. It has been shown that this relationship is not unique, but actually a hysteretic curve with increased discharge for the initial hydrograph rise and lowered discharge for the trailing hydrograph for the same stage (Vuuren 2000) and (Herschy 1995). It is typical to ignore these effects when determining a rating curve. This phenomenon was observed at the Kippley Gage at is discussed below in more detail in the discussion on observed velocities.

A further limitation to this method is changing stage-discharge relationship with time. It was observed that general baseflow levels in the wetland areas increased over the warmer months. Baseflow levels showed a steady and generally linear rise over the summer months. This rise was accounted for by subtracting out the rise in baseflow from when the rating curves were developed, and using that modified depth to calculate flowrate. At the Kippley Gaging station, this effect was not observed, and therefore corrections were not made to the stage for flowrate calculation.

0.4 Velocity Data

The velocity in the channel was monitored using an ECM velocity meter at the Kippley Gage Site. The velocity probe was located approximately 1.5 inches from the bed, and laterally at a location near the center of the channel. Transformation of the point velocity into an average velocity was accomplished by means of power law velocity profile complied by Gupta (1995), based on work of Dickenson (1967) and Daily and Harleman (1966).

$$\bar{V} = 0.88V_a\left(\frac{d}{a}\right)^{(1/7)}$$

Where V is the mean channel velocity, V_a is the measured velocity at point a, d it total water depth, and a is height of velocity measurement from the bed. This method is a good approximation of the average channel velocity. However, it assumes that the measured point is representative of the lateral velocity profile. Attempts were made to locate the velocity probe at a location of average lateral velocity, but errors may occur with changing depth as complex 3D flow patterns alter the velocities.

The results of the measured point velocity and average velocity obtained from the methods described above for the 2006 season are shown below.

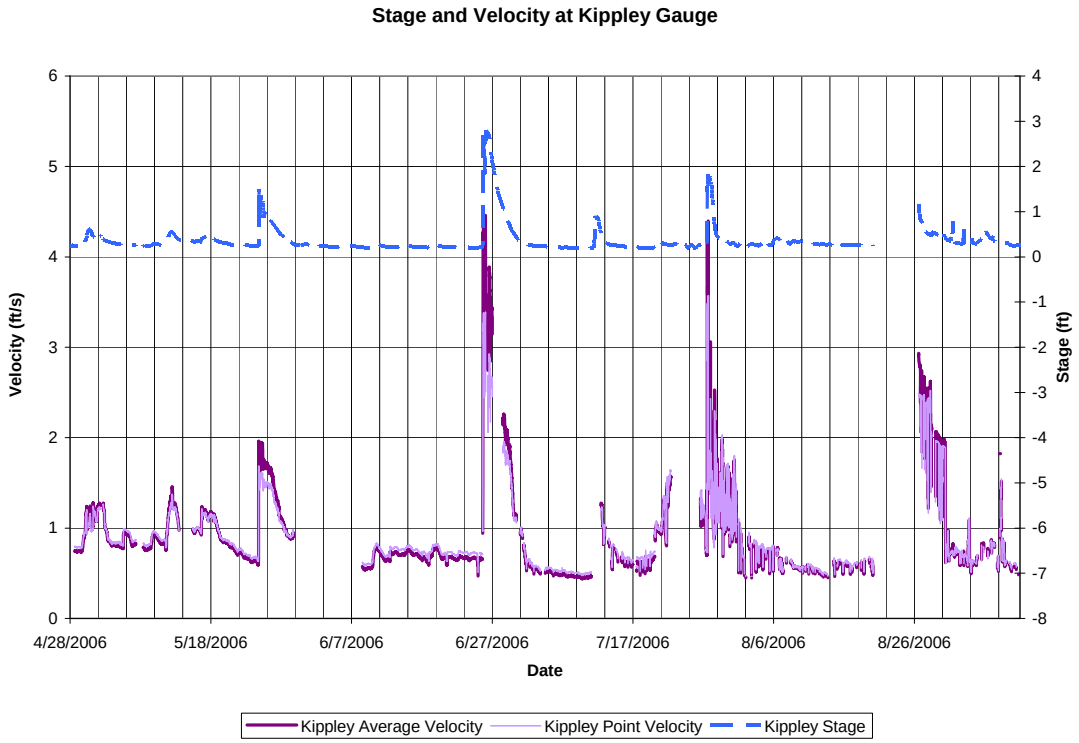

Figure 66: Stage and Velocity Data at Kippley Gage

The velocity data shown above shows a clear correlation between velocity and water depths. For the initial hydrograph, it has been well documented that there is a nonlinear behavior between stage and velocity between the hydrograph rise and fall. Shown below are several plots showing the initial hydrograph rise and hydrograph fall stage velocity relationship. It should be noted that the data points during the peak stages have been removed. This is due to a characteristic double peak at the site which does not clearly show the stage velocity relationship.

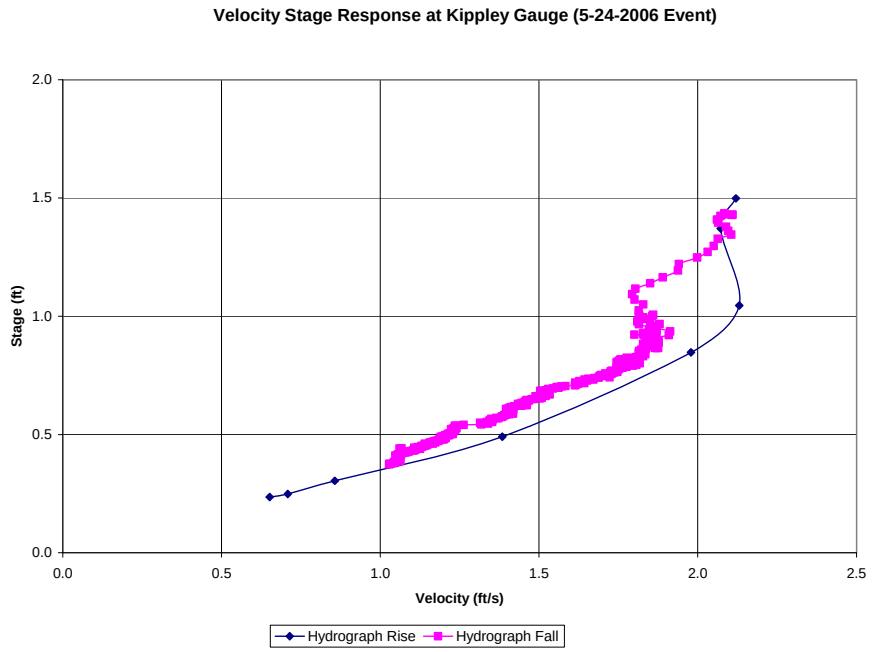

Figure 67: Velocity Stage Response at Kippley Gage for 5-24-2006 Event

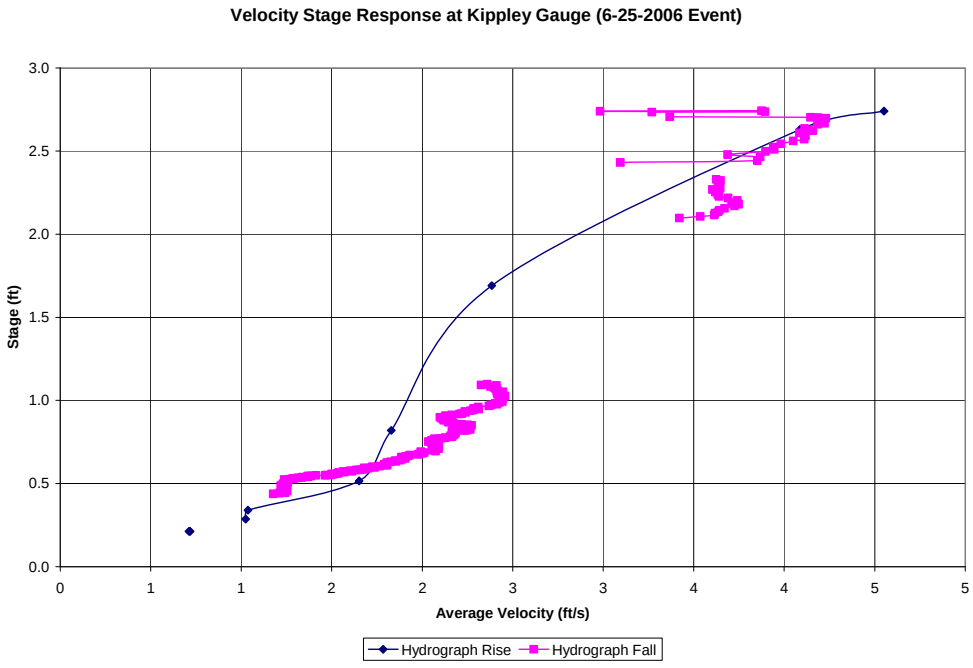

Figure 68: Velocity Stage Response at Kippley Gage for 6-25-2006 Event

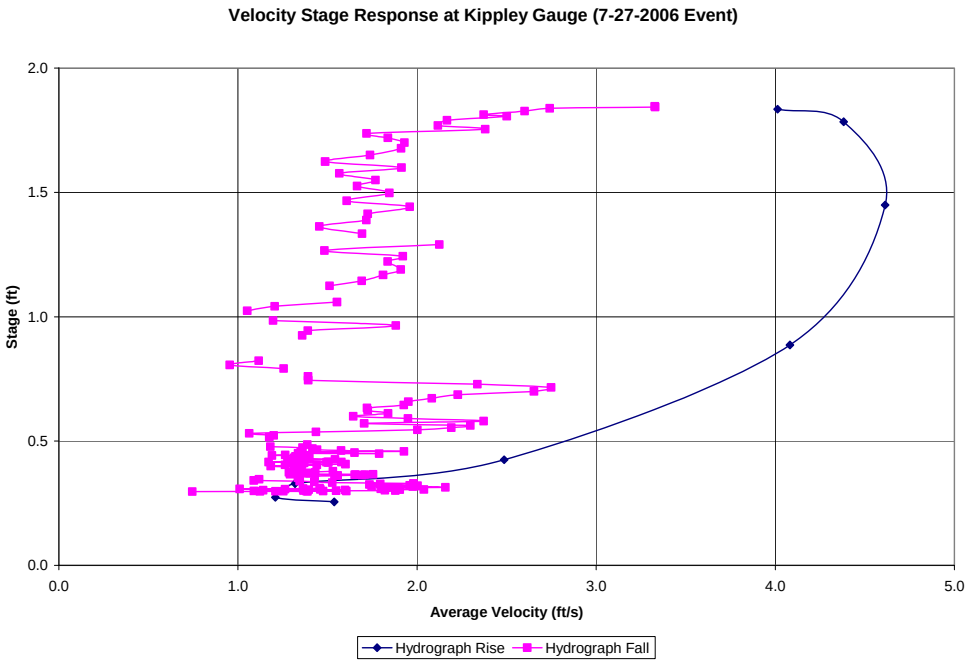

Figure 69: Velocity Stage Response at Kippley Gage for 7-27-2006 Event

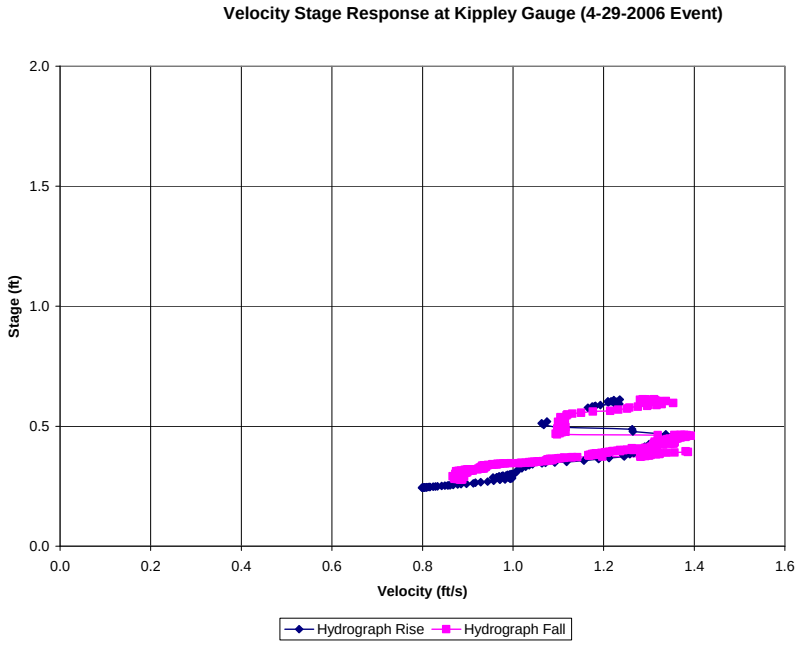

Figure 70: Velocity Stage Response at Kippley Gage for 4-29-2006 Event

In some cases, a clear hysteresis is observed in the velocity – stage relationship. This is especially true for the 5-24-2006 and 7-27-2006 events. For the other two events, there is no hysteresis observed. It is currently unclear how these relationships function, and could be a topic of further investigation.

0.5 Bed Shear and Roughness Data

The roughness of the channel was determined at the Kippley Gage using the average velocity relation described above. The Manning's roughness coefficient can be determined directly using the following relationship (Strum 2001).

$$n = \frac{1.49}{V} R^{(2/3)} S_0^{(1/2)}$$

Solving for the Manning's roughness coefficient at the Kippley site for the 2006 season yields Figure 71. Roughness values range between 0.022 and 0.092. However, this variability may be due to measurement error, and turbulent nonlinearities. A mean value for the entire 2006 season gives a value of 0.0508 with a standard deviation of 0.0114.

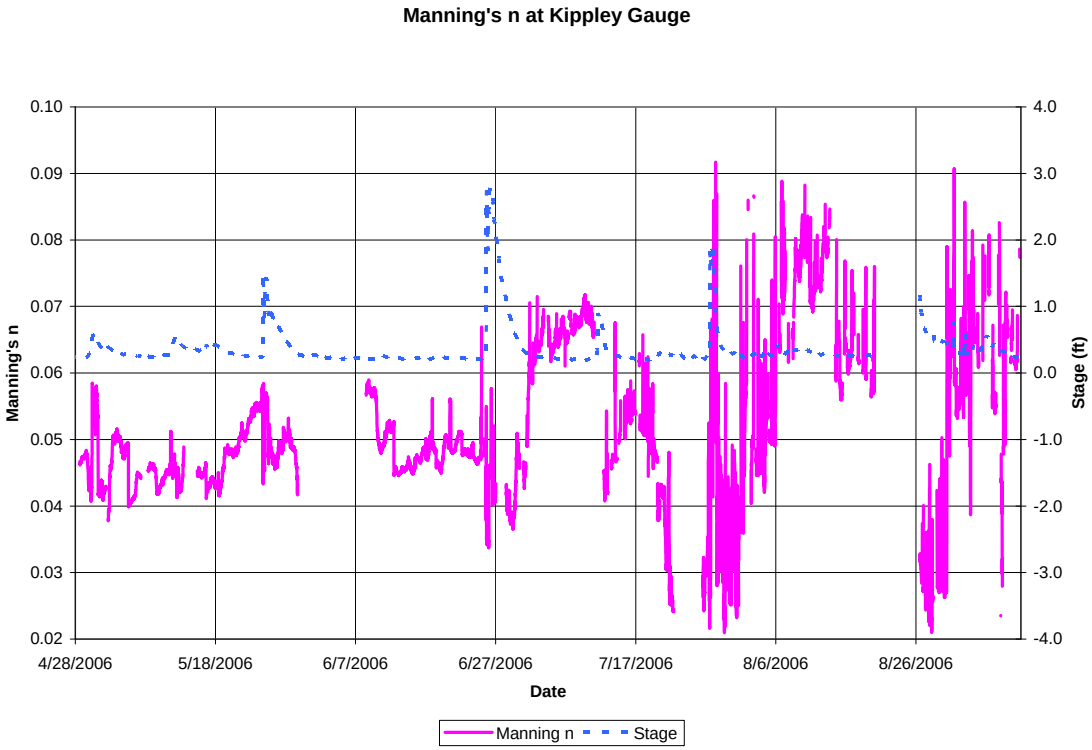

Figure 71: Manning's n Roughness Observed at the Kippley Gage for 2006 Season

Manning's n coefficient has been known to vary with depth (Strum 2001). A plot of Manning's n with depth is shown below for various storm events.

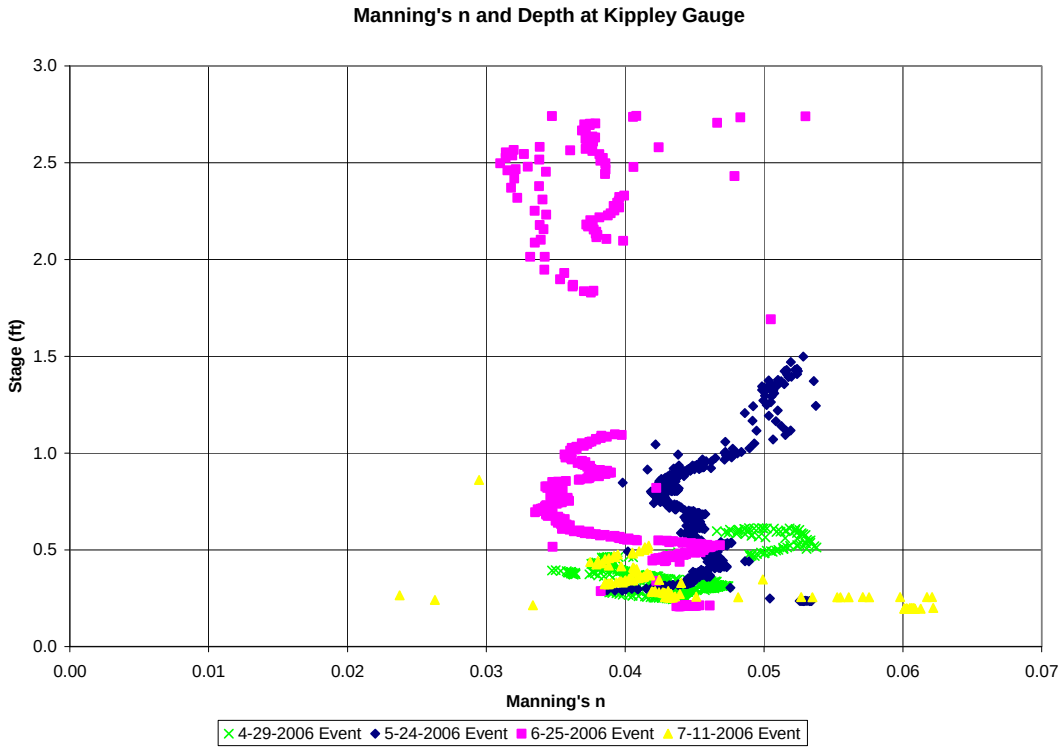

Figure 72: Manning's n Roughness and Depth for Various Storm Events at the Kippley Gage

As shown by Figure 72, there is less variability with the roughness coefficient than shown in Figure 71. There also does not appear to be a clear correlation between increasing Manning's n with depth.

The values of Manning's n obtained by this method (average 0.0508) are somewhat lower than those obtained by HECRAS calibration (0.061). There are probable reasons for this. Primarily, this technique involves transformation of a 1 dimensional point velocity to an average velocity for the entire cross section. There is some error in measurement and nonlinearities associated with this conversion, which are reflected in the relatively high standard deviation of 0.0114. Additionally, the 0.061 value for the HECRAS model is a calibration of the entire reach, which may be larger than the single cross section analyzed

here. Therefore the HECRAS Manning's n can be considered a composite value for the whole reach, and the direct measurement method is an approximate value for the Kippley Gage section.

0.6 References

Carter, R.W., and I.E. Anderson. 1963. "Accuracy of Current Meter Measurements. American Society of Civil Engineers Proceedings", Journal of Hydraulics Division 89: 105-115.

Chow, V.T., D.R. Maidment, and L.W. Mays. 1988. *Applied Hydrology*. New York: McGraw Hill, Inc.

Chow, V.T. 1959. *Open Channel Hydraulics*. New York: McGraw Hill, Inc.

Daily, J.W., and D.R. Harleman. 1966. Fluid Dynamics. Reading, Massachusetts: Addison-Wesley Publishing Company, Inc.

Dane County. 2006. "Dane County DCiMap". Dane County (WI) Land Information Office. http://dcimap.co.dane.wi.us/dcimap/index.htm.

Dickenson, W.T. 1967. Accuracy of Discharge Determinations. Hydrology Paper 20, Colorado State University, Fort Collins CO

Gupta, R.S. 1995. *Hydrology and Hydraulic Systems*. Prospect Heights, Illinois: Waveland Press, Inc.

Haan, C.T., B.J. Barfield, and J.C. Hayes. 1994. *Design Hydrology and Sedimentology for Small Catchments*. New York: Academic Press.

Herschy, R. 1995. *Streamflow Measurement, 2nd Edition.* Cambridge, UK: E&FN SPON.

Hughes, D.A. 1979. Floodplain Inundation: Processes and Relationships with Channel Discharge. Earth Surface Processes: 5, 297–304, 1980.

Krause, A.F. 1999. Modeling the Flood Hydrology of Wetlands using HEC-HMS. MS Thesis. University of California Davis.

Strum, T.W. 2001. *Open Channel Hydraulics*. New York: McGraw Hill, Inc.

US Army Corps of Engineers (USACE). 2006. HEC-RAS Introduction. USACE, Hydraulic Engineering Center. http://www.hec.usace.army.mil/software/hec-ras/hecras-hecras.html.

USACE. 2002. *HEC-RAS Hydraulic Reference Manual v.3.1*. Davis, California: USACE Hydrologic Engineering Center.

USACE 2002. *HECRAS User's Manual v.3.1.* Davis, California: USACE Hydrologic Engineering Center.

Vuuren, W.E. 2000. A Generalised Concept for Stage-Discharge Rating Curves for the Rhine and Meuse in Holland. Arnhem, The Netherlands.

APPENDIX D – ADDITIONAL HYDROLOGIC DATA

D.1 Overview

This appendix contains additional hydrologic data not presented in Section 4 of this report.

0.2 Watersheds

The Dorn Creek Watershed above the gaging stations is composed of 5 major watersheds as shown in Figure 73, and are named A through E. These watershed delineations were based on USGS mapping (USGS1983). Four of the watersheds were positioned so that their outlet is located at one of the four gaging stations. The impervious area of the watersheds was determined using aerial orthophotos (Dane County 2006). A summary of the area and percent impervious area is shown in Table 16. Additionally, the flow length and elevation change for each watershed is shown.

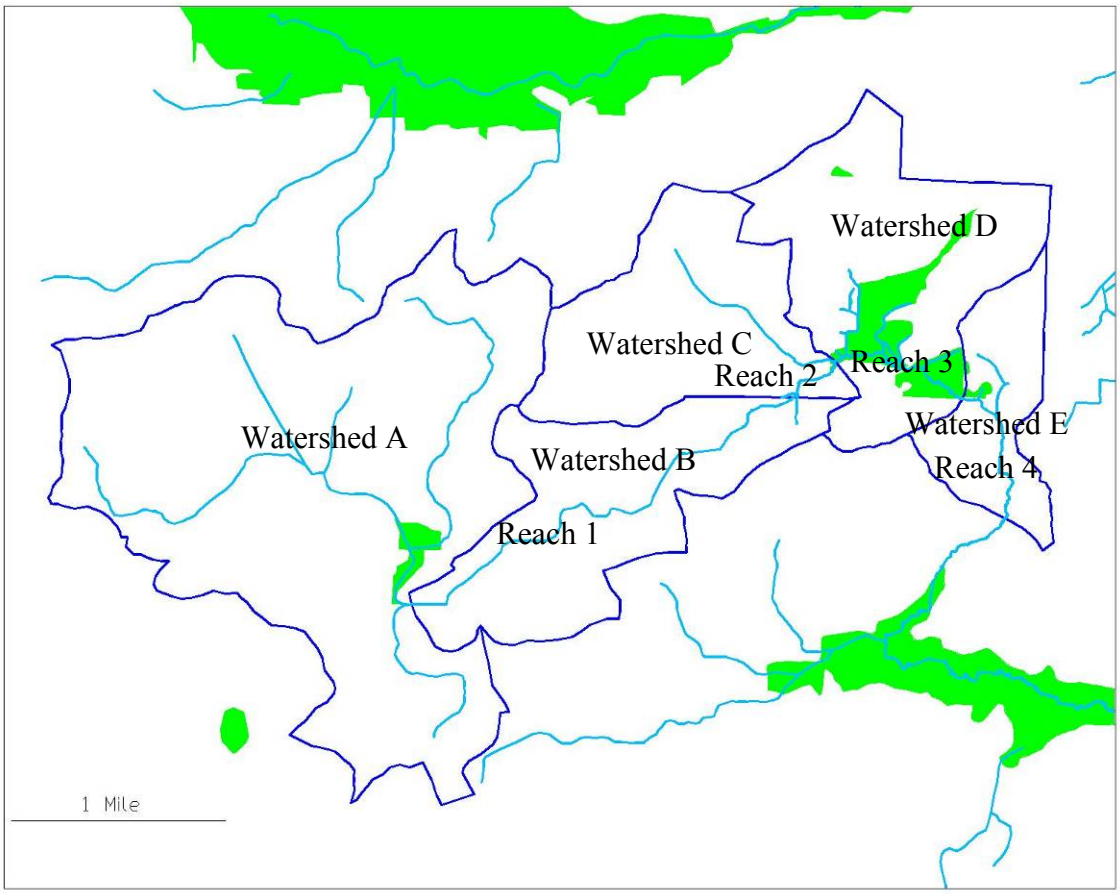

Figure 73: Watersheds and Major Reaches of Upper Dorn Creek Basin

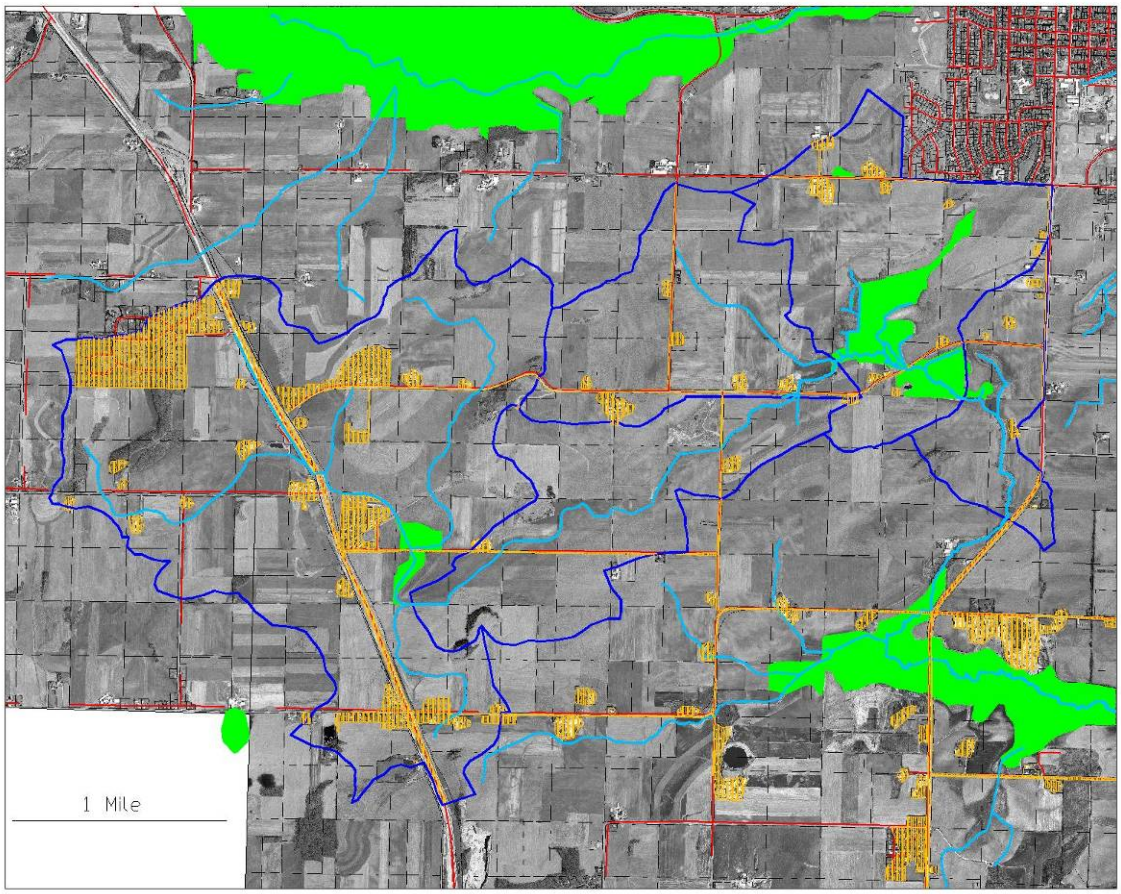

Figure 74: Watershed Map of Upper Dorn Creek Showing Impervious Area (yellow hatching)

Watershed	Area (mi^2)	% Impervious	Flow Length (mi)	Elevation Change (ft)
A	3.393	7.04	2.691	190.0
B	1.104	0.98	2.392	40.1
C	0.988	2.62	1.376	142.8
D	1.247	1.91	2.198	120.6
E	0.459	2.18	1.461	77.0

Table 16: Watershed Characteristic Summary

General information was gathered for the flow reaches within the watershed. The following is a general summary of these characteristics. Slopes were determined by the total elevation drop within the reach.

Reach	Length (mi)	Elevation Change (ft)	Slope (ft/ft)	General Description
1	2.345	40.05	0.003235	Grass-lined excavated channel, soil is primarily silt-loam.
2	0.284	2.73	0.001824	Small incised main channel surrounded by floodplain, with silt-clay sediment bottom
3	0.882	7.77	0.001668	Wetland reach, wide and shallow, with silt-clay sediment bottom
4	0.776	16.4	0.004005	Deeply incised channel with hard clay and sand bottom and boulder groups

Table 17: Reach Characteristic Summary

0.3 Hydrologic Data

As stated previously, gaging stations were placed at four locations within the watershed. The gages were located to give a better understanding of the hydrologic function of the wetland and surrounding stream reaches. Analysis of the observed hydrology at the site will be comprised of three primary topics, hydrogeology, meteorology, and stormflow.

0.3.1 Hydrogeology (Baseflow)

Although not specifically the topic of this investigation, the hydrogeology of the site plays an important role in the function of the wetland and system as a whole. Measurement of the baseflow at the gaging stations was accomplished by the use of rating curves as described in the hydraulics section. There were several difficulties in measurement of the baseflow. Primarily, a general rise in water levels was observed

throughout the season in the wetland areas. The following Figure 75 illustrates this phenomenon.

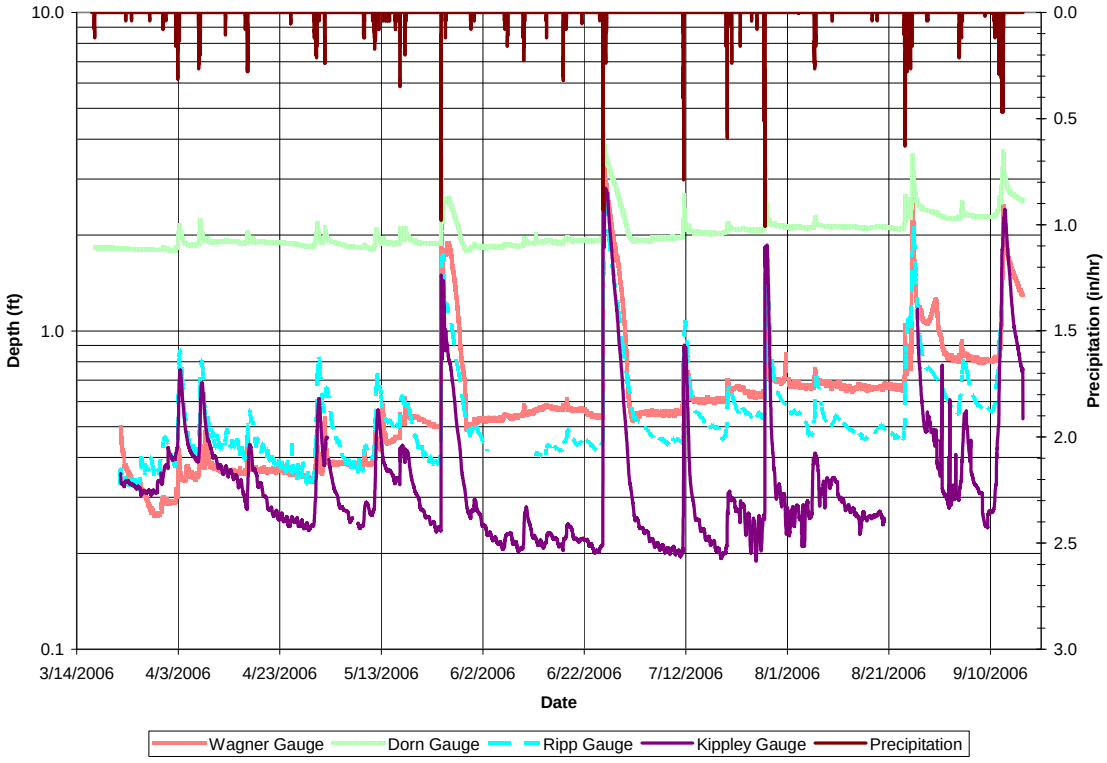

Figure 75: Water Levels for 2006 Season Showing Baseflow Rise for 3 Sites

The reason for this baseflow rise is probably due to increased roughness due to vegetation growth. This phenomenon was observed in the wetland areas (Wager, Dorn, and Ripp Gages). This baseflow rise leads to complications in calculating flowarate for the baseflow conditions. To reduce some of this error, baseflow rise curves were developed as a function of time, and are shown below. This rise was subtracted out from the water levels for flow calculations.

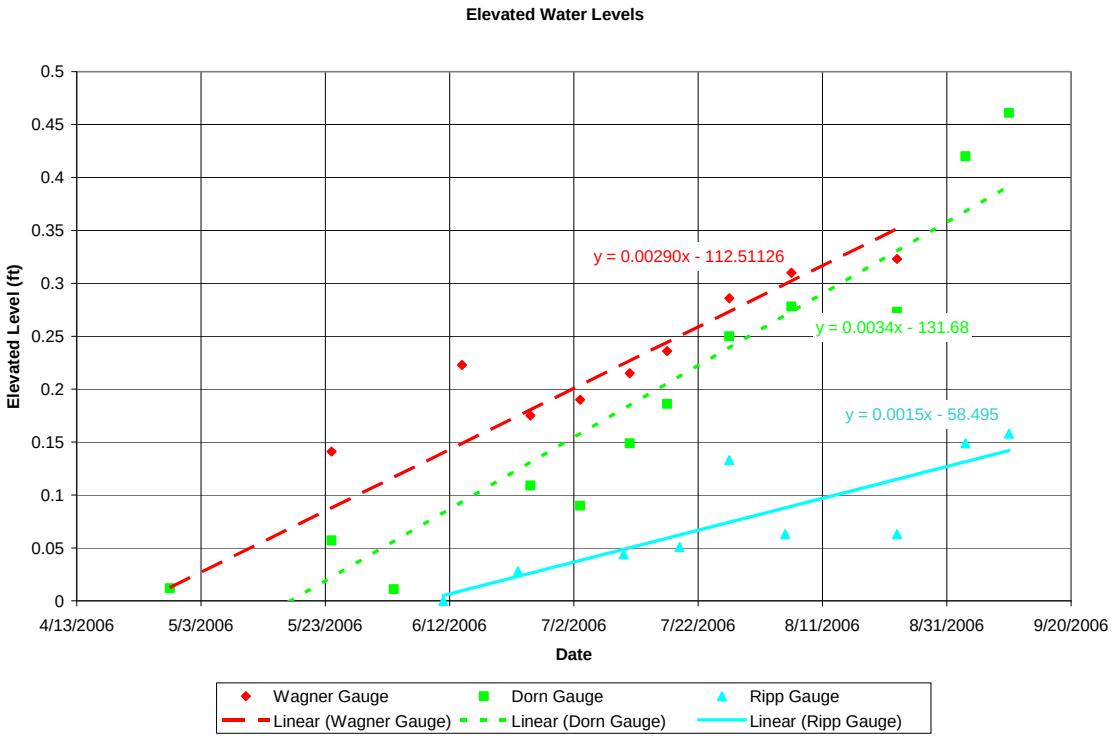

Figure 76: Elevated Base Water Levels During 2006 Season

These results indicate a general steady rise in base water level conditions. The upper wetland area experienced a 0.45 foot increase in water levels from early May to late September. The lower wetland area experienced a 0.15 foot increase in water levels from early June to late September. This data illustrates the effects of seasonal changes in the Wetland areas, and the difficulty in conversion of stage to flow in these areas.

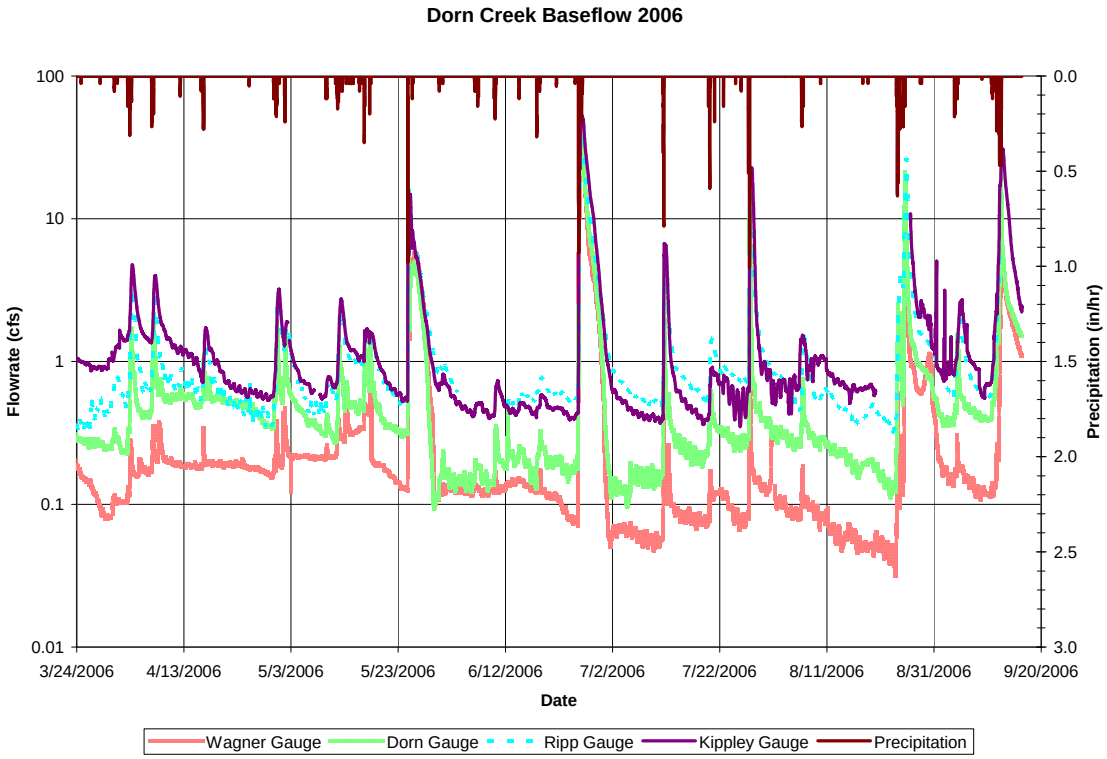

Figure 77: Dorn Creek Flow for 2006 Season

Based on the flow data shown above, the following conclusions can be drawn about the baseflow of the system. Baseflow for the Wager Gage results from a groundwater spring just upstream of the gage. The main channel upstream of this spring shows no baseflow and therefore is probably a groundwater recharge area. Baseflow between the Wager Gage and Ripp Gage, which encompasses the wetland area, shows strong baseflow increases. This indicates groundwater discharge in these areas. In the reach below the wetland, baseflow is generally increasing in small rates, indicating a small amount of groundwater discharge in this area. These locations are indicated in Figure 78.

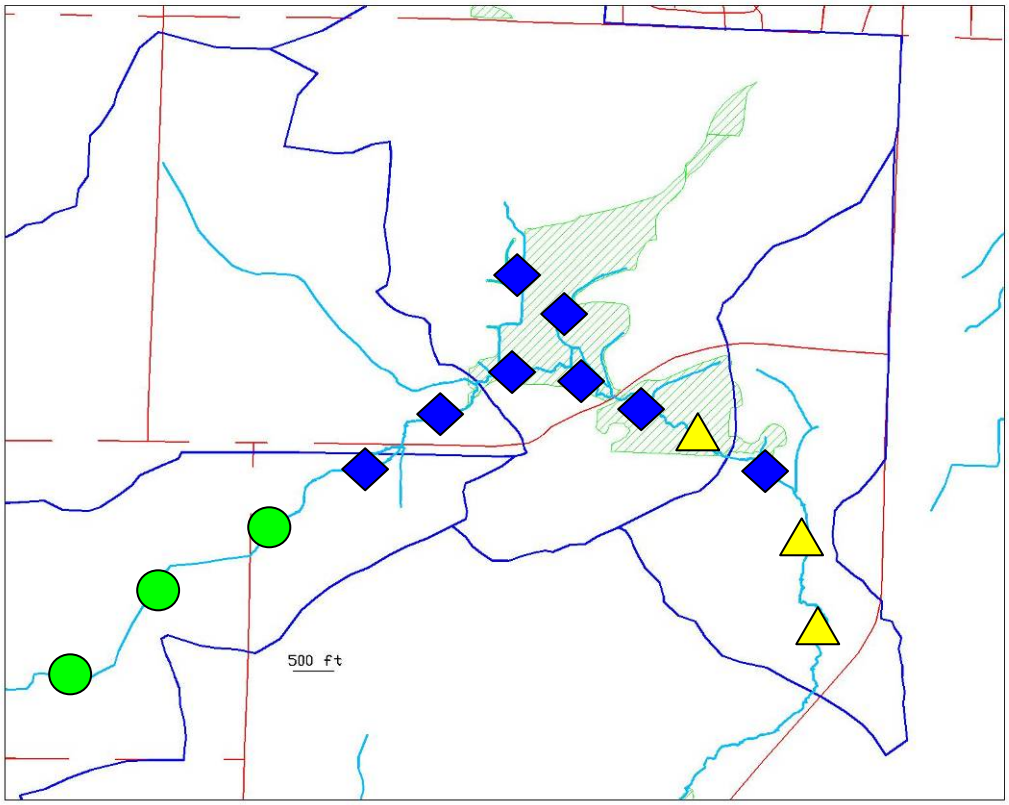

Figure 78: Probable Groundwater Discharge (Diamonds), Recharge (Circles), and No Effect (Triangles) areas of Dorn Creek

0.3.2 Metrologic Data

The meteorological data were obtained primarily through a weather station that it part of the Weather Underground (WU 2006) monitoring system. The 2006 season had many strong precipitation events. There was also a good variation between short, high intensity events, and longer low intensity events. Table 18 is a summary of the major storm events that occurred in the 2006 season. Average intensity and maximum intensity are rated according to the mean values for the 2006 season in terms of high or low. Duration of the event is rated according to the mean values for the 2006 season in terms of short or long.

The precipitation data were compared to three other weather station gages in the near area. The inverse distance weighted precipitation and Theissen polygon weighted values using this method did not vary significantly from the precipitation data from the KWAUNA1 Gage.

Name	Approx Date	Tot Precip (in)	Duration (hr)	Avg i (in/hr)	Max i (in/hr)	Avg i	Max i	Duration	Days since Last Rain	Conditions
1	3-Apr	1.14	18.8	0.061	0.35	low	low	long	15	dry
2	7-Apr	1.15	10.1	0.114	0.28	low	low	short	4	wet
3	16-Apr	0.79	13.3	0.059	0.31	low	low	short	9	wet
3.5	30-Apr	1.34	26.7	0.050	0.24	low	low	long	14	dry
4	11-May	1.18	31.1	0.038	0.20	low	low	long	11	dry
5	24-May	1.18	1.3	0.932	0.98	high	high	short	7	wet
6	25-Jun	2.48	4.6	0.541	0.94	high	high	short	16	dry
7	11-Jul	2.13	7.5	0.283	0.79	high	high	short	16	dry
8	27-Jul	1.02	1.8	0.577	1.02	high	high	short	7	wet
9	23-Aug	3.58	39.8	0.090	0.63	low	high	long	17	dry
10	12-Sep	2.46	46.1	0.053	0.47	low	low	long	6	wet

Table 18: Metrologic Storm Event Data for 2006 Season

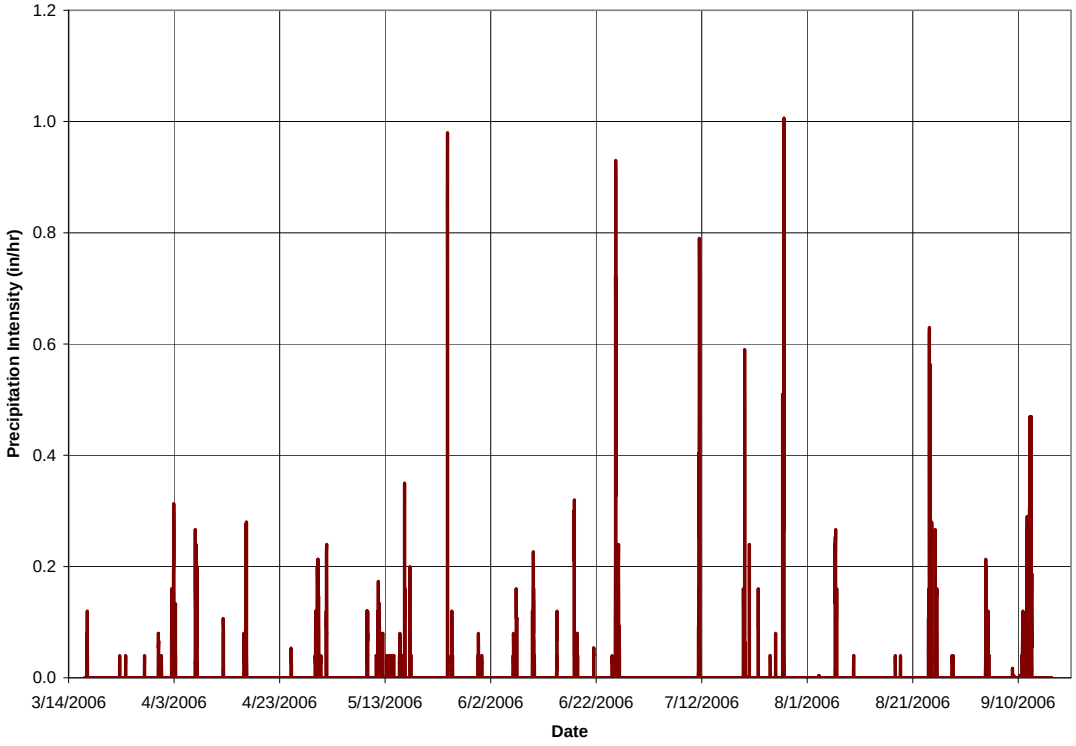

Figure 79: Precipitation Intensity for 2006 Season

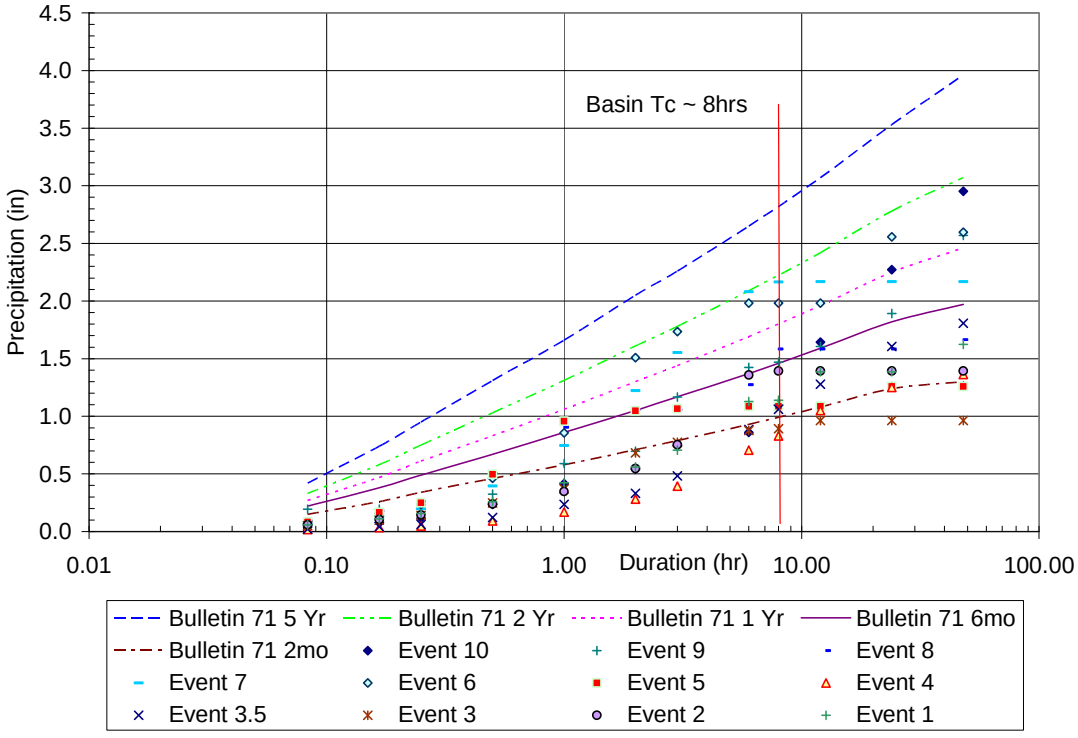

Figure 80: Rainfall Frequency Analysis of 2006 Record Compared to Bulletin 71 Data (Huff and Angel 1992)

The frequency of the observed rainfall events was analyzed by taking the maximum precipitation for each event in various time intervals of 5 minutes to 48 hours. These results are shown above with published values from Huff and Angel (1992). The basin has an approximate time of concentration of 8 hours, and therefore analysis of the recurrence interval for each storm event was performed based on this duration. This analysis indicated that Event 6 had approximately a 1.5 year recurrence interval.

Additional analysis comparing regression equations determined by Walker and Krug (2003), and observed flowrate at the Dorn Gage, indicated that Event 6 was a 1-2 year recurrence event. The following data were determined for the Dorn Gaging Station.

Recurrence (yr)	Q (cfs)
2	155
5	224
10	284
25	362
50	420
100	480

Table 19: Frequency Analysis at Dorn Gage (Walker and Krug 2003)

Historical monthly precipitation from 1948 to 2005 (NCDC 2006) was compared to the 2006 observed precipitation. Based on these results, the time period of measurement all months except March and September were statistically wetter than average. Additional data for 2003-2006 is presented below for correlation to E. Murdoc (2006) results.

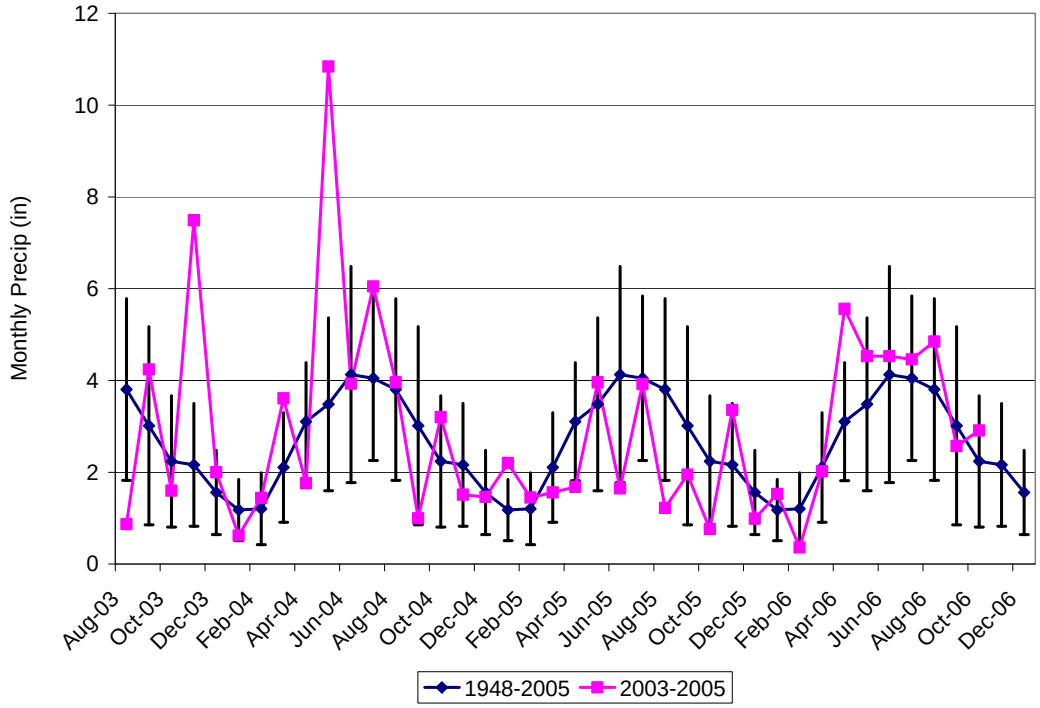

Figure 81: Comparison of Observed Monthly Precipitation to Historical Average 2003-2006

Month	Observed Precip (in)	Rank of 1948-2005	Quantile	Est Return Interval (yrs)	Average Precip (1948-2005)	Standard Deviation 1948-2005 (in)
Jan-06	1.53	18	0.30	3.3	1.18	0.67
Feb-06	0.36	51	0.85	1.2	1.21	0.78
Mar-06	2.02	29	0.48	2.1	2.11	1.19
Apr-06	5.56	3	0.05	20.0	3.10	1.29
May-06	4.53	12	0.20	5.0	3.48	1.88
Jun-06	4.53	22	0.37	2.7	4.13	2.35
Jul-06	4.46	19	0.32	3.2	4.05	1.79
Aug-06	4.85	19	0.32	3.2	3.80	1.98
Sep-06	2.57	29	0.48	2.1	3.02	2.16
Oct-06	2.91	17	0.28	3.5	2.24	1.43

Table 20: Comparison of Observed and Historical Monthly Rainfall for 2006

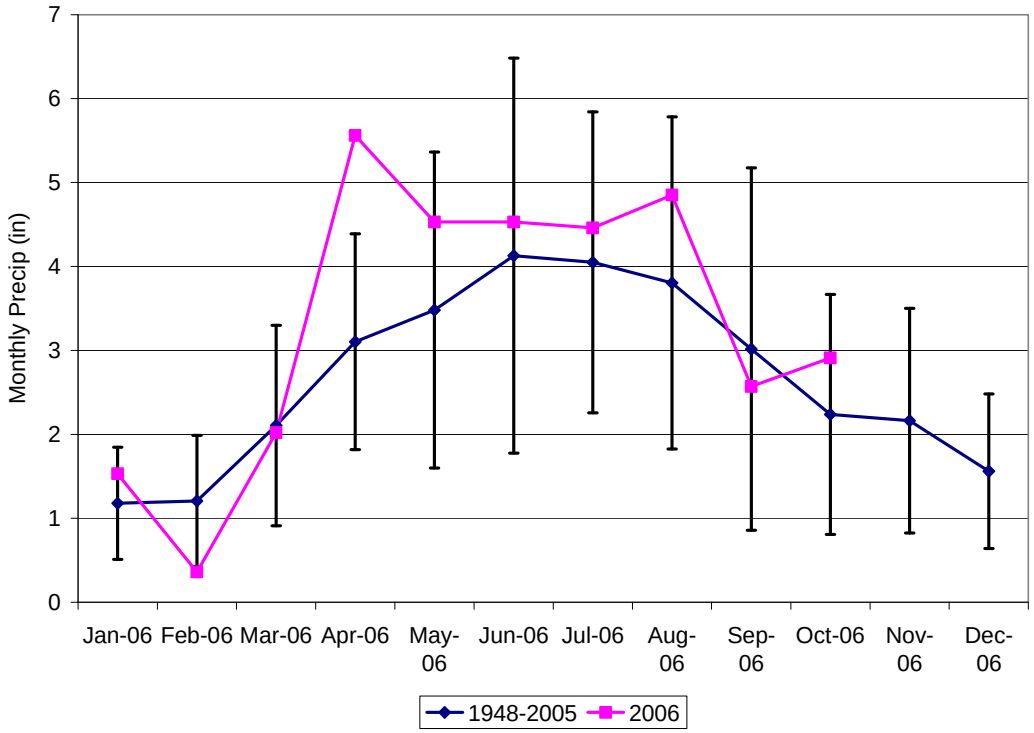

Figure 82: Comparison of Observed Monthly Precipitation to Historical Average 2006

0.3.3 Storm Hydrographs

The complete hydrographs from the 2006 season are presented in this section. Additionally, previous data collected by Even Murdoc (2006) is presented here for the 2003-2005 seasons. This data is added for a more complete hydrologic record. E. Murdoc states that his rating curve at the Kippley Gage is not accurate above the measured values of about 10 cfs. Analysis of this rating curve by using a combination of 2006 field measured data and HECRAS modeling, indicated that the two rating curves are similar below about 10 cfs. However, above 10 cfs, E. Murdoc's rating curve highly

over predicts flowrates. Conversion to a more accurate peak flowrate for high event flows was conducted for this report, and is listed on E. Murdoc's original figures.

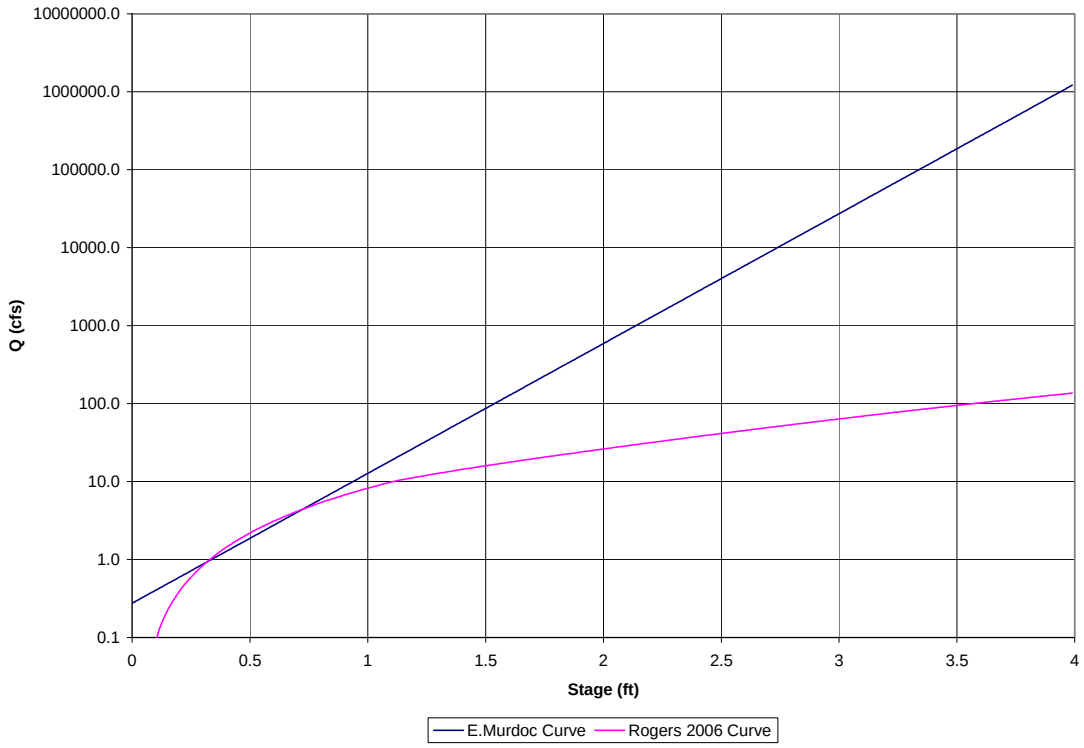

Figure 83: Comparison of E. Murdoc and Rogers 2006 Rating Curves

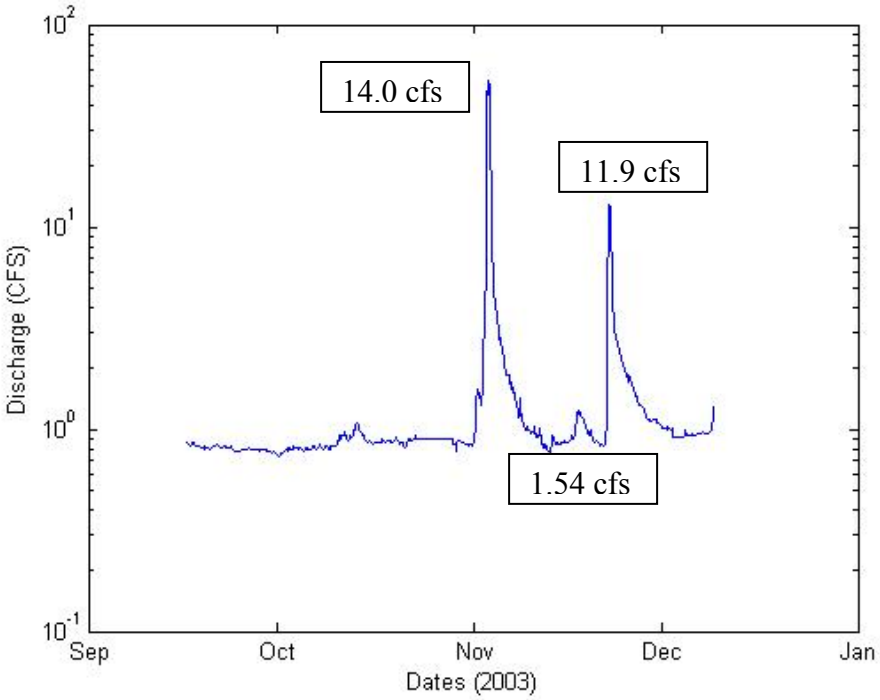

Figure 84: Complete discharge record for 2003 at Kippley Gage (Murdoc 2006)

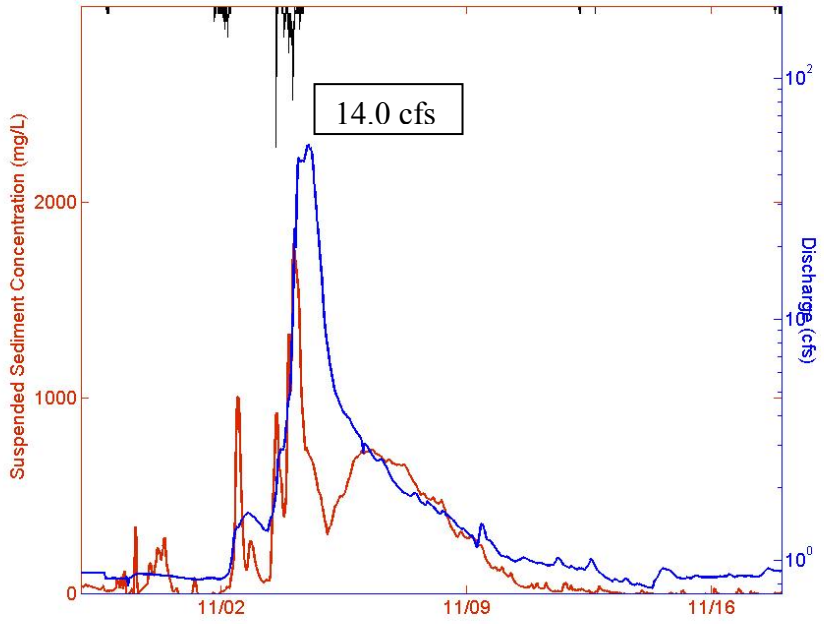

Figure 85: Discharge and SSC response to a 2.83 inch (7.2 cm) rainfall event in November, 2003 at Kippley Gage (Murdoc 2006)

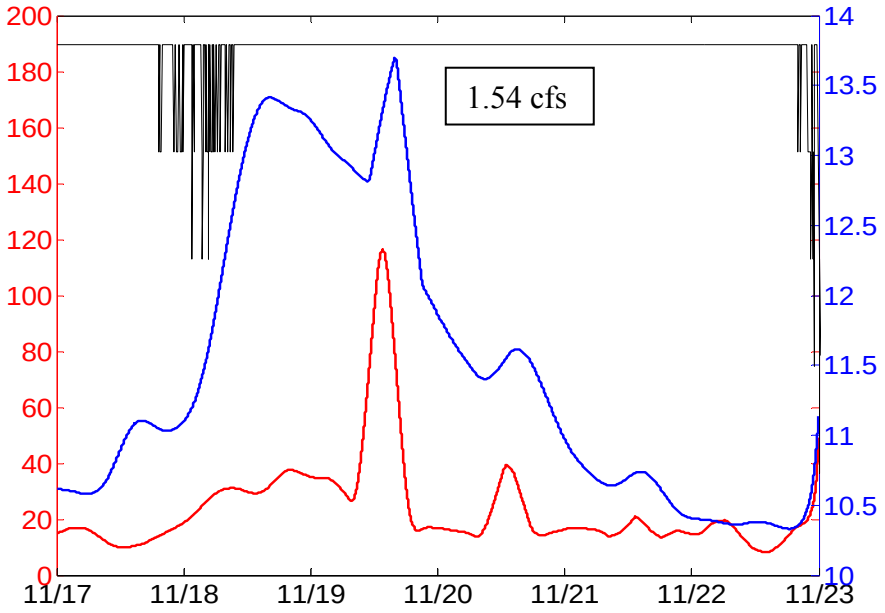

Figure 86: Small Event in November 2003 at Kippley Gage (2003). SSC (mg/l) on left scale and depth (cm) on the right scale

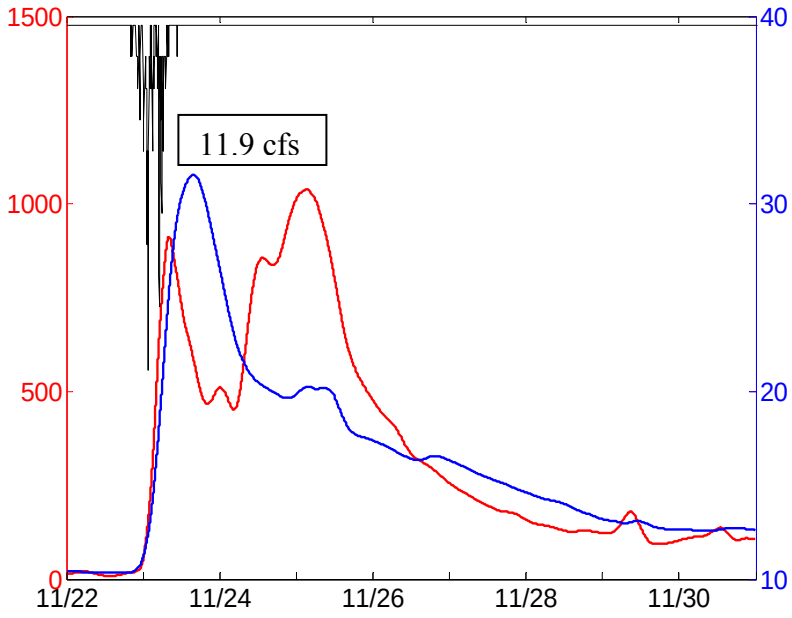

Figure 87: Discharge and SSC response to a 2.10 inch (5.3 cm) rainfall event in November, 2003 at Kippley Gage (Murdoc 2006)

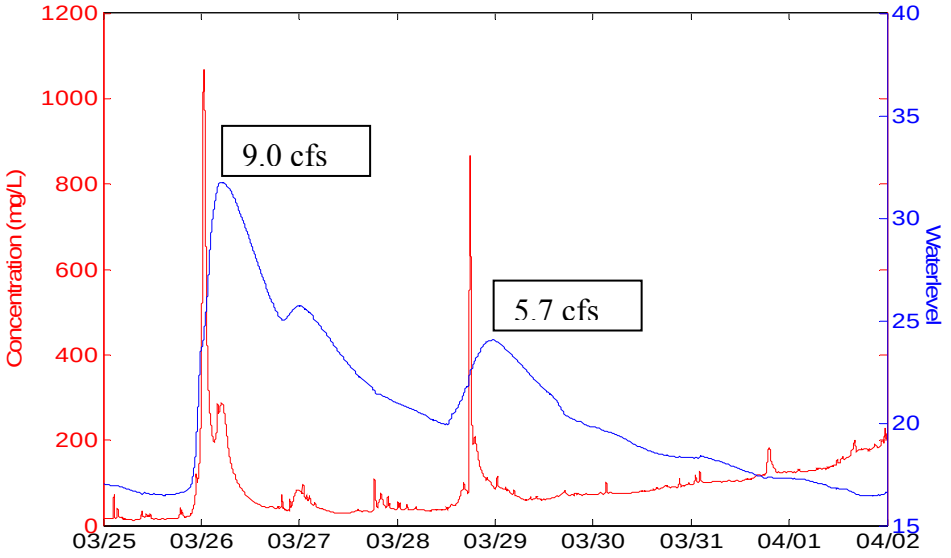

Figure 88: Response for March 2004 Events at Kippley Gage. Water level units are cm (Murdoc 2006)

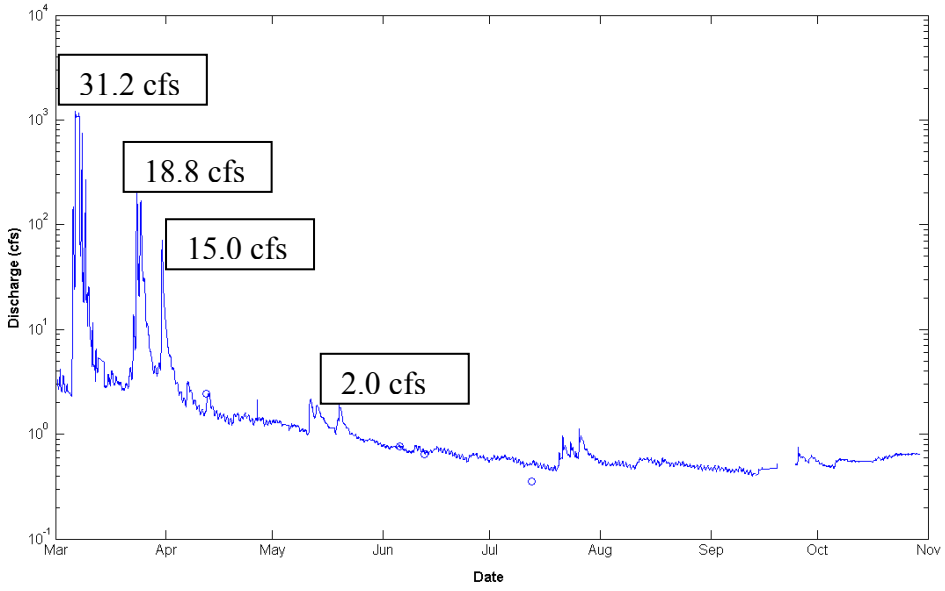

Figure 89: Calculated Discharge for the 2005 Field Season at Kippley Gage. Small circles show independent measurements of discharge. (Murdoc 2006)

The following figures and tables are data collected from 2006 season.

Event	Peak Flowrate (ft^3/s)				Stormflow Volume (ac-ft)			
	Wagner Gage	Dorn Gage	Ripp Gage	Kippley Gage	Wagner Gage	Dorn Gage	Ripp Gage	Kippley Gage
1	0.28	1.72	3.27	4.77	0.274	1.977	5.512	6.557
2	0.37	2.16	2.77	4.01	0.408	1.730	3.959	6.087
3	0.34	1.11	1.24	1.72	0.058	0.458	1.372	2.119
3.5	0.47	1.92	3.08	3.21	0.404	2.424	6.648	6.800
4	0.59	1.31	2.27	2.74	0.469	1.955	4.208	4.935
5	47.27*	71.46	17.13	15.89	30.996	31.198	36.395	36.216
6	134.02*	127.34	50.94	53.66*	116.140	122.343	123.591	137.82*
7	0.54	3.88	4.53	6.71	0.369	2.297	7.580	10.200
8	2.46	21.77	14.62	22.86	0.854	5.908	17.438	20.27*
9	15.30	21.35	26.66	30.00*	10.099	16.981	38.868	NA
10	10.58	23.07	27.00*	30.77	13.750	18.949	NA	30.00*

Table 21: Maximum Observed Flowrates and Storm Volume for 2006 Season Events. (*) Values were not directly measured. Interpolated values based on nearby Gage data, site data, and maximum flood stage

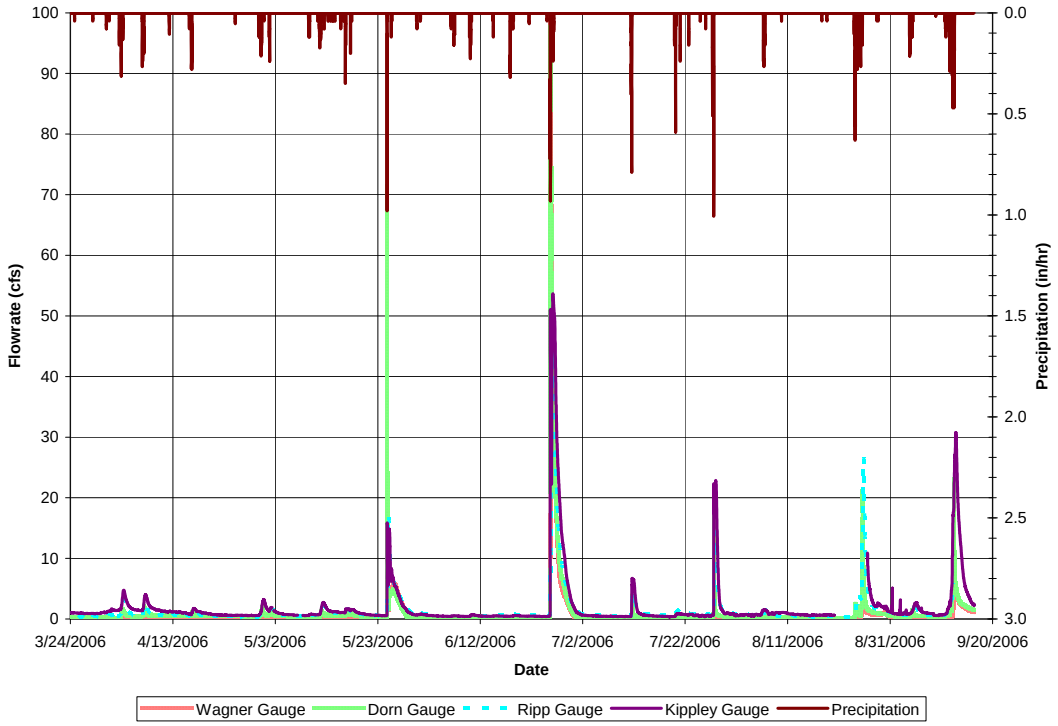

Figure 90: 2006 Season Summary

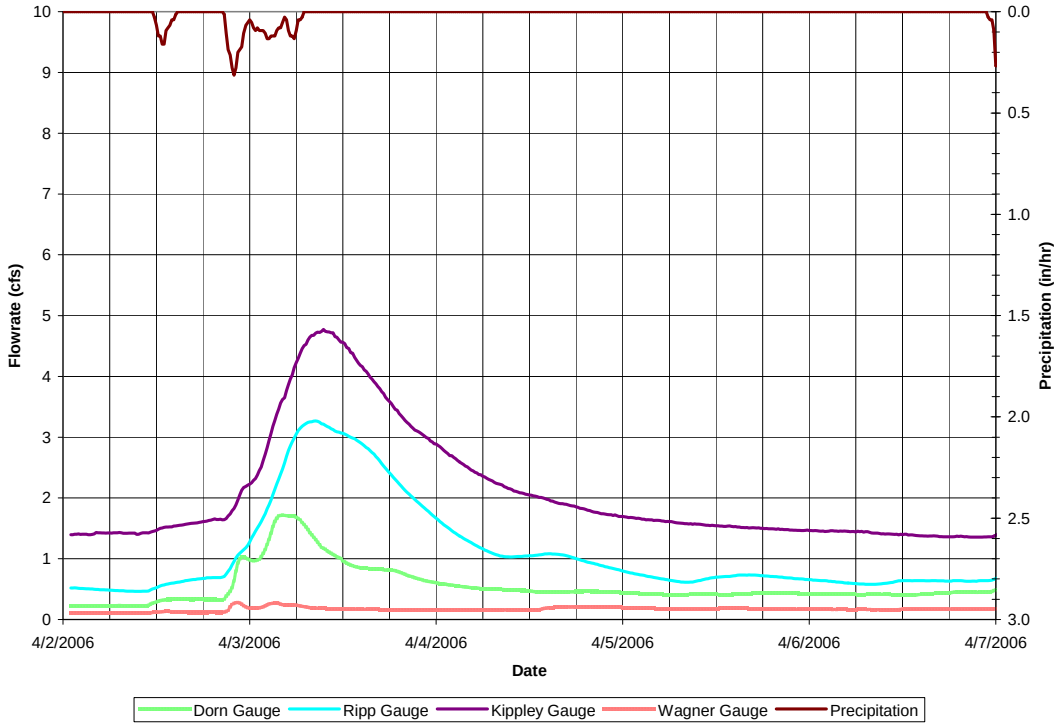

Figure 91: Event 1 Hydrograph

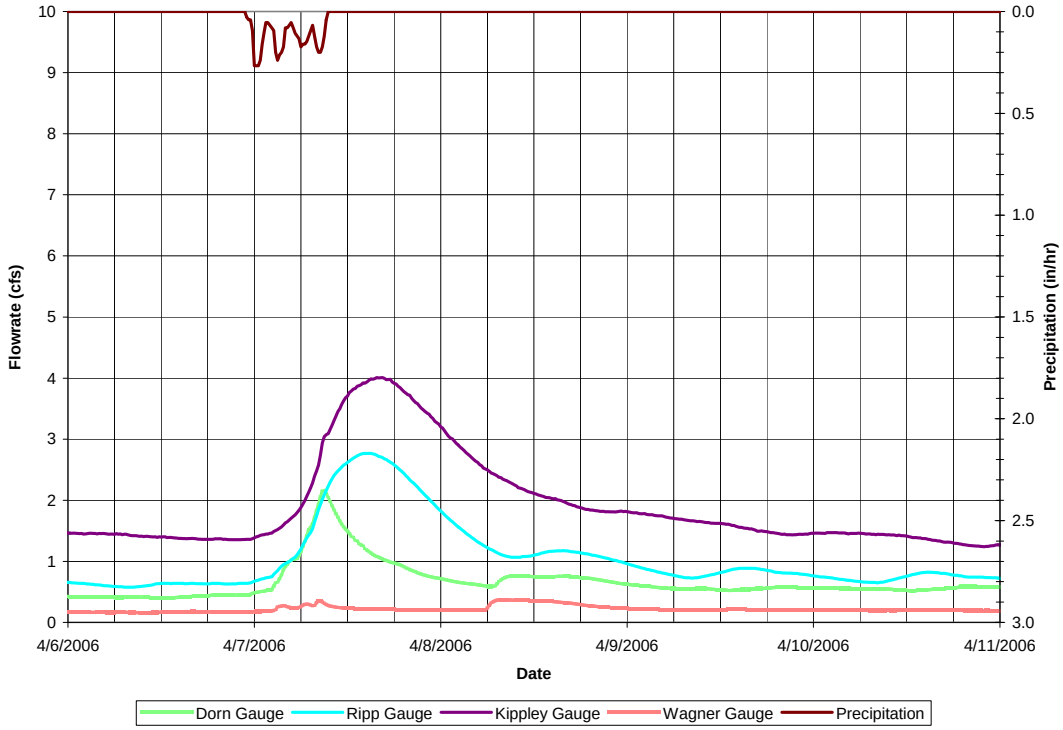

Figure 92: Event 2 Hydrograph

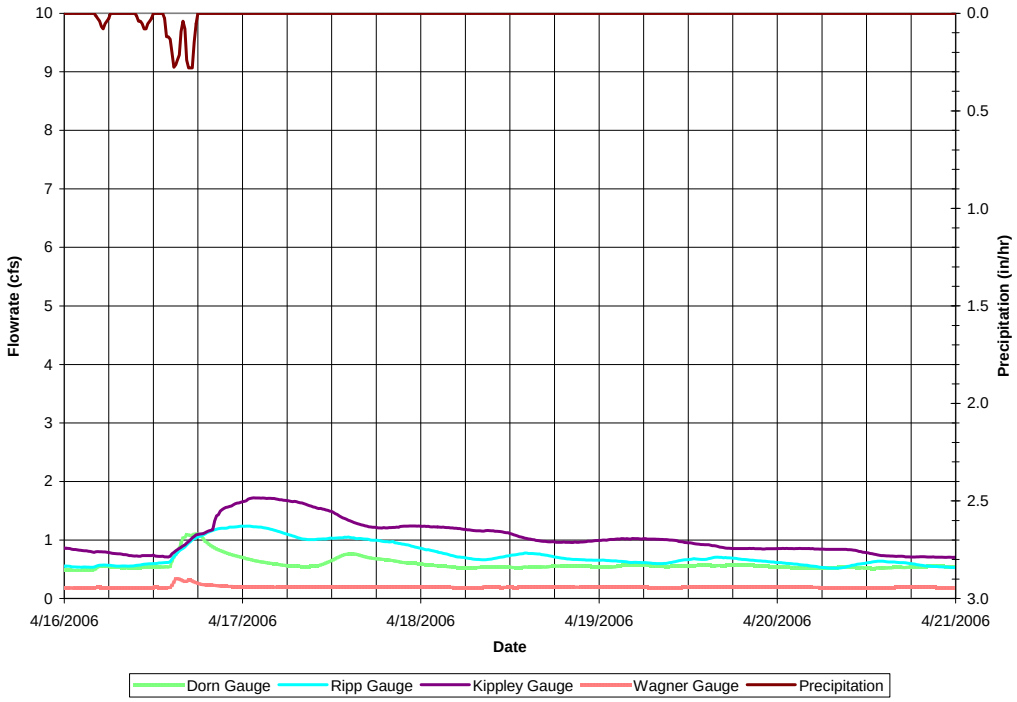

Figure 93: Event 3 Hydrograph

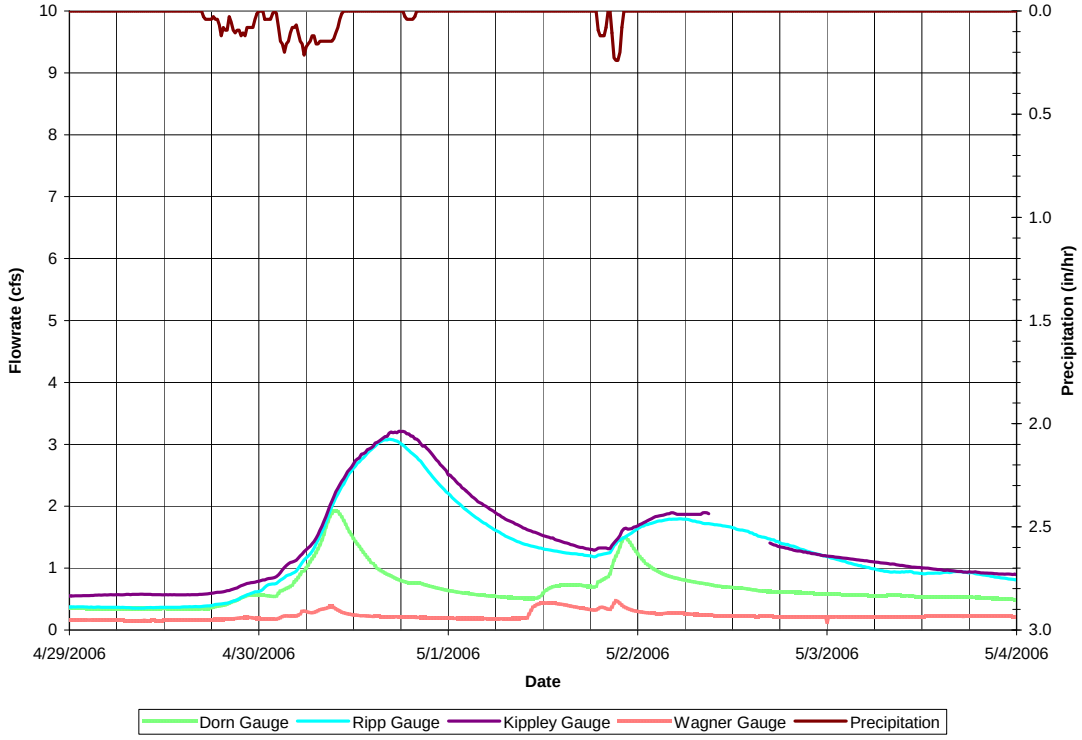

Figure 94: Event 3.5 Hydrograph

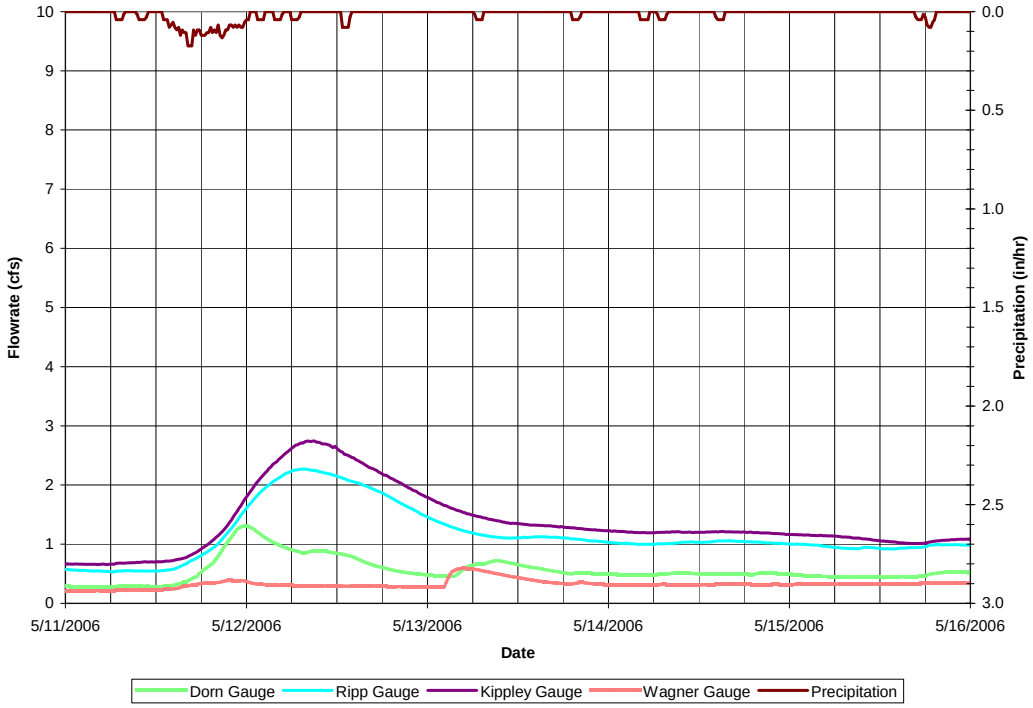

Figure 95: Event 4 Hydrograph

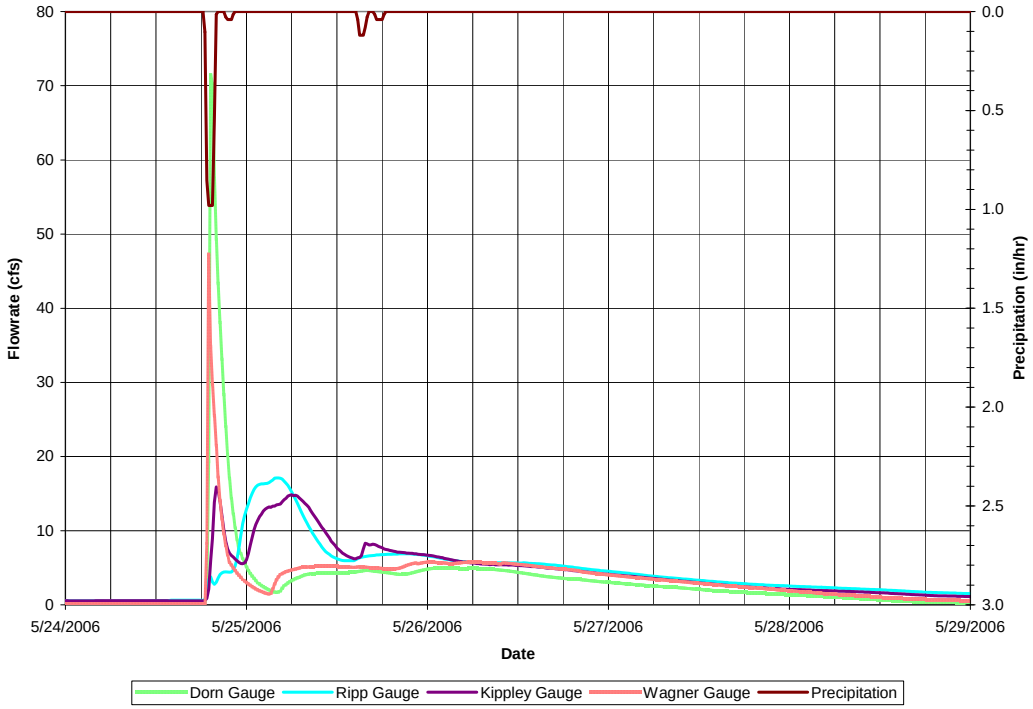

Figure 96: Event 5 Hydrograph. Wagner peak is interpolated. Post 5/26 Wagner flowrate inaccurate due to blockage

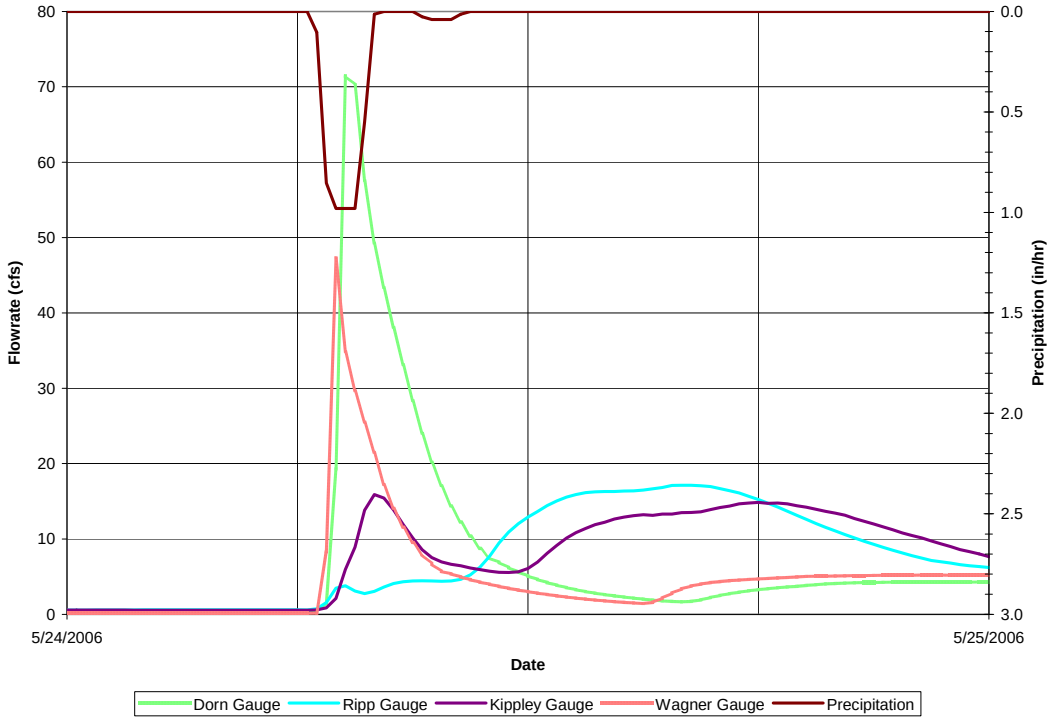

Figure 97: Event 5 Hydrograph Zoom

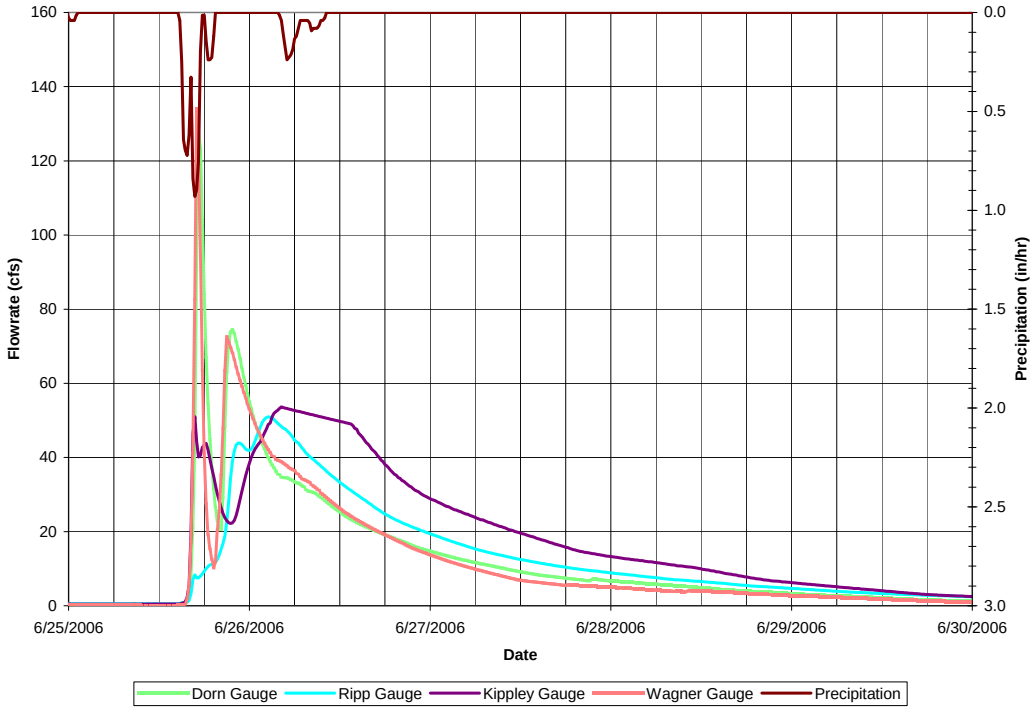

Figure 98: Event 6 Hydrograph (Wager and Kippley peaks are interpolated)

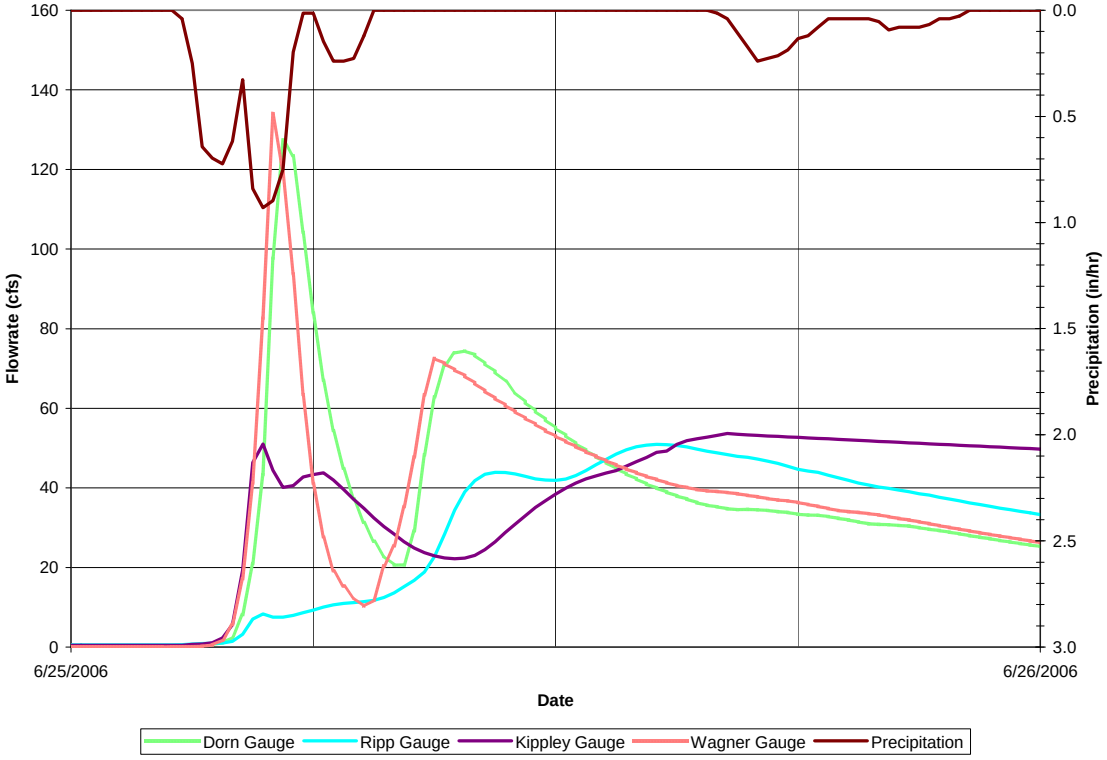

Figure 99: Event 6 Hydrograph Zoom

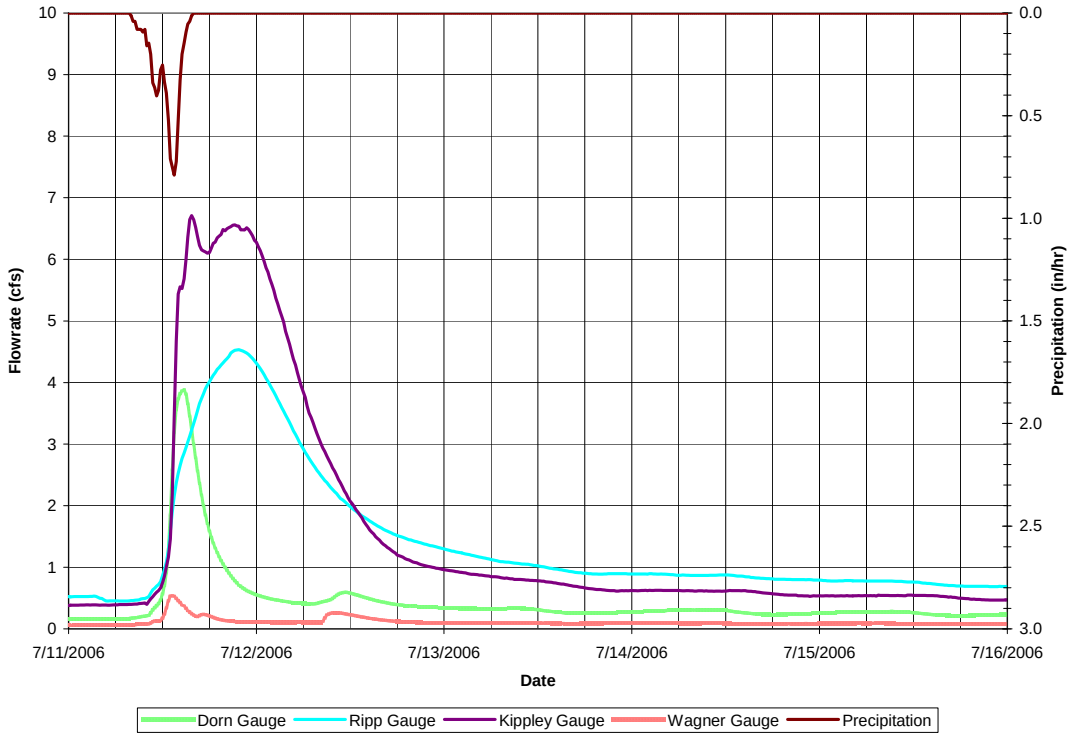

Figure 100: Event 7 Hydrograph. Possible inaccurate Kippley or Ripp flowrate.

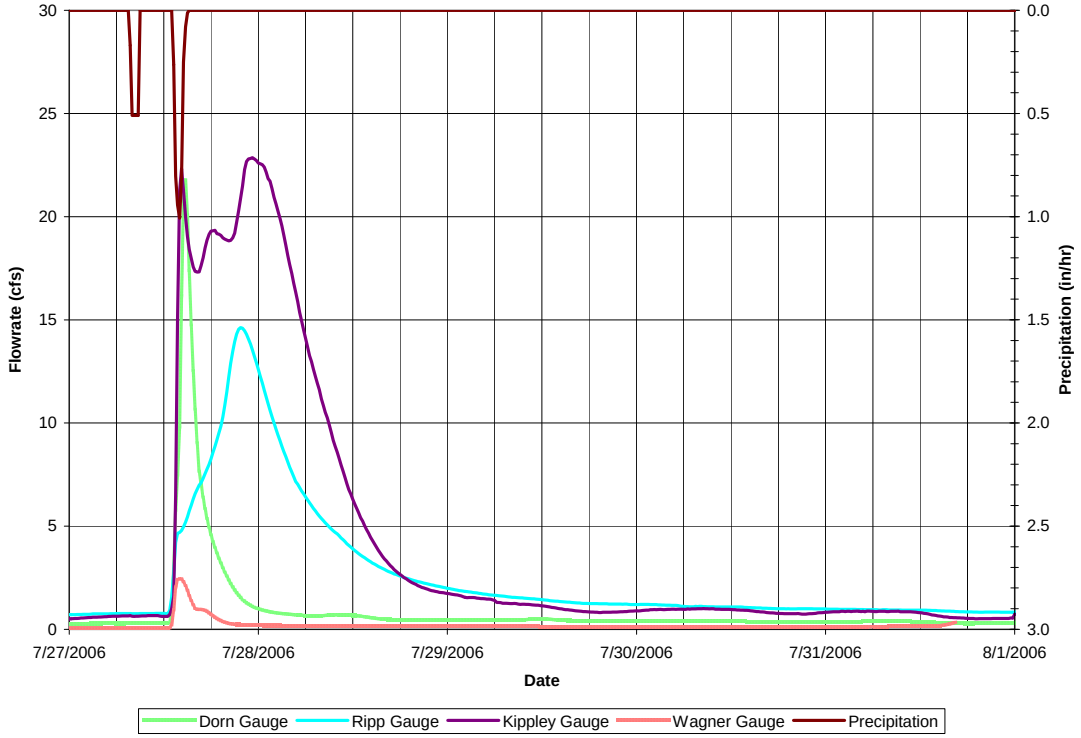

Figure 101: Event 8 Hydrograph. Possible inaccurate Kippley or Ripp flowrate.

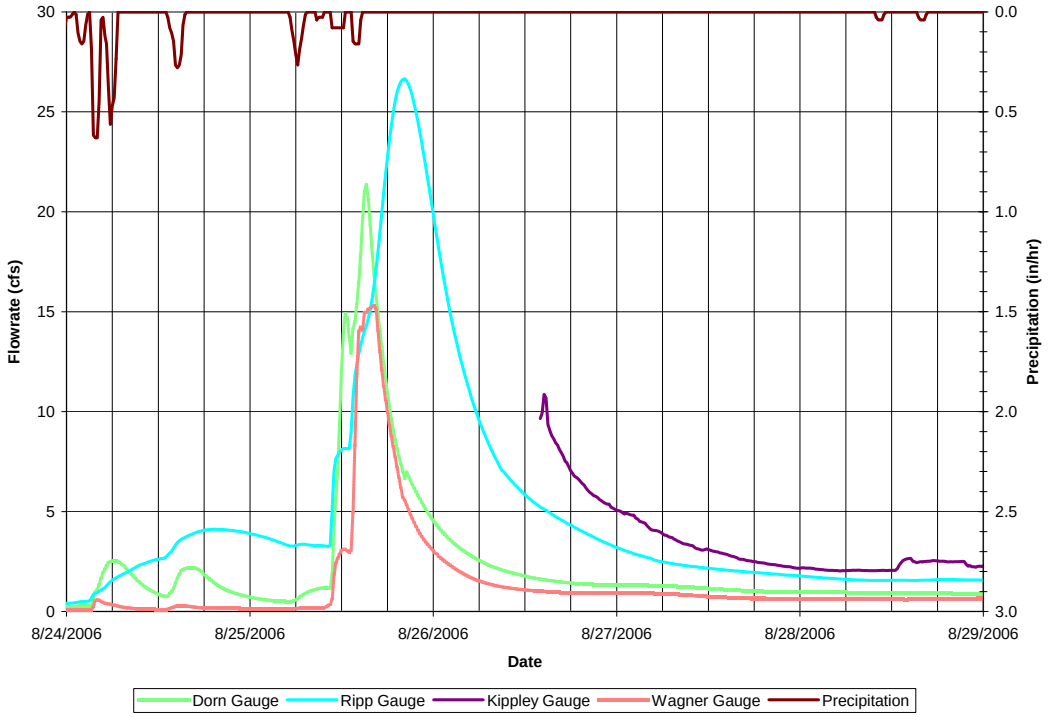

Figure 102: Event 9 Hydrograph. Kippley data missing.

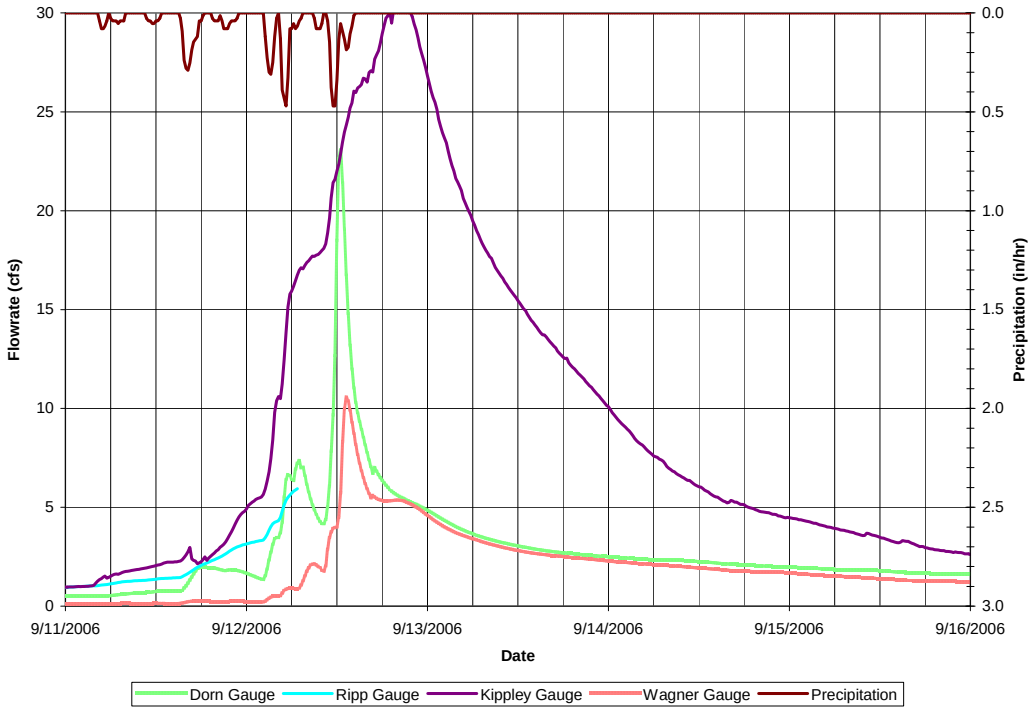

Figure 103: Event 10 Hydrograph. Probable inaccurate Kippley flowrate due to blockage. Ripp data missing.

Based on the 2006 flood record, flood peak reduction occurs for large events, but not small events. The incoming flowrate and outgoing flowrate for the wetland is plotted on Figure 104. Data points below the inflow = outflow line indicate reduction in peak flowrate, and data points above this line indicate an increase in peak flowrate. Large flows show a clear attenuation, while lower flowrate peaks are higher at the outlet. The transition seems to occur at about 20 cfs of incoming flowrate. This indicates that around this flowrate, flows enter into the overbank portions of the floodplain, and wetland storage becomes significant.

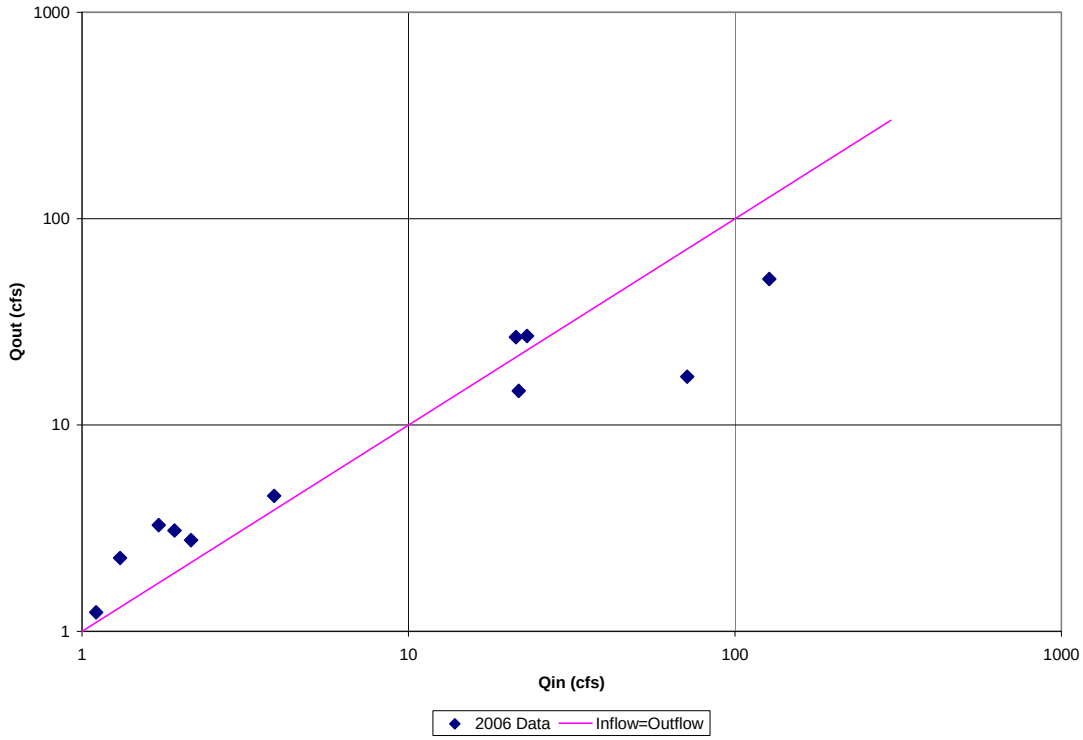

Figure 104: Incoming and Outgoing Flowrates for Wetland

0.3.4 Additional Hydrologic Data

For all of the recorded events, the peak time lag was recorded. Using this information and the distance between gages, the average peak flood wave speed was determined. The standard deviation was also determined. Theoretically, the flood wave speed will vary as a function of depth, however, there are additional factors such as channel roughness, and storage which influence the flood wave speed. Therefore some variation is expected.

Reach	Flood Wave Speed C (ft/s)	Standard Deviation (ft/s)
Wagner – Dorn Gages (2)	0.82	0.67
Dorn – Ripp Gages (Wetland) (3)	0.19	0.04
Ripp – Kippley	0.79	0.32

Gages (4)		

Table 22: Average Flood Wave Speed Through Watershed Reaches

It is of note that the wetland area experiences a low average flood wave speed of 0.19 ft/s, and a low standard deviation of 0.04, as compared to the other reaches. This indicates that the flood progression through the wetland is slow, and generally not different between events.

Figure 105 below shows the variation in runoff coefficient as compared to the total runoff volume. Most clear, and perhaps the most accurate is the plot of the runoff coefficient for the total watershed. This varies from 0.007 to 0.18, in a fairly linear response. This plot illustrates the dependence of the runoff coefficient on total storm magnitude, rainfall intensity and initial conditions.

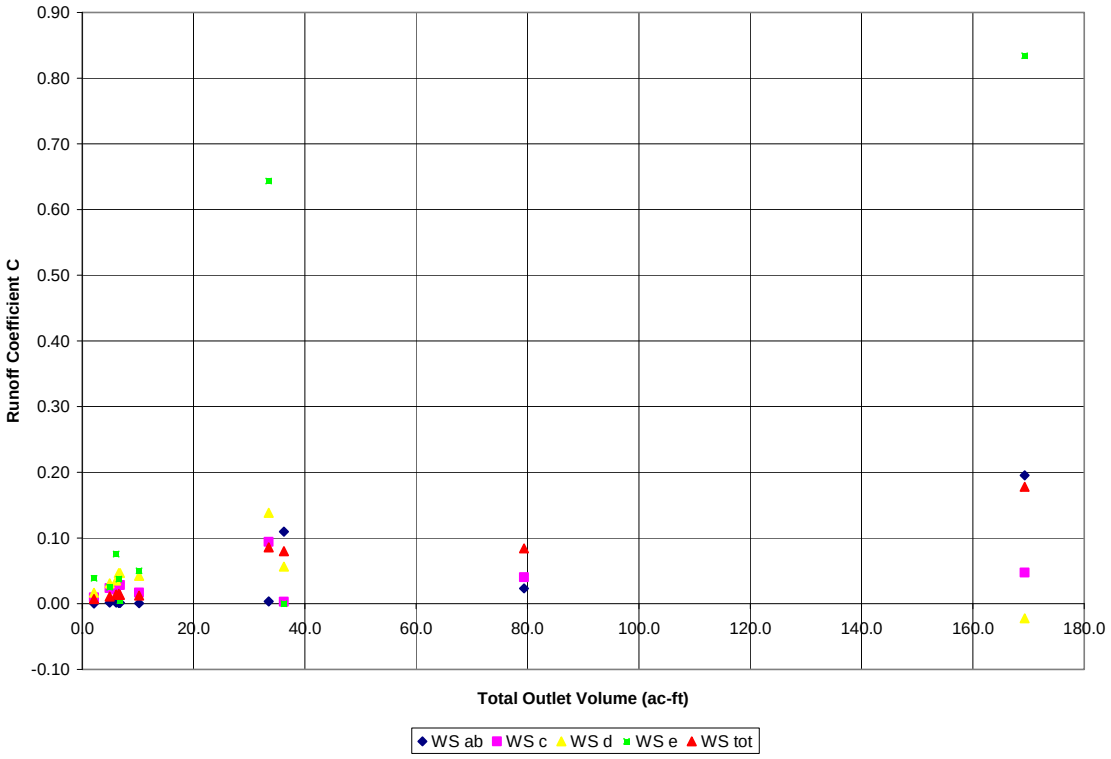

Figure 105: Observed Runoff Coefficient as a Function of Total Event Volume

Additionally, the temperature of the flow at both the Wager and Kippley Gages were monitored during the 2006 season. Ambient air temperature data were obtained from the KWIWAUNA2 weather gage. As shown below, the water temperature at the Wagner Gage is fairly constant through the season except for during stormflow events. This is due to groundwater spring flows during typical baseflow conditions which has a very constant temperature. The water temperature at the Kippley Gage is typically very well correlated with the ambient air temperature. This is because these flows are exposed to the ambient air for longer time periods which allows for equilibration of the temperature.

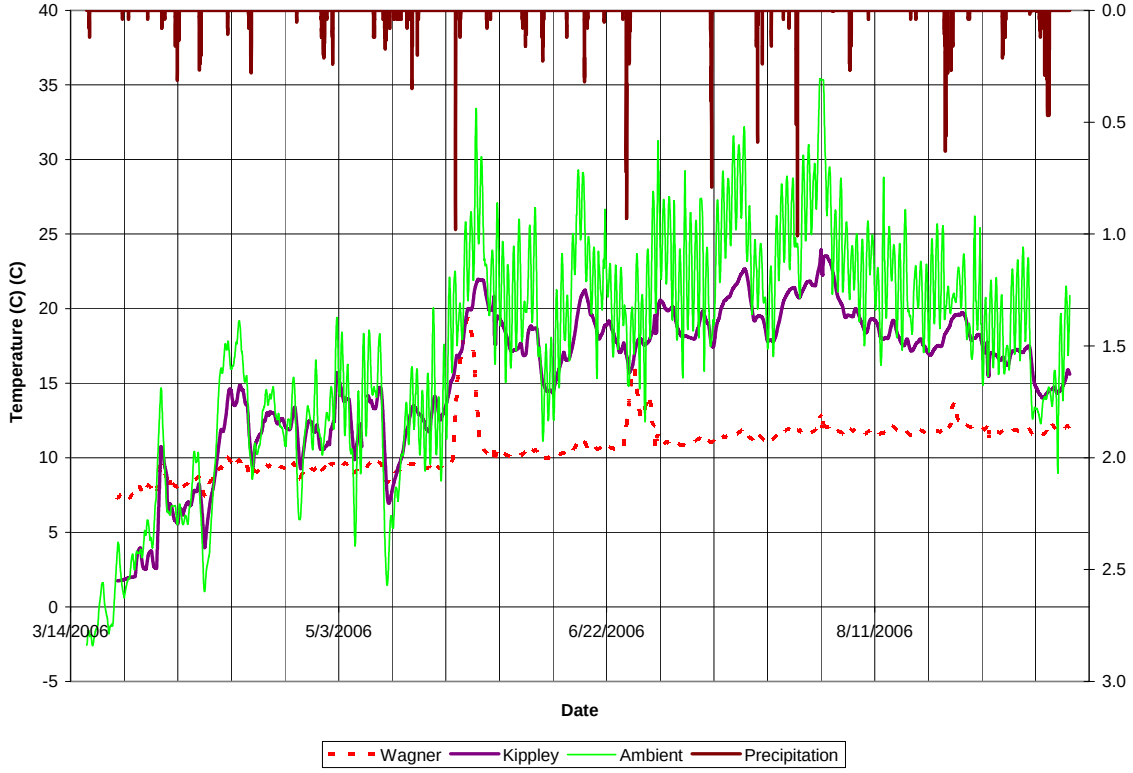

Figure 106: Water and Ambient Air Temperature for 2006 Season

0.4 References

Dane County. 2006. "Dane County DCiMap". Dane County (WI) Land Information Office. http://dcimap.co.dane.wi.us/dcimap/index.htm.

Huff, F.A., and J.R. Angel. 1992. Rainfall Frequency Atlas of the Midwest, Bulletin 71. Midwestern Climate Center Research Report 92.03.

Murdoc, Evan. 2006. Transport and Storage of Sediments and Solutes in a Small Agricultural Stream, Dane County, Wisconsin. MS Thesis. University of Wisconsin – Madison.

National Climate Data Center (NCDC). 2006. Madison, Wisconsin Historical Data. National Oceanic and Atmospheric Administration (NOAA). http://www4.ncdc.noaa.gov/cgi-in/wwcgi.dll?wwDI~StnSrch~StnID~20020992

Walker, J.F., and Krug, W.R., 2003. Flood-Frequency Characteristics of Wisconsin Streams. USGS WRI Report 03-4250.

Weather Underground (WU). 2006. “Weather Station History, KWIWAUNA2 Northwest of Waunakee Airport, Waunakee, Wisconsin” The Weather Underground, Inc. http://www.wunderground.com/weatherstation/WXDailyHistory.asp?ID=KWIWAUNA2

US Geological Survey (USGS). 1983. *7.5 Minute Quadrangle Maps: Springfield Corners, WI, and Waunakee, WI.* Madison, Wisconsin: Wisconsin Geological and Natural History Survey

APPENDIX E – ADDITIONAL SEDIMENT TRANSPORT DATA

0.1 Overview

This appenndix contains additional sediment transport information not presented in Section 4 of this report.

0.2 Sediment Data

0.2.1 Storm Event Data

Data from the sediment monitoring of the events at each of the gaging sites is presented in the following section. Total mass transport was determined by taking the measured concentration times the average flow for that period. Sediment transport data is presented with mean sediment diameter (D50) at the Dorn and Ripp Gages for most of the events.

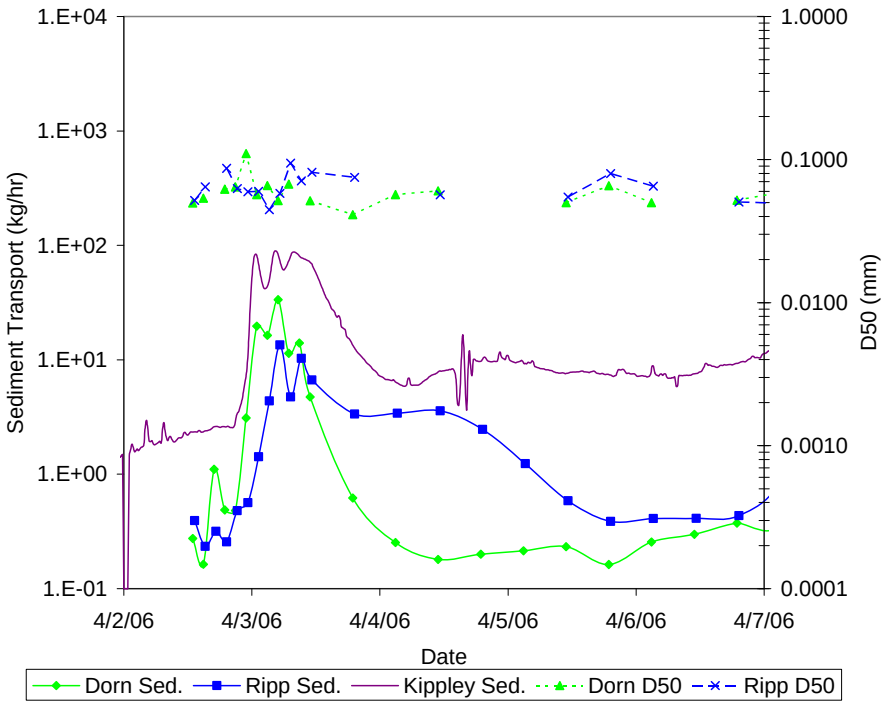

Figure 107: Event 1 Sediment Transport and Mean Suspended Particle Diameter

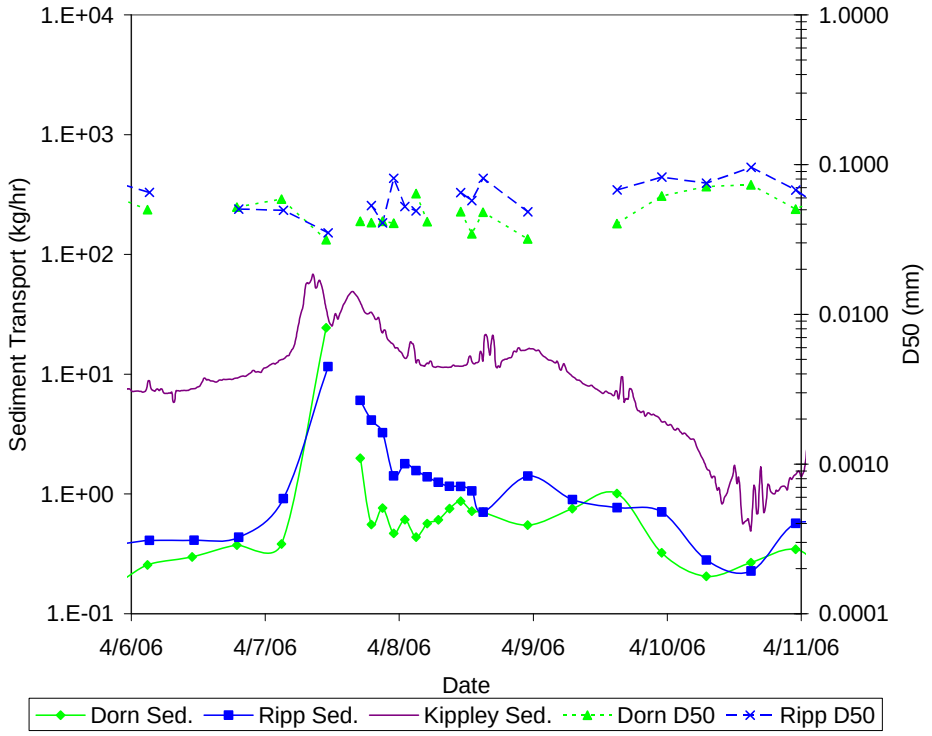

Figure 108: Event 2 Sediment Transport and Mean Suspended Particle Diameter

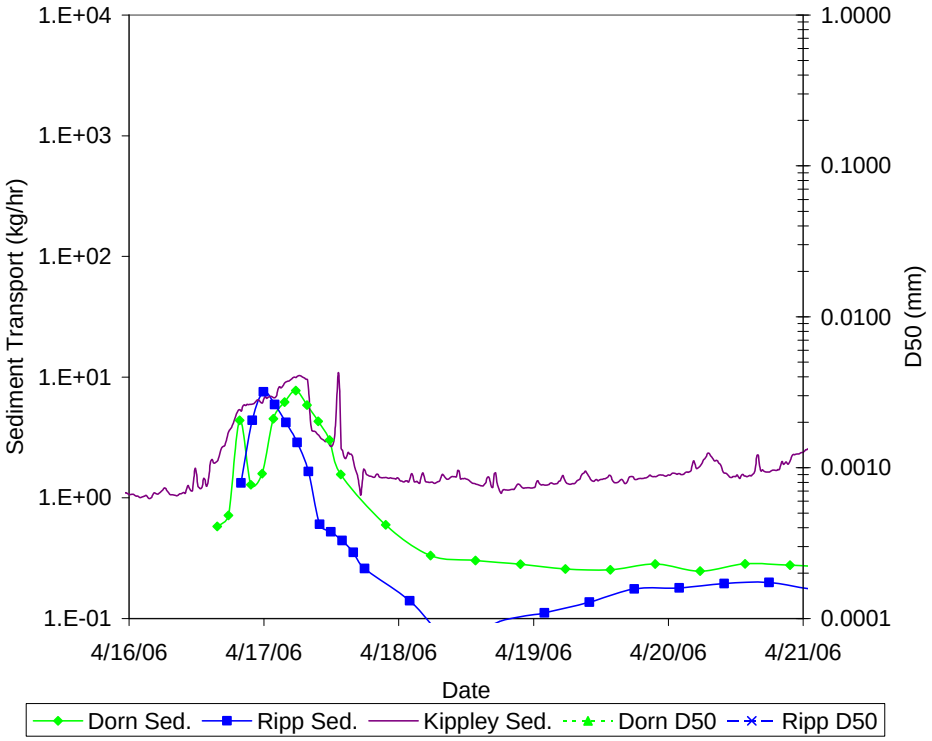

Figure 109: Event 3 Sediment Transport and Mean Suspended Particle Diameter

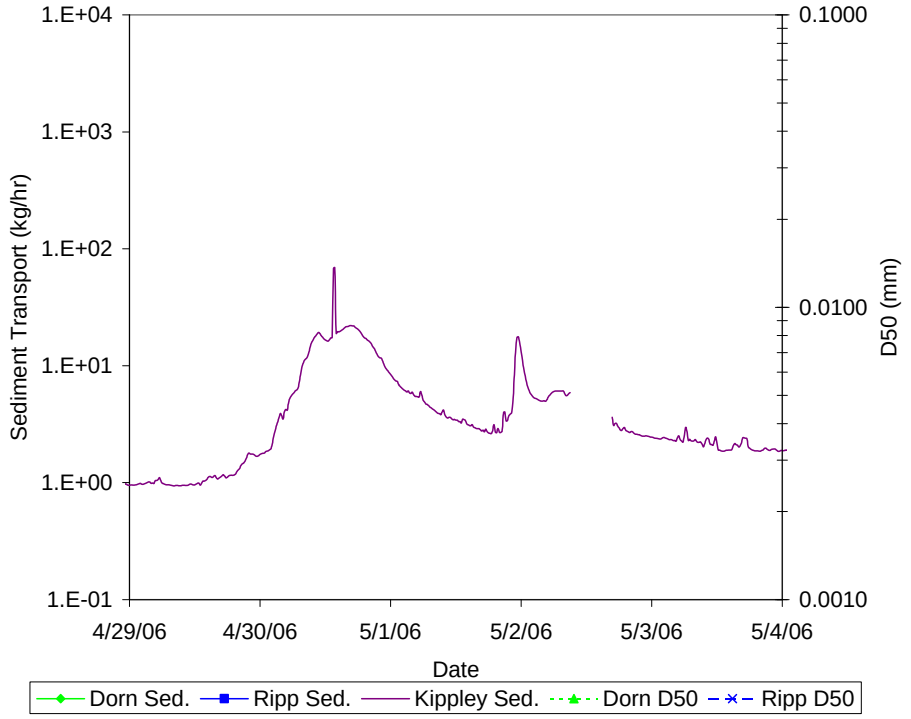

Figure 110: Event 3.5 Sediment Transport and Mean Suspended Particle Diameter

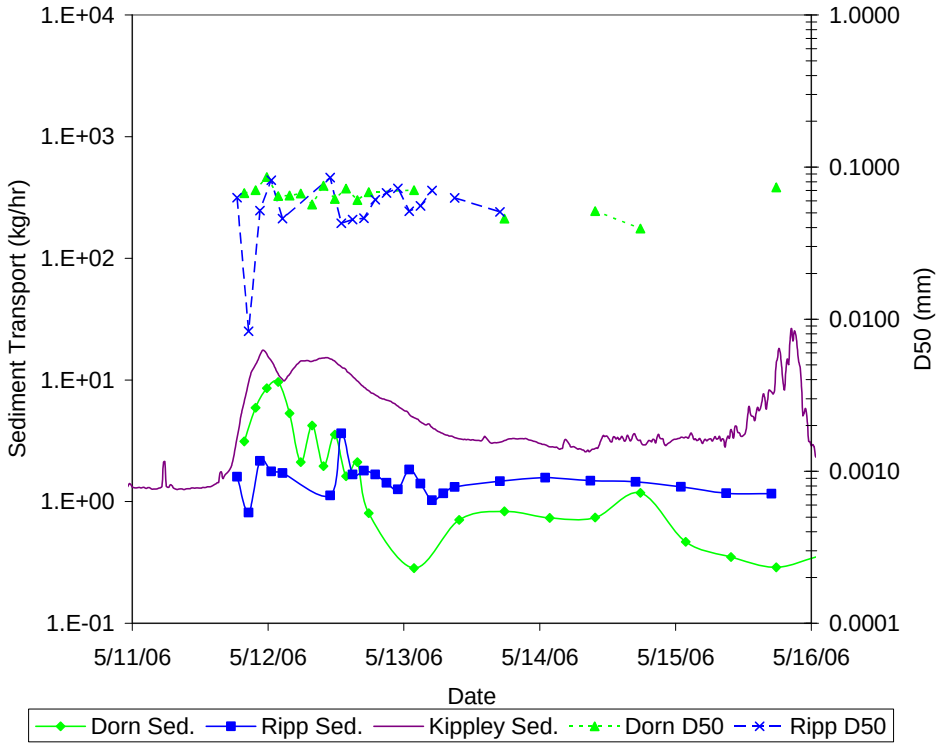

Figure 111: Event 4 Sediment Transport and Mean Suspended Particle Diameter

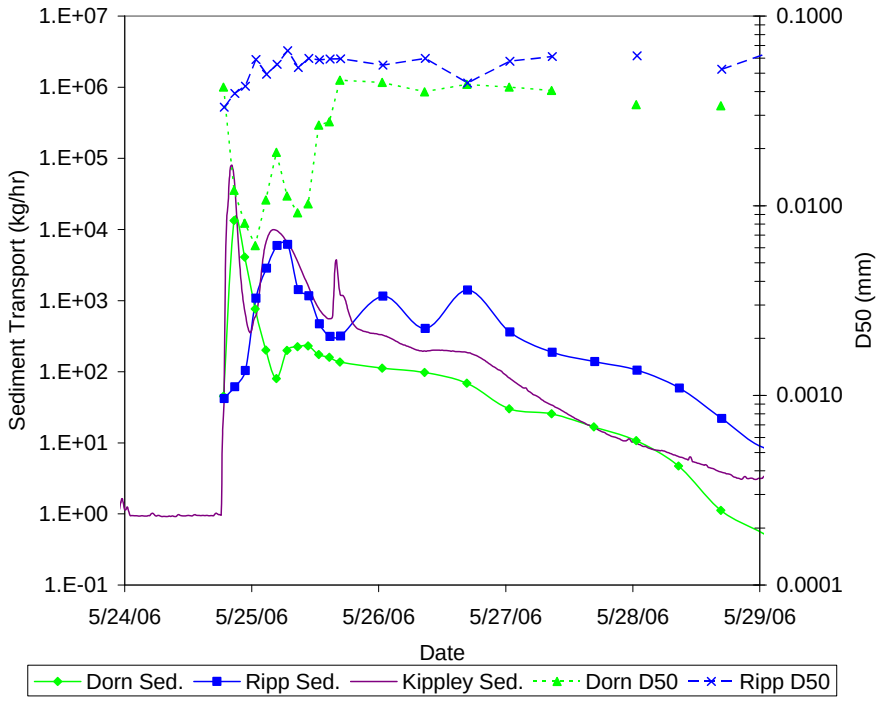

Figure 112: Event 5 Sediment Transport and Mean Suspended Particle Diameter

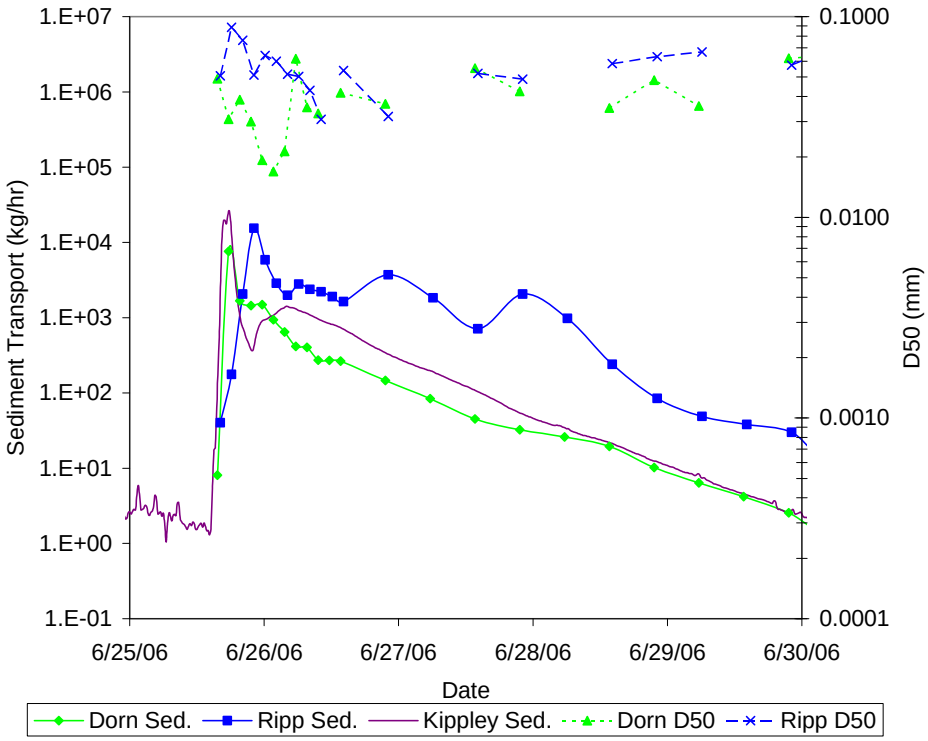

Figure 113: Event 6 Sediment Transport and Mean Suspended Particle Diameter

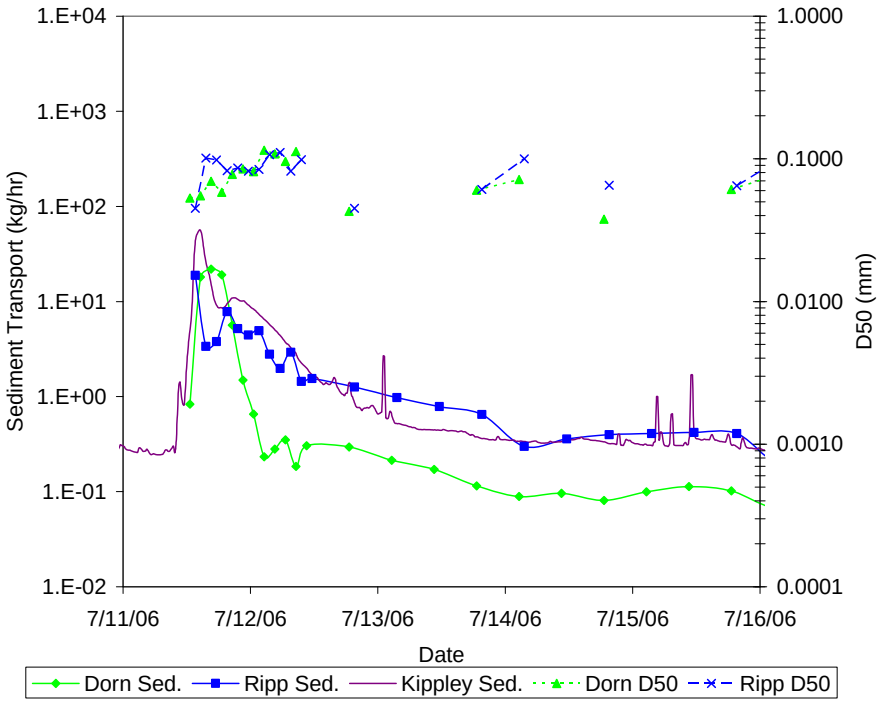

Figure 114: Event 7 Sediment Transport and Mean Suspended Particle Diameter

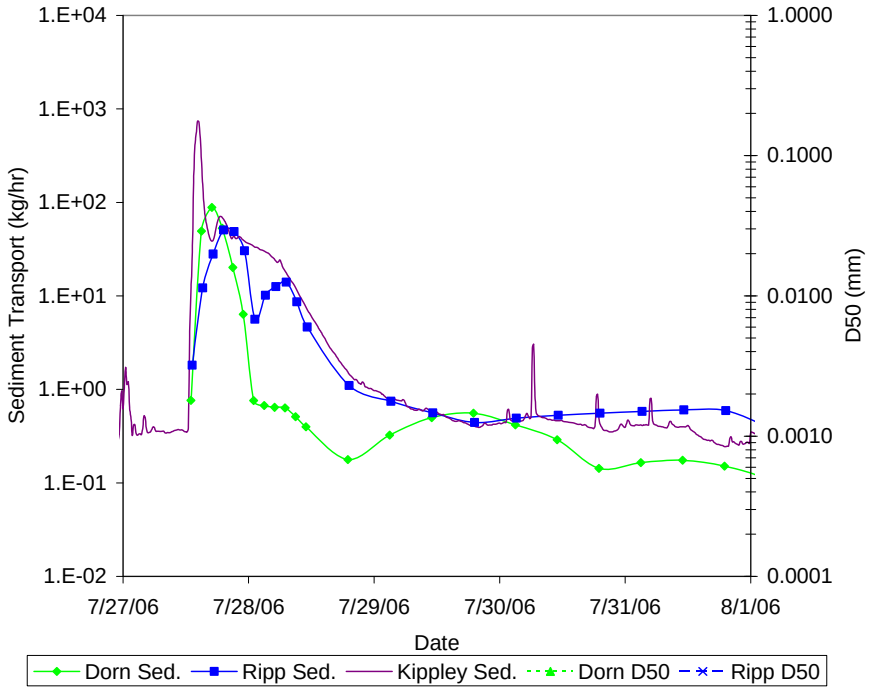

Figure 115: Event 8 Sediment Transport and Mean Suspended Particle Diameter

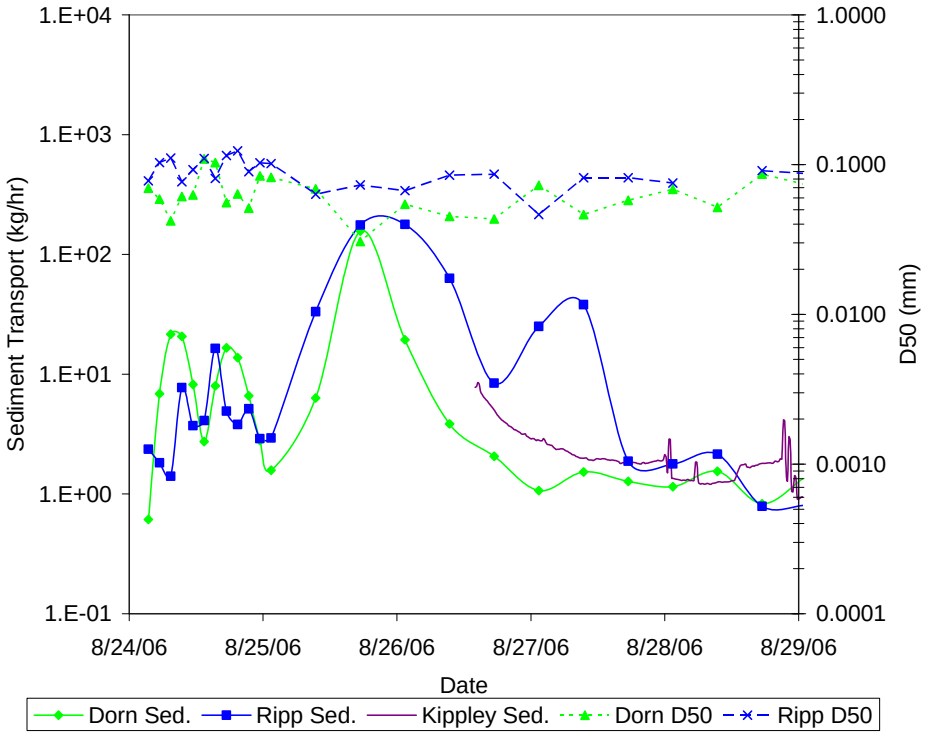

Figure 116: Event 9 Sediment Transport and Mean Suspended Particle Diameter

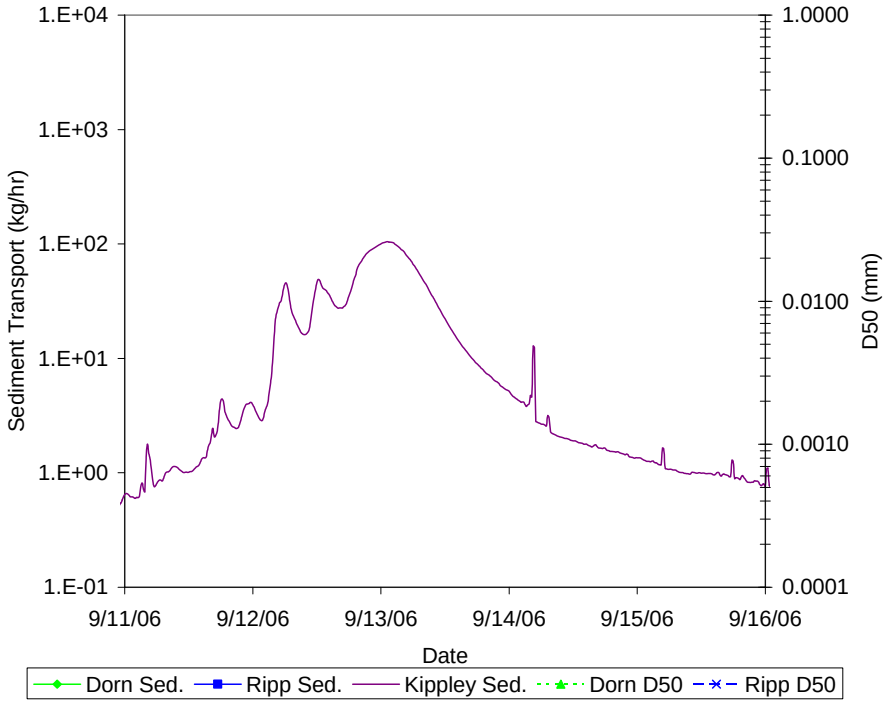

Figure 117: Event 10 Sediment Transport and Mean Suspended Particle Diameter

As shown in the previous figures, there does not seem to be a clear trend in the mean particle diameter with time during the events. This is most likely due to the surrounding soil type being primarily silt. One of the few visible trends in the D50 is during Events 5 and 6. A large amount of fines is observed and a lowering of the D50, which is probably a result of particles carried from upstream in Watersheds A and B.

0.2.2 Second Sediment Peak Explanation

A second sediment peak was observed by E. Murdoc (2006), to occur several days after the initial flood and sediment peak. This second sediment peak typically occurred 2-3 days after the initial peak, and was observed at the Kippley Gage in the 2003-2005 seasons.

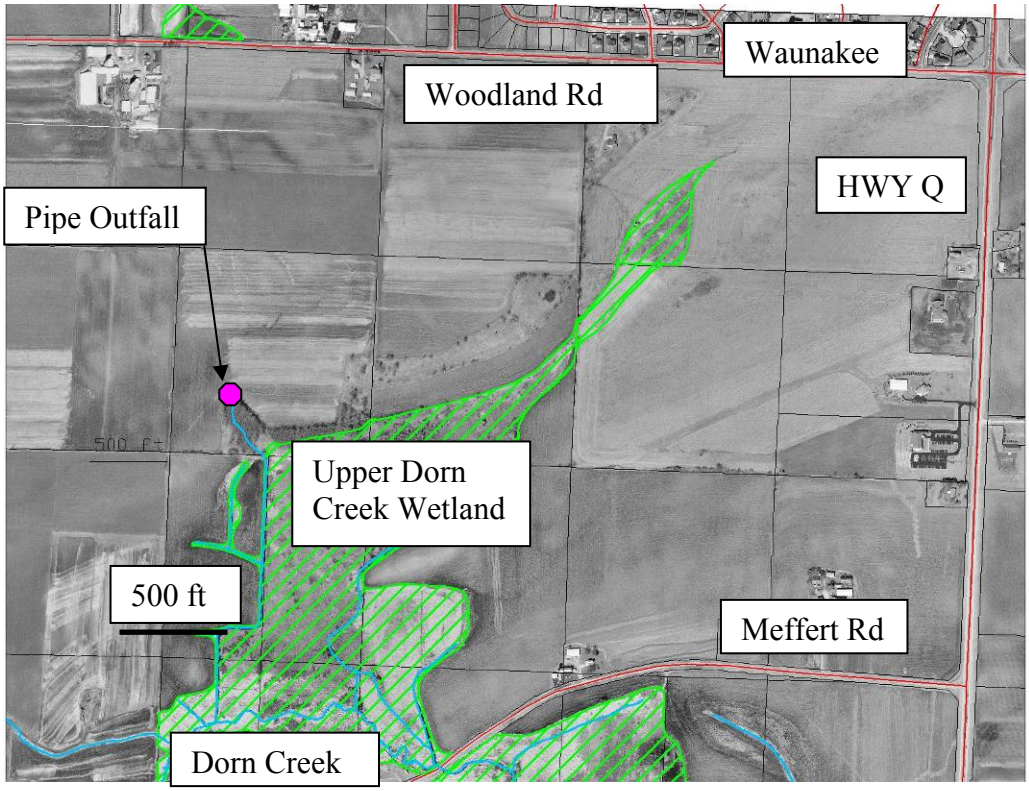

Figure 118: Pipe Outfall Location

The cause of this second peak was the subject of debate, and several theories were suggested as to its origin. Based on site data from 2006, it was observed that a major agricultural drainage channel just downstream of the Dorn Gage was observed to have very large sediment concentrations. Sediment-laden flow was also observed to be entering the main creek from this source several days after an event. The source of the very dark water was traced to a drainage pipe of unknown source at the top of the ditch at the north-western corner of the wetland. Samples of storm event water were taken on 5/12/2006 and analysis showed concentrations of TSS of 490 mg/l. Samples collected downstream near the entrance to the wetland on 4/5/2006 showed the following results:

total suspended solids 163 mg/l, bioavailable phosphorous 3.91 mg/l, and total phosphorous 5.92 mg/l.

Based on a hypothesis that this pipe discharge may be the cause of the second sediment peak, grab samples were taken of the flow in the agricultural channel several times per day after Event 3. Figure 119 shows the results for Event 3. Flow and sediment concentration are shown for the Dorn and Ripp Gages. Additional grab samples were taken of the suspected agricultural channel at various times.

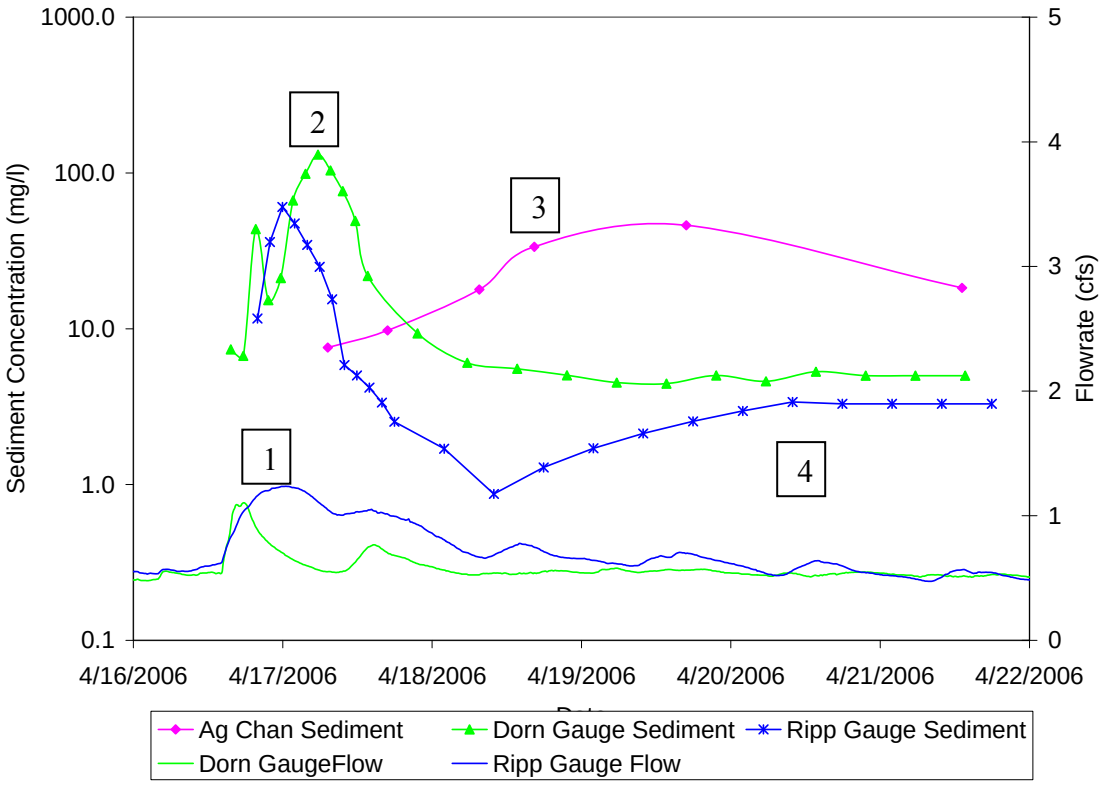

Figure 119: Delayed Second Sediment Peak and Agricultural Channel Input

Figure 119 clearly shows the agricultural channel having a low initial concentration, and a peak in concentration several days after the event. The Ripp Gage shows an initial

peak, which subsides by about 1.5 days after the event. However, the second peak rises again and peaks at about 3.5 days after the event. This data strongly suggests that the source of the second sediment peak is the agricultural channel which is fed by the pipe of unknown origin. A proposed mechanism for the second sediment peak is:

1. Rainfall event begins, and ends, while both Ripp and Dorn flowrates peak. Pipe discharge also peaks and ends (this was observed in the field).

2. Initial sediment transport of sediments in the channel begins due to increased shear from the event and causes initial peaks at Ripp and Dorn sites. Due to high stage in the agricultural channel outlet (at the creek), water from the pipe is stored in the large agricultural channel, and does not move.

3. Water levels at the channel outlet begin to drop, and thus the stored water in the agricultural channel begins to move to the outlet and concentrations increase.

4. Stored water from the agricultural channel moves to the outlet, and is transported through the system, which shows up in the second peak at the Ripp Gage.

This evidence does not fully prove the proposed mechanism due to lack of direct evidence. Tracing methods such as radionuclide or chemical methods might be more effective in conclusively proving this theory.

0.2.3 Shear-Sediment

Bed shear stress is thought to be the primary driver of sediment transport. Therefore prediction of sediment transport is determined by knowledge of the site bed shear and the critical shear stress values for the bed soil. Actual determination of the local bed shear is complex, as flows are nonuniform and in a flood situation are unsteady as well. For uniform, steady flow the bed shear stress can be determined by (Munson et al 2005):

$$\tau_0 = \gamma R_h S_0$$

However, values of the bed shear stress may differ significantly from this relationship under nonuniform conditions. Applying a one dimensional momentum balance, it can be shown that (Lee et al. 2004):

$$\tau_b = \gamma R_h \left(S_0 - \frac{dD}{dx}(1 - F^2) \right)$$

Where dD/Dx (which can be shown to equal S0-Sf) is the rate of change of the water depth, Rh is the hydraulic radius, and F is the Froude number. Using this relationship, the bed shear stress was calculated for the gages for the 2006 season. The friction slope (Sf) and Froude number (F) were determined using the HECRAS model and related to the depth. The hydraulic radius was determined from site survey data. The following is a presentation of the bed shear stress at the four gages plotted with sediment transport.

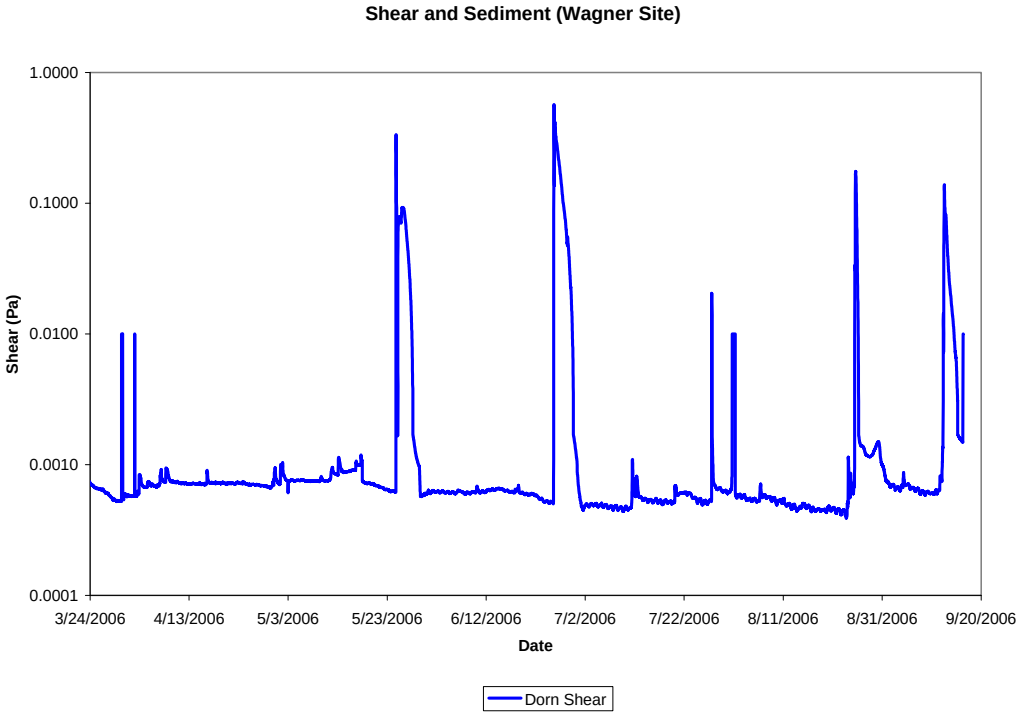

Figure 120: Bed Shear at the Wagner Gage for the 2006 Season

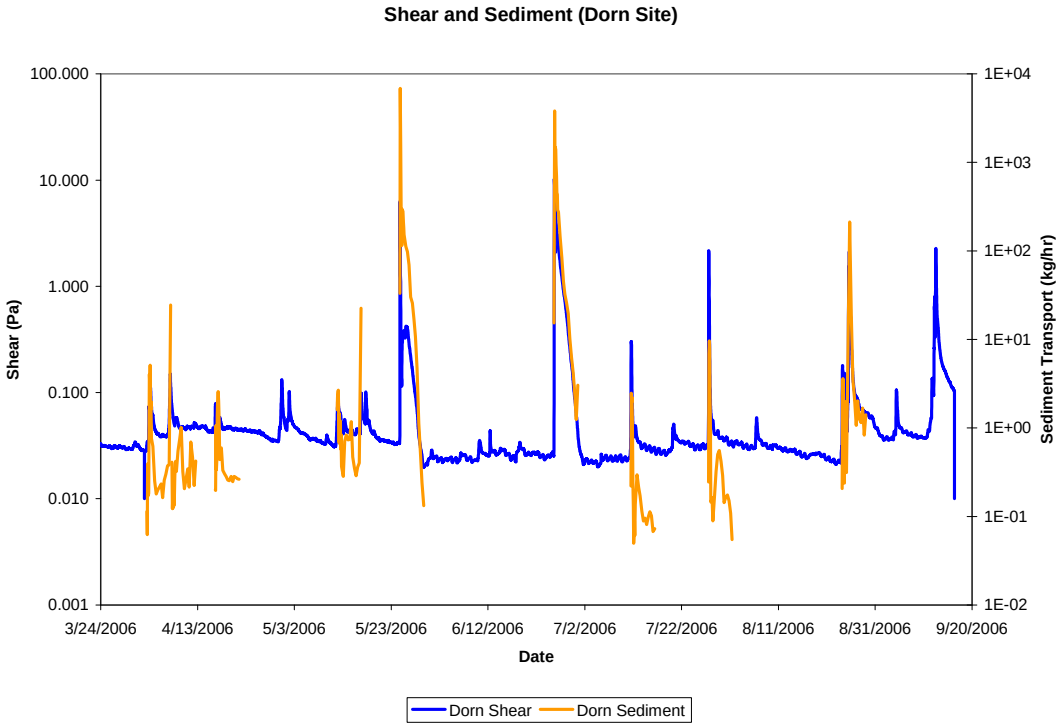

Figure 121: Bed Shear and Sediment Transport at the Dorn Gage for the 2006 Season

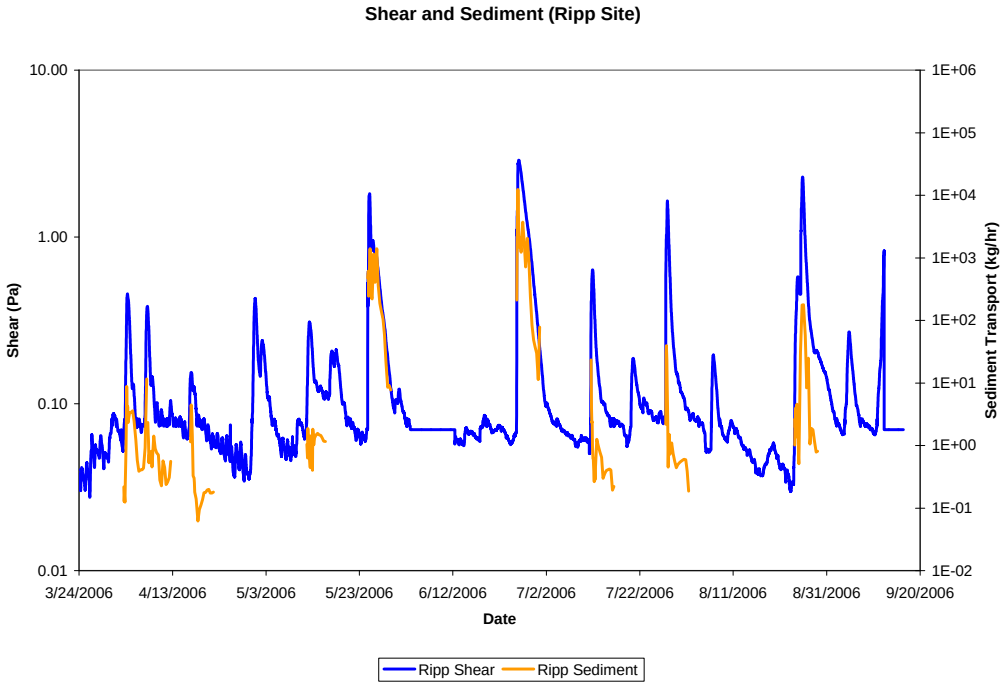

Figure 122: Bed Shear and Sediment Transport at the Ripp Gage for the 2006 Season

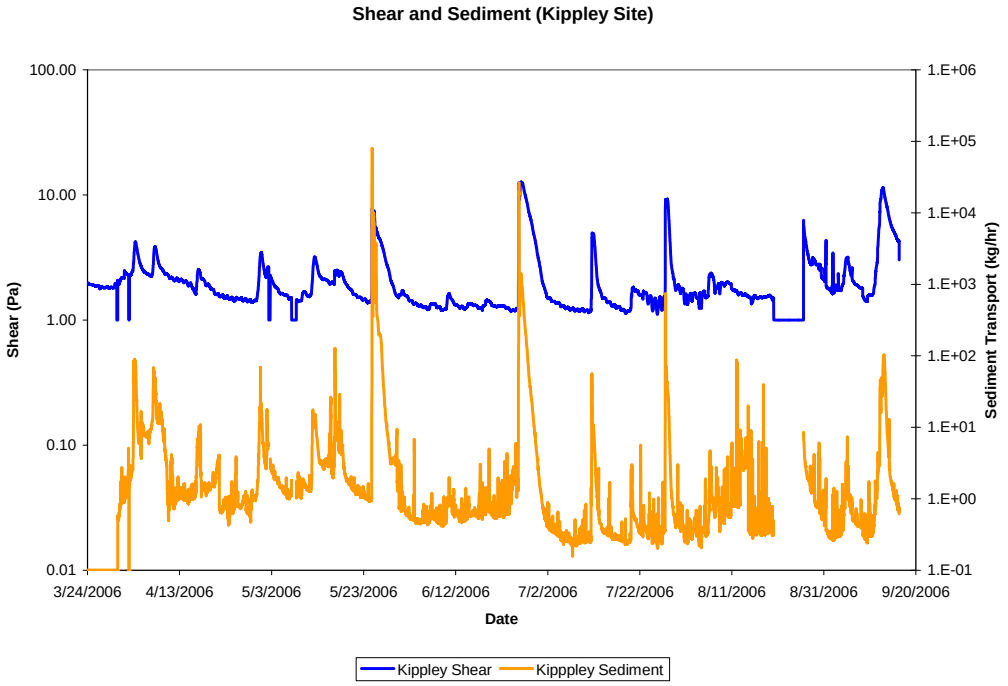

Figure 123: Bed Shear and Sediment Transport at the Kippley Gage for the 2006 Season

As shown by the previous figures, the bed shear stress seems well correlated with sediment transport. Additionally, it is important to note that the base shear levels are below typical transport rates for silt for the Wager and Dorn sites. This indicates an accumulation of fines during non-storm events, and a transport of silts during storm events. This information correlates well with published values of T_b, as well as site determined critical shear values as shown in this section.

The Ripp site shows a higher than expected base shear stress level, and may be influenced by several factors including localized effects of velocity, shear, depth, and sediment type. The Kippley site shows fairly high shear stress levels, which match well with the lack of sediment at that cross section. Only coarse sand and gravel are present, which matches this base bed shear stress level.

0.2.4 Velocity-Sediment

The velocity monitored at the Kippley Gage near the bed, as well as the sediment transport rate. The following results were observed:

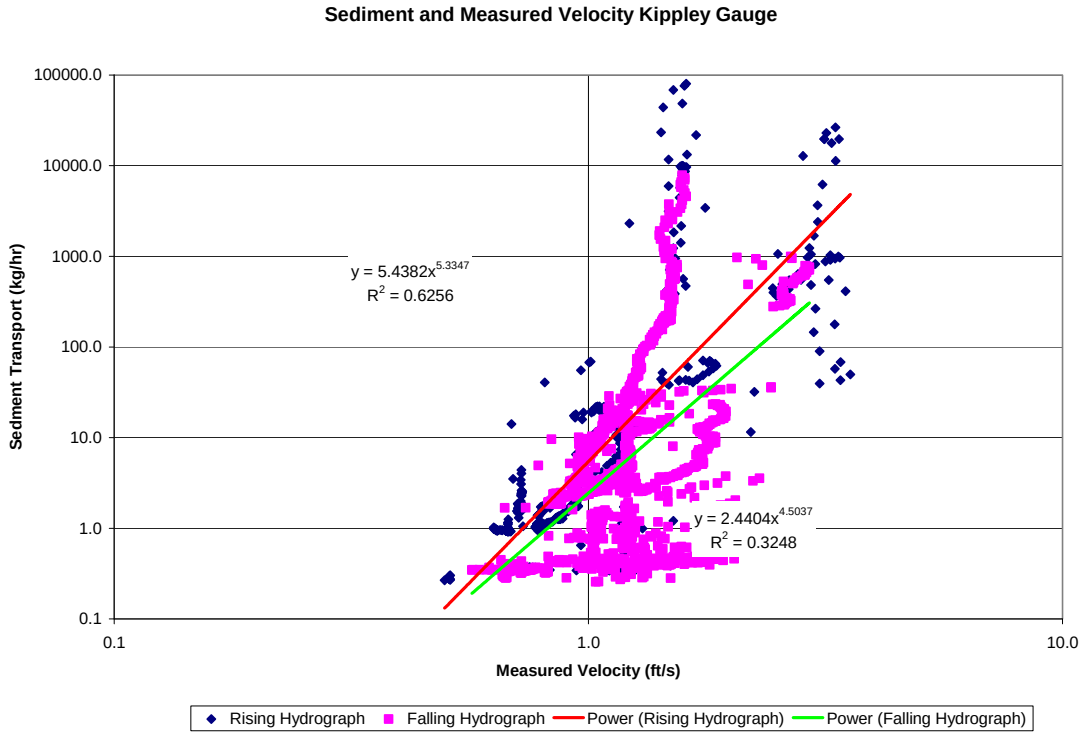

Figure 124: Sediment Transport and Measured Velocity Near Bed for 2006

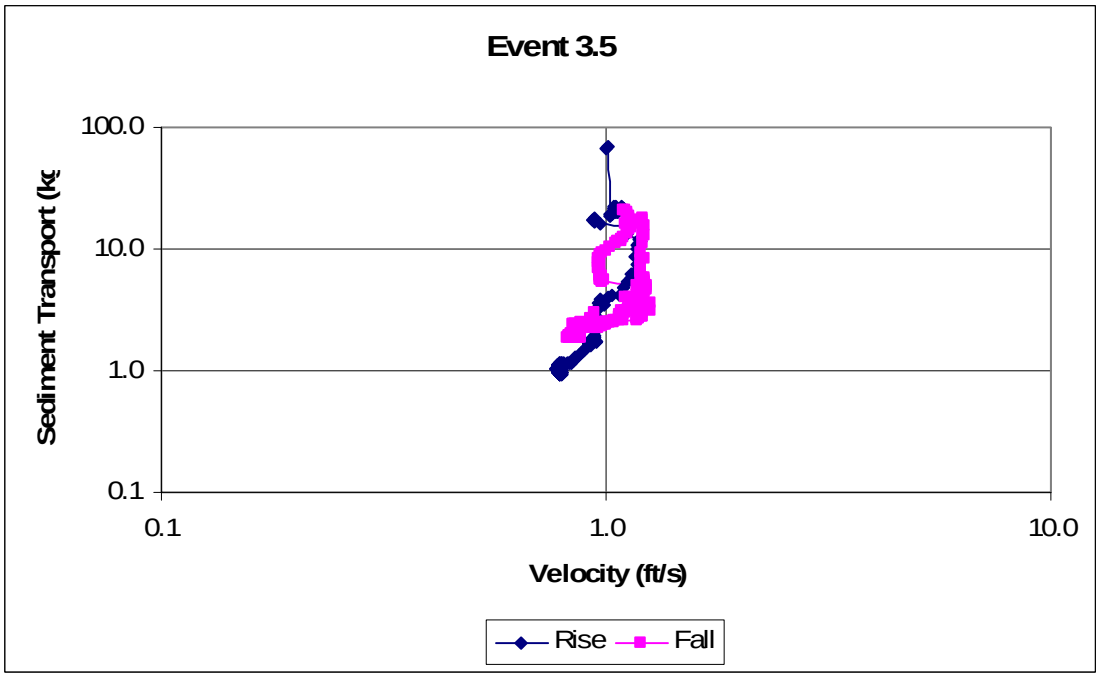

Figure 125: Event 3.5 Velocity and Sediment Transport

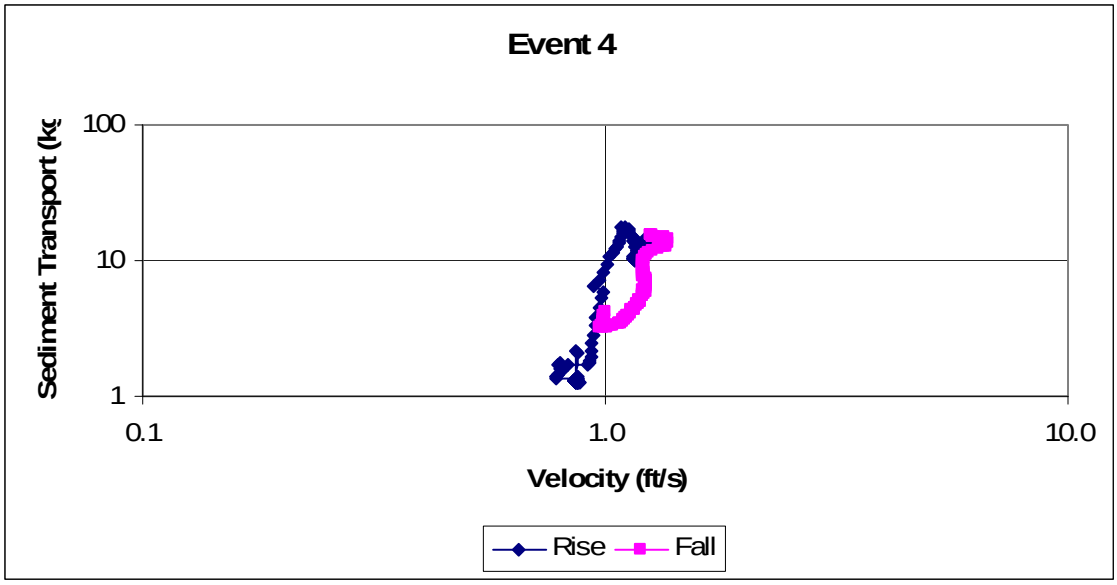

Figure 126: Event 4 Velocity and Sediment Transport

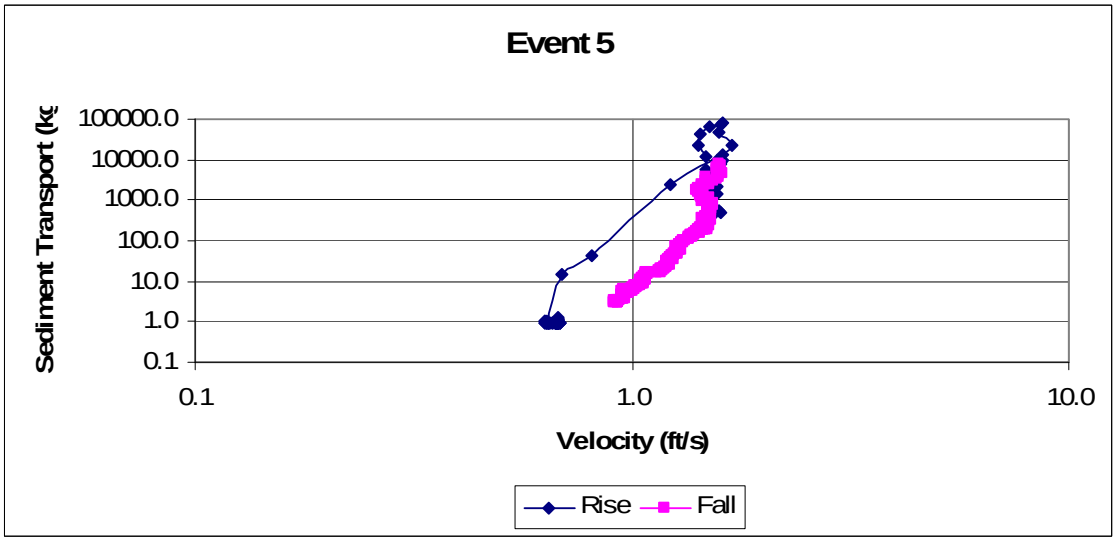

Figure 127: Event 5 Velocity and Sediment Transport

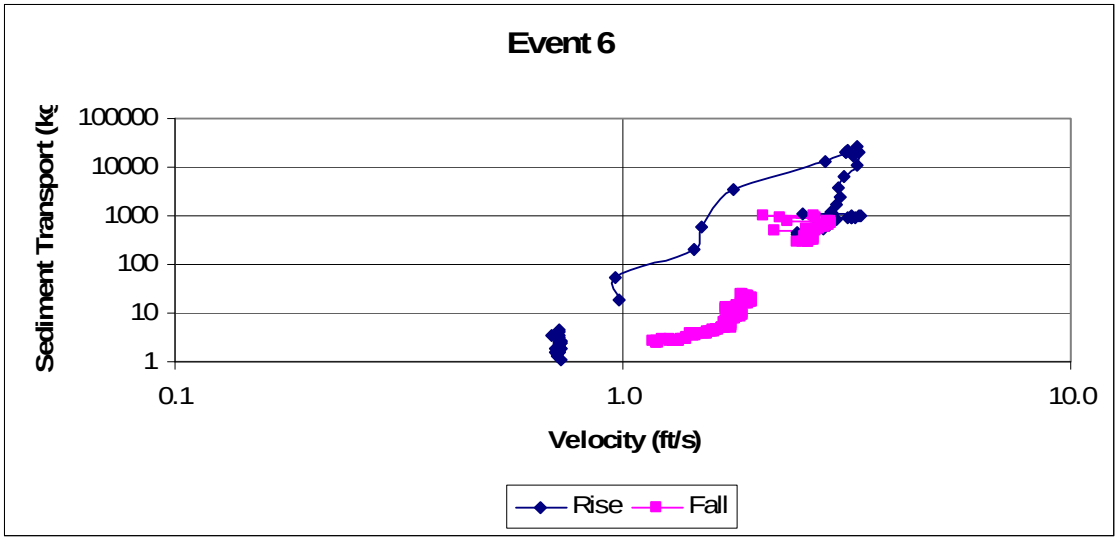

Figure 128: Event 6 Velocity and Sediment Transport

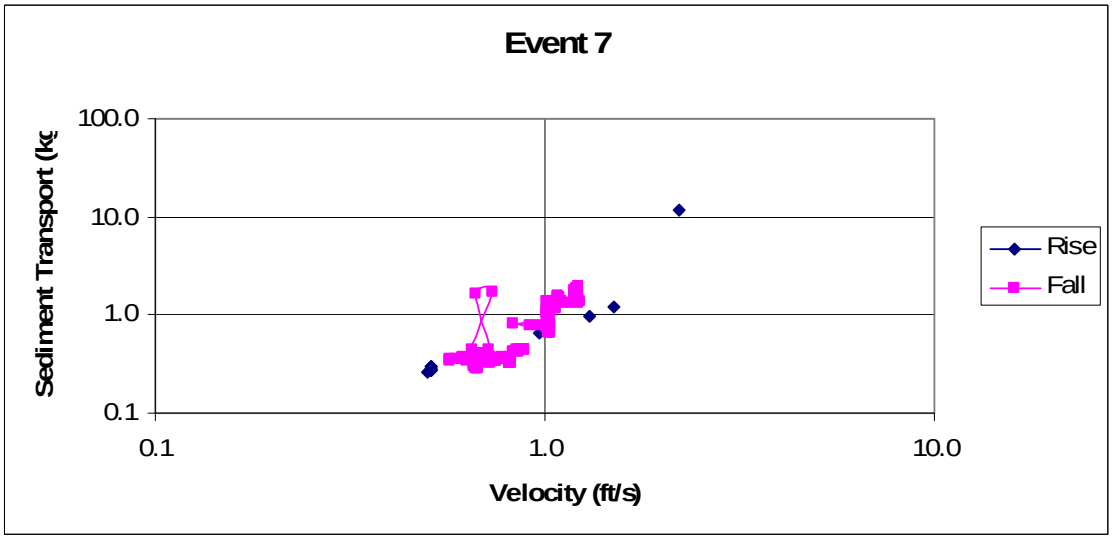

Figure 129: Event 7 Velocity and Sediment Transport

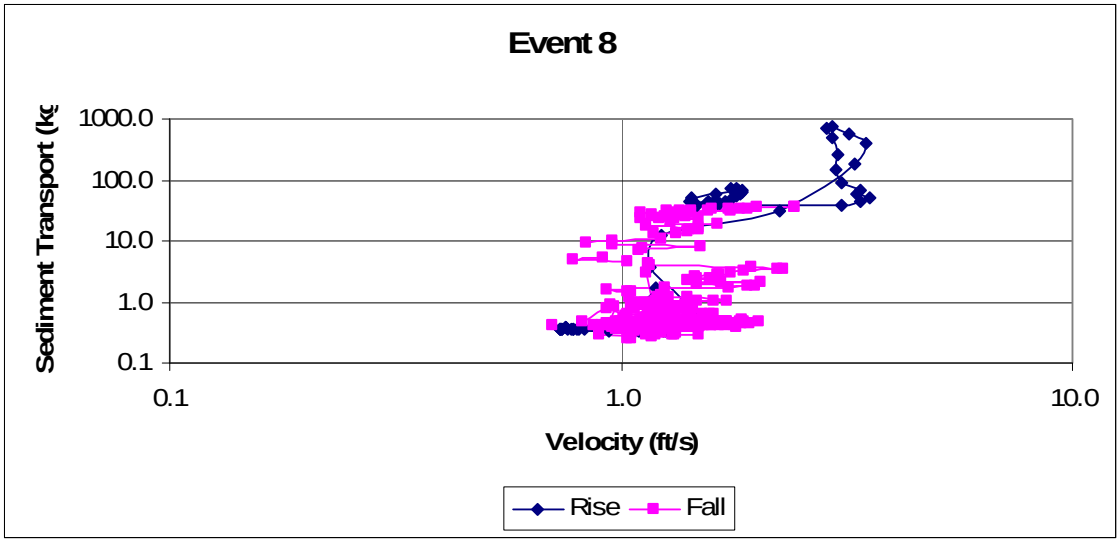

Figure 130: Event 8 Velocity and Sediment Transport

These results are similar to the flowrate versus sediment transport rate diagrams. Most of the events show a clear hysteresis of increased sediment transport in the rising limb of the hydrograph. As explained previously, the sediment transport of this reach is thought to be supply controlled, and therefore a unique relationship between velocity (and/or flow) and sediment transport does not exist.

0.2.5 Flume Core Shear Testing

Sediment cores were taken of the four gaging station and tested in the EFM lab in a 0.76m wide variable slope channel. Due to difficulty in determining slopes to the accuracy needed, a friction drag method was adopted to determine the critical shear stress values. Based on the Lee et al. (2004), the friction coefficient was related to the Reynolds for the flume as shown below. Using this relationship for the friction coefficient (Cf), the bed shear can be calculated as:

$$\tau_b = \frac{\rho C_f U^2}{2}$$

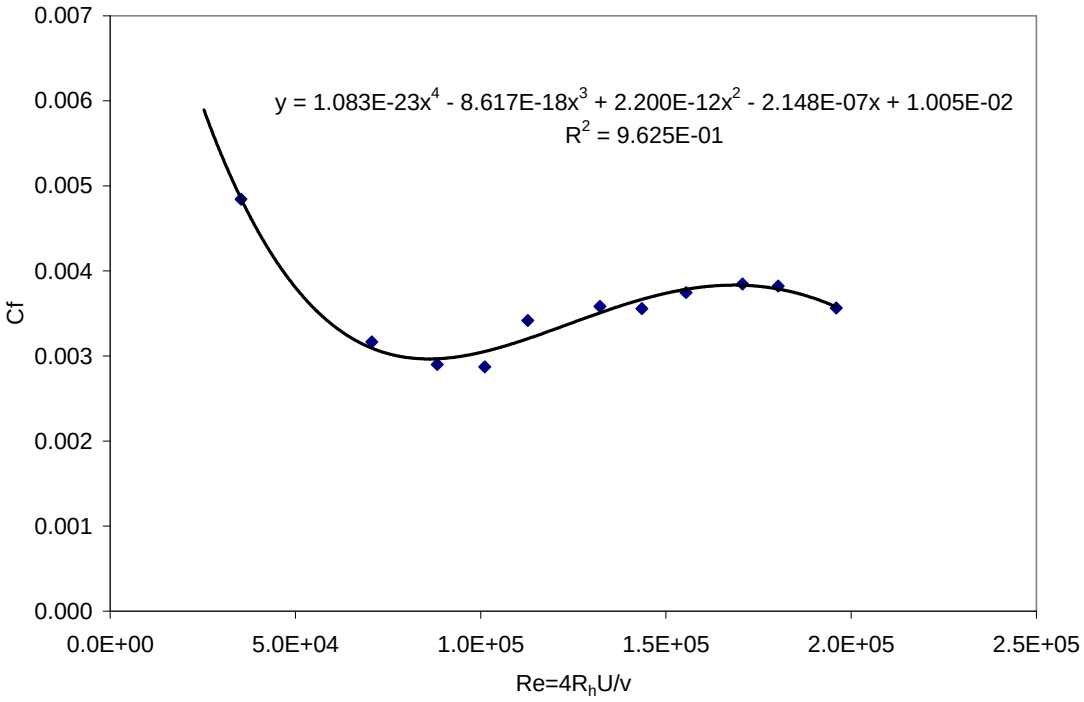

Figure 131: Friction Coefficient Values as a Function of the Reynolds Number

The results of the critical shear analysis are presented below. Julien (1998) lists the following approximate critical shear values for differing grain sizes:

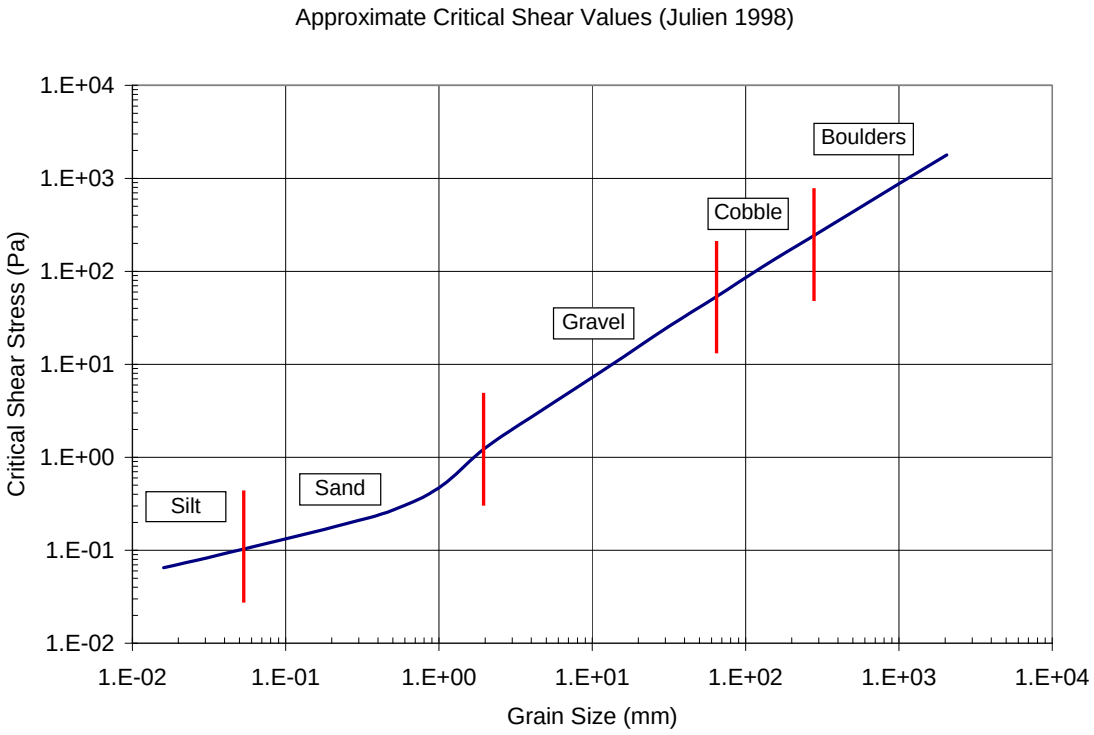

Figure 132; Approximate Critical Shear Stress Values as a Function of Grain Size for Non-Cohesive Sediments (Julien 1998)

The results of the flume critical shear testing are as follows:

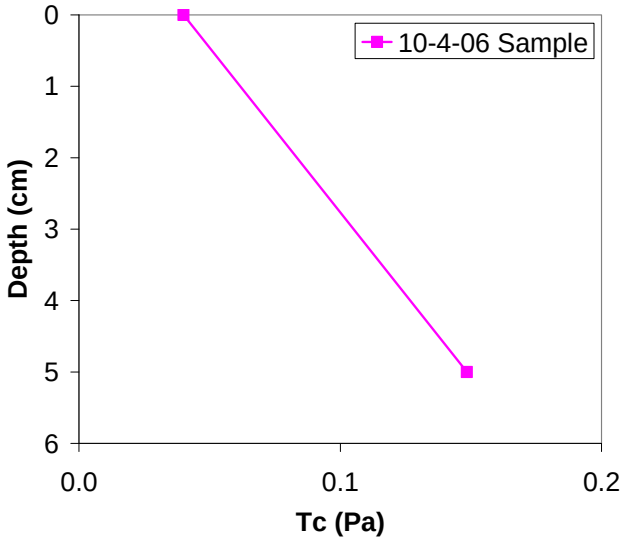

Figure 133: Critical Shear Profile for Wagner Gage Site.

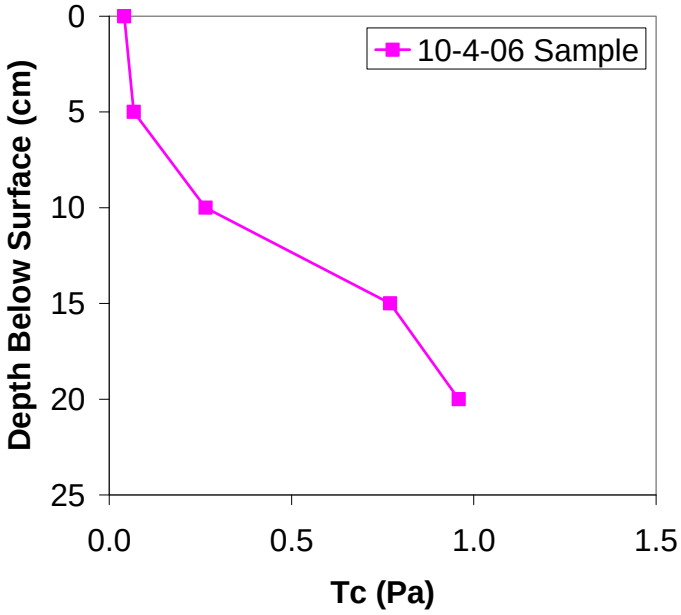

Figure 134: Critical Shear Profile for Dorn Gage Site

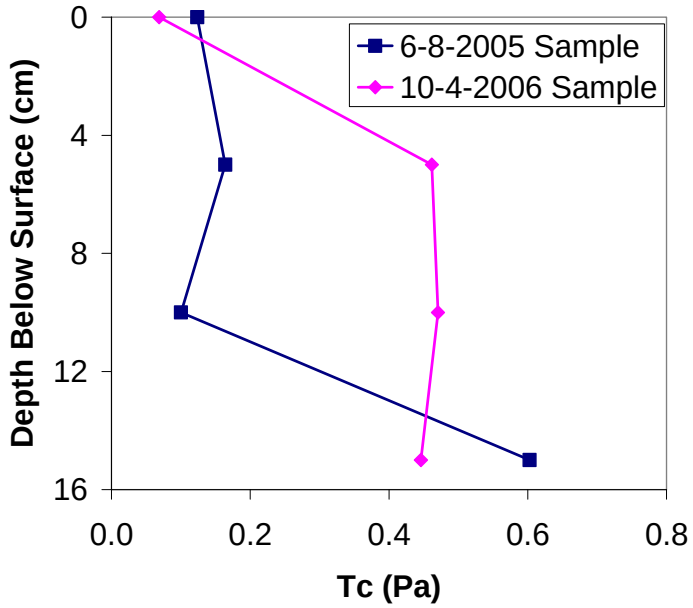

Figure 135: Critical Shear Profile for Ripp Gage Site (6-8-2005).

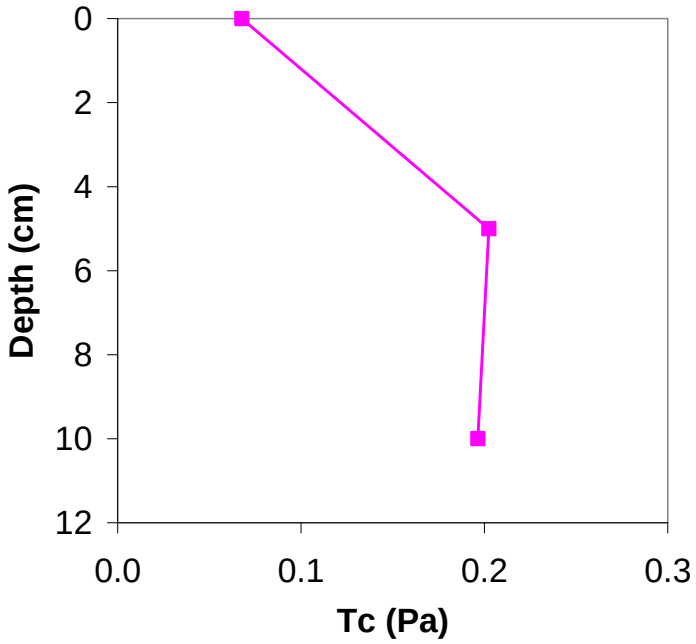

Figure 136: Critical Shear Profile for Kippley Gage Site.

The results indicate a thin layer of sediment in the samples with a low critical shear value. These values are consistent with the literature values presented earlier for silt. Lower layers of the samples indicate a much higher critical shear value, indicating highly cohesive sediments. This phenomenon was observed in the sediment cores, and high levels of roots and other vegetative matter were observed within the lower levels of the sediment cores indicating higher shear strength.

0.2.6 Bathymetry Measurements

Long-term measurements of the bathymetry of the channel at selected locations were performed since 2005. These measurements were initiated by Evan Murdoc in early 2005, and the same procedures were continued in the 2006 season. Essentially, measurements of the bed profile, and sediment thickness were taken at four main

locations along the creek. Site 1 is located just upstream of the Wagner Gage, Site 3 is located at the Ripp Gage, Site 6 has three cross sections at the Kippley Gage, and Site 9 is located just north of Highway K on Dorn Creek.

The measurements used to determine these results have a high standard deviation, and changes in the elevation of posts used to support the measuring bar may affect results. Nevertheless, some information can be gathered from this analysis. Changes in the sediment thickness are most notable at several locations.

The following results for channel cross section and sediment thickness for 2005-2006 are as follows:

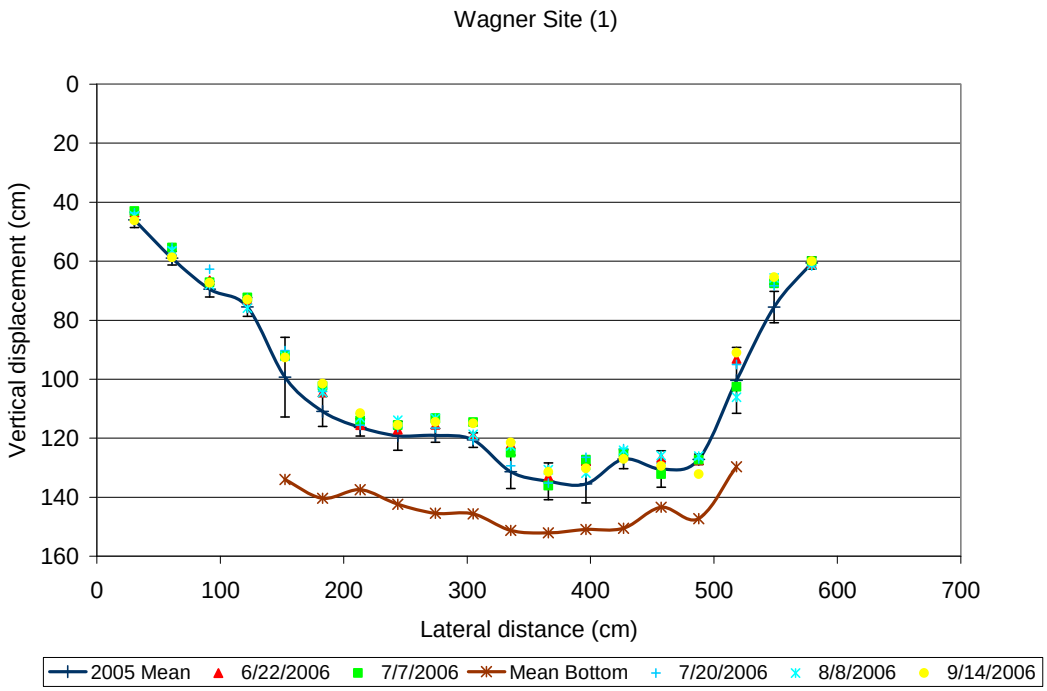

Figure 137: Bathymetry for Site 1 (Wagner) for 2005-2006

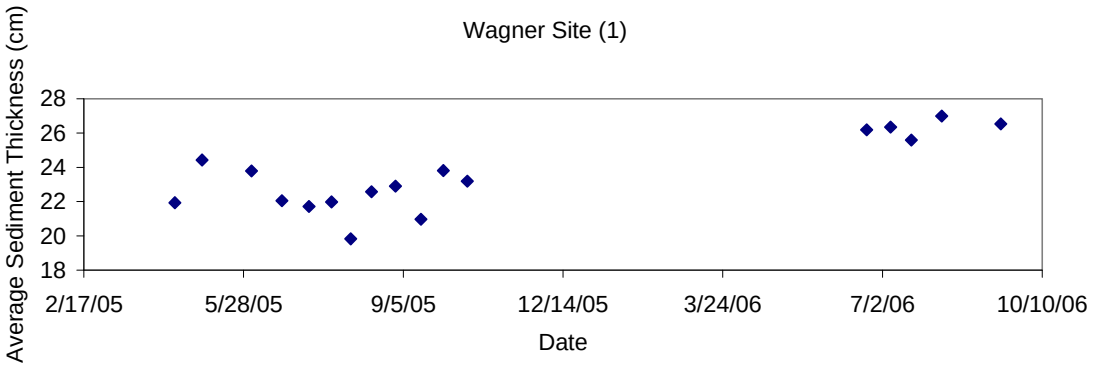

Figure 138: Sediment Thickness Variation for Site 1 (Wagner) for 2005-2006

The Wagner site shows an increase in sediment thickness of approximately 3 cm over the measured time period. Interviews of local residents indicated that this channel is artificially cut, and has to be cleaned out using a backhoe. This information agrees with a net sedimentation in this region.

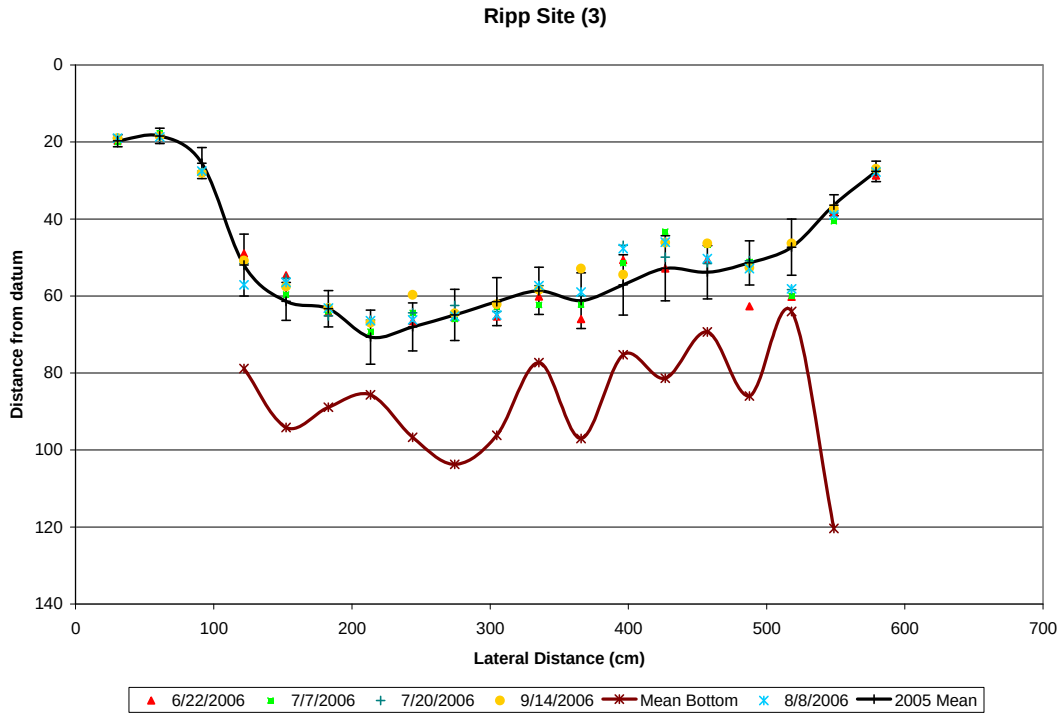

Figure 139: Bathymetry for Site 3 (Ripp) for 2005-2006

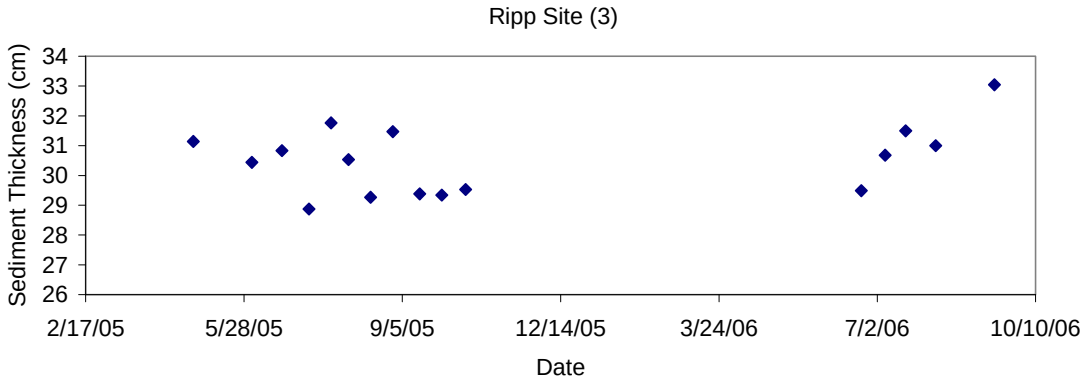

Figure 140: Sediment Thickness Variation for Site 3 (Ripp) for 2005-2006

The Ripp site shows no real change in the overall levels of sediment thickness. Between storm events, there does appear to be variations in sediment thickness, but for the time measured, there does not appear to be a net change. Of note is the rise in sediment thickness near 6/26/06, when sediment stormflow measurements indicate a large sediment transport from the wetland and deposition in the Kippley-Ripp Reach.

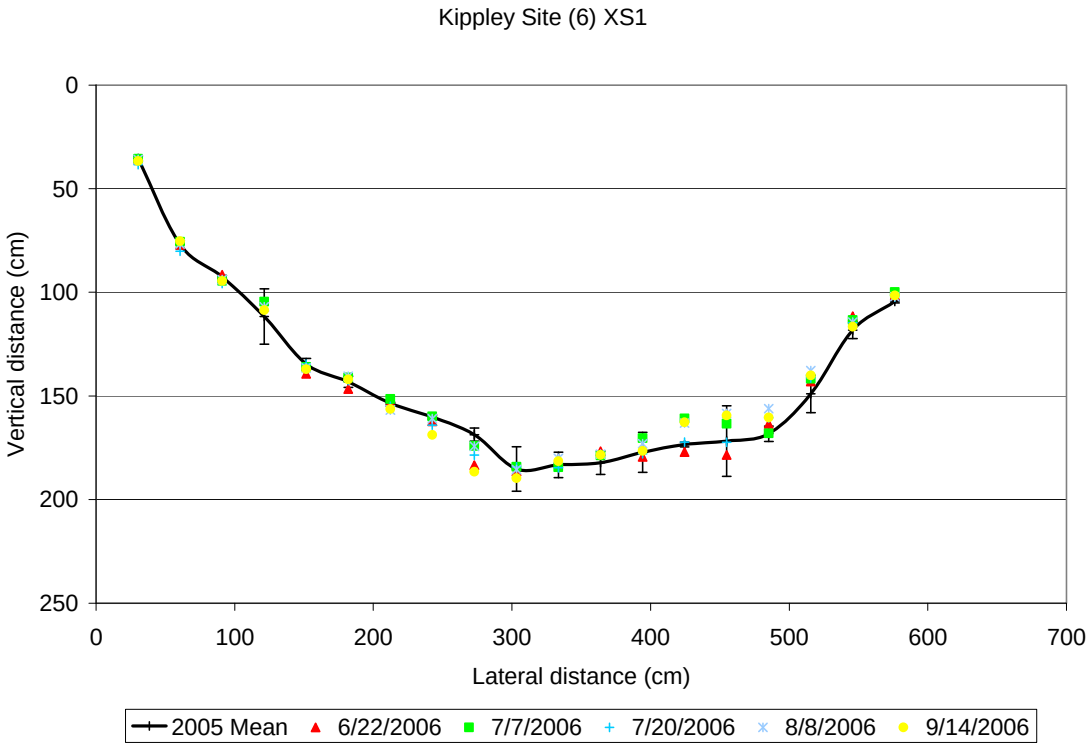

Figure 141; Bathymetry for Site 6 (Kippley) Upstream Cross Section for 2005-2006

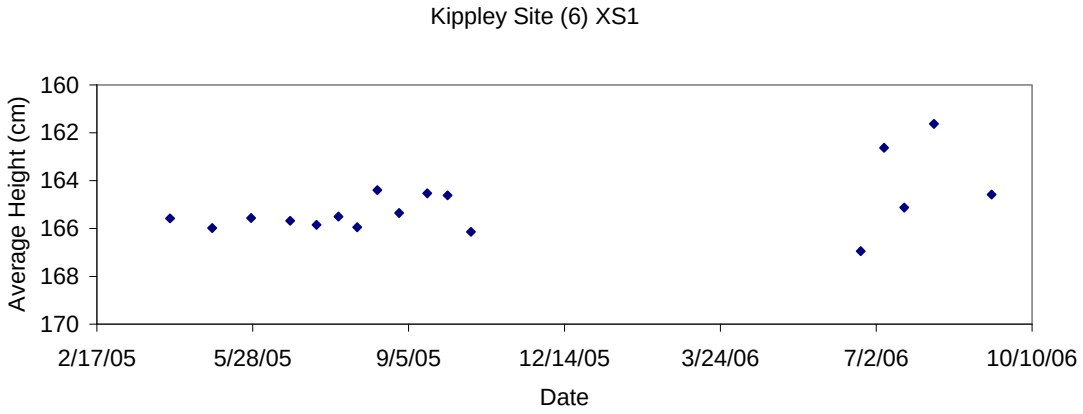

Figure 142: Sediment Thickness Variation for Site 6-XS1 (Kippley) for 2005-2006

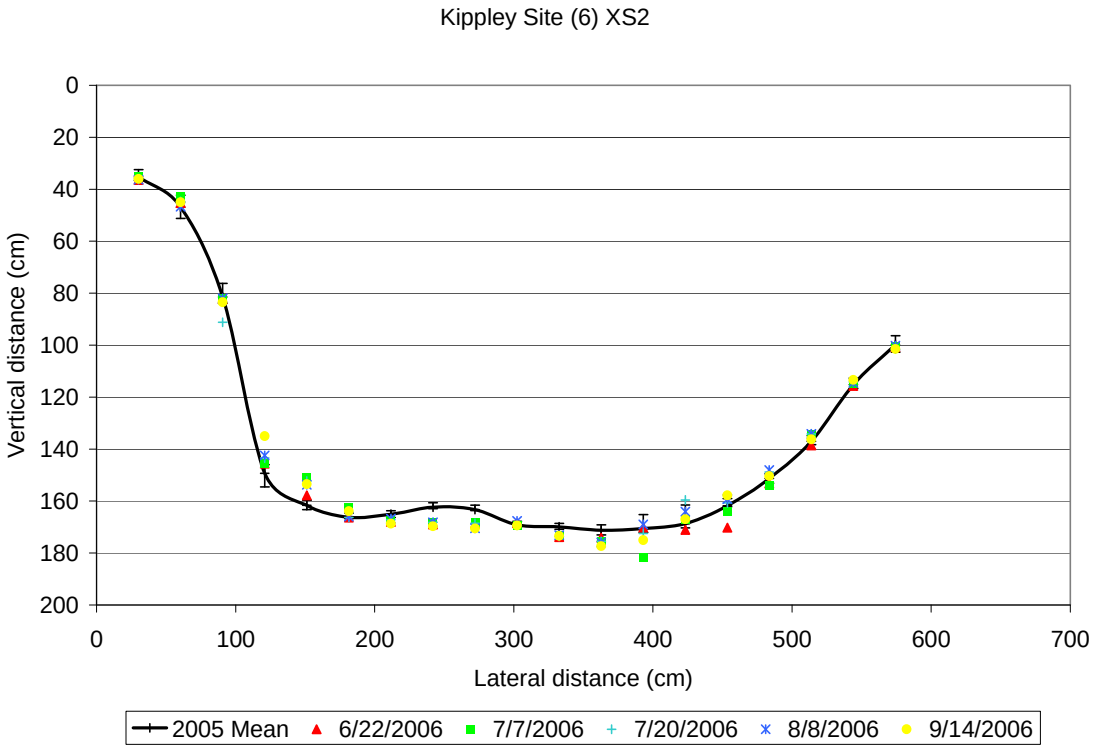

Figure 143: Bathymetry for Site 6 (Kippley) Mid Cross Section for 2005-2006

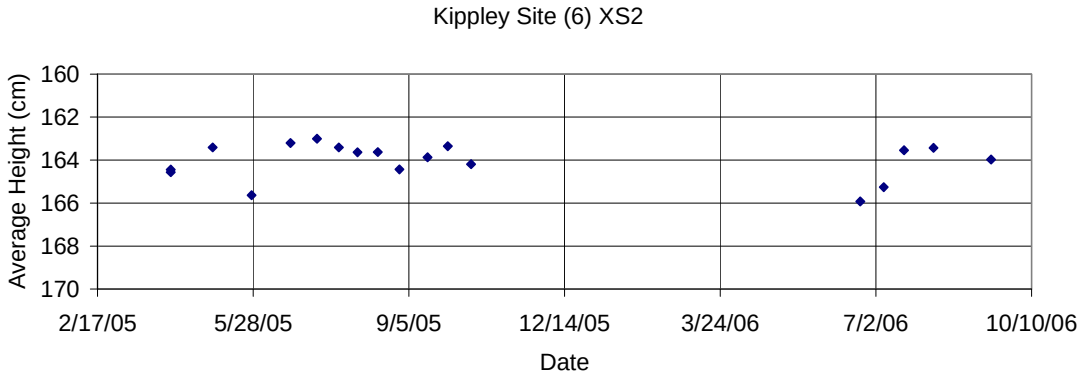

Figure 144: Sediment Thickness Variation for Site 6-XS2 (Kippley) for 2005-2006

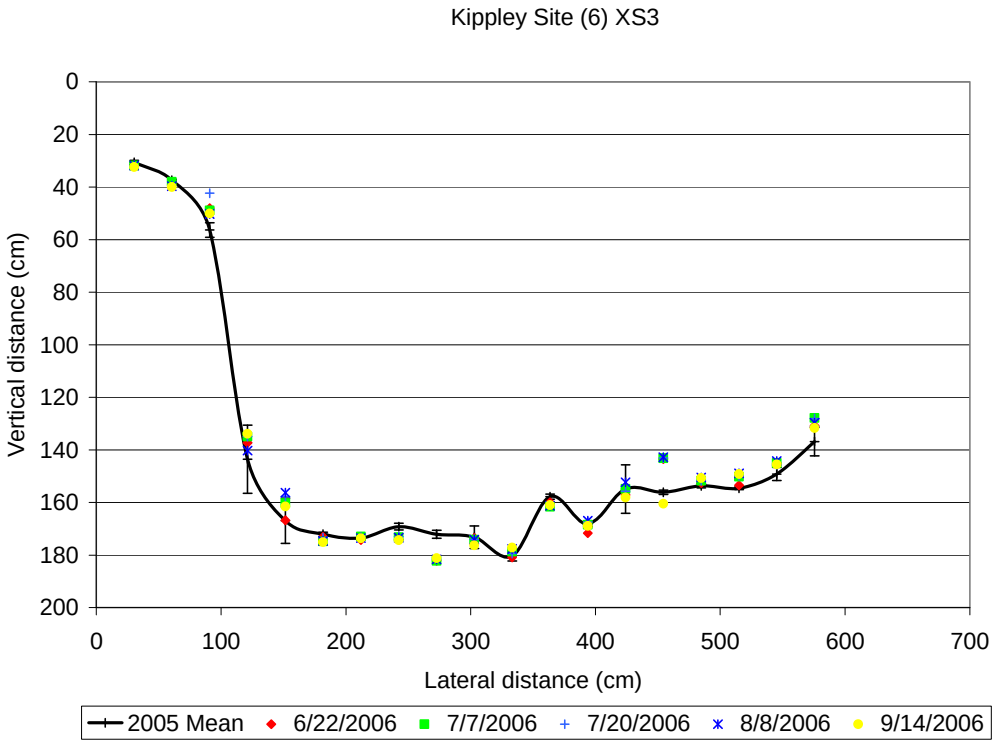

Figure 145: Bathymetry for Site 6 (Kippley) Downstream Cross Section for 2005-2006

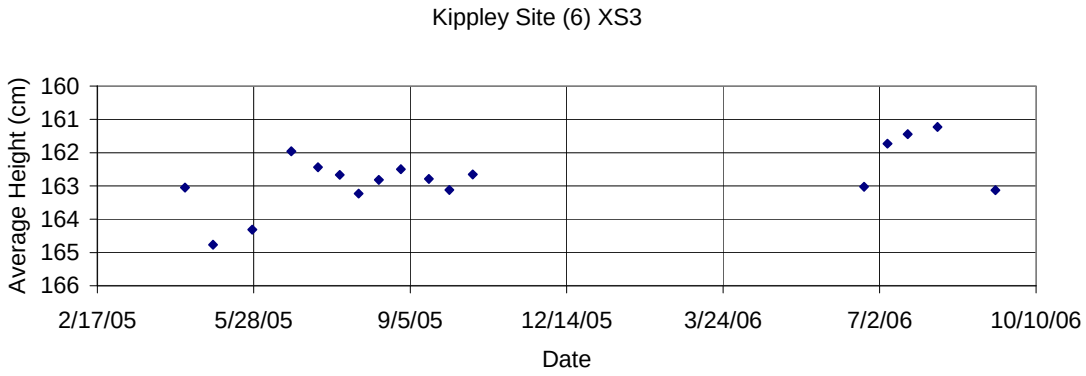

Figure 146: Sediment Thickness Variation for Site 6-XS3 (Kippley) for 2005-2006

The bathymetry measurements at the Kippley Gage show no real change in the overall channel cross section. There are no appreciable sediment deposits at this site, so the average depth below the datum was calculated. Cross Section 1 appears to be changing

based on individual events, but overall sedimentation or deposition was not observed for any of the cross sections during the 2005-2006 time period.

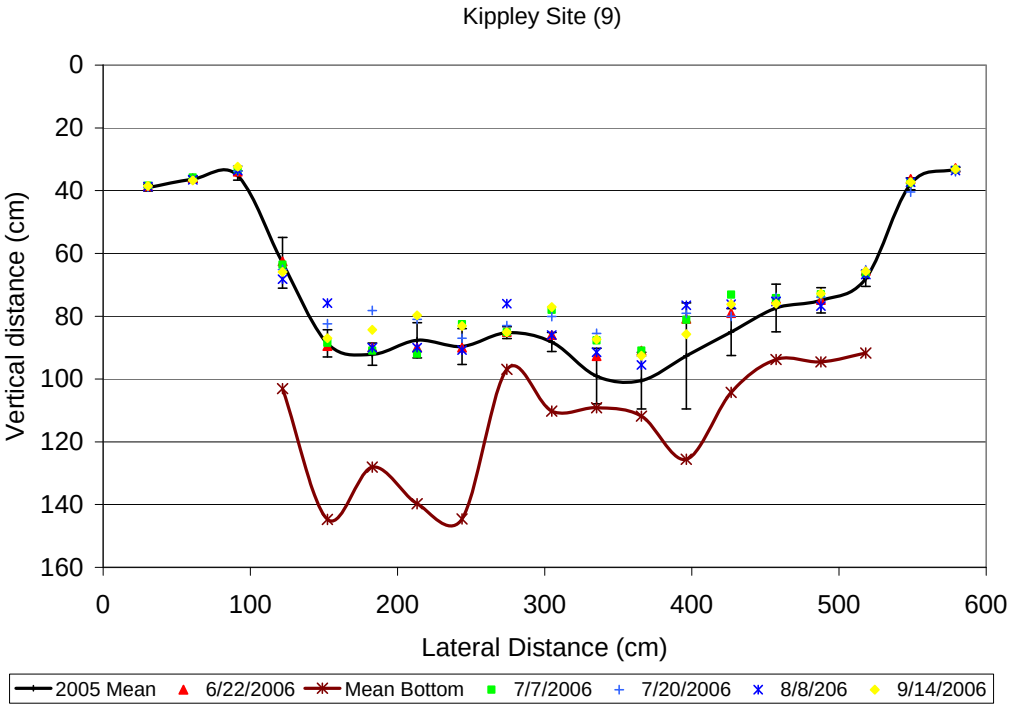

Figure 147: Bathymetry for Site 9 (Kippley) for 2005-2006

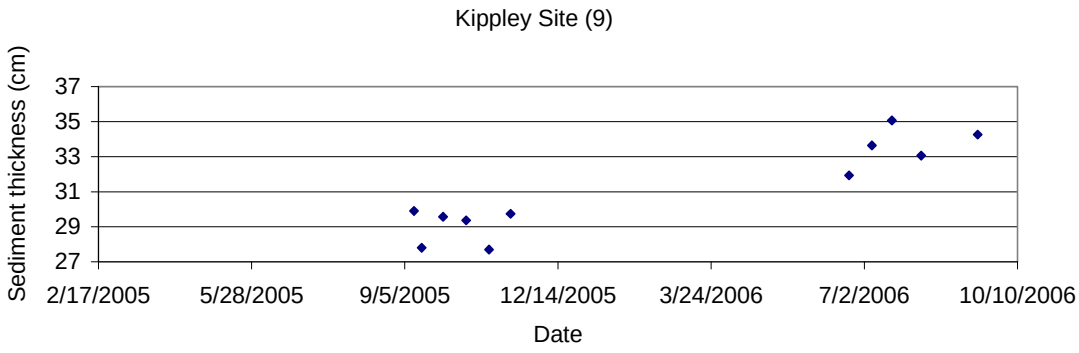

Figure 148: Sediment Thickness Variation for Site 9 (Kippley) for 2005-2006

The measurements of the cross section near Highway K at the beginning of the Lower Dorn Creek Wetland indicate an overall increase in sediment thickness of about 4 cm. The presence of thick layers of fine silty sediment at the site further confirms this result.

0.2.7 Event Sediment Rating Curves for Kippley Site

The following are the sediment transport and flowrate figures for the 2006 season. As shown by the figures, all events show a clear hysteresis with higher mass transport in the rising limb of the hydrograph. However, the relationship is not unique, and varies by event.

Analysis of the individual events shows a clear hysteresis for all events with higher transport in the rising limb of the hydrograph. As shown by the figures, there is not a unique relationship between flow and sediment transport rate. This indicates that the sediment transport in the reach in strongly controlled by sediment availability, and that sediment that enters the reach is typically flushed through quickly.

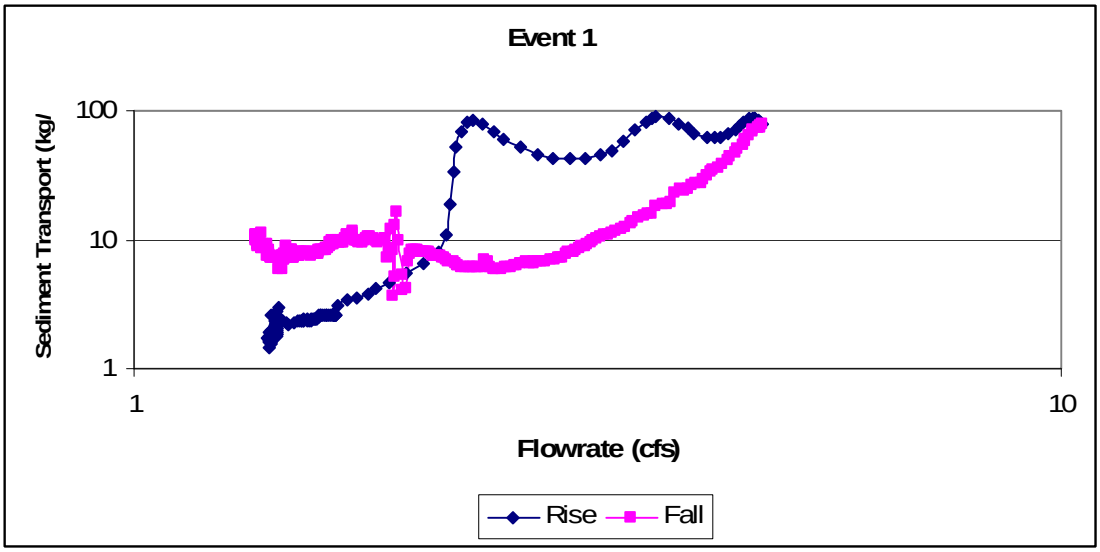

Figure 149: Event 1 Flowrate and Sediment Transport Rate

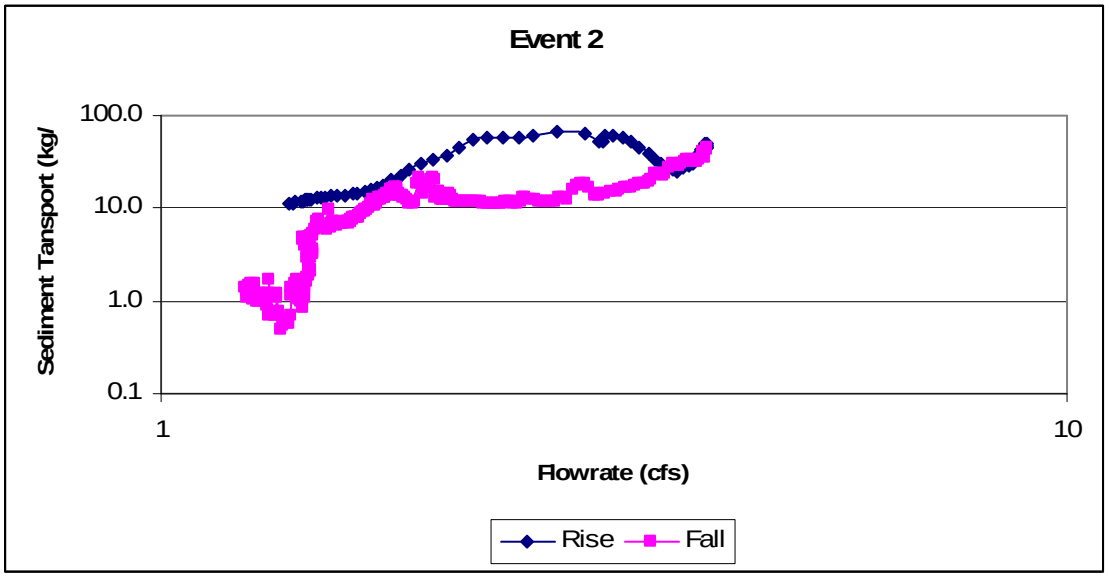

Figure 150: Event 2 Flowrate and Sediment Transport Rate

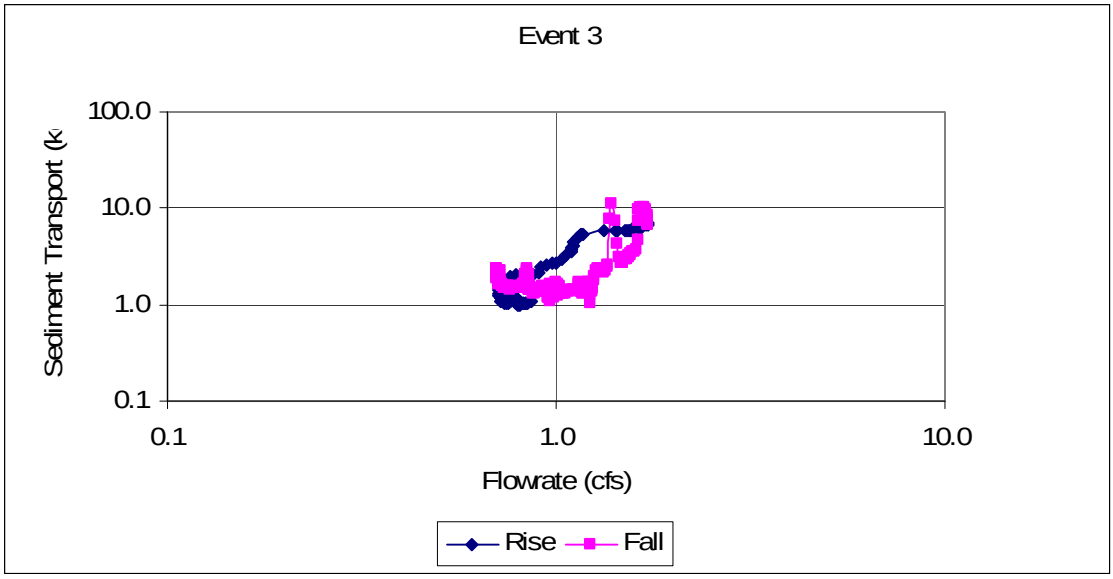

Figure 151: Event 3 Flowrate and Sediment Transport Rate

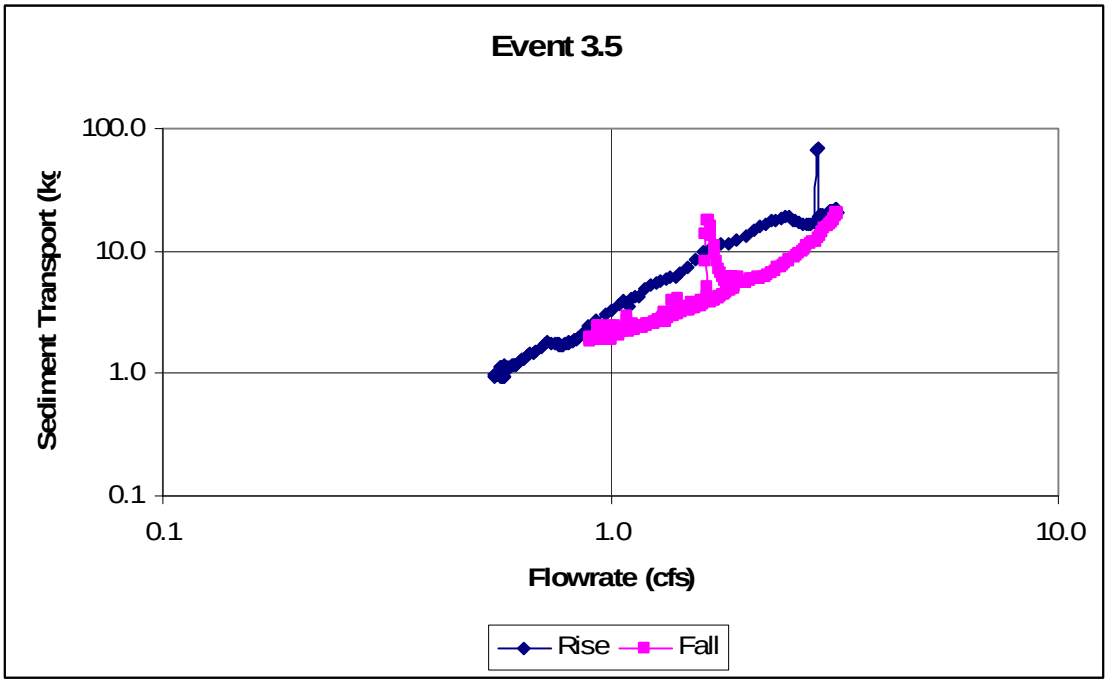

Figure 152: Event 3.5 Flowrate and Sediment Transport Rate

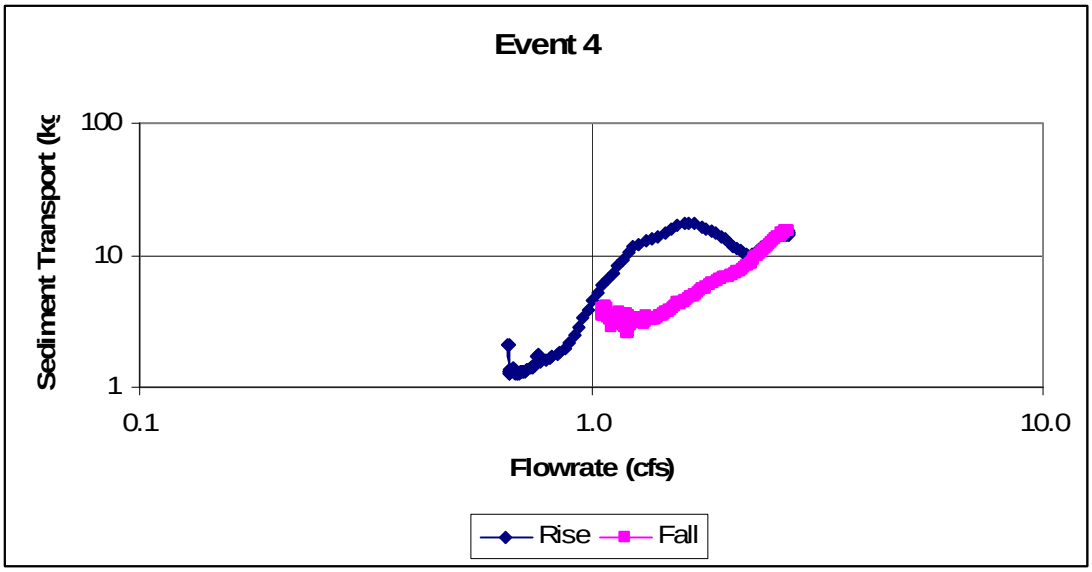

Figure 153: Event 4 Flowrate and Sediment Transport Rate

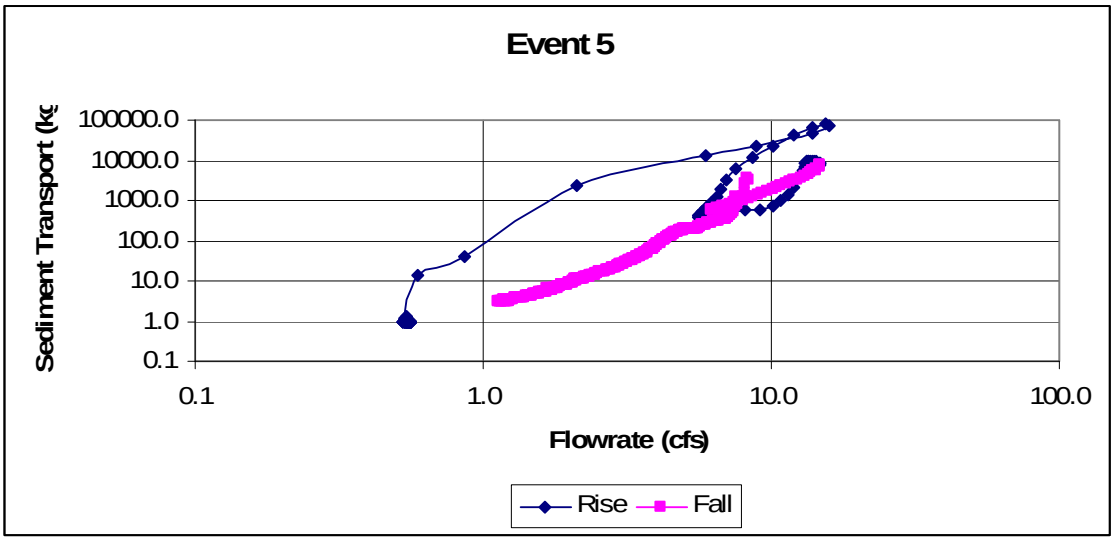

Figure 154: Event 5 Flowrate and Sediment Transport Rate

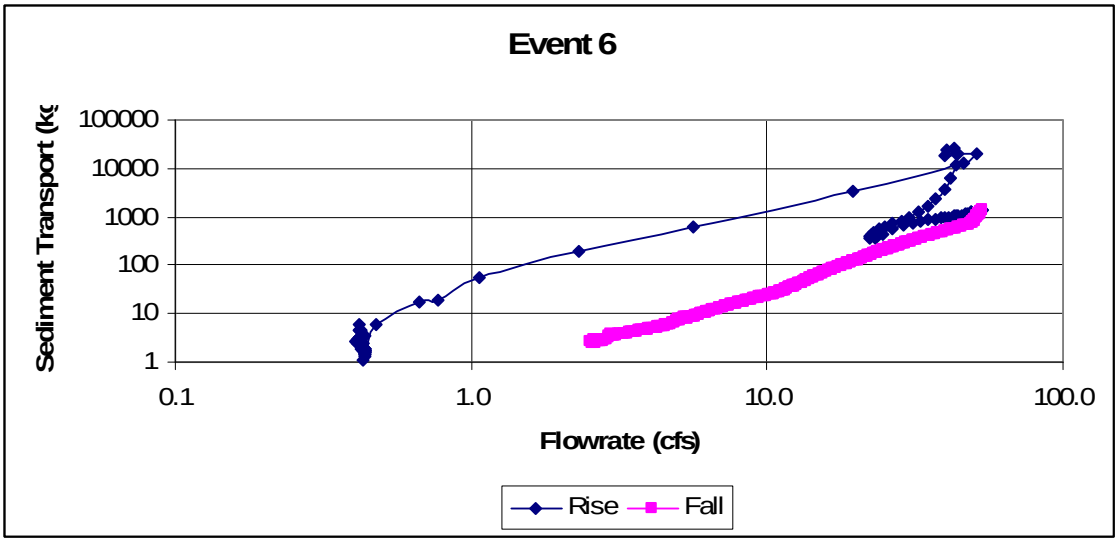

Figure 155: Event 6 Flowrate and Sediment Transport Rate

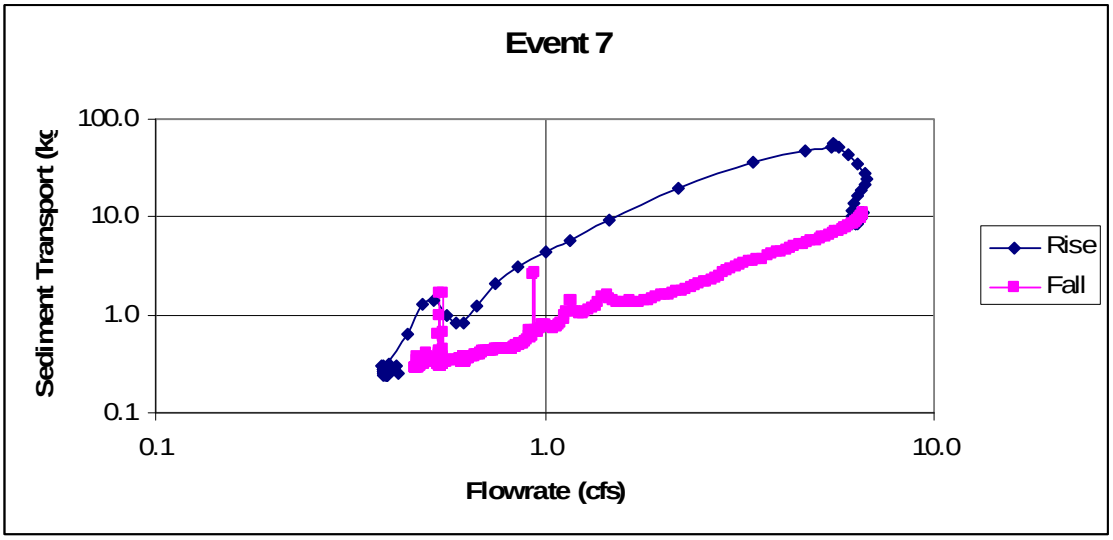

Figure 156: Event 7 Flowrate and Sediment Transport Rate

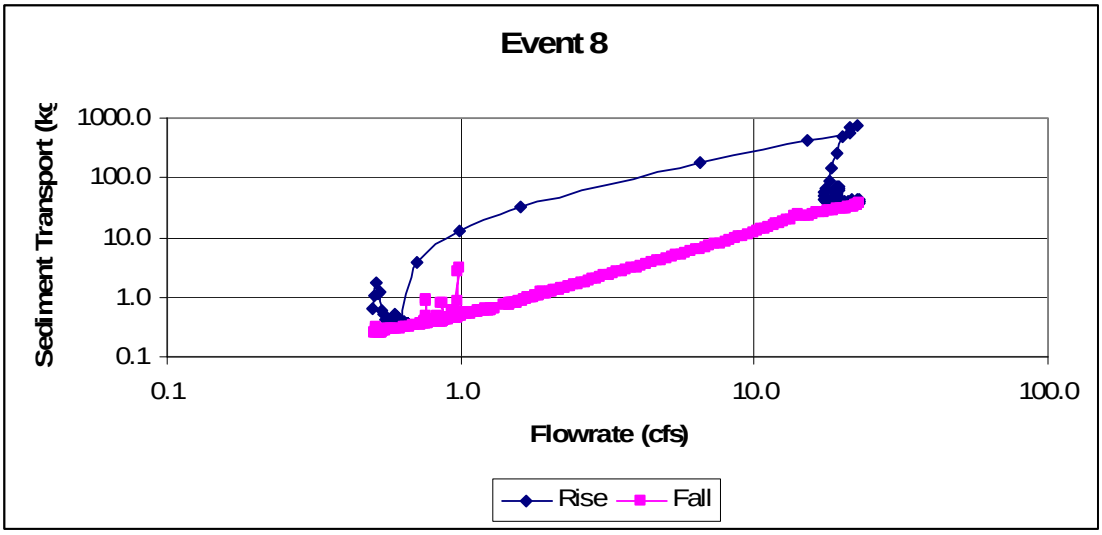

Figure 157: Event 8 Flowrate and Sediment Transport Rate

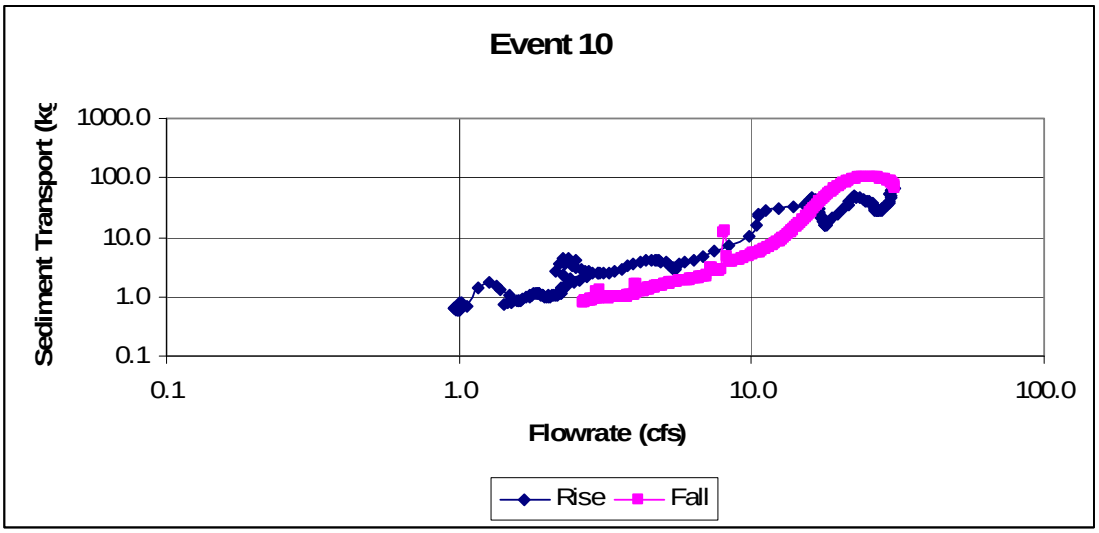

Figure 158: Event 10 Flowrate and Sediment Transport Rate

0.3 References

Julien, P. 1998. *Erosion and Sedimentation*. New York: Cambridge University Press.

Lee, C., et al. 2004. Automated Sediment Erosion Testing System Using Digital Imaging. Journal of Hydraulic Engineering 130(8): 771-782.

Muson, B., et al. 2005. *Fundamentals of Fluid Mechanics 5th Ed.* New York: John Wiley and Sons.

Murdoc, E. 2006. Transport and Storage of Sediments and Solutes in a Small Agricultural Stream, Dane County, Wisconsin. MS Thesis. University of Wisconsin – Madison.

APPENDIX F – INSTRUMENTATION WIRING INFORMATION

0.1 Overview

This appendix contains additional information concerning the wiring and programs used for this project not contained in Section 3.

0.1.1 Marsh-McBirney Model 201 Electromagnetic Current Meter (ECM)

Wiring diagram for connecting the MMB 201 for continuous velocity measurement.

Pin Output

A: Signal Ground
B: (+) 4.5 V
C: (-) 4.5 V
D: Magnet Ground
E: Output Signal
F: Signal Ground for Recorder

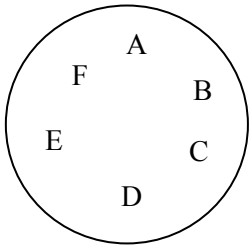

Output voltage was measured between pins E and F.

There appears to be some malfunction with meter. Output works for a period of time, and then will stop. Perhaps this is due to a bad connection within the meter.

Battery Wiring

Battery 1 (12V)
Red (+): voltage regulator (A) in
Black (-): voltage regulator (A) ground, and pin C

Battery 2 (12V)
Red (+): voltage regulator (B) in
Black (-): voltage regulator (B) ground

Voltage Regulator A (5V, 1A)
IN: Battery 1 (+)
GRD: Battery 1 (-), and Pin C
OUT: Pin A

Voltage Regulator B (5V, 1A)
IN: Battery 2 (+)
GRD: Battery 2 (-)
OUT: Pin B

0.1.2 Campbell-Scientific CR-10 Datalogger

Wiring for CR-10

For year 2006, this was the Meffert/Wagner Gage (Site 2)

OBS-3 Turbidity Probe (D&A Instruments)
1H: White
1L: Green
G: Black
12V: Red

107 Temperature Probe
2H: Red
AG: Purple
E1: Black
G: Clear

Differential Voltage (Water Level 400)
3H: High (Black)
3L: Low (Jumper to GRD)
G: Shield
3H-3L: (130 ohm Resistor Jumper)
12V: Red

-Measurement Labels-

Default Measurements
1 Batt_Volt
2 Prog_Sig

OBS-3 Turbidity Probe (D&A Instruments)
3 Turbidity

107 Temperature Probe
4 Temp

Differential Voltage
5 WaterLev

202 Output_Table 1.00 Min
1 202 L
2 Year_RTM L
3 Day_RTM L

```
4 Hour_Minute_RTM  L
5 Turbidity_AVG  H
6 Temp  L
7 WaterLev_AVG  L
8 Batt_Volt  L

Estimated final storage locations used per day:   12960
```

CR-10 DLD Program

```
};CR10
;CR10-SM2.DLD
;Created by Short Cut (2.5)
;$
;:Batt_Volt:Prog_Sig :Turbidity:Temp     :WaterLev

;$

;%
;Final Storage Label File for:  CR10-SM2.SCW
;Date:  7/6/2006
;Time:  19:50:59
;
;202 Output_Table   1.00 Min
;1 202 L
;2 Year_RTM  L
;3 Day_RTM  L
;4 Hour_Minute_RTM  L
;5 Turbidity_AVG  H
;6 Temp  L
;7 WaterLev_AVG  L
;8 Batt_Volt  L
;
;Estimated final storage locations used per day:   12960
;%

MODE 1
SCAN RATE 10.0000

1:P10
1:1

2:P92
```

1:0
2:1440
3:30

3:P19
1:2

4:P95

5:P2
1:1
2:25
3:1
4:3
5:0.4
6:0

6:P11
1:1
2:3
3:1
4:4
5:1.0
6:0.0

7:P2
1:1
2:25
3:3
4:5
5:1.0
6:0.0

8:P92
1:0
2:1
3:10

9:P80
1:1
2:202

10:P77
1:1220

11:P78
1:1

12:P71
1:1
2:3

13:P78
1:0

14:P70
1:1
2:4

15:P71
1:1
2:5

16:P70
1:1
2:1

MODE 2
SCAN RATE 10.0000
1:P96
1:71

MODE 3

MODE 10
1:28
2:106
3:0

MODE 12
1:0000
2:0000
3:0000

0.1.3 Campbell Scientific CR-10X Datalogger

Wiring for CR10-X

For the year 2006, this was the Kippley Site Gage (Site 6)

OBS-3 Turbidity Probe (D&A Instruments)
G: Black
1H: White
1L: Green
C1: Jumper to SW 12V CTRL
SW 12V CTRL: Jumper to C1
SW 12V: Red

107 Temperature Probe
G: Clear
AG: Purple
3H: Red
E1: Black

Differential Voltage (1) (Water Level 400)
G: Shield
2H: High (Black)
2L: Low (Jumper to GRD)
2H-2L: (130 ohm Resistor Jumper)
12V: Red

Differential Voltage (2) (Velocity Meter 201)
G: Shield
4H: High (Pin E)
4L: Low (Pin F)

-Measurement Labels-

Default Measurements
1 Batt_Volt
2 Prog_Sig

OBS-3 Turbidity Probe (D&A Instruments)
3 Turbidity

107 Temperature Probe
5 Temp

```
 Differential Voltage (1)
   6  Waterlev

 Differential Voltage (2)
   7  Velocity

101 Output_Table   1.00 Min
1 101 L
2 Year_RTM  L
3 Day_RTM  L
4 Hour_Minute_RTM  L
5 Turbidity_AVG  H
6 Temp  L
7 Waterlev_AVG  L
8 Batt_Volt  L
9 Velocity_AVG  L

Estimated final storage locations used per day:   14400
```

CR-10X DLD Program

```
};CR10X
;CR10X SM1.DLD
;Created by Short Cut (2.5)
;$
;:Batt_Volt:Prog_Sig :Turbidity:_________:Temp
;:Waterlev :Velocity
;$

;%
;Final Storage Label File for:  CR10X SM1.SCW
;Date:  4/28/2006
;Time:  15:05:53
;
;101 Output_Table   1.00 Min
;1 101 L
;2 Year_RTM  L
;3 Day_RTM  L
;4 Hour_Minute_RTM  L
;5 Turbidity_AVG  H
;6 Temp  L
;7 Waterlev_AVG  L
;8 Batt_Volt  L
```

```
;9 Velocity_AVG  L
;
;Estimated final storage locations used per day:   14400
;%


MODE 1
SCAN RATE 10.0000

1:P10
1:1

2:P92
1:0
2:1440
3:30

3:P19
1:2

4:P95

5:P86
1:41

6:P22
1:1
2:0
3:300
4:0

7:P2
1:1
2:25
3:1
4:3
5:0.4
6:0

8:P86
1:51

9:P11
1:1
```

2:5
3:21
4:5
5:1.0
6:0.0

10:P2
1:1
2:25
3:2
4:6
5:1.0
6:0.0

11:P2
1:1
2:25
3:4
4:7
5:1.0
6:0.0

12:P92
1:0
2:1
3:10

13:P80
1:1
2:101

14:P77
1:1220

15:P78
1:1

16:P71
1:1
2:3

17:P78
1:0

18:P70
1:1
2:5

19:P71
1:1
2:6

20:P70
1:1
2:1

21:P71
1:1
2:7

MODE 2
SCAN RATE 10.0000
1:P96
1:71

MODE 3

MODE 10
1:28
2:108
3:0

MODE 12
1:0000
2:0000
3:0000